EXPERIMENTAL INVESTIGATION, MODELLING AND OPTIMIZATION OF LASER BEAM WELDING OF POLYMERS AND TITANIUM BASED ALLOYS

Thesis submitted by

DHIRAJ KUMAR

DOCTOR OF PHILOSOPHY (ENGINEERING)

DEPARTMENT OF PRODUCTION ENGINEERING

FACULTY COUNCIL OF ENGINEERING & TECHNOLOGY

JADAVPUR UNIVERSITY

KOLKATA – 700 032, INDIA

2025

JADAVPUR UNIVERSITY
KOLKATA – 700 032, INDIA

Index no. 109/19/E

Registration No. 1021916007

Title of the thesis:

Experimental Investigation, Modelling and Optimization of Laser Beam Welding of Polymers and Titanium Based Alloys

Name, Designation & Institution of the supervisor:

Prof. (Dr.) Arunanshu Shekhar Kuar

Designation: Professor

Institution: Department of Production Engineering,

Jadavpur University, Kolkata – 700 032, India.

LIST OF PUBLICATIONS

International Journal

1. **Kumar, D.**, Ganguly, S., Acherjee, B., & Kuar, A. S. (2024). Performance evaluation of TWIST welding using machine learning assisted evolutionary algorithms. *Arabian Journal for Science and Engineering*, *49*(2), 2411-2441. **[SCI, Scopus Indexed]**

2. **Kumar, D.**, Pratap, U., Acherjee, B., & Kuar, A. S. (2023). Modeling and optimization of conflicting responses in the laser transmission welding process using RSM, PSO, and TLBO algorithm. *Materials Today: Proceedings*. **[Scopus Indexed]**

3. **Kumar, D.**, Sarkar, N. S., Acherjee, B., & Kuar, A. S. (2022). Beam wobbling effects on laser transmission welding of dissimilar polymers: Experiments, modeling, and process optimization. *Optics & Laser Technology*, 146, 107603. **[SCI, Scopus Indexed]**

4. **Kumar, D.**, Ghosh, S., Kuar, A. S., & Maity, N. (2021). Enhancement of Laser Transmission Welds in Acrylic and Polypropylene Copolymer (PPCP) Using Snap Drift Cuckoo Search (SDCS) Optimization. *Lasers in Engineering*, 49(4-6), 205-225. **[SCI, Scopus Indexed]**

5. **Kumar, D.**, Kuar, A. S., & Maity, N. (2021). Low Power Laser Transmission Welding (LTW) of Clear-to-Clear Acrylic Transparent Polymers. *Lasers in Engineering*, 50(4-6), 311-330. **[SCI, Scopus Indexed]**

6. **Kumar, D.**, Pratap, U., Roy, N., & Kuar, A. S. (2021). Sensitivity analysis for process parameters in laser transmission welding of transparent polymers. *Materials Today: Proceedings*. **[Scopus Indexed]**

7. **Kumar, D.**, Ghosh, S., Kuar, A. S., & Paitandi, S. (2020). Laser transmission welding of thermoplastic with beam wobbling technique using particle swarm optimization. *Materials Today: Proceedings*, 26, 808-813. **[Scopus Indexed]**

National Journal

Nil

Book Chapter

1. **Kumar, D.,** Acherjee, B., & Kuar, A. S. (2021). Laser transmission welding: A novel technology to join polymers, *In: Encyclopedia of Materials: Plastics and Polymers*, Editor: S. Hashmi, Elsevier. **[Scopus Indexed]**

2. **Kumar, D.**, Paitandi, S., Kuar, A. S., & Bose, D. (2021). Experimental investigation on laser transmission welding of Polycarbonate and Acrylic. *In Machine Learning Applications in Non-Conventional Machining Processes*, (pp. 160-180). IGI Global. **[Scopus Indexed]**

Patents

Nil

Presentations in National/International/Conferences/Workshops

International Conference

1. Kumar, D., Acherjee, B., & Kuar, A. S. (2024, October). Microstructural and Corrosion Behaviour of Laser Welded NITINOL for Marine Engineering Application. 24th International Association of Maritime University Conference (IAMUC – 2024), Massachusetts Maritime Academy, Massachusetts, USA.

2. Kumar, D., Pratap, U., Acherjee, B., & Kuar, A. S. (2023, April). Modeling and Optimization of Conflicting Responses in the Laser Transmission Welding Process using RSM, PSO and TLBO algorithm. International Conference on Advances in Materials, Mechanics, Mechatronics and Manufacturing (IC4M – 2023).

3. Kumar, D., Kumar, R., & Kuar, A. S. (2022, August). Experimental Investigation into Fiber Laser Beam Welding of TI-6AL-4V Superalloy. International Conference on Laser Assisted Material Processing (LAMP – 2022), Indian Institute of Technology, Kharagpur, India.

4. Kumar, D., Pratap, U., Roy, N., & Kuar, A. S. (2021, November). Sensitivity analysis for process parameters in laser transmission welding of transparent polymers. 1st International Conference on Applied Research and Engineering (ICARAE – 2021), Cape Peninsula University of Technology, Cape Town, South Africa.

5. Kumar, D., Ghosh, S., Kuar, A. S., & Paitandi, S. (2020, February). Laser transmission welding of thermoplastic with beam wobbling technique using particle swarm optimization. 10th International Conference on Materials Processing and Characterization (ICMPC – 2020), GLA University, Mathura, India.

6. Kumar, D., Kuar, A. S., & Maity, N. (2019, July). Experimental Investigation on Low Power Laser Transmission Welding of Transparent Polypropylene. 40th MATADOR International Conference on Advanced Manufacturing and Design, Hangzhou, China.

National Conference

Nil

- ❖ Awarded Best Paper Presentation at 1st International Conference on Applied Research and Engineering ICARAE 2021 organized by Department of Mechanical Engineering, Cape Peninsula University of Technology, Cape Town, South Africa.

"Statement of Originality"

I Dhiraj Kumar registered on 06th June 2019 do hereby declare that this thesis entitled "**EXPERIMENTAL INVESTIGATION, MODELLING AND OPTIMIZATION OF LASER BEAM WELDING OF POLYMERS AND TITANIUM BASED ALLOYS**" contains literature survey and original research work done by the undersigned candidate as part of Doctoral studies.

All information in this thesis have been obtained and presented in accordance with existing academic rules and ethical conduct. I declare that, as required by these rules and conduct, I have fully cited and referred all materials and results that are not original to this work.

I also declare that I have checked this thesis as per the "Policy on Anti Plagiarism, Jadavpur University, 2019", and the level of similarity as checked by iThenticate software is 8 %.

Signature of Candidate: Dhiraj Kumar

Date : 26-11-25

Certified by Supervisor(s): 26/11/25

(Signature with date, seal)

Dr. Arunanshu Shekhar Kuar
Production Engineering Department
Jadavpur University
Kolkata - 700 032, India

JADAVPUR UNIVERSITY

FACULTY OF ENGINEERING AND TECHNOLOGY

DEPARTMENT OF PRODUCTION ENGINEERING

CERTIFICATE FROM THE SUPERVISOR

*This is to certify that the thesis entitled "**Experimental Investigation, Modelling and Optimization of Laser Beam Welding of Polymers and Titanium Based Alloys**", submitted by Shri. Dhiraj Kumar, who got his name registered on 6th June 2019 for the award of Ph.D. (Engg.) degree of Jadavpur University is absolutely based upon his own work under the supervision of Dr. Arunanshu Shekhar Kuar and that neither his thesis nor any part of the thesis has been submitted for any degree/diploma or any other academic award anywhere before.*

Arunanshu Shekhar Kuar 9/6/11/25

(Signature of the Supervisor with date and official seal)

Dr. Arunanshu Shekhar Kuar
PROFESSOR
Production Engineering Department
Jadavpur University
Kolkata - 700 032, India

ACKNOWLEDGEMENT

The insight presented in this thesis is undoubtedly a result of the contributions made by numerous outstanding individuals. The author wishes to express his deep sense of gratitude to the PhD (Engg.) thesis supervisor Dr. Arunanshu Shekhar Kuar, Professor, Production Engineering Department, Jadavpur University for his constant guidance, valuable advice, helpful suggestions, support, encouragement and continuous association at every aspect from the budding stage to the final stage of this research work. Without his helpful and timely advice, this thesis would not have been progressed as smoothly as it did towards its completion.

The author also extends appreciation for the cooperation and encouragement received from Dr. Soumya Sarkar, Dr. Souren Mitra, Dr. Biplab Ranjan Sarkar, Dr. Ajoy Kumar Dutta, and the Head of the Department, Dr. Bijan Sarkar and all the faculty members of the Prodcution Engineering Department at Jadavpur University during the research work. Special thanks to Shri Dipten Misra, School of laser science and engineering, Jadavpur University, Dr. Dipankar Bose, Mechanical engineering department, NITTTR Kolkata, CRNN, Calcutta University and IIT Kharagpur for helping me at different stages of my research work. The author expresses his gratitude to Professor Sanjib Acharya, Mechanical Engineering department, Jadavpur University for his guidance and support.

The author expresses sincere gratitude to fellow colleagues Dr. Nilanjan Roy, Dr. Debal Pramanik, and Dr. Kingshuk Mandal, as well as to former undergraduate students Srinjoy Ghosh and Samriddhi Ganguly, and former postgraduate students Utkarsh Pratap and Agnibha Banerjee of the Department of Production Engineering, Jadavpur University, for their invaluable assistance, cooperation, and unwavering support throughout the research work. The author also extends heartfelt thanks to former postgraduate students Nandakishor Maity and Niladri Shekhar Sarkar of the School of Laser Science and Engineering, Jadavpur University, for their helpful contributions and collaboration. Special thanks are extended to the FET office and Research section for their cordial assistance and administrative support. The author acknowledges the All India Council for Technical Education, New Delhi, for providing the fellowship under NDF (Engg.) scheme during the research work. The author gratefully acknowledges the co-operation and encouragement received from all the

faculty members and staff members of Production Engineering Department, Jadavpur University for carrying out research work successfully.

A very special thanks to Dr. Bappa Acherjee, Associate Professor, Birla Institute of Technology, Mesra for his constant guidance and support during the time needed. Last but not least, the author would express his gratitude to Almighty for his blessings, without which, this would have never been possible.

The author thanks his family members and friends for their continuous support and motivation. Also, the author sincerely thanks all those who contributed directly or indirectly to this research work and helped the author make the research work a success.

Dhiraj Kumar 26/11/25

Dhiraj Kumar

PREFACE

Engineers and researchers in the field of manufacturing are working on the joining of different lightweight materials, advanced materials, polymers, and recently developed smart or intelligent materials, with a primary goal of achieving precise and high-quality weld. In this regard, there is a also requirement of minimizing the greenhouse gas emission, it is found that one of the most effective ways of increasing the fuel economy and minimizing the emissions is achieved through reduced vehicle weight. Thus, various types of lightweight structural materials are being produced and used for component manufacturing in automotive and aerospace industries. However, manufacturing engineers are facing challenges of development of approximate joining technology for joining of different classes of materials such as lightweight materials, polymeric materials and smart materials. Welding has been identified as one of the most effective joining method used in the manufacturing industry. Previous studies show that as compared to the conventional welding process, laser beam welding stands out as a versatile solution offering exceptional precision, productivity and versatility. Laser welding offers a number of benefits, such as regulated bead size, faster and more productive welding, less distortion, a small heat-affected zone, and low contamination. Despite this, laser welding is not as common as expected owing to material constraints. The optical qualities of the material are critical in laser beam welding.

The main challenge of laser beam welding is difficulty to weld several types of engineering material combination due to differing degree of incompatibility. Althogh, polymers and titanium alloys are fundamnentally different materials but they share various challenges in laser beam welding such as thermal management, absorption characteristics and process control. Despite having advantages over conventional welding technique, laser welding faces material constraint, that limits its full potential.

For this research, two different laser sources are employed to address the specific requirements of each material class. A low-power diode laser (10W) is used for welding of transparent and opaque polymers, such as polymethyl methacrylate , polycarbonate, and polypropylene copolymer, and a high-power fiber laser (500W) is used for welding of titanium-based alloys, including titanium and NiTinol superalloy. While substantial research has been conduced in this field, yet the incompatibility in the thermal and optical properties presents challenges and builds a scope for optimizing laser welding parameters,

develop defect free prevention strategies and enhancing material compatibility across diverse material classes. However, limited studies have focused on the simultaneous exploration of laser welding in both low-melting polymers and high-melting titanium alloys using different laser sources. In particular, the effect of process parameters on weld quality and defect minimization across these diverse materials remains under-investigated. Based on feasibility, the goals of the current research activity have been merged in accordance with the resources available, as follows:

1) To assess the laser weldability of acrylic and polypropylene copolymer and assess the laser weldability of clear transparent polymers without the use of any additives.
2) To carry out experimental investigation into laser transmission welding (LTW) of polymers by low power laser and determine the influence of significant laser welding parameters on the weld quality characteristics:
    a) to study LTW of acrylic to polypropylene copolymer
    b) to study LTW of polycarbonate to acrylic
    c) to study LTW of clear to clear acrylic transparent polymer
    d) to study LTW of clear acrylic to clear polycarbonate transparent polymer
3) To study the effect of beam wobbling parameters on the weld quality characteristics.
4) To develop the mathematical model based on response surface methodology for correlating the influence of the various laser welding process parameters on responses of weld joint. To test the adequacy of the developed mathematical models, analysis of variance test.
5) To carry out interactive multi-response optimization analysis for different responses such as weld strength, weld seam width and HAZ width, from the developed mathematical models effective for laser welding process parameters for the purpose of determining optimal parametric combinations leading to minimum HAZ thickness, weld seam width and maximum weld strength.
6) To carry out experimental investigation into laser beam welding of NiTinol alloys by high power laser, determine the influence of significant laser welding parameters on the weld quality characteristics and find out parametric process optimization to develop mathematical model
7) To carry out experimental investigation into laser beam welding of Titanium super alloys by high power laser, find out the influence of significant laser welding parameters on the weld quality characteristics and by using the developed mathematical model to determine the optimal process parameter

In order to accomplish the objective of the study, this thesis is prepared in a well-organized manner into nine chapters. A summary of each chapter is provided as below:

Chapter 1 frameworks an outline of laser welding process, fundamentals of laser beam welding process, current needs, and applications. Several kinds of laser systems applied for welding processes are discussed in this chapter. This chapter accomplishes with the explanation of more suitability of of laser beam welding over other welding process. Laser welding of polymers and laser welding of metals and alloys are also discussed in this chapter.

Chapter 2 contains literature review of past research works of laser beam welding of different class of materials, which support to plan the research objectives by exclusion of knowledge gaps found during literature review.

Chapter 3 provides the details of both low power and high power Laser beam welding set up used for experimental investigation. Experimental methodology which applied not only for plan using of the experiments but also for analysis of experimental explanations has also been discussed in this chapter. Different optimization method used for this present investigation is also discussed in this chapter.

Chapter 4 focusses on experimental studies of low power laser transmission welding of acrylic to polyrpoylene copolymer to study the influence of process variables on weld quality characterisics. Emphasis is given here to increase the weldability by using white ink as compatibilizer. A second order rotable polynomial model is established during laser beam welding by response surface methodology (RSM) to create the correlation between input and output of the process. Multiobjective optimization technique is also applied to optimize the responses at optimal parameter settings.

Chapter 5 highlights the experimental investigation into low power laser transmission welding of polycarbonate to black carbon filled acrylic with or without beam wobbling technique. In this chapter, the effects of process parameters on the responses have been analysed. The efficacy of beam wobbling technique on weld quality characteristics is also studied. Multiobjective optimization technique is also applied to find out optimal parameter settings to enhance weld quality.

Chapter 6 provides the experimental studies of low power laser transmission welding of clear transparent polymers with or without beam wobbling technique and to study the influence of process variables on weld quality characterisics. This research also addresses the challenges of predicting appropriate parameter values and optimizing conflicting objectives in TWIST welding. The effects of wobble LTW parameters on weld quality and weld morphology are investigated through experimental work and statistical analyses.

Chapter 7 highlights the experimental investigation into high power laser beam welding of NiTinol alloys and the effects of process parameters on the responses have been analysed. Multiobjective optimization technique is also applied to find out optimal parameter settings to enhance weld quality.

Chapter 8 highlights the experimental investigation into high power laser beam welding of titanium super alloys and the effects of process parameters on the responses have been studied. Multiobjective optimization technique is also applied to find out optimal parameter settings to enhance weld quality

Chapter 9 contains the overall conclusions of the present research work based upon various experimental results and discussions which have been summarized in brief. Apart from that, the chapter also contains the future scope of the present research work which can be used by any researchers in order to enhance the work in the areas of laser marking.

VITA

The author, Dhiraj Kumar, son of Mr. Yamuna Prasad Gupta and Mrs. Vimala Devi, was born on 15th November, 1993 in Hariharganj (Palamu District), Jharkhand, India. The author did his entire schooling in his mother tongue, Hindi.

He studied up to Class X at R. K. Sita High School, Hariharganj (Palamu District), Jharkhand and Class XI to Class XII at S. N. Sinha College, Aurangabad, Bihar, India. He passed Annual Secondary Examination (Class X) in the year 2008 under Jharkhand Academic Council and the Higher Secondary Examination (Class XII) in the year 2010 under Bihar School Examination Board.

The author graduated in Mechanical Engineering in 2015 from RCIT Bishrampur. University - Nilamber Pitamber University, Medininagar in First Class with Distinction. The author qualified GATE (Graduate Aptitude Test in Engineering) and received AICTE approved post graduate fellowship for a period of two years i.e. 2016-2018. He completed his Masters degree (M.Tech) in Manufacturing Technology in First Class with Distinction in the year 2018 from National Institute of Technical Teachers Training and Research Kolkata, West Bengal, India. The author acknowledges the support from NDF (National Doctoral Fellowship) for 2 years as JRF (August, 2018 –July, 2020) and another two years as SRF (August, 2020 – July, 2022) during the tenure of research for Ph.D work. The author has published seven research papers in international journals, two book chapters as well as presented six research papers in reputed international conferences related to advanced welding process during his tenure of research in Production Engineering Department, Jadavpur University.

The author has spent last six years in pursuing Ph.D. (Engg.) at Production Engineering Department of Jadavpur University, Kolkata, West Bengal, India.

Currently, the author is working as a faculty at Indian Maritime University Kolkata Campus, since August, 2022.

Humbly dedicated to the grace of Lord Mahakal

TABLE OF CONTENTS

CHAPTER: 1

INTRODUCTION

1.1. Introduction

Engineers and researchers in the field of manufacturing are continuously working on the joining of different lightweight materials, advanced materials, polymers and recently developed smart or intelligent materials, with a primary goal of achieving precise and high-quality weld. The growing global need to minimize greenhouse gas emissions is continually pushing the transportation sector to search for ways to reduce fossil fuel combustion, a significant source of anthropogenic greenhouse gas emission. One of the most effective ways to increase fuel economy and lower emissions is to reduce vehicle weight. In general, a 10% weight reduction may result in a 3–7% reduction in actual fuel consumption [1]. As a result, a variety of lightweight structural materials are being created and utilized in the aerospace and automotive industries [2]. Polymeric materials are rapidly being used in various applications, including packaging, appliances, medical, electronics, automotive, and aerospace [3,4]. It is not easy to comprehend how essential plastics have been in our everyday lives [5]. Plastics allow for the development of elegant, well-designed products from the many different plastic materials that are readily available today. Titanium based alloy, renowned for its distinctive attributes like high strength to weight ratio, pseudo elasticity, exceptional biocompatibility, and resistance to corrosion, making it a viable material for a number of industries. Currently, manufacturing engineers and researches are facing the challenges of development of approximate joining technologies for the joining of different class of materials such as lightweight materials, polymeric materials and smart materials. One of the most significant joining methods in the manufacturing sector today is welding. More than any other conventional process, laser welding stands out as a versatile solution applicable to diverse materials, offering exceptional precision, productivity and versatility as compared to other traditional or non-traditional welding. Compared to conventional and arc welding, laser welding offers a number of benefits, such as regulated bead size, faster and more productive

welding, less distortion, a small heat-affected zone, and low contamination. Nowadays, lasers are used in the automotive and aerospace industries as a clean, non-contact source of heating and fusing to join sheets. The aerospace, automotive, electronic, medical, shipbuilding, and military defense industries have all made extensive use of laser beam welding (LBW) because of its many advantages, including its small fusion and heat-affected zones, low distortion, quick cycle time, and flexibility. Despite this, laser welding is not as common as expected owing to material constraints. The optical qualities of the material are critical in laser beam welding. Researchers are concentrating on laser welding of engineering material combinations that are challenging to join because of their differing degree of incompatibility [6]. As a result, laser welding processes have seen progressive development and enhancement over the last twenty years. However, challenges such as material limitations, process complexity and cost need to be addressed to fully leverage its potential. Ongoing research and technological developments are expected to further enhance LBW, making it a pivotal technique in modern manufacturing.

1.2. Laser Beam Welding (LBW): An Overview

Most consumers nowadays choose small, attractive and high-quality items. Everyone is concerned with the appearance, quality and weight of a product, whether it is a laptop, smartphone, or bicycle. Since 1962, there are numerous application of lasers in metallurgical contexts, including welding. The first laser welding was documented in the year 1963, focusing on butt welding steel sheets utilizing a pulsed ruby laser. By the year of 1965, laser systems had been specifically engineered for welding electronic circuitry, the interior of vacuum tubes, and various specialized applications where traditional methods were insufficient. Because of the precise placement of the laser spot and the fast-processing speed, lasers are widely utilized to execute micro welding of miniaturized components successfully. Laser welding is easily automatable and there are hand-held laser welding and cutting devices in the market as well. When compared to other traditional welding techniques, laser welding generates seams that are exceptionally strong and have a very narrow width, necessitating no post-processing. The use of laser welding in manufacturing has many advantages, including reduced material use, shortened processing times and more effective output. With the recent development of precision technology, Laser welding is one of the most important joining technologies in manufacturing industry. Lasers are currently being implemented in the automobile sector to make seam or stitch welds as a substitute for traditional resistance spot

welding, which is commonly used to join auto-body panels to subassemblies, in the fields of biology, medicine, and even nuclear fusion. Laser welding offers distinct advantages over resistance spot welding, including a smaller laser spot size, greater weld penetration, and the requirement for only single-sided access to the workpiece [7]. Laser welding offers significant benefits such as narrower flange widths, increased structural durability, and compatibility with rapid automated manufacturing processes. Since the introduction of high-power gas and solid-state lasers, lasers have been instrumental in material joining processes [8]. Recently, fiber lasers are gaining attention for producing narrow and deep penetration welds due to their high power and high beam quality.

1.3. Fundamentals of Laser Beam Welding Process

Laser is surely one of the greatest innovations of 20th century. A coherent, convergent, monochromatic beam of electromagnetic radiation with wavelengths ranging from ultraviolet to infrared is what is known as a laser, which stands for light amplification by stimulated emission of radiation. A laser is an artificial light composed of electromagnetic waves that may be concentrated at a specific point using lenses or mirrors, transforming it into a high-power density heat source. By nature, laser consists of a coherent (same frequency) and monochromatic (same wavelength) beam of photons. Einstein established the basic framework of laser theory [9]. Einstein's prediction was then confirmed experimentally for the first time by Kopfermann & Ladenburg [10]. It was Maiman [11] who created the first ruby laser in 1960. Much of the fundamental development of lasers took place between 1962 and 1968. This period saw the invention of nearly all significant laser types, including semiconductor, Nd:YAG, CO_2, dye, and other gas lasers. The current lasers were designed and manufactured with improved durability and dependability after 1968. More dependable lasers were made accessible by the middle of the 1970s for industrial uses including drilling, labeling, welding, and cutting that were actually useful. Lasers were investigated for surface-related uses in the 1980s and early 1990s, including thin film deposition, alloying, heat treatment, cladding, and glazing.

Figure 1.1 illustrates the fundamental layout of the laser generation and welding process. In this setup, a completely focused laser beam is directed towards the workpiece or joint at the specified level and speed. A shielding gas is employed to protect the weld pool from oxidation and to ensure appropriate atmospheric conditions during welding. The laser energy melts the adjoining edges of the workpiece, enabling fusion upon solidification after

the laser beam is removed. Typically, the movement required for welding is achieved by translating the workpiece rather than the laser source, allowing for controlled heat input and the minimization of the heat-affected zone (HAZ).

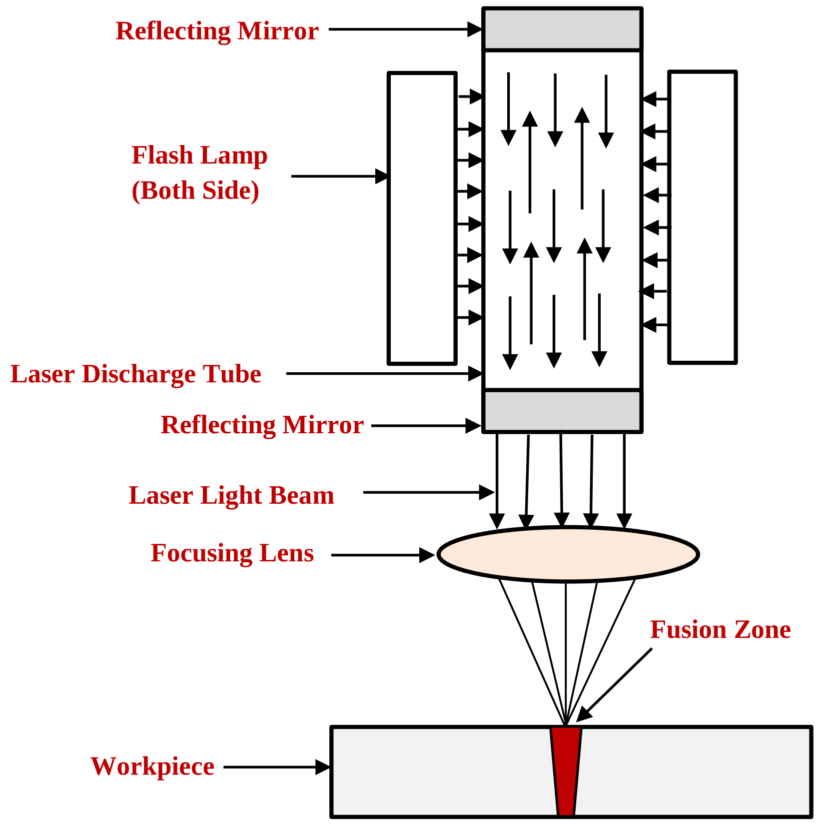

Figure 1.1. Schematic diagram of the basic scheme of the laser generation process

1.4. Laser Material Interaction

The phenomenon of laser material interaction is complex and laser is seen as a heat source only in some special cases. Over the decades, lasers are widely used in industrial production. Laser is a monochromatic source of coherent beam. Ordinary light contains many colors and electromagnetic radiation, thus it is difficult to collimate ordinary light without hampering its beam intensity. Monochromatic source of radiation can be used to focus very tiny spot of any size by the use of an optical lens without hampering its intensity.

When the intensity of laser beam strikes the material, some part of it has absorbed, some parts reflected and other part is transmitted, as shown in Figure 1.2.

$$\alpha + \rho + \tau = 1 \quad \text{……………………………………}(1.1)$$

Where, α stands for absorptivity, ρ for reflectivity and τ for transmissivity.

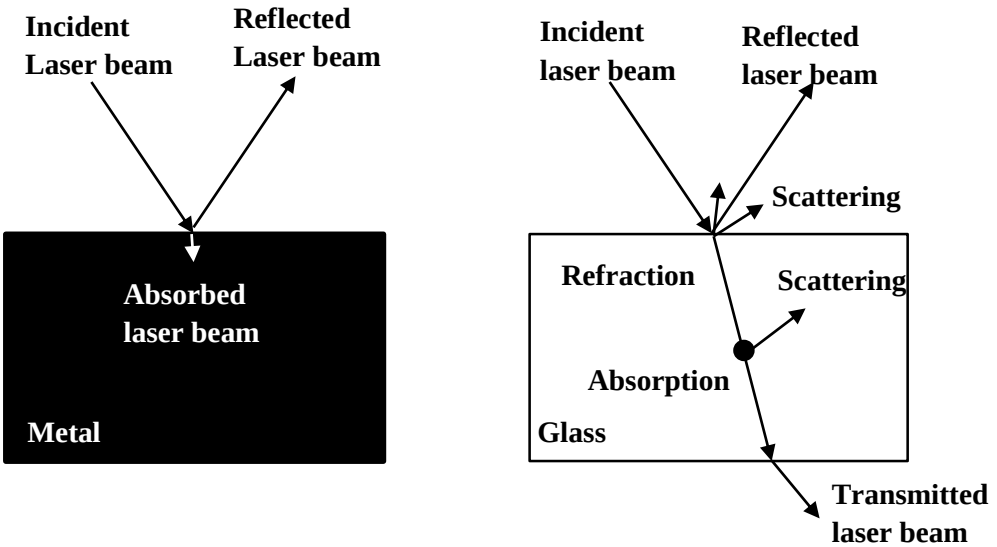

Figure 1.2. Schematic representation of physical interaction of absorption, reflection, transmission, refraction, and scattering between laser beam and material

The function of laser beam welding relies on thermo-optic interaction between the laser beam and work material. Thus, selection of workpiece is such that it should not reflect most incident radiation of laser beam. Metals have high reflectivity at the wavelength of CO_2 laser as compared to operating wavelength of Nd:YAG and diode laser. This is because diode and Nd:YAG laser are commonly used. Some parts of the laser beam which interact with the work piece have been absorbed as thermal energy and are gradually transferred to the molecular structure of material as kinetic energy.

$$E_{photon} = h\nu = E_1 - E_2 \quad \text{..... (1.2)}$$

E_{photon} is the energy absorbed by each photon of laser beam and E_1 and E_2 are the two states of the absorbed material [12].

In general, homogeneous polymer materials are non-absorbent to laser radiation, until or unless any kind of additive or pigmentation has been incorporated. The volumetric absorption on the surface of workpiece material is defined by Lambert's law which indicates the relation between penetration by the laser beam and intensity of laser beam [13].

$$I(z) = I_{(z=0)}\, e^{-Kz} \quad \text{..... (1.3)}$$

Where, I (z) is the light intensity (W/m^2) at a distance z within the work material and K is the extinction coefficient (m^{-1}). Absorption coefficient can also be written as reciprocal of penetration depth dp [14].

$$K_{absorption} = dp^{-1} \quad \ldots\ldots\ldots\ldots\ldots\ldots\ldots\ldots\ldots\ldots\ldots\ldots \quad (1.4)$$

Some part of heat is also lost to the surroundings by convection and radiation. When the temperature exceeds the melting point of polymers at interface, a thin layer of plastic melts from both the transparent and absorbent parts. Clamping pressure has maintained the proper contact in between two parts and helps to form a melt pool and flows across the path of laser beam. The formed melt pool has been quenched and the weld zone appeared.

1.5. Different types of Laser Source used for Welding

Various types of lasers are applicable for laser beam welding (LBW), including fiber lasers, Nd: YAG pulsed lasers and Nd: YAG continuous-wave lasers. However, the particular application determines which laser source is best for LBW. Because of their affordability and versatility, fiber lasers may be used for a wide range of tasks, from welding heavy components in the automotive and aerospace industries to precisely joining micro components in the medical engineering and electronics industries. Their affordability and versatility make them ideal for achieving high-quality spot welds. The state of matter of the active medium is usually used to classify laser sources. The laser medium might be solid, liquid, or gaseous, depending on the desired wavelength and laser type. Various laser type are frequently named based on the active medium's condition or physical characteristics. Figure 1.3 summarizes the commercially available lasers for material processing.

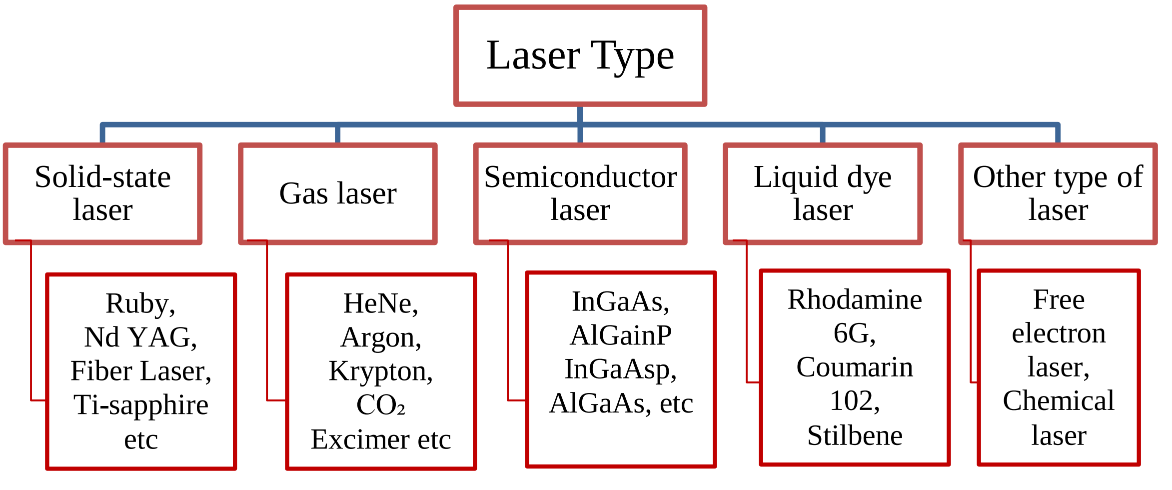

Figure 1.3. Various type of laser source

Different types of laser have been used in the field of laser transmission welding (LTW) of polymers. Diode, fiber and Nd: YAG lasers with wavelength spectrum of 0.8–1

µm are successfully used for LTW of parts having millimeter thickness. In early days, Nd:YAG laser (1064 nm) has commonly used as the source for welding of polymers. But, this kind of laser machine took lot of space and require high maintenance cost. The requirement of laser welding of polymers remained unfulfilled because of heavy maintenance cost and low efficient system. Modern diode and fiber lasers have replaced the Nd: YAG laser significantly in terms of cost and efficiency. Modern lasers are more compact, reliable and comparatively economical in nature which improves its efficiency as a tool to weld the polymers by laser transmission welding technology.

CO_2 lasers (10.64 µm wavelength) are generally not used for LTW process due to low absorptivity of polymers in that range of spectrum. It is mainly used in welding of thin polymer films for industries. The drawbacks of the system are large cycle time, reduced energy efficiency and less control over the weld heat input. Absorbing agent free LTW in the wavelength range of 1.4–2.2 µm has carried out to use the full potential of intrinsic absorption of polymers. Wavelength is a very critical parameter in LTW as it affects the optical properties of polymers. Among all other diode, fiber and solid state laser, thulium fiber laser has emerged as a promising tool to perform absorbing agent free LTW.

1.6. Types of Laser Welding based on Welding Methods

Laser exhibits a high concentration of energy, offering distinctive welding abilities characterized by optimal penetration and minimal heat application. There are three distinct laser beam welding techniques, each characterized by unique operational principles crafted for specific applications. The primary distinction among these three modes lies in the power density applied to the welding region. The three modes mentioned are (a) Conduction mode, (b) Transition mode and (c) Keyhole or Penetration mode [15,16]. Figure 1.4 visually depicts these three welding modes.

a.) Conduction mode welding

This technique involves employing a concentrated laser beam to liquefy the surface of the base materials. Upon the joint's solidification, a precise and seamless weld seam is generated. Welds produced using the conduction method typically require no further finishing, as the quality is excellent from the outset. Conduction welding takes place with a low energy density, usually around 0.5 MW/cm^2, resulting in the creation of a weld nugget that is broad and not deeply penetrating [17]. The heat required to form the weld within the material is

generated through conduction from the surface. This mode creates shallow welds due to low gas absorption within the molten metal. It is used in high-quality welds such as battery sealing applications.

b.) Transition mode welding

This mode emerges at a moderate energy density, approximately 1 MW/cm², leading to deeper penetration compared to conduction mode. While the keyhole exists, its penetration is shallow, yielding a typical weld aspect ratio (depth/width) of about 1 [16,17]. This method is predominantly employed by pulsed Nd:YAG lasers in numerous spot and seam welding.

c.) Keyhole or Penetration mode welding

In the keyhole mode, the applied intensity is sufficient to induce vaporization, leading to the development of a keyhole within the molten pool. Increasing the peak power density to over 1.5 MW/cm² shifts the welding process into the keyhole mode, resulting in narrow, deep welds where the aspect ratio is more than 1.5. Upon laser irradiation, the material quickly heats up and melts. If the intensity reaches a sufficient level, it leads to the formation of a key-shaped cavity filled with vapor from the base metal. The laser beams high-power density creates a vaporized material thread known as a keyhole, which extends into the bulk material, allowing efficient delivery of the beam into the joint. This direct energy transfer maximizes reduces the amount of heat that is applied to the base metal during welding, reducing the heat-affected zone (HAZ) and workpiece distortion.

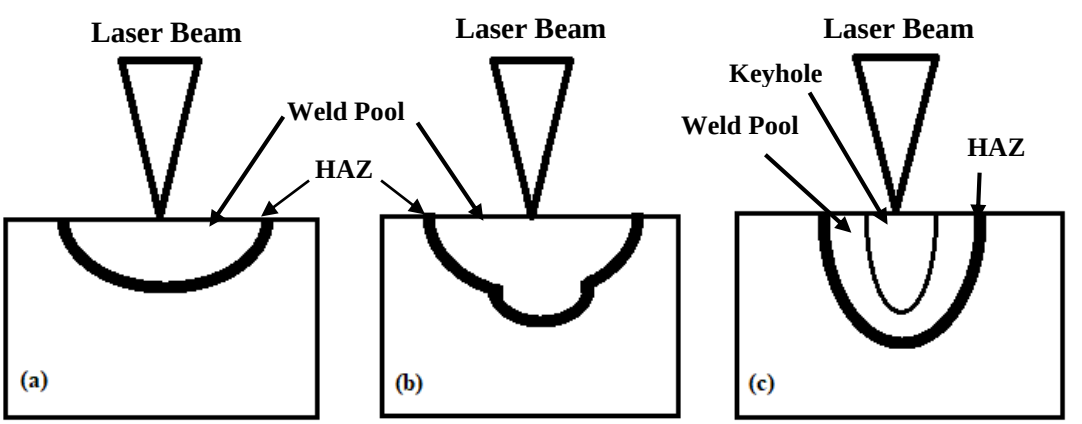

Figure 1.4. Schematic of different modes of laser welding (a) Conduction mode, (b) Transition mode and (c) Keyhole/Penetration mode.

The primary distinction between these LBW methods lies in how they interact with the weld pool surface. The weld pool surface is left intact in the initial mode, but in penetration welding, it is opened to let the laser beam enter the molten pool. Conduction welding minimizes gas absorption as the laser beam doesn't penetrate deeply into the material. However, in penetration welding, sporadic closure of the keyhole raises the risk of porosity formation in the weld pool. As LBW operates on high energy density, it achieves deep penetration without relying on thermal conduction, unlike traditional arc and gas welding methods that rely on escalating heat input for penetration. In conduction LBW, the weld width is typically surpasses the depth and the heat input exceeds the necessary amount of penetration. On the other hand, laser heat is transported from the surface into the joint during penetration or keyhole welding, creating a narrow and deep weld pool.

1.7. Different type of Laser Pulse Regime used for Welding

The categorization of lasers is determined by the type of medium they employ, which could be gas, solid-state, semiconductor or dye. The attributes of a continuous wave laser and a Q-switched laser are determined by factors such as the wavelength or the duration of the laser emission. Temporal mode refers to how the laser power is modulated over time, which significantly impacts the welding process as well as weld quality, influencing factors like weld depth, heat input and material interaction. It is divided into continuous-wave (CW) and pulsed modes according to the temporal mode. The beam is transmitted intermittently in the pulsed mode and constantly and uninterruptedly in the CW mode. A continuous wave laser operation necessitates a consistent and uninterrupted output power. The measurement of this output power for continuous wave lasers is typically expressed in watts. Within the cavity of a Q-switched laser lies a nonlinear crystal known as a Q-switch, which serves to prevent the premature release of laser light. Once energy has accumulated within a Q-switched laser, it is released upon the opening of the Q-switch, resulting in the generation of a highly intense laser pulse.

Pulsed mode lasers possess lower average power but higher peak power per pulse which results in a large power density and the formation of deep keyholes, enabling the creation of weld profiles with high aspect ratios or the drilling of materials to form micro-holes when the vaporization temperature is surpassed.

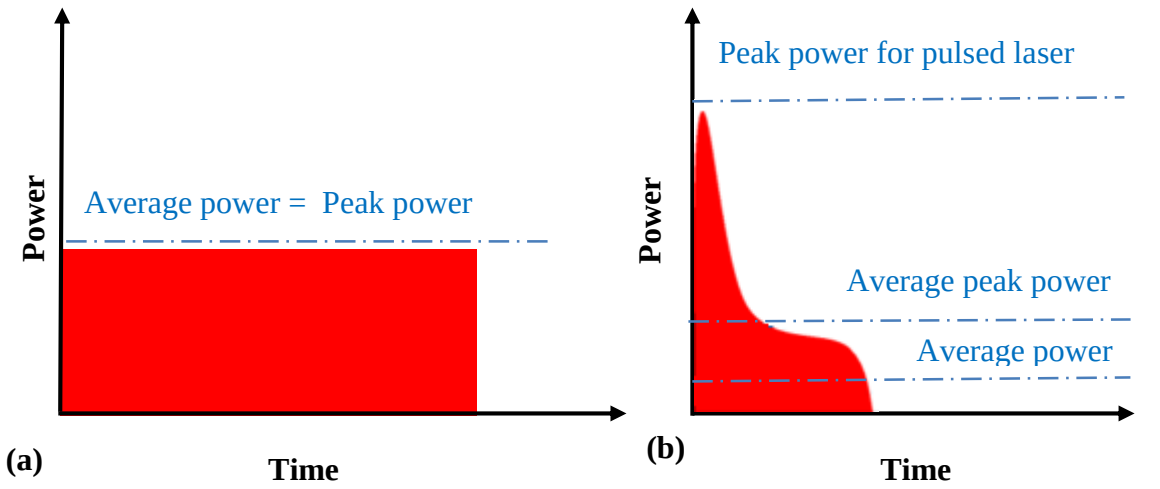

Figure 1.5. Differentiation of lasers in terms of temporal outputs in (a) continuous wave and (b) pulsed wave mode

The increased peak power encourages more vaporization compared to continuous wave (CW) lasers at equivalent average power levels. In continuous wave (CW) mode, the material's energy distribution per unit length is well defined. On the other hand, energy is delivered in the form of discrete pulses or sequences of pulses in nanosecond pulsed-width seam welding, as shown in Figure 1.5. Each pulse has a unique peak power, duration, and energy.

1.8. Variables affecting Laser Beam Welding

An ideal weld represents the absolute best possible weld, characterized by complete fusion, full penetration, smooth and uniform bead and the absence of any defects, while a desired weld is a weld that meets the specific requirements, allowing for some minor variations or imperfections that still ensure structural integrity and functionality. In order to obtain an excellent weld with an acceptable appearance, it is essential and sufficient to accomplish optimal conditions. Studying the factors and aspects influencing LBW is essential.

- **Parameters related to laser source**: There are some variables which directly impact the performance of laser welding, such as laser wavelength, continuous or pulsed laser, laser power, pulse frequency, pulse width and beam quality.
- **Parameters related to the operation of the system and the welding process:** The distance from the center of the beam to the surface of the workpiece, welding speed/scanning speed and gas shielding type also affect the performance of the laser welding.

1.9. Laser Beam Welding of Polymers

Laser materials processing has undergone significant advancements over the years and has become an essential technique in various industrial sectors due to its unique benefits [18]. Among these techniques, laser welding has gained prominence as an effective method for joining polymers, a trend that has been evident since the late 1990s [19-21]. This non-contact process facilitates precise and spatially selective energy deposition, making it suitable for welding a diverse range of polymers using different laser sources [22]. Compared to traditional polymer joining techniques such as adhesive bonding, hot plate welding, ultrasonic welding and vibration welding, laser welding offers distinct advantages, establishing it as a viable alternative [23-24]. A comparative analysis of various polymer joining methods is presented in Table 1.1, highlighting the superior performance of laser polymer welding over conventional techniques [25-27].

Table 1.1. Comparison of the various polymer bonding techniques [25-27].

Welding Systems	**Laser welding**	**Bonding technologies**	**Ultrasonic/ vibration welding**	**Hot-plate welding**
Design freedom	4	4	3	3
Investment	3	3	3	3
Maintenance	4.5	2	4	2
Tool costs	4	3	2	3
Joint quality	5	3	3	3
Material combination	4	5	3	3
Process flexibility	4.5	4	2	2
Part Flexibility	4	4	2.5	3
Cycle time	5	2	4	3

Laser welding techniques for polymers can be commonly categorized into two major types: laser butt welding and laser transmission welding (LTW) [18]. In laser butt welding, the polymer components are arranged side by side in a butt joint configuration, where a laser beam is directed onto the joint interface to facilitate fusion and bonding (Figure 1.6(a)) [22]. To enhance the welding process, mirrors are often used to preheat the joining surfaces before

they are pressed together in a molten state. This method is widely utilized for welding polymer pipes, shafts and similar components and is commonly known as direct laser welding of polymers. In LTW, the laser beam is projected onto overlapping polymer components to generate a weld at the joint interface. This process relies on the differential transmission and absorption of the laser beam within the polymer materials to induce localized heating and melting (Figure 1.6(b)) [22]. One polymer component must be transparent to the laser beam and the other absorbent (at least initially) for the welding to be successful. In cases where both polymer components are transparent, an intermediate absorption coating is applied at the interface to start efficient heat absorption [28-29]. During welding, the transparent polymer is positioned above the absorbing polymer, ensuring direct contact at the joint interface for effective energy transfer and bonding [30].

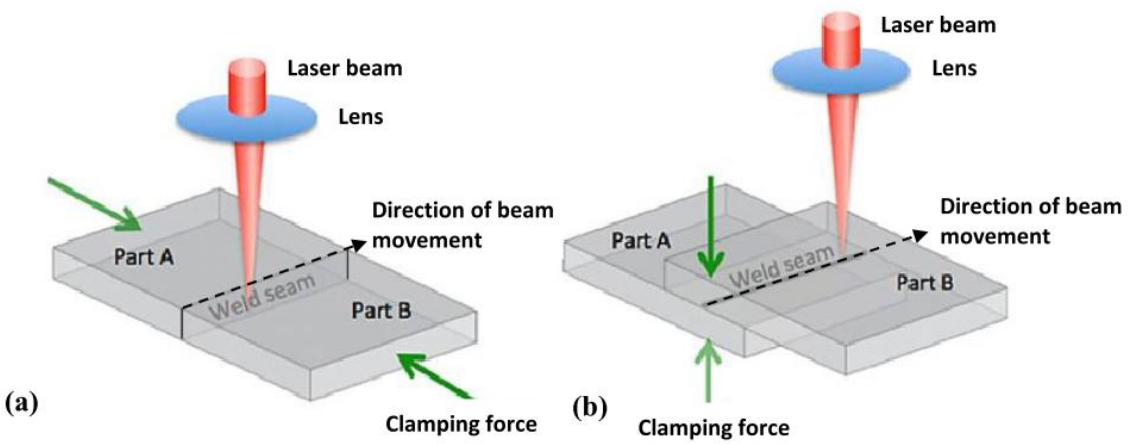

Figure 1.6. Typical joint configuration for (a) laser butt welding, and (b) laser transmission welding [22]

1.9.1. Laser Transmission Welding

Laser transmission welding is a promising technique for joining polymers. It is still regarded as a highly advanced technology even after its commercial use in the mid-1990s. In the early 1990s, laser transmission welding was considered as an emerging unconventional technology suitable only for a few applications. Laser welding has become a well-established welding technique after more than a decade of extensive testing. It also presents significant challenges to conventional polymer joining methods such as ultrasonic welding or adhesive bonding [31]. This versatile technique produces weld seams closer to the ideal than any other polymer welding method for components with a suitable configuration. Various research activities are

being undertaken in polymer laser welding to investigate and recognize current principles that can be used with new material varieties and therefore, novel areas of application for this joining technology. Laser transmission welding is now being used to weld thermoplastic combinations that could not previously be welded. Several laser systems developments for joining complex 3D geometries and lowering investment costs have been reported in the recent years [57].

On the other hand, material restriction remains the most crucial impediment to polymer laser welding. Significant efforts have been made to investigate laser welding of different materials. As a result, numerous compatibility matrices have been published recently. Furthermore, recent advancements have allowed the joining of a wide range of colored polymers and the consolidation of numerous color variations through modified additives and pigments. Not only is it possible to achieve a high degree of complexity, such as when welding transparent/transparent configurations, but still there are many realistic choices. Moreover, a laser absorber can be blended and concealed within the color of the components for the welding of different color combinations and transparent parts.

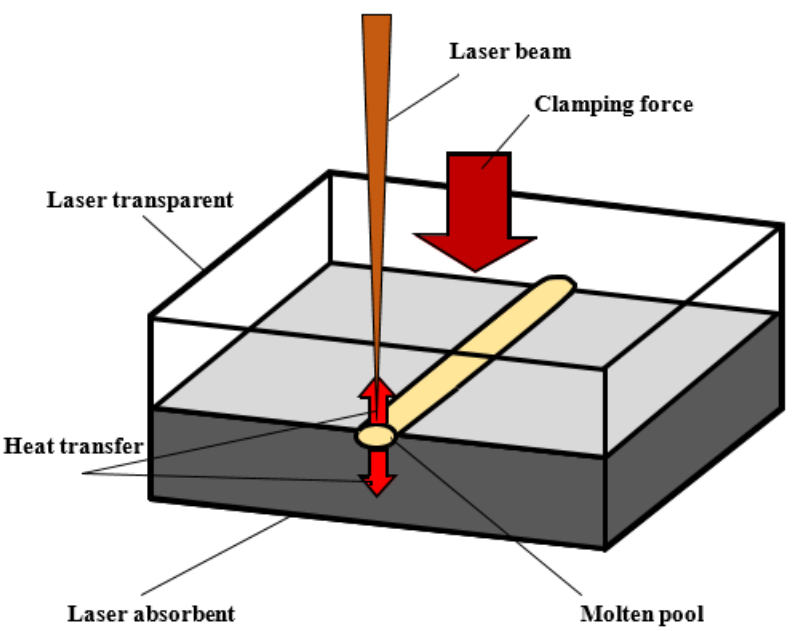

Figure 1.7. Working principle of the laser transmission welding process

For LTW of polymers, the upper part should be transparent to the laser wavelength, while the lower part should be absorbent. The laser beam strikes the polymers, travels through the upper portion, and arrives at the joining interface, as shown in Figure 1.7. The laser beam

is absorbed in to the near-surface layer of the second joining component in the weld region. The lower part absorbs the laser beam and transforms the radiation into heat immediately in the welding zone. The heat energy melts the lower part of the polymer, and it also softens the upper layer through heat conduction at the weld interface [32]. Sufficient pressure is also applied between two joining parts to ensure the proper fusion of both materials. After melting or softening of both joining polymer at weld interface, weld pool generates and intermixing of material happens. Finally, joining occurs following cooling and material diffusion. Four primary requirements must be met to carry out the laser transmission welding, as described below [33-34].

1.9.1.1. Transparent top polymer part

The upper part of the assembly must be transparent to laser wavelengths in the infrared and near-infrared range [30]. The transmittance of laser radiation is not equivalent to the optical transparency of the plastic. While many lasers welded thermoplastics do have optical translucency, it is not needed and welds with optically opaque upper layers can be realized.

1.9.1.2. Absorbing bottom polymer part

The bottom polymer part must absorb laser radiation to transform the optical energy into heat energy. Most thermoplastics emit infrared laser light naturally, but absorptive properties may be achieved by incorporating soot or pigmentation. The most popular and efficient absorbent additive is carbon black doped at a rate of around 0.5% by weight. Nonetheless, as this technology gained popularity, a range of other additives explicitly designed for laser polymer welding are developed.

1.9.1.3. Clamping and contact

The bottom polymer part absorbs the laser radiation and converts it to heat; this heat must be transferred to the upper part for it to soften and melt. The intimate contact between the parts is needed for heat energy to be transferred from the bottom to the upper part. The mating parts typically work together well, but the force is used to provide robust and reliable contact clamping.

1.9.1.4. Material compatibility

For the plastics to be fused using LTW, they must have a common chemical structure, as required in any welding process. The most critical aspect is that the two plastics should have similar melting or softening temperatures.

The upper joining part facing the focusing optic needs to have a high transmittance in the laser wavelength range. This is required for the laser beam to pass through the upper part and reach the joining interface [35]. The bottom polymer component should be opaque in order to absorb the laser beam and turn the radiation into heat. The lower joining section must be pigmented with additional substances to enhance the laser absorptivity. Carbon black is commonly used for pigmentation because of its low cost. However, this results in the coloring of at least one joining sheet, which is undesirable in certain situations.

1.9.2. Joint design used for laser transmission welding

The joint design is an important step for performing laser transmission welding. Various types of joint can be created using transmission laser welding of polymers, i.e. Lap joint, T joint and I joint. A suitable arrangement must be made to ensure that the laser traverse the transparent part and reached the weld interface [36].

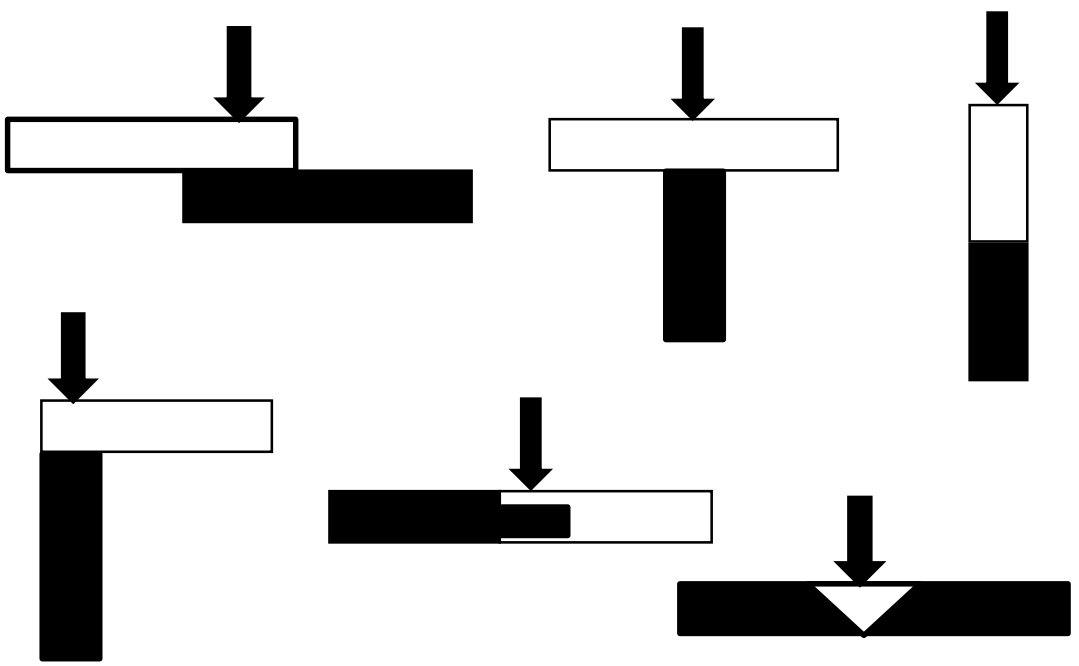

Figure 1.8. Different possible joint configuration for laser transmission welding process.

In order to ensure contact conduction, the materials should have a high degree of surface finish to decrease any air gap between the joining sections. Figure 1.8 shows various probable joint design for the process of LTW. Lap joint and T joint are mostly preferred over other joints for transmission laser welding process [37-41]. However, Butt joint formation with LTW is more difficult because it necessitates a deep penetration in a transparent area. It's also challenging to maintain close contact between joining components for butt joints.

1.9. 3. Laser transmission weldability of polymers

The polymeric material constraint remains the barrier for transmission laser welding. Most of the thermoplastic material can be joined using LTW including Polymethylmethacrylate (PMMA), Polycarbonate (PC), Acrylonitrile Butadiene Styrene (ABS), Polyamide (PA), Poly Vinyl Chloride (PVC), Polypropylene (PP), Polyethylene (PE), Polystyrene (PS), Polyethylene Terephthalate (PET), Polyether Ether Ketone (PEEK) and so on. Nearly all of these materials have weld strengths that are on par with or even greater than the tensile strengths of their parent materials. If elastomers or thermoplastic polymers are compatible, they can be welded together. Figure 1.9 lists the various polymers that have been tested along with their combinations. Using conventional welding techniques to join dissimilar polymers is extremely difficult. Compatibility signifies that the crystal structure of both polymers should be same and viscosity of both polymers should not differ much in melting range. Molecular structure of polymer shows how the various polymer molecules can arrange themselves in a solid-state. The molecular masses, melting temperature and degree of branching of polymers affect the compatibility of polymers maximum [42]. Amorphous polymers have good compatibility but may not properly welded with semicrystalline polymers. Amorphous polymers consist of random structure of molecular arrangement whereas semi-crystalline polymers have characterized by regions of ordered molecular arrangements. Amorphous polymers do not have any sharp melting point and they can be softened over a wide range. Crystalline polymers consist of exact melting and solidification point. It is very difficult to join incompatible polymers because molten materials do not interfuse with each other and form distinct phases. For complex plastic parts it is often important to combine different thermoplastics to meet various requirements. In addition, the combination of various thermoplastics provides significant potential for financial savings.

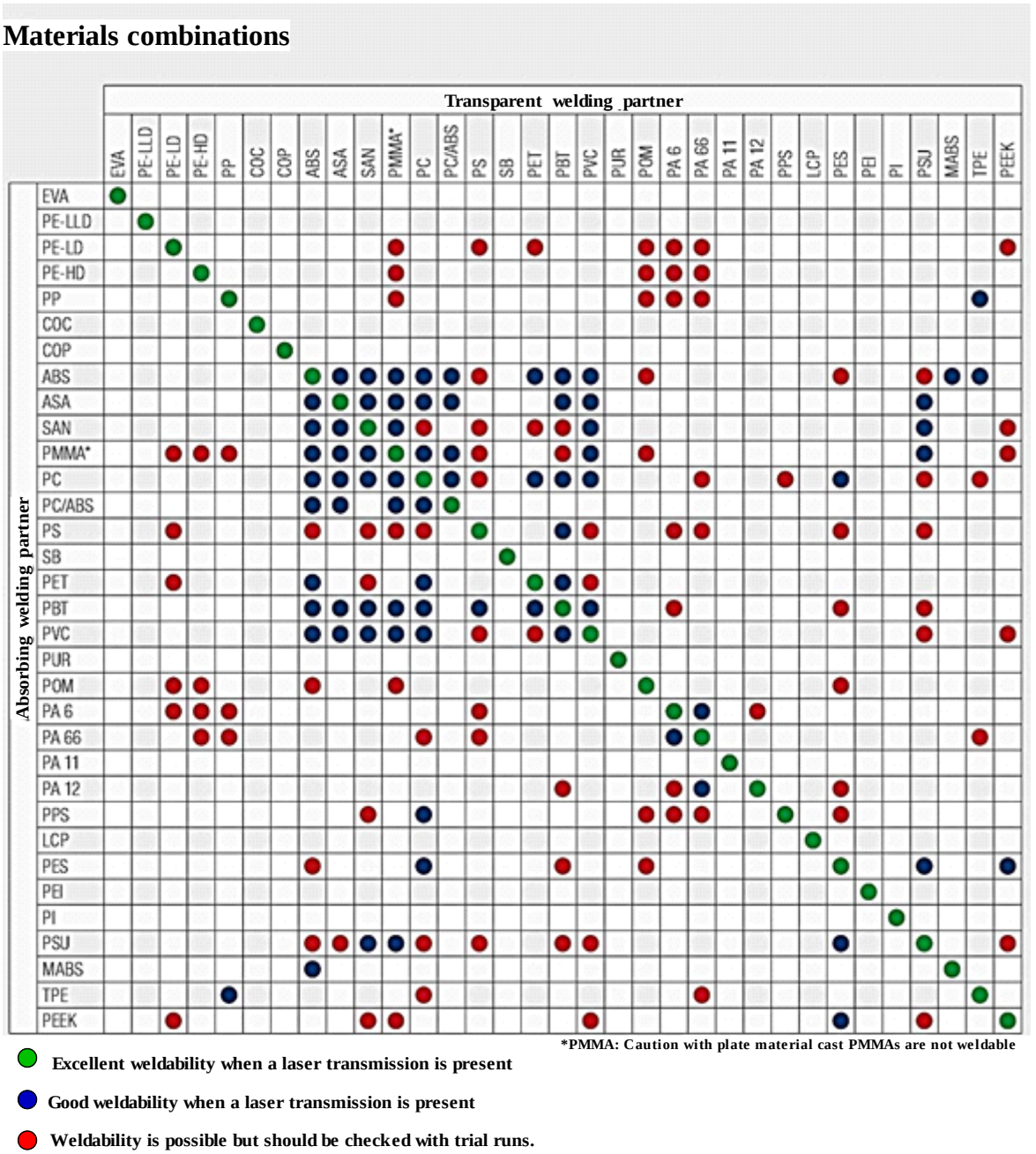

Figure 1.9. Laser weldability chart for possible polymer combinations [32]

In the automotive industry, for example, the replacement of polyamide (PA) with cost-effective polypropylene (PP) or polyethylene (PE) must be stated. One example is the joining of connection branches made of PA12 (polyamide 12) and conduits, the exterior of which is sometimes made of PE (polyethylene). The ingenious fusion of LTW with the technique of plasma activation produces new possibilities for creating polymer joints that have not been welded before. Homogeneous bubbles occur during the process of laser welding that allow the microinterlocking. It is not possible to weld PE and POM (Polyoxymethylene) because of poor compatibility [43]. However, oxygen plasma is used to pretreat the surface of PE and

POM to enhance their laser weldability. PA6 (nylon 6) and PVC (Polyvinyl chloride) are not compatible with each other and thus, a thin aluminum coating of 20 µm is used as transition layer through sputtering technique on absorbing part PA6 (nylon 6) and transparent part PVC is joined during the laser welding. Similarly, polycarbonate (PC) and glass-fiber reinforced polyamide 66 (PA66GF) are effectively welded through sputtering technique [44]. Bubble formation between joining materials stimulate micro anchor mechanism which improves the strength [45]. Intermediate layer method can also be used for joining of incompatible polymeric materials.

The main parameters that regulate laser heat input during LTW depend upon the laser power density and laser material interaction time [46]. The independent controllable process parameter used in LTW are laser power, scanning speed, pulse frequency and spot diameter which control the heat input per unit length. Line energy is defined as the ratio of laser power and welding speed [3]. Another welding parameter is clamping pressure, which is used to keep the work pieces in contact with the joining parts. Laser power is an important parameter which directly affects the heat input. Weld strength is achieved at higher laser power because laser power increases the weld heat input, results in increased melt volume and weld strength. Welding speed simply signifies the interaction time between laser and polymers. Low welding speed is expected to increase the laser interaction time, and therefore increase the total energy input, which also can result in higher heat affected zone due to more conduction. High welding speed results in low line energy. Another significant parameter is number of scans, which is generally used in quasi-simultaneous welding technique. One important parameter of LTW is wavelength of laser source as it affects mostly the optical properties of polymers. Different laser wavelength ranges have used to LTW of different combination of polymers.

1.9.4. Different laser transmission welding techniques

The contour, simultaneous, quasi-simultaneous, and mask welding procedures are the four fundamental process variations of LTW. They vary in cycle time, process flexibility, and laser scanning techniques. The part size, variety, and production volume, as well as the necessary weld contour and standards, all influence their particular choice [3]. LTW is largely impacted by the laser irradiation techniques used. Another variant of this process is radial welding, which is an implantation of the contour welding process that often uses scanning optics similar to quasi-simultaneous welding.

In contour welding, the laser beam and the joining members are moved relative to each other as shown in Figure 1.10. A path is already defined in contour welding and laser beam is used to scan over defined path for performing welding with a comparatively low scanning speed. Scanning speed should not exceed 100 mm/s in contour welding reported by several researchers [3]. The contour laser welding is clear, versatile and cost effective.

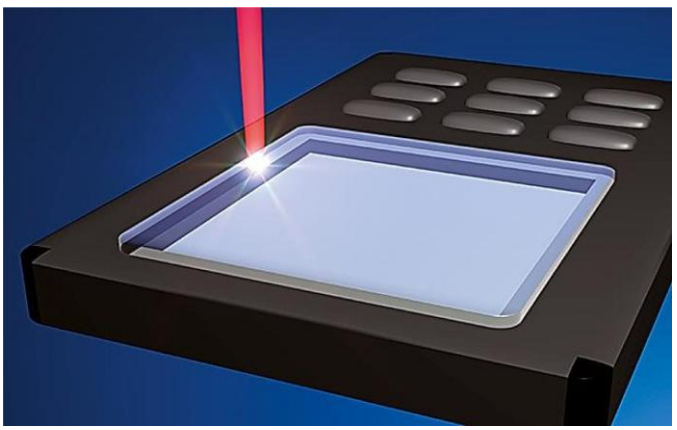

Figure 1.10. Working principle of contour welding [47]

In simultaneous welding, welding is performed in single exposure using precise arrangement of an array of laser modules to irradiate the entire weld simultaneously as shown in Figure 1.11 (a). This technique is quick and does not have dynamic motion system, but it is more complicated, costly and not effective as contour welding. In order to prevent overlapping of laser beam spots and non-irradiated areas in the whole weld seam contour, the key consideration is to organize the diode laser module. This kind of optical feature makes it possible for simultaneous welding of the entire weld contour with a high-power laser.

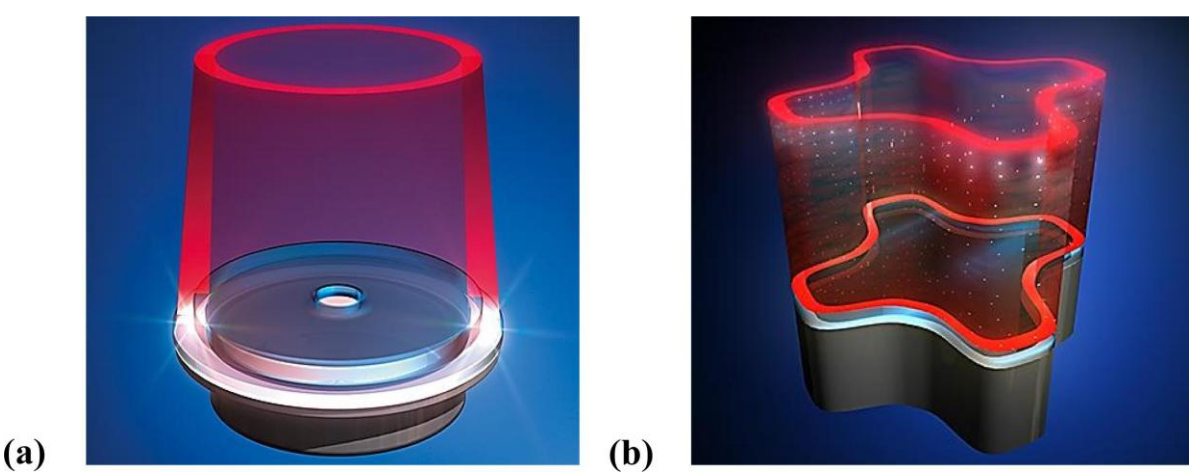

Figure 1.11. Working principle of (a) simultaneous welding, and (b) simultaneous welding with DOE [47]

With the use of specialized beam-shaping diffractive optical elements (DOE), the weld geometry can be welded concurrently. (Figure 1.11 (b)). Lizotte [47–48] presented a new beam-shaping method for laser beam machining and welding that makes use of diffractive and holographic optical components. Diffractive optics is used in the process, which enables the welding of free geometries in accordance with the specified optical component.

Welding head and path are fixed in quasi-simultaneous welding and laser beam scans the predefined path repeated times along the desired weld contour with speed up to 15 m/s, using galvo mirror system. With repeated laser scanning, the temperature at the weld zone increases and eventually approaches to the point of fusion. The entire weld area heats up uniformly due to the low thermal conductivity of polymers, ensuring that the weld seam melts quasi-simultaneously as shown in Figure 1.12. The beauty of this process is to eliminate the defect, re-solidification during welding because of higher scanning speed. The application of this process is found in manufacturing of automotive sensors and electronic housings. Simultaneous and quasi-simultaneous welding are very less sensitive to air gaps since collapse occurs in the entire weld line when the weld seam is simultaneously heated. This process is proved to be superior in terms of welding strength and better bridging capacity than contour welding with PA, PP and PC samples. This can also be the reason it gives higher joint strength than contour welding.

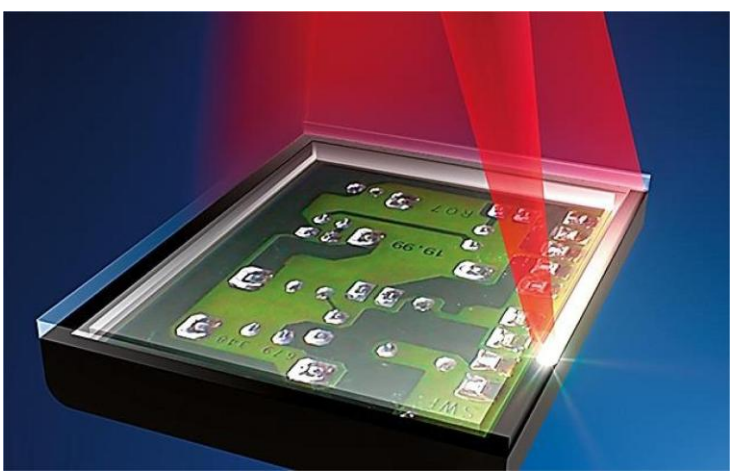

Figure 1.12. Working principle of quasi-simultaneous welding [47]

Another process variant is mask welding technique in which the laser reaches the uncovered surface that adheres to weld seam by using a mask as shown in Figure 1.13. This method offers a practical approach to the simultaneous welding technique's seam geometry constraints. Mask welding is used in micro-technology area that requires special profiles.

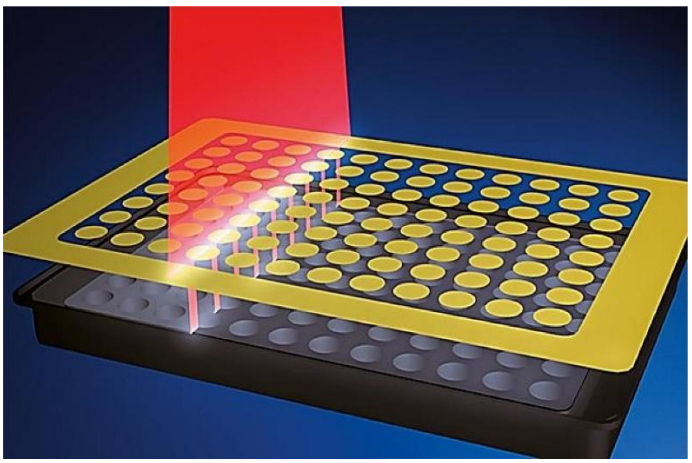

Figure 1.13. Working principle of mask welding [47]

In radial welding method, either the object rotates or laser beam oscillates dynamically to perform the welding as shown in Figure 1.14. It is used for welding of rotary symmetrical components. The joining part is rotated along the horizontal axis under the laser beam by holding the component in a spinning chuck. The laser beam is directed through object using a galvo mirror in second approach.

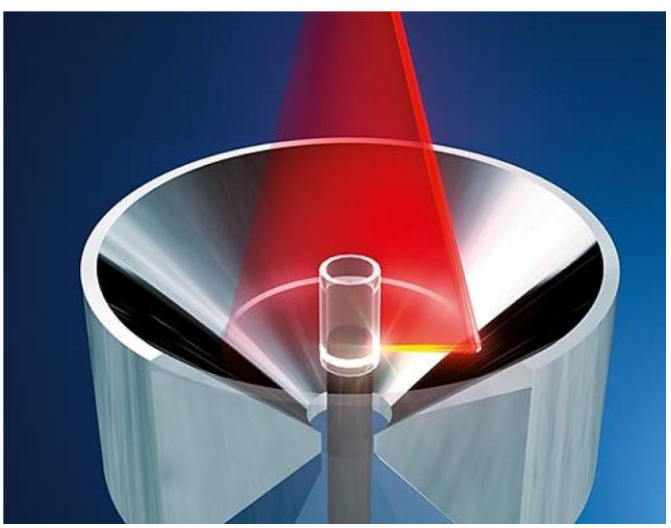

Figure 1.14. Working principle of radial welding [47]

1.10. Laser Beam Welding of Metals and Alloys

Laser welding of metals and alloys is becoming an important technology due to its ultimate properties, such as focusing of high-power laser beam to a small area and almost zero mass of the welding tool, which results in fast and flexible movement of the laser beam along the welding path. The technology is emerging where welding of thin sections, minimal heat affected zone, high welding speed, and minimization of thermomechanical distortions are

expected. Research and development of novel welding processes must also incorporate the creation of new materials with enhanced mechanical and chemical characteristics. Because of its exceptional strength-to-weight ratio, resistance to corrosion, and biocompatibility, titanium-based alloys—including pure titanium and shape memory alloys like NITINOL (Nickel-Titanium Alloy)—are frequently utilized in high-performance applications. Because of their strong reactivity with oxygen, nitrogen, and hydrogen, these materials are difficult to weld and can develop flaws including porosity, oxidation, and embrittlement. Renowned for its unique qualities, such as shape memory effect, pseudo elasticity, corrosion resistance, and superior biocompatibility, nitinol is a material that shows promise in a number of industries. Its uses include micro-electromechanical systems, aircraft, and heat-recoverable couplings in shipyards. However, obstacles including poor machinability, a lack of connecting methods, and expensive material prices currently prevent it from being fully utilized in real-world applications. The welding of titanium is very much difficult because it is highly reactive toward atmospheric gases like oxygen, nitrogen, carbon or hydrogen at temperatures exceeding 550°C, predominantly in the molten stage, which causes severe embrittlement and crack formation. Contamination in the weld region can be caused by inadequate cleaning of the joint, poor shielding environment around the weld zone or impurities in the shielding gas, which results in a crack formation. Although there are variety of welding technique such as solid-state welding and fusion welding are used to join titanium alloy, but advanced welding technique such as laser beam and electron beam welding has clear cutting edge over the conventional welding processes. However, because it doesn't require a vacuum, laser beam welding offers several advantages over electron beam welding. With advantages including exact control over heat input, penetration depth, and limiting the heat-affected zone, laser welding is emerging as a promising fabrication technique for titanium-based alloys. Laser beam welding produces fine seam width, high precision and less thermal distortion for joining the intricate metal assemblies. Figure 1.15 shows the operating principle of laser beam welding. In laser beam welding, the laser serves as a focused heat source, melting the material and causing the molten material to fuse together during the coalescence phase, creating a weld. Fundamentally, the laser beam interacts with the material in two ways, such as keyhole welding and conduction, and this is mostly determined by the laser heat source's power density. If power density is high ($>10^7$ W/cm^2), then it is usually considered as keyhole welding and if power density is less ($<10^5$ W/cm^2), then it is said to be conduction welding.

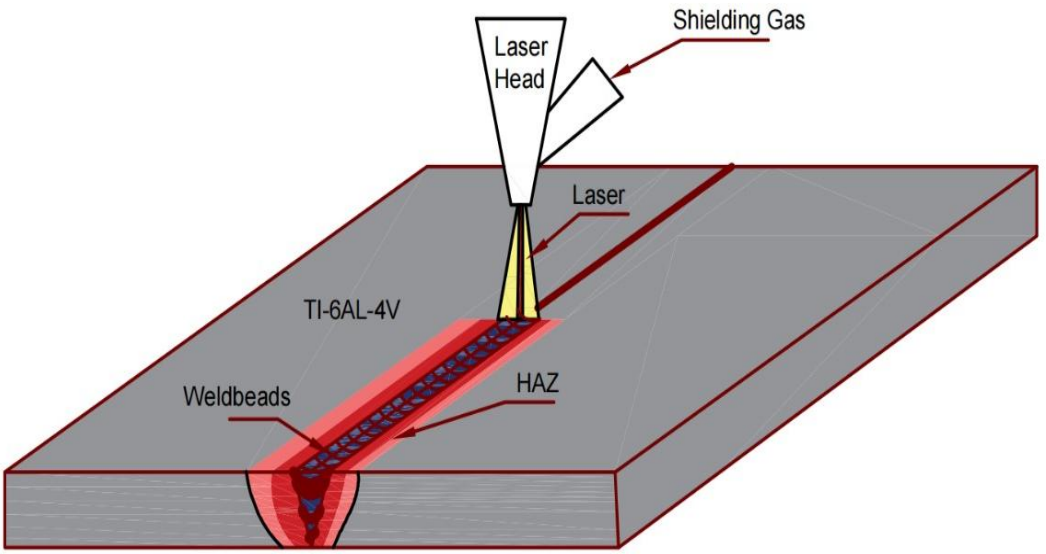

Figure 1.15. Operating principle of Laser beam welding

One notable benefit of laser welding over other fusion welding technologies is its versatility. Components with diverse geometries can be joined using laser welding, which also readily generates a weld quality that is acceptable in the workplace. Nonetheless, the keyhole mode welding procedure frequently uses laser butt welding. After the welding materials have gone through both the melting and solidification stages, they can be fully bonded. Actually, a lot of manufacturing uses this kind of joint. The efficiency in laser butt welding relies on the gap between weld materials.

1.10.1. Joint design used for laser beam welding

One remarkable benefit of laser welding over other welding processes is its adaptability. Components with diverse geometries can be joined using laser welding, which also readily generates a weld quality that is appropriate in the industrial setting. The types of joint geometry that can be used for laser welding are shown in Figure 1.16. Butt welds do not require a chamfer for thicker pieces, T-joints can be welded from a single side with full strength and lap welds can be welded through the top sheet or along the seam. This allows for flexibility when designing your parts and weld locations.

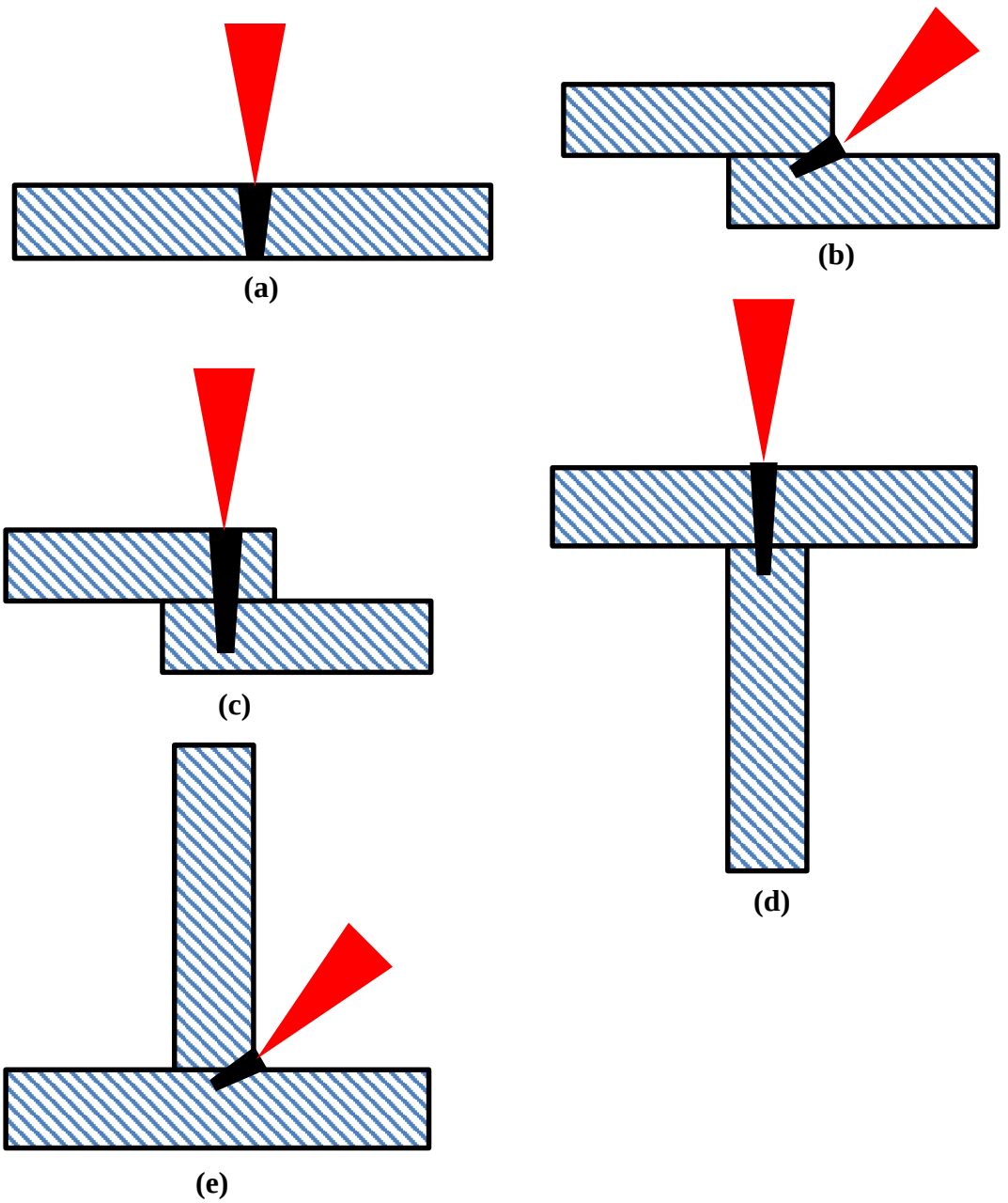

Figure 1.16. Joint Configurations: (a) Butt, (b) Lap along the seam (c) Lap through the top sheet (d) T through the top sheet and (e) T from a single side

1.10.2. Weldability of similar materials

Welding similar materials may seem straightforward compared to dissimilar materials, but it presents several challenges that can affect weld quality, mechanical properties and performance. When welding similar materials, key challenges include: controlling heat input to avoid distortion, managing residual stresses that can lead to cracks, selecting the correct filler metal for optimal fusion, potential for porosity due to trapped gases and ensuring proper joint design to minimize stress concentrations; all while considering the specific properties of

the material being welded. These challenges vary depending on the material type, welding process and operating conditions [49,50].

1. **Heat-Affected Zone (HAZ) Issues:** In materials like stainless steel and titanium, excessive heat input can cause coarse grain growth in the HAZ, leading to reduced mechanical strength [49].
2. **Solidification Cracking & Hot Cracking:** Some materials, like austenitic stainless steel and aluminum alloys are prone to hot cracking due to shrinkage stresses during solidification [51].
3. **Porosity Formation:** Entrapment of gases (like hydrogen, oxygen, or nitrogen) during welding can lead to porosity, reducing weld integrity. This issue is common in aluminum and titanium alloys, requiring proper shielding gas selection and welding parameters [52].
4. **Oxidation and Contamination:** Reactive metals like titanium, aluminum and stainless steel easily form oxides, affecting weld strength. Proper shielding gas (Argon/Helium) and cleaning procedures are essential to prevent contamination [50].
5. **Difficulty in Maintaining Uniform Mechanical Properties:** Achieving consistent strength, toughness and corrosion resistance across the weld zone can be challenging, especially for high-performance materials like stainless steels and titanium [49].
6. **Selection of Proper Welding Process & Parameters:** Improper heat input and welding speed may lead to various defects like undercutting, lack of fusion or excessive reinforcement. The choice of welding method (SMAW, TIG, MIG, Laser and Friction welding) depends on the material's thermal and mechanical properties [52].

However, there are several mitigation strategies such as proper shielding gas and contamination control to prevent oxidation. Also, optimized welding parameters (power, scanning speed, pulse frequency) can be used to enhance the weldability of similar materials.

1.10.3. Weldability of dissimilar materials

Welding dissimilar materials presents significant challenges due to differences in their chemical compositions, mechanical properties, thermal properties and metallurgical behaviors. Welding of dissimilar materials is always performed in response to a specific demand from industry. The differences in physical and chemical properties between the weld

materials and their metallurgical incompatibilities cause problems in the weld, such as asymmetric welding shapes, the formation of intermetallic brittle phases, segregation and residual stresses. These various challenges impact the weldability, strength and durability of the joint [53].

1. **Differences in Thermal Properties:** Dissimilar metals have different coefficients of thermal expansion, leading to residual stresses, cracking or distortion after cooling. One material may absorb or conduct heat faster than the other, causing uneven melting, incomplete fusion or overheating [52].
2. **Formation of Brittle Intermetallic Compounds (IMCs):** Certain material combinations (e.g., aluminum-steel, titanium-steel, or copper-nickel) tend to form brittle intermetallic compounds at the interface, leading to reduced mechanical strength [54].
3. **Differences in Melting Points:** A significant difference in melting points between the materials (e.g., aluminum-steel, titanium-nickel) can cause uneven melting, excessive dilution and poor fusion [49,53].
4. **Poor Wettability & Lack of Fusion:** Some metals, such as aluminum and steel, have poor wettability with each other, making it difficult to achieve proper bonding [52].
5. **Mechanical Property Mismatch:** Variations in hardness, ductility and strength across the welded joint can lead to stress concentration and premature failure [53].

1.11. Laser Beam Welding with Wobbling Technique

The wide spread usage of laser beam welding is still constrained by material issues [32]. Wobble laser welding has emerged as a cutting-edge technology in the field of laser welding. Wobble welding is performed by oscillating the laser beam longitudinally at a high wobble frequency, resulting in a stirring action inside the molten weld pool. As a consequence, the weld pool is controlled by the oscillating beam, which affects the critical features of the weld [29]. The wobbling mode might be circular, linear, eight or infinite. When compared to welding without beam oscillation, wobble welding expands the weld fusion area. It has been demonstrated that beam oscillation has a significant impact on weld strength when laser welding incompatible metals because it increases material intermixing. The wobbling approach improves weld quality by reducing flaws, increasing uniformity and allowing for higher tolerance for controllable parameters. Laser beam wobbling is said to be useful in dissimilar metal welding because it enhances deposition rate and dissimilar metal

intermixing. The heat input to the work piece is relatively minimal in wobble welding and the weld width may be easily regulated. TWIST (transmission welding using incremental scanning technique) is a promising technology for welding dissimilar polymers and the newest innovation in the field of LTW. In TWIST welding, the laser beam moves incrementally along the welding line while also making rapid circular oscillations, partly overlapping neighboring circles, at a high velocity [46], as shown in Fig. 1.17. TWIST welding solves the drawbacks of LTW by allowing for micro-welding and enhanced joint strength [55]. The wobbling modes used in TWIST welding cause turbulence inside the weld pool and increase weld strength by boosting material intermixing. In addition to the standard LTW process parameters like laser power, pulse frequency, scanning speed and clamping pressure, wobble amplitude and wobble frequency, which regulate the circular overlap, also impact the performance of TWIST welding [56]. The beam wobbling parameter may be adjusted to control the weld width. TWIST welding finds widespread industrial application in the automotive, aerospace, battery, micro components and food packaging industries for seaming, sealing and welding [57]. TWIST welding produces narrower heat affected zone and much more uniform welded zone. Weld strength and weld width are two performance metrics that are commonly used to gauge the effectiveness of the TWIST process, while a defect-free seam, minimal distortion and pleasing seam appearance are indicators of weld quality.

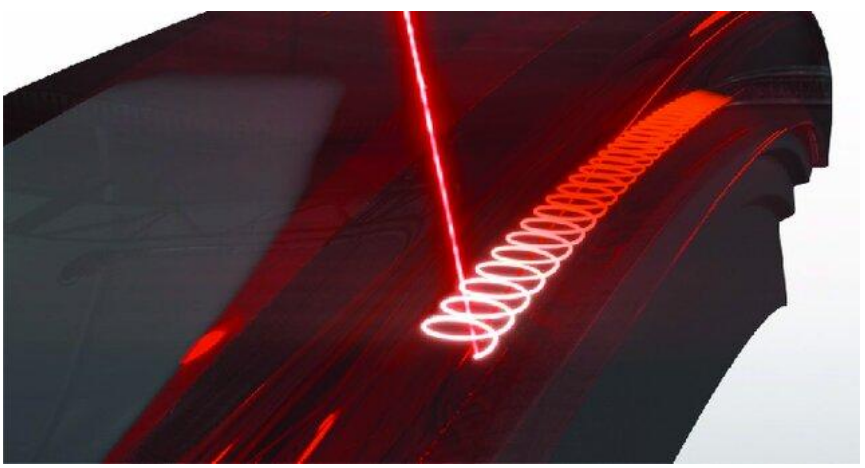

Figure 1.17. Operational strategy of wobble welding process

1.12. Advantages, Limitations and Applications

Laser beam welding provides numerous process benefits as compared to other conventional and advanced welding processes. It offers the finest, non-porous welding for medical

technology and precision spot welding for electronics or the jewelry industry. This process offers high quality joint and aesthetic due to its flexibility and non-contact nature and production of a minimal heat affected zone around the welded zone [27, 34, 58]. Localized heat affected zone has produced due to concentrated heat source of laser beam which could be improve by shape and size of laser beam and control of flow of molten flash. This process is not limited to the welding of thermoplastic polymers only, it can be used for welding of elastomers and semi-crystalline polymers in similar or dissimilar material combination [59,60]. The geometry of the components to be welded have minimal constraints. In addition, the process is completely free of debris, unlike other welding methods. This process is capable of hermetic and is appropriate for welding of microfluidic devices and 3-D weld contours [61, 62].

There are also some negative aspects that limit the extensive use of laser transmission welding process. Although, it has evolved as an efficient method for mass production, the higher capital outlay is required for equipment [63]. The efficiency of this process largely depends upon optical properties of polymers. The infrared absorbing layer in terms of addition of absorbent is used for clear-to-clear polymer welding, which may be increase the cost of processing. This process requires conduction of transmitted heat from absorbent part to the transparent part for welding and thus, close robust contact is needed in between the mating parts. Some points can be noted as major disadvantages of this process [31]:

1. **Material constraint –** Presently, this is the most important drawback of LTW. The requirement to match the optical properties to satisfy the LTW criteria (transparent and absorbing joining partner) and the limited potential to weld dissimilar materials significantly restricts the product designers' independence.
2. **Shape limitation –** Generally, 2D surfaces has involved in the majority of LTW applications. However, with the growing versatility of polymeric materials, 3D contours are becoming increasingly important for LTW.
3. **Investment cost –** From the beginning, this factor has followed the polymer welding narrative and heavily restricted the viability of laser transmission welding technique.

LBW has a vast application in several industries and manufacturing unit. In recent years, this process has been evolved a reliable technique whenever we need fast welding speed, flexibility, good cosmetic properties with less residual stresses.

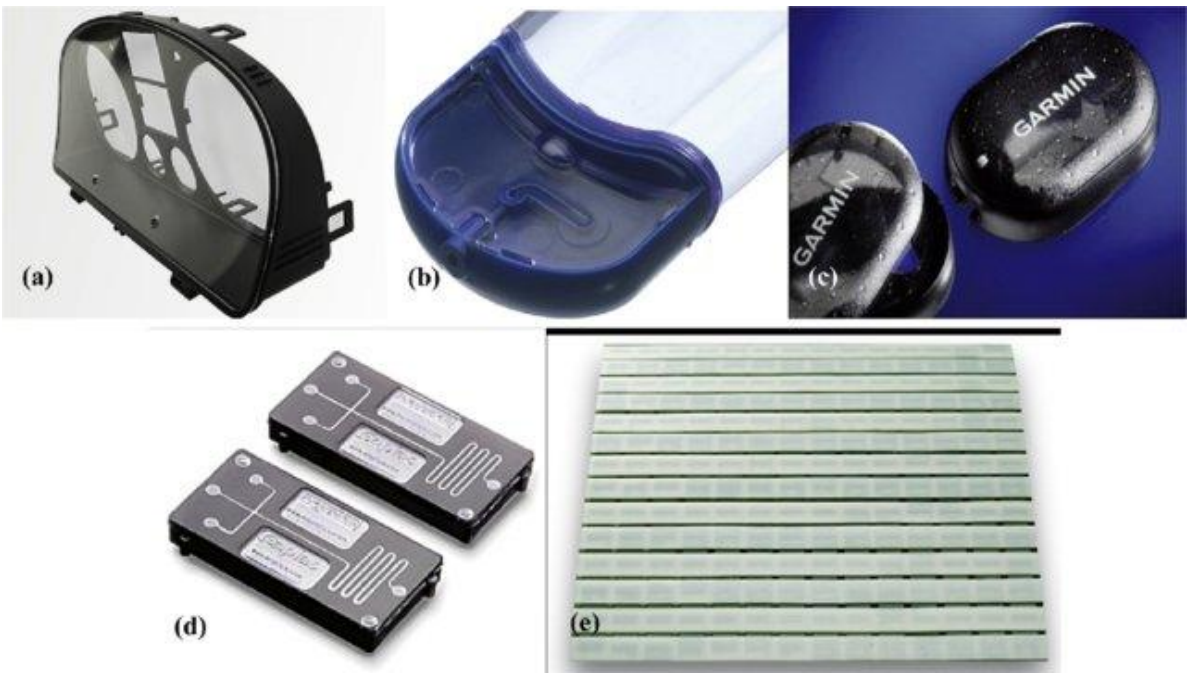

Figure 1.18. Application of LTW in different industries: (a) automotive (car dashboard assembly), (b) medical devices (drug delivery system), (c) electronics (sensor housing), (d) micro-technology (microfluidic device), and (e) textile (technical textile).

Industries like automobile, textile, medical, electronics etc. (Fig. 1.18) use LTW as a prime method for clean and leak proof welding, shock free and stress-free bonding, accurate and concentrated energy applications. A keyless car entry system developed by Marquardt, a German maker, in 1997 was the first mass-produced consumer product to use the LTW technique. This technique has been used in medical industries for leak proof polymeric micro-channels, to join microfluidic devices used for DNA profiling and fabrication of medical packaging such as blood bags etc.

Automotive manufacturers rely on laser welded blanks (LWBs), which comprise of metal sheets of different thicknesses and grades, to minimize and control the amount of material employed in different regions of a car, such as the frame and body [64]. On talking about electrical and electronics industries, LBW is primary used in joining parts of sensors and switches, also where the work involves high degree of positioning and welding precision in micrometer range. LBW is best and safest method for welding electronics housing as other methods like ultrasonic welding has a chance of damaging the internal electronics part. The cost of using this technique is comparatively much lower than other technique like adhesive bonding so the future of this technology is bright and it will grow more and more.

In view of the above background, the present study indicates that fiber laser welding has gained prominence as a cost-effective and advanced alternative to conventional solid-state and gas laser systems. The main objective of present research work is to develop and optimize fiber laser welding processes for polymers and titanium-based alloys. The study will systematically investigate the effects of laser power, pulse frequency, scanning speed, defocusing distance, wobble width, and wobble frequency on weld quality. It assesses the laser weldability of acrylic to polypropylene copolymer and clear transparent polymers without the use of any additives. The present study also discusses experimental investigation into laser transmission welding (LTW) of polymers by low power laser and determine the influence of significant laser welding parameters on the weld quality characteristics. In addition, the effect of beam wobbling parameters on the weld quality characteristics is also investigated. The study also carries out experimental investigation into laser beam welding of NiTinol alloys and titanium superalloys by high power laser, determine the influence of significant laser welding parameters on the weld quality characteristics and find out parametric process optimization to develop mathematical model.

This study aims to establish a new guideline of research for optimizing fiber laser welding across different material classes, improving weld quality, and expanding the application potential of laser welding in marine, biomedical, and aerospace industries.

CHAPTER: 2

LITERATURE REVIEW & OBJECTIVE

2.1. Literature Review of Laser Beam Welding Process

Laser beam welding (LBW) offers high precision, deep penetration and minimal heat-affected zones, making it suitable for applications in various industries. Fiber lasers, in particular, have gained prominence due to their high efficiency and beam quality. LBW is employed for welding components such as gear parts, transmission components and body parts. Industries like automobile, textile, medical, electronics etc. use laser transmission welding as a prime method for clean and leak proof welding, shock free and stress-free bonding, accurate and concentrated energy applications. It is also used in manufacturing critical components like turbine blades, fuel tanks and structural parts in aerospace sector. However, the complexity of controlling various parameters (e.g., laser power, focus, and welding speed) requires advanced understanding and precise control to achieve optimal welds. When welding different classes of materials, such as polymers, metals and alloys, the welding mechanisms, thermal responses, and joint characteristics vary significantly. Corrosion behavior, surface morphology, metallurgical characteristics such as heat affected zone, grain structure, bubble formation and mechanical properties such as Tensile strength, weld seam width, microhardness, etc. remain to be interesting attribute features of fiber laser beam welding. With the progress of technology, optimization plays a significant role in improving quality and lowering operational costs, which benefits both the producer and the consumer. Optimization of process variables is necessary to improve performance of welded structure.

2.1.1. Review on laser beam welding of polymers

Kagan et al. [33] reported optical characteristics (transmittance, absorbance, etc.) for semicrystalline thermoplastic nylon 6 polymers of significant relevance to laser transmission welding (LTW) technology. The author examined the impact of particular factors like fiber-glass, mineral filler, impact modifier content, additives, and color versions on the Near InfraRed transmission properties and found that energy deposition can be controlled by

optimizing laser parameters like laser power, choice of beam focusing optics, sweep rate, etc. It has been found that when the amount of fiber glass in nylon 6 plastic increases, laser energy transmission decreases. Plastics of different color exhibit considerable variations in laser energy transfer. Red specimens transmit nearly naturally, whereas yellow and green pigments can cut transmission by 75–85%. Transmission is reduced to incredibly low levels (almost undetectable) by carbon black. The thickness and composition of the joined part transmitting the laser beam significantly influence the beam width and energy density at the joint interface.

Potente et al. [65] utilized finite element modeling (FEM) to simulate melt displacement and temperature distribution during laser through-welding, with a particular focus on the quasi-simultaneous welding mode. The findings revealed a high degree of agreement between the simulated results and experimental measurements. Under the specified boundary conditions, the maximum temperature was observed not in the joining zone but beneath the surface of the absorbent material. Consequently, the melt layer in the absorbent material was found to be thicker compared to that in the transparent material. The study also demonstrated that the squeeze flow of the melt initiates in the absorbent material before extending to the transparent material. During the steady-state phase, the weld strength and the residual melt layer thickness were shown to remain relatively constant. Similar behavior is anticipated in simultaneous welding processes concerning melt displacement and temperature distribution.

Ghorbel et al. [66] in their investigation, attempted to examine the microstructure and geometry of the polypropylene weld zone during laser transmission welding. It was also reported how the welding parameters affected the material's crystallinity, flaws, and seam geometry. It has been found that the optical characteristics of the absorbent polymer and process parameters both significantly affect the seam weld qualities. These characteristics had a strong correlation with the dimensions of the weld seam. A micrograph shows that a greater volume of the weld zone with more significant depth penetration results from increasing the laser power and decreasing the scanning speed. Conversely, lowering the laser power and increasing the speed resulted in a decline in the highest level the crystallinity index could reach. Crystallinity index is described as a measurement of the proportion of crystalline phase in a polymeric material, usually ascertained by differential scanning calorimetry (DSC). The crystallinity index is crucial because it affects the polymer's mechanical strength, thermal stability, and optical characteristics [67]. Geometry of the weld zone is found to be elliptic. Microscopic Fourier transform infrared (FTIR) spectroscopy method shows that diode laser welding induces thermal degradation of the polypropylene by random chain scissions. An

increase of the crystallinity along the cross section of the welding joint was observed with a maximum reached in the center of the weld zone.

Mayboudi et al. [68] developed a three-dimensional transient thermal model to simulate T-shaped joints in unreinforced polyamide (PA6) specimens. Utilizing the ANSYS finite element method (FEM) code, the study successfully generated spatial transient temperature distributions. The model demonstrated versatility, accommodating various plastic materials, boundary conditions, optical properties, geometries, and process parameters. It proved effective in predicting both the molten zone depth and the temperature distribution along the weld line. Furthermore, the authors highlighted the utility of a two-dimensional model for similar predictions. The numerical results from the 3D thermal model were compared with experimental weld dimension data after normalization, revealing reasonable agreement. Discrepancies were attributed to multiple potential sources, underscoring the model's reliability for thermal analysis of plastic welding processes.

Acherjee et al. [69-73] have conducted extensive and systematic research on laser transmission welding (LTW) of polymers, with an emphasis on numerical modelling, experimental analysis, and process parameter optimization to improve weld quality.

In their initial work, Acherjee et al. [69] investigated the laser transmission welding (LTW) of acrylics using Taguchi design. The study optimized process parameters to enhance weld quality and revealed through ANOVA that all process parameters significantly influence weld strength. Laser power (58%) had the most substantial impact on total variation, followed by focal distance (31%) and welding speed (11%). Weld strength increased with welding speed up to 5 mm/s but decreased afterward. The energy deposition and heat diffusion into the material depend on laser power density and irradiation time. At low welding speed, higher irradiation time cause material deterioration and overheating, which reduces joint strength. Increment of welding speed strengthens the joint due to optimum heat input. Nevertheless, an increment of more than 5 mm/s shortens the irradiation duration, resulting in inadequate melting and absence of fusion, which weakens the joint. The optimal welding parameters for maximum weld strength were identified as laser power of 28 W, welding speed of 5 mm/s, and a focal distance of 9 mm, which were validated through confirmation testing.

Extending their work to dissimilar materials, Acherjee et al. [70] studied laser transmission welding (LTW) of dissimilar thermoplastics, specifically acrylonitrile butadiene styrene (ABS) and polymethyl methacrylate (PMMA) using response surface methodology (RSM).

The study examined how weld shear strength and weld seam width were affected by four important input parameters: clamp pressure, stand-off distance, welding speed, and laser power. The results demonstrated significant interaction effects among laser power, welding speed, and stand-off distance on both weld strength and width. Analysis of variance (ANOVA) was conducted to validate the developed models, revealing that stand-off distance was the most influential parameter affecting weld strength and seam width. Furthermore, a numerical multi-objective optimization technique based on RSM was employed to achieve optimal welding conditions, maximizing weld strength while minimizing weld width. This research provides a robust framework for process optimization in LTW of dissimilar thermoplastics.

In another contribution, Acherjee et al. [71] examined the impact of carbon black on temperature distribution and weld profile during laser transmission welding of polymers by developing a transient numerical model based on conduction-mode heat transfer. Their findings revealed that an increase in carbon black content in the absorbing polymer enhances both the molten depth ratio and weld width. This increase shifts the absorption type from volumetric to surface absorption. At lower carbon black concentrations, the weld geometry is asymmetrical, with maximum penetration occurring in the absorbing polymer, whereas higher carbon black content leads to a more symmetrical weld geometry. Additionally, increasing carbon black concentration reduces the laser power required for welding.

Further advancing numerical modeling approaches, Acherjee et al. [72] combined Finite Element Method (FEM) and RSM to study the impact of process parameters on the temperature distribution and weld bead characteristics in laser transmission welding of polycarbonates. A three-dimensional transient heat diffusion model was developed using ANSYS, incorporating temperature-dependent material properties. RSM was then used to create mathematical models based on the outcomes of the simulation. These second-order models were found to predict response values with high accuracy, and their adequacy was verified within a 95% confidence interval. The study revealed that key responses such as maximum temperature (Tmax), weld temperature (Tweld), weld width (WW), depth of penetration in transparent material (DT), and depth of penetration in absorbing material (DA) increases with increase of laser power and welding time. Among these factors, laser power was identified as the most influential on Tmax, Tweld, and WW, followed by the welding time as well as beam width. The increase in laser power along with welding time resulted in higher heat input to the irradiation zone, thereby raising Tmax and Tweld. This heat input is

directly correlated with the applied laser fluence (energy delivered per unit area during laser irradiation). Laser fluence is inversely proportional to the beam spot area and directly related to the laser power and irradiation duration. Conversely, welding time emerged as the key factor affecting DT and DA, with power and beam width following in importance.

Finally, Acherjee et al. [73] developed a three-dimensional finite element (FE) model for laser transmission welding (LTW) of circular contours using polycarbonate. The utilized model successfully predicted transient temperature distributions and molten pool geometry for different combinations of process parameters. The findings showed that welding speed had a negative impact on weld responses, whereas laser power had a positive influence. The combination of high laser power and high welding speed produced the greatest temperatures for a constant line energy. The study also demonstrated that how the amount of carbon black in the absorbing medium significantly affects the ratio of the molten depth between the material's transparent and absorbent components. This work underscores the potential of the developed FE model as a robust tool for process simulation and optimization in LTW applications.

Mingareev et al. [22] have made their investigation regarding the absorber free transmission welding of different polymers in butt joint configuration using 2 µm thulium fiber laser. Different polymers in the following top/bottom material combinations were used in the transmission welding experiments: PETG/PETG, PMMA/PMMA, PMMA/PP, and PP/PE-LD. The joining partners were subjected to the same normal-to-surface pressure of 0.59 MPa as in the melting and butt-welding tests. According to the experimental findings, increasing the laser power first causes the melt track's depth and width to increase until the maximum depth (full sample thickness) and width are reached. Due to the decreased viscosity of the molten material, the track width then lowers as the laser intensity increases. The transmission welding of PETG/PETG and PMMA/PMMA, two comparable polymers, produced a large-area material intermixing in the interface region, as seen in the micrograph. When PETG and PETG are joined, no interface barriers are discernible. Although there is no effective material intermixing when PMMA/PP and PP/PE-LD are joined, the bead formed at the lower, stronger absorbing material passes across the interface and reaches the weaker absorbing higher joining partner.

Vidal et al. [39] investigated the laser transmission welding of polymeric joints comprising two acrylonitrile/butadiene/styrene (ABS) sheets—one transparent (natural ABS) and the

other doped with varying concentrations of carbon nanotubes (CNTs) to serve as the absorbent partner. Their research demonstrated how doped ABS with high CNT concentrations is extremely sensitive to changes in incident laser intensity, which can affect the integrity of the material and the production of welds. The glass transition temperature of the doped ABS was largely unaffected by the inclusion of CNTs. The CNT content, however, had a significant impact on the absorption and reflection coefficients; higher CNT concentrations led to greater absorption and lower laser energy needs for weld formation. Subsequent investigation showed that because of its higher absorption coefficient, ABS with a higher CNT content was especially sensitive to variations in input power. Remarkably, for all tested CNT concentration, no discernible relationship between weld width and shear force values was found.

Singare et al. [74] studied the impact of laser welding parameters like laser power and welding speed on weld strength. The transparent and absorbing acrylic polymers are welded in lap joint configuration. It has been found that the weld strength rises with laser power; for example, welding clear and absorbent acrylic parts with a 20W laser produces a stronger weld than welding with a 15W laser. Weld strength decreases and voids are created in the weld region when welding speed is increased beyond 65 mm/s while maintaining the same power. This results in a better-quality weld. This is because voids in the weld zone get more and bigger as the welding speed increases; the highest welding speed seems to exacerbate void formation in the polymer. A high welding speed may result in heat loss or poor heat transfer between the two components; this heat loss may have contributed to the formation of voids, which will weaken the weld. On one hand, the weld strength is discovered to be restricted by extremely high welding speed, while on the other hand, weld strength is limited by extremely high heat input, which leads to overheating and partial material decomposition, and a very low heat input, which results in lack of fusion.

Aden et al. [75] examined the impact of carbon black (CB) and indium tin oxide (ITO) absorbers, along with titanium dioxide (TiO_2), on the laser transmission welding of polypropylene (PP). Thermal simulations demonstrated that ITO enabled deeper heat penetration compared to carbon black. However, achieving comparable maximum temperatures for ITO required an order-of-magnitude increase in laser power relative to CB. The inclusion of 2% TiO_2 in the absorbing material was found to reduce the required laser power. Experimental results, including tensile shear tests of welded PP parts, indicated that higher laser power was necessary when using ITO to achieve welding strength equivalent to

that of CB. Additionally, the study quantified the absorption coefficients for ITO and carbon black particles, alongside the scattering properties of polypropylene loaded with TiO_2. At similar concentrations, ITO exhibited an absorption coefficient that was an order of magnitude smaller than that of carbon black, highlighting the differences in their optical and thermal behaviors during the welding process.

Berger et al. [76] explored innovative joining techniques and enhancements to the laser transmission welding (LTW) process for bonding two opaque polymers. Traditional LTW typically requires one of the joining materials to be transmissive at the wavelength of the incident laser radiation. However, the study introduced the use of filler materials, which act as adhesive promoters, enabling an innovative approach for joining carbon fiber-reinforced thermoplastic (CFRTP) polymers. This modified LTW process closely resembles conventional LTW, with both joining materials being absorbent to the laser radiation, while the filler material remains transparent. The laser radiation passes through the transparent filler material and is absorbed by the joining partners, facilitating the welding process. The studies evaluated material combinations, such as unmodified PA 6 natural, PA 6 with carbon black, and CFRP, using a diode laser operating in the near-infrared range at a wavelength of 940 nm. The findings highlighted that the choice of materials, along with their thermal and optical properties, significantly influenced the welding process. This approach underscores the potential of using filler materials to expand the applicability of LTW for opaque and reinforced polymer materials.

Xu et al. [77] conducted studies to understand how laser energy behaves when it travels through the polymer's transparent portion. They investigated how the optical characteristics of amorphous and semi-crystalline polymers were affected by thickness, glass fiber content, and crystallinity. The findings indicated a linear correlation between sample thickness and the logarithm of transmission. The apparent absorption coefficient and reflectance were computed based on the ratio of transmitted power to incident laser power. The findings revealed that the apparent absorption coefficient increases linearly with the glass fiber volume fraction in reinforced polymers, with similar trends observed for crystallinity. This coefficient was determined to be a material-specific parameter. Both the apparent absorption coefficient and reflection were found to increase with crystallinity due to enhanced scattering, although the apparent reflection in glass-fiber-reinforced polymers exhibited more complex behavior.

Wang et al. [78] investigated the application of an intermediate material technique to improve the weld strength in laser transmission welding (LTW) of polymethyl methacrylate (PMMA) and polybutylene terephthalate (PBT), which are known to exhibit poor compatibility. To address this challenge, a polycarbonate (PC) film was introduced as an interlayer material due to its superior compatibility with both PMMA and PBT. Their study revealed that the inclusion of PC film significantly enhanced weld strength, achieving more than four times the strength compared to welds without the film at a laser power of 19 W. Under other parametric conditions, welds incorporating the PC film demonstrated strength improvements of two to four times over those without the interlayer. The study also examined the effects of process parameters, noting that a reduction in laser power and welding speed resulted in increased weld strength. Furthermore, laser power was identified as a more influential factor than welding speed in determining weld strength when considering their interaction effects. Additionally, clamping pressure applied up to the center of the weld joint further improved weld strength. The observed enhancements in weld strength were attributed to the superior bonding properties of PMMA/PC and PC/PBT interfaces. Microstructural analysis provided insights into the mechanism underlying the improved weld strength. The presence of bubbles in the weld zone, formed during the LTW process with the PC interlayer, was noted. These bubbles contributed to micromechanical riveting, which played a significant role in strengthening the weld joint.

Gisarrio et al. [79] investigated the LTW of Poly (Ethylene Terephthalate) and Poly (Ethylene Terephthalate) modified by an additive that promotes the biodegradation of the primary polymeric phase. Polymers were welded by superimposing two surfaces and blackening the faying surface of the underlying substrates using a continuous wave High Power Diode Laser. Thus, it is discovered that local heating of the absorbing surface results in local polymer melting and the creation of the welded junction. Tensile tests were used to characterize the mechanical properties of the welded joints. The results of the tensile test indicate that the welded specimen has a satisfactory mechanical response, as evidenced by the elongation and rupture at break of the welded joints. According to experimental findings, the concentration of the additive, which is distributed throughout the primary phase as tiny spherical droplets, affects the Young's modulus of the welded joints. FT-IR analysis was used to identify the main routes of thermal degradation of polymers. Thermal degradation can be attributed to the breaking of the C–O single bonds of the ester groups, featured by both PET and PEVA in the additive, similarly to what happens during typical hydrolytic degradation of polyesters.

Herthoge et al. [80] investigated the laser transmission welding (LTW) of unfilled polytetrafluoroethylene (PTFE) and PTFE filled with 10 wt.% short carbon fibers (fiber length up to 0.2 mm, average diameter 20 μm). Their study focused on the effect of line energy on the lap shear strength of the welds. Optimal welding conditions were identified as a laser power of 12 W and a speed of 5 mm/s, with the mean lap shear strength per parameter setting varying between 0.081 N/mm² and 0.297 N/mm² across different power and speed combinations. Micro-computed tomography (μ-CT) and optical microscopy revealed the presence of tunnel defects in the weld pattern, while differential scanning calorimetry (DSC) demonstrated a reduction in the molecular weight of PTFE within the welded region. Spectroscopic analyses using attenuated total reflectance infrared (ATR-IR) and nuclear magnetic resonance (NMR) with hexafluoro-isopropanol (HFIP) detected no evidence of new chemical compounds in the weld zone.

Literatures based on LTW suggest that weld quality characteristics are influenced by polymer optical properties, filler content and process parameter. It is also learned that additives, pigments, carbon black, Crystallinity and CNTs significantly impact transmissivity, absorptivity and seam formation of the weld. On the other hand, scanning speed, laser power and focal length affect the weld strength, seam width and melt behavior. It is also revealed that interlayers, additive and alternate absorbers enable welding of opaque or dissimilar polymers. Some of the researcher conducted microstructural and mechanical analysis, and figured out that proper interfacial melting associated with stable temperature distribution and balanced energy input are necessary for achieving perfect joint. Overall, the above studies have covered various aspects of modeling, effect of process parameters, optical behavior but there is hardly any research which investigates the collective impact of the said variables on weld integrity. This provides an opportunity to explore this area with reference to similar and dissimilar or reinforced polymer combination.

2.1.2. Review on laser beam welding of metals and alloys

El-Batahgy et al. [81] explored the influence of laser welding parameters on the fusion zone (FZ) shape and solidification structure of austenitic stainless steels. Their study revealed that the composition of the FZ was largely unaffected by variations in heat input. However, a higher welding speed or lower laser power led to a finer solidification structure, attributed to reduced heat input. The welded samples predominantly exhibited austenitic microstructures without solidification cracking, which the authors attributed to primary ferrite or mixed-mode

solidification, as predicted by Suutala and Lippold diagrams. The penetration depth of the welds increased with higher laser power, although laser power had minimal impact on the overall weld profile. In contrast, welding speed significantly influenced the size and shape of the FZ; an increase in welding speed resulted in a higher depth-to-width ratio and a smaller FZ size. The study emphasized the critical role of minimizing heat input and optimizing energy density—achieved by carefully adjusting laser power, welding speed, and defocusing distance—in ensuring high weld quality with a desirable FZ size and profile. Additionally, the choice of shielding gas was found to affect weld quality, with helium providing superior results compared to argon in achieving an acceptable weld profile.

Reed et al. [82] conducted an investigation into the welding of V-Cr-Ti alloy sheets using a pulsed Nd:YAG laser, with a focus on assessing the resulting joints' microstructural and mechanical properties. Their study demonstrated that achieving deep penetration and defect-free welds depended on optimizing laser parameters such as lens focal length, pulse energy, pulse repetition rate, beam travel speed, and the arrangement of shielding gas. A critical factor for producing defect-free welds was the stabilization of the keyhole and the provision of an escape path for gases trapped in the molten weld pool. Furthermore, the application of post-weld heat treatment using a diffuse laser beam revealed that multiple passes—specifically, five—over the welded region effectively softened the material, particularly in the root area of the weld.

Caiazzo et al. [83] examined the effect of shielding gases, helium (He) and argon (Ar), on the mechanical properties of titanium alloy welds during CO_2 laser beam welding. Their study explored the impact of different nozzle configurations and revealed that helium provided greater penetration depth compared to argon. This was attributed to argon's lower ionization energy, which limits energy transfer to the material. Furthermore, micro-hardness analysis indicated an increase in HV values from the base material through the heat-affected zone (HAZ) to the melted zone. This trend was associated with the high cooling rates experienced by the melted zone during the laser welding process.

Khan et al. [84] explored the mechanical properties of Nitinol welded using a pulsed Nd:YAG laser, analyzing weld strength, pseudo elastic behavior, and cyclic loading characteristics under varying welding parameters. Their findings indicated that higher peak power combined with lower pulse frequency enhanced the mechanical performance of the welds. A detailed fracture surface analysis revealed distinct failure mechanisms: the base material exhibited

ductile dimpled surfaces, whereas the welded specimens displayed both brittle fracture at lower peak power and ductile failure at higher peak power.

Schneider et al. [85] successfully conducted laser beam welding (LBW) of a 16 mm thick titanium sheet using a 20 kW fiber laser. Their study highlighted the adverse impact of plume formation on the welding process, emphasizing the importance of adequate inert gas shielding to minimize its effects in the welding zone. Additionally, they noted that shielding the weld metal during the cooling phase is crucial to prevent contamination from atmospheric gases. Both destructive and non-destructive testing methods were employed to evaluate the weld quality. Charpy impact test results indicated that reducing the temperature from room temperature to 0°C did not affect the ductility of the welded material, demonstrating its resilience under varying thermal conditions.

Fang et al. [86] studied the influence of welding parameters on weld defects such as distortion, tensile properties and microstructure of the weld joint during pulsed laser beam welding of thin titanium alloy sheets. Specific heat input plays an important role, because under-fill defects are observed after exceeding specific heat input of 328.5 J/cm, and also both angular and bending distortion increases with an increase of specific heat input. The dominating martensite phase structure that forms in the heat affected zone (HAZ) and fusion zone (FZ) makes the welded joints stronger than the base metal. Reducing the underfill rate using a transversal pre-extrusion load can make up for the tensile characteristics lost due to underfill flaws in the weld zone.

Kannan et al. [87] reviewed recent advancements in the micro-joining of both similar and dissimilar NiTinol sheets. Their study highlighted that achieving crack-free welded joints with minimal porosity and superior surface quality is possible by selecting appropriate welding techniques and parameters. However, they emphasized the challenges associated with welding NiTinol, particularly the alterations in microstructural characteristics that lead to a decline in mechanical strength and corrosion resistance. The review concluded that further research is necessary to address fundamental weldability issues and enhance the metallurgical, mechanical, and corrosion properties of welded NiTinol joints.

Kumar et al. [88] conducted a comprehensive investigation into the laser beam welding of Ti-6Al-4V superalloy using a statistical design of experiments approach. The study concentrated on investigating how important process variables, such as welding power, welding speed, and the laser beam's defocused position, affected crucial reactions like the width of the fusion

zone (FZ), the size of the heat-affected zone (HAZ), and the general properties of the fusion zone. Their findings revealed that optimal welding conditions produced smooth, uniform weld beads with acceptable micro-pore sizes, a shiny surface devoid of spatter, and no observable cracks. High welding power and low welding speeds allowed the weld bead to penetrate completely, but they also resulted in flaws such undercuts, bead decay, and excessive melt-through. According to the study, the main factors influencing full penetration were welding power and speed, with welding strength directly influencing the welding reactions and welding speed having an inverse effect. Additionally, by changing the power density on the workpiece surface, the laser beam's defocused position had a substantial impact on the geometry of the beads. Microstructural analysis validates that the hardness of the fusion zone is higher than that of the HAZ and base material (BM), attributed to the faster cooling rates in the fusion zone, which promoted the formation of the α′ martensitic phase. Despite achieving satisfactory bead quality, the welded samples exhibited reduced ultimate tensile strength and elongation compared to the base material.

Datta et al. [89] examined the influence of process parameters on the quality of bead-on-plate welding of NiTinol sheets. Their study revealed that the Ti/Ni ratio on the top surface decreased with increasing scan speed at a constant power level. A similar trend was observed for oxide contamination during welding. Microhardness measurements indicated a gradual increase from the weld centerline towards the base metal. However, the formation of brittle intermetallic compounds led to a significant reduction in tensile strength post-welding. Despite this, corrosion testing demonstrated that the welded samples exhibited superior corrosion resistance compared to the parent material.

Kramar et al. [90] assessed the suitability of various welding techniques, including micro-plasma arc, laser, electron beam, resistance, and capacitor discharge welding, for joining fine pseudo elastic NiTi wires. Their findings indicated that, regardless of the welding method used, the welded joints exhibited a similar behavior, primarily characterized by a deterioration in mechanical properties due to recrystallization and the formation of brittle intermetallic phases. However, they noted that with optimal shielding conditions and minimal heat input, the welds could largely retain their original properties, thereby mitigating the adverse effects of welding on the material.

Several studies conducted across different alloys suggest that laser welding performance is impacted by heat input, energy density and proper shielding. In order to produce finer

structure with acceptable fusion zone geometry, lower heat input from higher welding speed or less power may be applied. It is also learned that for deeper penetration and perfect weld adequate gas escape, stable keyhole formation and suitable shielding gas environment are needed. In general, microstructural and mechanical evaluations exhibit higher level of hardness in fusion zone. Optimized parameters result in smoother and uniform weld with suitable pore sizes and microstructure free of cracks. The literature has suggested that challenges exist in welding of nitinol due to intermetallic compound formation, change in Ti/Ni ratio, effect of recrystallization and minimization of tensile strength. In a nutshell, it may be said that it is necessary to control process parameter for achieving desirable weld quality. Despite several studies have investigated process optimization and metallurgical behavior of metals and alloys but there is an absence of unified frame work which predicts weld quality in a reliable manner while minimizing the defects.

2.1.3. Review on laser beam welding with beam wobbling technique

Boglea et al. [91] introduced a novel method called Transmission Welding using Incremental Scanning Technique (TWIST) for micro-welding of polymers using fiber lasers. Experimental findings confirmed the feasibility of the TWIST approach, demonstrating its capability to weld polymers effectively even at high laser intensities. The technique leverages high dynamic movement, ensuring a uniform distribution of laser energy within the absorbing joint material. When compared to traditional laser welding of polypropylene, which achieved maximum weld strengths of 25–30 N/mm², the TWIST method delivered superior weld strength, reaching values as high as 35 N/mm². This highlights the enhanced performance and reliability of the TWIST approach in polymer welding applications.

Kuryntsev and Gilmutdinov [92] examined the effect of laser welding with beam wobbling on the microstructure and mechanical characteristics of structural steel. Their study revealed that the second welding pass in the wobbling laser beam mode reduces the microhardness of the cap and middle sections of the weld seam due to the annealing effect. While the ductility of the weld joint was found to be comparable to that of the base metal, the upper surface of the seam exhibited greater ductility than the root weld. The wobbling pass, by enabling lower cooling rates, minimizes phase transitions, reduces shrinkage, and enhances the ductility of the weld metal.

Barbieri et al. [93] explored the advancements in laser welding achieved through an innovative beam wobbling head for joining tailored blanks, which are commonly employed

in the automotive industry to fabricate aluminum components with varying stiffness. The study involved producing butt and lap joints from two industrial aluminum grades, AA-6082 T6 and AA-5754 H111, of differing thicknesses. The wobbling technique notably increased the width of the strength section in lap joints without affecting penetration depth, resulting in improved surface aesthetics on the visible side. However, the study also noted the presence of residual porosity in the lap joints, attributed to the inability to fully evacuate gas or metallic vapor during the laser process, inherent in non-fully penetrating welding.

Mann et al. [56] studied the effect of oscillation frequency and focal diameter on weld pool geometry and temperature distribution during laser beam welding of high-strength steels using beam oscillation. Their findings indicate that higher oscillation frequencies help mitigate variations in melt pool geometry during welding but also contribute to increased spatter formation. Additionally, higher frequencies result in elongated and narrower melt pools, which may raise concerns regarding hot cracking susceptibility. This highlights the need for careful control of oscillation parameters to optimize weld quality and minimize defects.

Khodabakhshi et al. [94] examined the weldability of dissimilar lap joints between AA6022 aluminum (bottom layer) and AZ31 magnesium alloys (upper layer) using a novel laser beam wobbling technique. To mitigate metallurgical incompatibility, a pure nickel interlayer with a thickness of 0.1 mm was employed. The study assessed how the incorporation of the nickel interlayer, travel speed, laser power, and laser beam wobbling characteristics affected the final microstructures and phases. It was discovered that the laser beam wobbling technique was very successful in lowering the likelihood of cracking during welding. This was accomplished by improving the intermixing between the different metals and changing the nugget zone's shape to disperse the intermetallic compounds evenly within the nugget metal matrix rather than continuing the intermetallic compound formation at the interface. The presence of the nickel interlayer further suppressed undesirable Al-Mg chemical reactions, leading to the formation of more stable and uniformly dispersed phases compared to conventional Al-Mg intermetallic at the interface. The study demonstrated that joint formation strongly depends on the degree of intermixing and the dimensions of the fusion zone, which influence the Al- and Mg-rich interaction zones and are controlled by laser power. Because beam wobbling and laser processing parameters have a direct impact on molten pool circulation, it was demonstrated that hardness profiles are quite sensitive to these factors. In comparison to the base magnesium and aluminum alloys, the mean Vickers

hardness values of the Mg- and Al-rich interaction zones increased significantly as a result of the creation and uniform dispersion of complex intermetallic compounds in the metal matrix. These increases were roughly 225% and 140%, respectively. This study demonstrates how laser beam wobbling in conjunction with a nickel interlayer can improve the mechanical characteristics and overall quality of dissimilar lap joints.

Shah et al. [95] investigated the laser welding of Al-Mg alloys with a Ni foil interlayer using linear and wobble laser sources. According to the study, a brittle lower fusion zone caused fractures in joints that were welded using a linear laser. On the other hand, because of the ductile upper fusion zone of the weld, the wobbling laser welding created unbroken joints after cutting. By encouraging a ductile fusion zone rich in magnesium and attaining a greater bonded width, the wobbling laser approach improved joint integrity. These results imply that by increasing the joint area and decreasing the development of brittle secondary phases in the fusion zone, laser beam wobbling enhances joint quality.

The literature proposes a novel incremental scanning technique for transmission welding (TWIST) which help to achieve uniform energy distribution in polymer joint thereby leading to much higher weld strength than the traditional LTW. It is observed that beam wobbling technique enhances ductility, minimizes hardness and shrinkage. Higher oscillation frequency is found to stabilize melt pool geometry but at the same time increases the spatter and narrow the pool. This raises hot cracking risk. Studies have suggested that using an Ni interlayer with beam wobbling for dissimilar Al-Mg joints help to improve intermixing, uniform intermetallic dispersion, hardness and joint integrity while suppressing undesirable reactions. Experts have suggested that wobble mode welding generates wider bonded zones and more ductile and crack free joints as compared to linear welding. Although, the benefits of beam wobbling have been revealed in both similar and dissimilar material welding but there is a insufficient research for understanding of how the specific wobbling parameters interact with material behavior to impact the microstructure, defect formation and mechanical performance with respect to different class of materials.

2.1.4. Review on modeling and optimization of different class of materials

Jeng et al. [96] employed an ANN with back propagation and learning vector optimization to reliably predict weld quality, such as weld width, undercut, and distortion as a function of laser welding parameters with minimal error. Their study demonstrated the model's reliability, with prediction results closely aligning with experimental data. The ANN model provided a

comprehensive and practical approach for predicting optimal laser welding parameters for butt joints. Additionally, the model's predictions were valuable for selecting appropriate welding parameters and avoiding unsuitable welding designs, underscoring its potential to enhance laser welding efficiency and accuracy.

Nagesh et al. [97] employed back propagation ANN to establish the relationship between weld geometry and process factors and showed that the resulting model accurately predicts bead and penetration geometry in shielded metal arc welding, which was confirmed by test data. The network exhibited strong alignment with the training dataset and satisfactory generalization capabilities. The findings indicate that the ANN model can be effectively employed for estimating weld bead and penetration parameters, with minimal error observed between predicted and experimental values, confirming its reliability and applicability in welding process optimization.

Okuyucu et al. [98] employed ANN to estimate tensile strength, yield strength, weld zone hardness, and heat affected zone as a function of process factors in friction stir welding of aluminum. The ANN model demonstrated excellent predictive performance, enabling the calculation of mechanical properties as functions of welding speed and tool rotational speed (TRS). Simulations revealed the combined effects of these parameters on the mechanical properties of welded aluminum plates. Strong agreement was found when comparing the measured and projected values; the root mean square (RMS) error values for the hardness of HAZ and weld metal, elongation, yield strength, and tensile strength were 0.0115, 0.0064, 0.0566, 0.0253, and 0.018, respectively. Furthermore, the model's accuracy and dependability in forecasting the mechanical behavior of welded aluminum were highlighted by the R^2 values exceeding 0.99 for all outputs with the exception of elongation, which had a value of 0.985.

Rao et al. [99] used the PSO algorithm to optimize the process variables of ECM and compared the results to other optimization approaches in terms of convergence and accuracy. Their study revealed that the PSO algorithm demonstrated superior convergence and accuracy compared to the other methods. The comparison between single-objective and multi-objective optimization using PSO indicated that the combined objective function provided better overall results. However, it was observed that in both cases, the tool life exceeded requirements, as reflected by the minimal number of sparks. Consequently, single-objective optimization was deemed preferable for achieving maximum dimensional accuracy while maintaining adequate tool life. The proposed PSO algorithm also exhibited efficiency,

requiring only 30 to 40 iterations to converge to an optimal solution. Furthermore, it demonstrated the capability to effectively handle multi-objective optimization models, underscoring its versatility and robustness in complex optimization scenarios.

Chandrasekaran et al. [100] examined how soft computing methods like fuzzy sets, ant colony optimization, and genetic algorithms (GA) are used in different manufacturing processes and shown their ability to handle challenging optimization problems. GA is a popular and well-tested optimization approach because it can handle both discrete and continuous variable objective functions and automatically searches for a non-linear relationship between process variables and responses. In machining, GA has been employed for two primary purposes: optimizing internal parameters of neural networks, fuzzy systems, and neuro-fuzzy systems, and optimizing machining processes, highlighting its versatility and effectiveness in manufacturing optimization tasks.

Rao et al. [101] proposed an optimization method, Teaching learning based optimization algorithm for solving the large nonlinear scale problems. Due to multimodality, complexity, and differentiability, traditional techniques are unable to address such large-scale issues, particularly when dealing with non-linear objective functions. It is discovered that, in contrast to previous population-based techniques, TLBO provides algorithm parameter-free simplicity by operating without the necessity for algorithm parameter fine-tuning. The TLBO method has a significant advantage over the PSO algorithm in that the latter requires the user to set some algorithm parameters, including acceleration coefficients and inertial weight, while the former does not. Both algorithms yielded encouraging results in all of their endeavors and found several uses in manufacturing process improvement.

Rao et al. [102] applied the TLBO algorithm for parametric optimization of a variety of nontraditional machining processes, demonstrating its usefulness in terms of accuracy and convergence in comparison to all other contemporary algorithms. The study demonstrated that TLBO outperformed contemporary algorithms, such as Genetic Algorithm (GA), Simulated Annealing (SA), Artificial Bee Colony (ABC), Harmony Search (HS), Shuffled Frog Leap (SFL), and Particle Swarm Optimization (PSO), in terms of accuracy and convergence. Notably, TLBO achieved significant improvements, including a 12% enhancement over GA in Ultrasonic Machining (USM), 8% and 20% improvements in Abrasive Jet Machining (AJM) for brittle and ductile materials respectively, and considerable advancements over ABC in Wire Electrical Discharge Machining (WEDM). These results

establish TLBO as a superior optimization method for solving constrained and multi-objective models in nontraditional machining processes.

Rao et al. [103] presented a modified version of TLBO for heat exchanger multi-objective optimization, demonstrating its potential for thermal system optimization. Compared to the Genetic Algorithm (GA), the modified TLBO exhibited a faster convergence rate and produced improved results, highlighting its potential for thermodynamic optimization tasks. The algorithm's robustness was further validated by altering cost and objective functions, where it consistently delivered accurate and reliable outcomes. This underscores the modified TLBO algorithm's capability to handle complex thermal optimization challenges effectively.

Satpathy et al. [104] improved the TLBO algorithm by way of incorporating orthogonal design (OTLBO) for the purpose of improving speed and robustness, hence leading to much better quality as well as stability of solution. Performance evaluations demonstrated that OTLBO outperformed the basic TLBO and other evolutionary algorithms such as Particle Swarm Optimization (PSO), Differential Evolution (DE), Artificial Bee Colony (ABC), and their variants across multiple benchmark functions. The proposed OTLBO algorithm also showed superior efficiency in terms of the number of function evaluations (FEs), highlighting its effectiveness and stability compared to alternative optimization techniques.

Yildiz [105] applied a newly developed Cuckoo Search (CS) algorithm to address a manufacturing optimization problem, demonstrating its effectiveness by solving a milling operation optimization case. The outcomes were compared to those of other algorithms, such as the ant colony algorithm, genetic algorithm, hybrid particle swarm algorithm, immune algorithm, and hybrid immune algorithm. These techniques were surpassed by CS, which offered better ways to optimize machining parameters in milling processes. The authors emphasized how readily CS can be tailored to different optimization models with a wide range of goals and constraints, making it a versatile generalized optimization tool. Overall, the study confirmed the robustness and efficacy of the CS algorithm for machining optimization problems.

Mohamad et al. [106] conducted a comprehensive review of the cuckoo search (CS) algorithm across various domains. The study highlights that CS consistently outperforms other evolutionary algorithms, including genetic algorithms (GA), particle swarm optimization (PSO), Tabu Search, artificial bee colony (ABC), and differential evolution (DE). Experimental findings demonstrate that CS excels in computation efficiency, time,

convergence rate, and cost. Additionally, prior research indicates that CS effectively addresses diverse optimization challenges, such as engineering design optimization, unconstrained optimization problems, and pattern recognition tasks. Overall, the review underscores the efficiency and robustness of CS in solving a wide range of test problems.

Rao et al. [107] found that the tensile strength and hardness of the casting process significantly improved as compared to the previously employed optimization strategy after applying the TLBO algorithm to improve the performance of three different casting processes. For the die casting process, the model, which previously required 1000 generations using Genetic Algorithm (GA), was successfully optimized with only 10 generations using TLBO, significantly reducing computational effort. Additionally, the solution was identified as a global optimum. The study highlights TLBO's effectiveness in handling complex mathematical models for parameter optimization in casting processes, with the potential for application to other casting techniques.

Huang et al. [108] introduced a modified version of the Cuckoo Search algorithm, called Chaos-Enhanced Cuckoo Search (CCS), which leverages chaotic sequences to increase solution diversity. This variant incorporates a step-size parameter and a boundary-handling mechanism to address challenges with solutions exceeding boundaries, a limitation commonly encountered in the standard Cuckoo Search algorithm. Numerical evaluations demonstrated that CCS significantly enhances the exploration capability of CS, preventing premature convergence to local optima and effectively identifying global optimal solutions. The integration of chaos-driven boundary handling further strengthens the algorithm's robustness in locating host nests within feasible solution spaces.

Gupta et al. [109] applied the RSM and PSO algorithms for optimizing the turning variables by way of using the minimum-quantity lubrication approach and figured out that PSO and DFA provided nearly identical results. The study highlighted the effectiveness of MQL in reducing temperature at the tool-chip interface, thereby preventing built-up edge formation. However, the process generated laminar structures with coarse microstructures, leading to higher shear stresses, increased cutting forces, and elevated tool wear. Optimal machining parameters for turning Titanium Grade-II alloy under MQL conditions were identified as a lower cutting speed (200 m/min), lower feed rate (0.10 mm/rev), and a higher approach angle (90°).

Rakhshani and Rahati [110] developed an enhanced variant of the Cuckoo Search (CS) algorithm, termed SDCS, which incorporates a learning strategy and an information-sharing search mechanism for improving the convergence speed and global search efficiency. The learning strategy in SDCS integrates local and global search modes, termed snap and drift modes, to meet convergence conditions effectively. Furthermore, the information-sharing mechanism refines the search process, guiding solutions toward optimal outcomes. The performance of SDCS was assessed using well-known benchmark functions, with statistical analyses comparing its results to those of CS, modified CS (MCS), and other advanced optimization algorithms. The findings indicate that SDCS exhibits superior convergence rates and robustness in most scenarios, outperforming its counterparts.

Joshi et al. [111] reviewed the use of the cuckoo search (CS) algorithm for solving various optimization problems and highlighted challenges related to its parameter tuning. Typically, the parameters of CS are held constant for a specific duration, which can reduce the algorithm's efficiency. The authors emphasized the need for a well-defined strategy to dynamically adjust CS parameters to enhance performance. They also drew an analogy to the unique reproductive behavior of cuckoo birds, such as Ani and Guira species, which strategically lay their eggs in host nests to improve the survival chances of their offspring. This analogy illustrates the adaptive and opportunistic nature of the algorithm, aligning it with the optimization strategies it employs.

Elsheikh et al. [112] examined the suitability of PSO for optimizing different solar energy systems and found that it is a reliable technique that raises the efficiency of solar systems. While numerous metaheuristic methods have been explored to improve solar energy systems, PSO has shown versatility across domains such as engineering, manufacturing, and medicine. The algorithm's core process involves identifying the optimal position for each particle within the population. Their review suggests that PSO is a highly effective and promising technique for advancing the performance of solar energy systems.

Basset et al. [113] successfully predicted the unknown variables of a photovoltaic model using a modified TLBO approach; in comparison to state-of-the-art methods, the modified TLBO algorithm performed better than the competing algorithms, particularly for PV models with a large number of unknown parameters. The modification involved dividing the teaching and learning phases into three levels—low, medium, and high—based on the scoring levels of

individual learners. This enhanced structure improved the algorithm's accuracy and reliability, establishing its advantage over competing metaheuristic methods.

Diyaley and Chakraborty [114] evaluated the effectiveness of the TLBO algorithm relative to the other four algorithms—the firefly algorithm, the differential evolution algorithm, the cuckoo search algorithm, and the quantum particle swarm optimization algorithm—in order to improve the performance of ring and rotor spinning processes in the textile industries. The results demonstrated that the TLBO algorithm outperformed these methods in terms of computational speed, accuracy, and consistency of the solutions. Convergence diagrams and boxplots further validated its superiority. Additionally, sensitivity analysis confirmed the robustness of the TLBO algorithm, even with variations in population size.

Diaz et al. [115] examined 62 papers on the engineering applications of TLBO, exposing a range of hybridized and altered versions created by researchers to improve optimization performance. Despite these advancements, the original TLBO algorithm has proven effective across multiple optimization domains. The main benefit of TLBO is its speed and practicality; it simply needs the population, design variables, maximum iterations, and the goal function, negating the need for parameter changes.

Hassan et al. [116] proved that, in the context of smart water-assisted foam technology, the ANN machine learning method is effective in modeling and forecasting the contact angle in oil and gas applications. Using 1,615 datasets from various published sources, they developed an ANN-based model that offers advantages such as speed, reliability, and ease of use. Statistical error analysis confirmed the model's robustness, demonstrating no issues of underfitting or overfitting. The model accurately predicted contact angles, achieving high R values of 0.9988, 0.9985, and 0.9967 and AAPRE values of 1.68, 1.62, and 1.81 for training, validation, and testing datasets, respectively. This study underscores ANN's potential in advancing predictive modeling in the oil and gas sector.

The research paper revealed that artificial intelligence-based approaches show high level of predictive accuracy and strong convergence behavior. The ANN models accurately forecast weld geometry, mechanical properties and process quality responses. On the other hand, metaheuristic algorithm like PSO, GA, TLBO and Cuckoo search help in improving optimization of machining, casting, thermal system, solar energy application etc. comparison of the said algorithms suggests that TLBO outperforms the other algorithm, the common evaluation metrics are accuracy, convergence speed, stability and computational efficiency.

In addition to this, the ANN based models applied to oil and gas segment, depict high reliability and statistical accuracy. Several studies have applied the above machine learning algorithms for the purpose of modelling and optimizing welding, machining, thermal systems and other manufacturing processes. Very less research has been conducted to understand how the above discussed computational techniques perform across various classes of material. This indicates a peer research gap.

2.2. Problem Identification

Laser Beam Welding (LBW) is a versatile and highly efficient joining process, but achieving high-quality welds requires addressing material-specific challenges, optimizing process parameters, and minimizing defects. Although polymers and titanium-based alloys are fundamentally different materials, they share certain challenges in laser welding, such as thermal management, absorption characteristics, and process control.

Laser welding relies on opto-thermo-mechanical phenomena, including laser propagation, absorption, heat conduction, material melting, and solidification. The optical properties of the materials being welded, along with the type of laser used, significantly influence welding performance. Despite its advantages over conventional welding techniques, laser welding faces material constraints that limit its full potential.

For this research, two different laser sources are employed to address the specific requirements of each material class:

- A low-power diode laser (10W) for welding transparent and opaque polymers, such as polymethyl methacrylate (PMMA), polycarbonate (PC), and polypropylene copolymer (PPCP).
- A high-power fiber laser (500W) for welding titanium-based alloys, including titanium and NiTinol superalloy.

While substantial research has been conducted on laser welding of metals and some polymers, Yet, material constraints continue to be a significant impediment to realizing the full potential of laser welding. The incompatibility in their thermal and optical properties presents challenges in achieving defect-free, high-strength welds. More research is needed to optimize laser welding parameters, develop defect prevention strategies, and enhance material compatibility across these diverse material classes.

2.3. Objective of the Present Research Work

In recent years, fiber laser welding has emerged as a cost-effective and advanced alternative to conventional solid-state and gas laser systems. A review of existing literature indicates that researchers have explored the weldability of different material combinations using various techniques, with a focus on process optimization and mechanical performance enhancement. However, limited studies have focused on the simultaneous exploration of laser welding in both low-melting polymers and high-melting titanium alloys using different laser sources. In particular, the effect of process parameters on weld quality and defect minimization in these diverse material combinations remains insufficiently investigated.

To bridge this research gap, the present study aims to develop, optimize, and compare fiber laser welding processes for polymers and titanium-based alloys. The study will systematically investigate the effects of laser power, pulse frequency, scanning speed, defocusing distance, wobble width, and wobble frequency on weld quality. The research objectives are divided into the following modules:

1) To assess the laser weldability of acrylic and polypropylene copolymer and assess the laser weldability of clear transparent polymers without the use of any additives.
2) To carry out experimental investigation into laser transmission welding (LTW) of polymers by low power laser and determine the influence of significant laser welding parameters on the weld quality characteristics:
    a) to study LTW of acrylic to polypropylene copolymer
    b) to study LTW of polycarbonate to acrylic
    c) to study LTW of clear to clear acrylic transparent polymer
    d) to study LTW of clear acrylic to clear polycarbonate transparent polymer
3) To study the effect of beam wobbling parameters on the weld quality characteristics.
4) To develop the mathematical model based on response surface methodology for correlating the influence of the various laser welding process parameters on responses of weld joint. To test the adequacy of the developed mathematical models, analysis of variance test.
5) To carry out interactive multi-response optimization analysis for different responses such as weld strength, weld seam width and HAZ width, from the developed mathematical models effective for laser welding process parameters for the purpose

of determining optimal parametric combinations leading to minimum HAZ thickness, weld seam width and maximum weld strength.

6) To carry out experimental investigation into laser beam welding of NiTinol alloys by high power laser, determine the influence of significant laser welding parameters on the weld quality characteristics and find out parametric process optimization to develop mathematical model
7) To carry out experimental investigation into laser beam welding of Titanium super alloys by high power laser, find out the influence of significant laser welding parameters on the weld quality characteristics and by using the developed mathematical model to determine the optimal process parameter

This study aims to establish a new guidelines of research for optimizing fiber laser welding across different material classes, improving weld quality, and expanding the application potential of laser welding in marine, biomedical, and aerospace industries.

CHAPTER: 3

MATERIALS & METHOD

3.1. Introduction

This section discusses the selection of materials and the methodologies employed for executing laser beam welding on different class of materials. A solid-state diode Nd: YVO_4 laser (EMS 100; Electrox Ltd.) was utilized for the welding of low melting polymers, demonstrating significant potential for welding various polymers. A multi-diode pump CW fiber laser welding (SILFLDP004, Suresh Indu Lasers Pvt. Ltd.) is utilized to perform the laser beam welding of high melting titanium-based alloy. Detailed specifications and operational parameters of the laser are provided in the subsequent subsection. Additionally, the concepts of various modeling techniques and optimization methods employed in the study are elaborated in the following subsections.

3.2. Materials used as Workpiece for Laser Beam Welding

In this study, five different class of materials such as polymethylmethacrylate (PMMA), polycarbonate (PC), polypropylene copolymer (PPCP), titanium superalloy, and NITINOL alloy were utilized for performing laser beam welding using various techniques. These materials are widely used across diverse fields such as engineering, biomedical applications, automotive, electronics, and textiles. Additionally, their potential to create leak-proof joints makes them suitable for applications in micro-technology, including microfluidic devices. A brief overview of these materials is provided below:

3.2.1. Polymethyl methacrylate (PMMA)

Polymethyl Methacrylate or acrylic is rigid thermoplastic polymer possesses excellent strength and stiffness. PMMA (poly-methyl methacrylate) is widely used in microfluidic chips, aircraft windshields and automotive panels etc. due to its robust, longevity and lightweight. Excellent thermal, electrical, mechanical and chemical properties of PMMA

makes it well suited for biological as well as micro electro mechanical applications. PMMA or acrylic is an incredible useful clear plastic which is superior than glass in many ways. It is used in number of applications such as airplane windows, turrets, and acrylic nails because of transparency. It is safer than polycarbonate (PC) because it does not contain potentially harmful substances such as bisphenol- A. The physical along with mechanical properties of acrylic are presented in Table 3.1 [117].

Table 3.1. Physical and mechanical properties of PMMA [117]

Property	**Value**
Density	1190 kg/m^3
Thermal Conductivity	0.167 W/m.K
Specific Heat	1466 J/kg.K
Coefficient of Linear Thermal Expansion	80×10^{-6} /K
Yield Stress	67 MPa
Yield Strain	3 %
Tensile Modulus	3200 MPa
Refractive Index (Clear Acrylic)	1.49
Luminance Transmission	92 %
Glass Transition Temperature	100 ºC
Vicat Softening Point	96 ºC
Water Absorption	1.8 %
Humidity Absorption	0.6 %

3.2.2. Polycarbonate (PC)

Polycarbonate is a clear, colorless polymer with great strength, hardness, heat resistance, and dimensional stability, which is used extensively for engineering and optical applications. Its most widely used commercial name is LEXAN. PC is a member of the thermoplastics engineering family of high-performance polymeric heterochain materials. PC is a superb material alternative in industry not only because of its features but also because it can be recycled and its manufacturing is environmentally beneficial. Polycarbonate is tough thermoplastic polymers offers excellent strength and impact resistance. The physical and mechanical properties of polycarbonate are presented in Table 3.2 [118].

Table 3.2. Physical and mechanical properties of PC [118]

Property	**Value**
Density	1200 kg/m^3
Thermal Conductivity	0.19 – 0.22 W/m.K
Specific Heat	1200 - 1300 J/kg.K
Coefficient of Linear Thermal Expansion	65 × 10^{-6} /K
Yield Stress	66 MPa
Yield Strain	6.1 %
Tensile Modulus	2400 MPa
Refractive Index (Clear Polycarbonate)	1.58
Luminance Transmission	89 %
Glass Transition Temperature	145 - 150 ºC
Vicat Softening Point	144 ºC
Water Absorption	0.3 %
Humidity Absorption	0.12 %

3.2.3. Polypropylene copolymer (PPCP)

Polypropylene copolymer (PPCP) thermoplastic is semi-crystalline, non-reactive and colorless material and thus it is difficult to join. It has numerous applications in automotive manufacturing, packaging, laboratory accessories, etc. PPCP can also replace polyvinyl chloride (PVC) in some applications.

Table 3.3. Physical and mechanical properties of PPCP [119]

Property	**Value**
Density	905 kg/m^3
Coefficient of Linear Thermal Expansion	1.0 × 10^{-4} / ºC
Tensile Strength	25 MPa
Yield Strain	12 %
Flexural Modulus	1200 MPa
Solidus Temperature	210 ºC
Liquidus Temperature	290 ºC
Water Absorption	0.03 %

PPCP has excellent mechanical, physical, thermal and electrical properties which differ it from other thermoplastic materials. Polypropylene is used in the manufacturing of piping systems, both ones concerned with high purity and ones designed for strength and rigidity (e.g., those intended for use in potable plumbing, hydronic heating and cooling, and reclaimed water). The physical and mechanical properties of polypropylene copolymer are presented in Table 3.3.

3.2.4. Titanium superalloy (Ti-6Al-4V)

Ti-6Al-4V are the primary titanium alloys that are commonly utilised in a variety of manufacturing and biomedical industries. But Ti-6Al-4V alloy holds a larger share of the titanium market. Ti-6Al-4V, which is α-β allotropic phase alloy, are the mostly used among all titanium alloy. It has the ability to alter the mechanical and physical properties by changing the amount of alloying elements or by regulating the microstructural evolution during thermo-mechanical processing. The HCP structured α phase alloy remains stable up to 882°C before changing into BCC β structured material. Ti-6Al-4V is presently considered as the workhorse of titanium alloy because of its high strength and fabrication. It contains about 6% aluminium for α stabilization and 4% vanadium for β stabilization. About 4% of it is vanadium for β stability and 6% is aluminium for α stabilization. Table 3.4 lists the chemical composition of Ti-6Al-4Valloy. Table 3.5 lists the mechanical and physical characteristics of Ti-6Al-4V.

Table 3.4. Chemical compositions of Ti-6Al-4V

Elements	Ti	Al	V	Alloying element
Composition	89 %	5.55 %	3.95 %	Rest

Table 3.5. Physical and mechanical properties of Ti-6Al-4V

Property	**Value**
Density	4430 kg/m³
Tensile Strength	895–930 MPa
Yield Strength	825–869 MPa
Young's Modulus	110–114 GPa
Elongation	6–10 %
Thermal conductivity	6.7 W/m·K
Solidus Temperature	1604 °C
Liquidus Temperature	1660 °C

3.2.5. NITINOL alloy

Nitinol, an equiatomic Ni–Ti system, having the trade name of NiTinol, was first discovered by Buehler and Wiley in Naval Ordnance Laboratory in the year 1960 [120]. It is the most widely used shape memory alloy (SMA) among product developers and designers since its creation. Due to its exceptional qualities, such as shape memory effect (SME), great corrosion resistant behavior, extremely good biocompatibility, and superelasticity (SE), this alloy has been widely used in the biomedical and medical business for the past ten years [121, 122]. The equiatomic Ni and Ti alloy NiTinol (50 atomic percent Ni, 50 atomic percent Ti) possesses several exceptional qualities, such as corrosion resistance, shape memory effect, and pseudoelasticity. It is a well-liked and novel smart material that finds usage in a variety of disciplines, including medical, micro-electro-mechanical (MEMS), structural and civil, hydrospace, aviation, and aerospace, among others. Table 3.6 lists the mechanical and physical properties of NiTinol alloy.

Table 3.6. Physical and mechanical properties of NITINOL

Property	**Value**
Density	6450 kg/m^3
Thermal conductivity	18 W/m·K
Specific Heat Capacity	620 J/kg·K
Solidus Temperature	1513 K
Liquidus Temperature	1583 K
Melting Temperature	1310 K
Vaporization Temperature	2760 K
Latent Heat, Melting	0.2×10^6 J/kg
Latent Heat, Evaporation (J/kg)	7.6×10^6 J/kg

3.3. Details of Low Power ND: YVO_4 Laser System (10 watt) used for Welding of Polymers

In this experimental study, an Nd: YVO_4 laser (EMS 100; Electrox Ltd.) equipped with a galvo scanning system was employed. The Nd: YVO_4 (Neodymium-doped yttrium orthovanadate) laser, operating at a wavelength of 1064 nm, with an average power output of 9.28 W in continuous wave mode, was utilized for the transmission laser welding of thermoplastics. The laser system is operated through its dedicated control unit and a computer

interface. The computer interface incorporates software called Marker COMSOL, which facilitates the operation of the laser unit. The control unit connects to the computer interface using the Marker Comsol program when the main power source for the laser and control units is turned on, allowing the laser system to function smoothly. The pictorial view and the scheme of the experimental setup are shown in Figure 3.1 & 3.2.

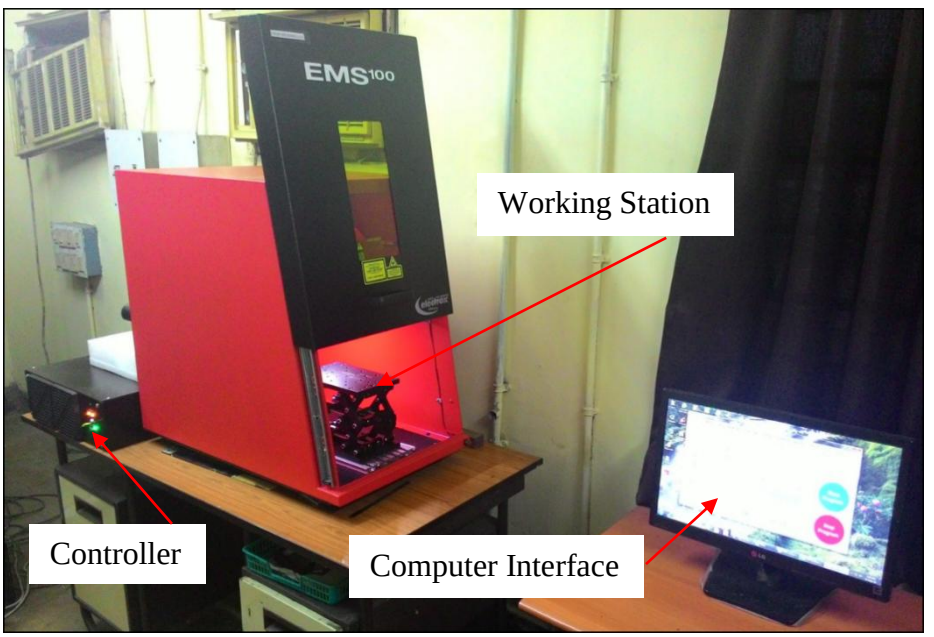

Figure 3.1. Photographic view of the experimental setup

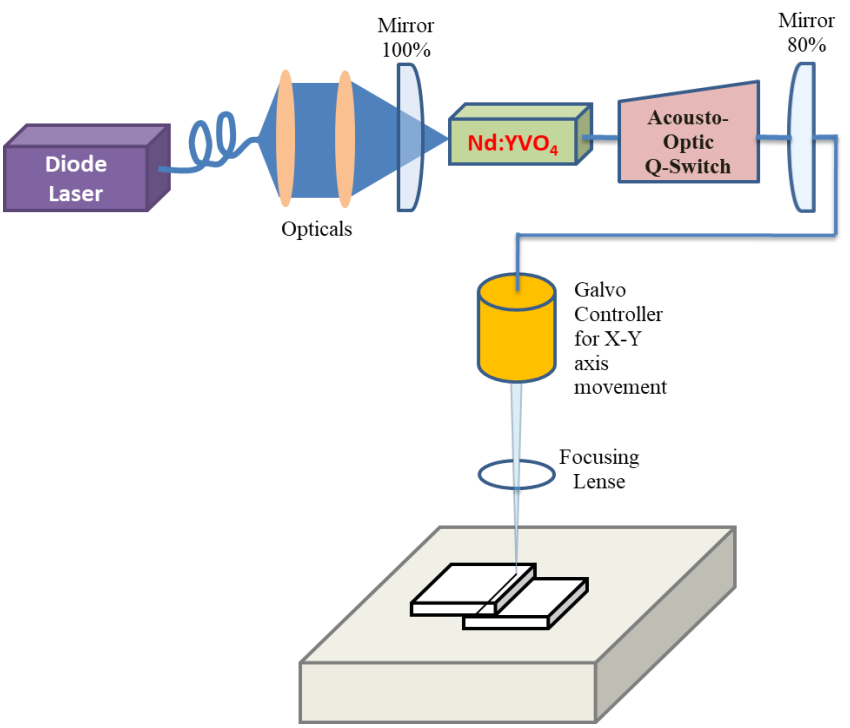

Figure. 3.2. Schematic diagram of the experimental setup

3.3.1. Laser system

Laser produces a monochromatic light of high intensity beam at the wavelength of 1064 nm. Light is properly focused through a lens and it has adequate power to vaporize materials or change the thermal and mechanical characteristics of material. The light beam is steered by two motorized moving mirrors which is controlled by a computer. Raptor laser system contains laser enclosure and scanning system, controller and the control unit. The units are interconnected by fiber optics and cable which give light, power and data communications. The laser enclosure and the control unit are shown in the Figure 3.3.

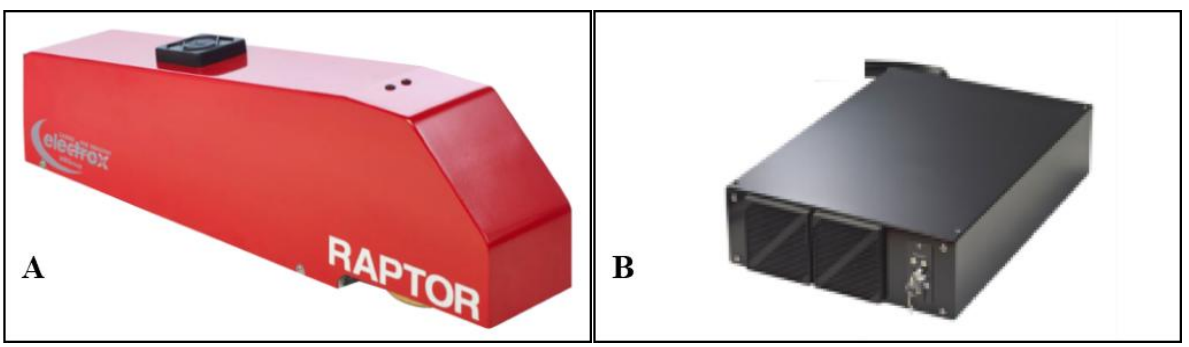

Figure 3.3. Pictorial view of (A) raptor laser enclosure and, (B) laser control unit

3.3.2. Specification of ND: YVO_4 laser system

The specifications of the laser system used for the experimental work are listed in Table 3.7.

Table 3.7. Specification of the ND: YVO_4 laser system

Specification	**Description**
Laser type	Q – switched, solid state fiber laser
Wavelength	1064 nm
Maximum laser average power	10 W
Available laser power	9.28 W
Beam diameter	1.2 mm
Pulse width	4.2 ns
Beam divergence	< 2 mrad
Q – switch pulse frequency	0.1 – 250 kHz
Laser beam spot diameter	50 µm

3.3.3. Laser beam production

3.3.3.1. Laser resonator and amplifiers

The laser beam is generated within the laser enclosure by a component called the resonator, which includes a full reflector, a gain medium, a pumping source, and a partial reflector that emits the laser beam as shown in Figure 3.4. The pumping source energizes the gain medium, turning it into a light amplifier. Amplification is the process by which light of a particular wavelength gains power as it travels through the electrified gain medium.

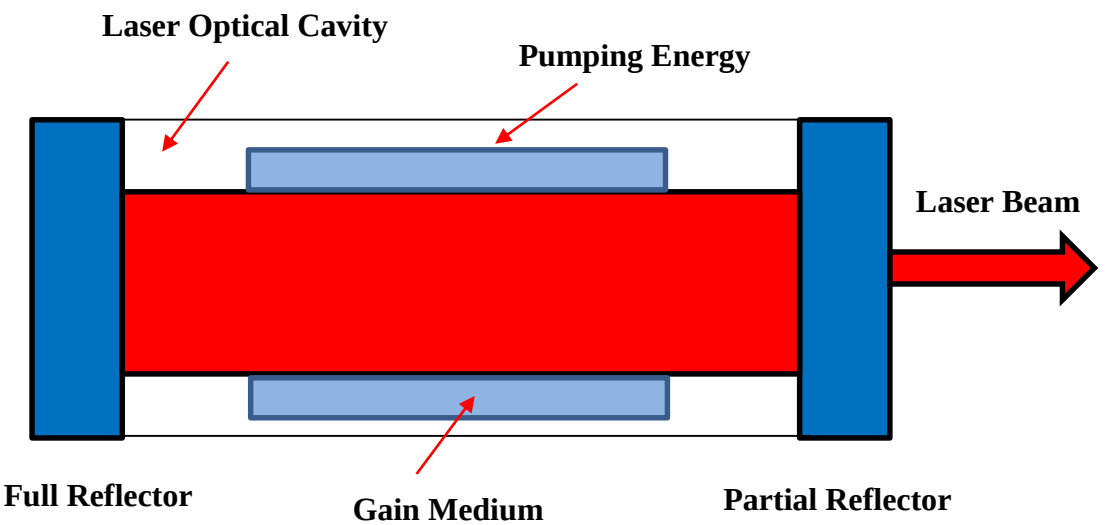

Figure 3.4. Schematic diagram of a laser resonator

The full and partial reflectors facilitate multiple passes of light through the gain medium, amplifying it with each pass. The partial reflector transmits a portion of this amplified, highly parallel light as the laser beam. For additional power, the laser beam can be passed through amplifier stages, where energized gain media without reflectors further amplify the beam without compromising its quality. This allows low-power, high-quality beams to be converted into high-power, high-quality outputs.

3.3.3.2. Q – switch

A Q-switch in a laser serves as a high-frequency light switch, rapidly toggling the laser beam by deflecting light when an electrical signal is applied. It also enables energy storage in the gain medium during beam interruption. Upon signal removal, the stored energy is released as

a brief, high-power pulse, producing peak powers up to 1,000 times higher than normal operation, essential for marking materials like metals.

3.3.3.3. Laser cooling system

The Raptor is an air-cooled laser, requiring sufficient space around the control unit and laser enclosure to ensure proper airflow.

3.3.3.4. Laser workstation

The Electrox EMS100 is a compact, cost-effective industrial desktop laser workstation, ideal for low-volume applications or cell manufacturing. Its ergonomic design ensures easy access, and the compact footprint offers a large working envelope. It is fully compatible with all Electrox fiber laser markers. Figure 3.5 shows the pictorial view of Electrox EMS100 laser work station

Figure 3.5. Pictorial view of Electrox EMS100 laser work station

3.3.3.5 Laser control system

The Raptor laser is equipped with a central processing unit (CPU) housed within the control unit, alongside other electronic components. The control unit includes the following modules:

- Diode laser power supply
- Q-switch power supply
- Auxiliary power supplies
- DSP (Laser beam scanner) PCB
- CPU PCB
- Laser Interface PCB
- I/O Interface PCB
- Fiber-coupled laser diode

3.4. Details of High-Power Fiber Laser System (500 Watt) used for Welding of Titanium based Alloys

In this experimental study, a multi-diode pump CW fiber laser welding (SILFLDP004, Suresh Indu Lasers Pvt. Ltd.) is utilized to perform the laser beam welding of titanium-based alloy. The fiber laser beam welding used for the experimental work contains spot diameter of 500 µm, wavelength 1064 nm, and maximum power of 500 watt. The specification of the Fiber laser welding system used in this experimentation is given in Table 3.8.

Table 3.8. Specification of the CW Fiber laser system

Laser type	Multi-diode pump CW Fiber laser
Maximum power	500 Watt
Wavelength	1064 nm
Mode of operation	Continuous mode
Mode of laser beam	Fundamental/Gaussian mode (TEM_{00})
Laser beam spot diameter	500 µm

A fiber laser source is used in continuous mode with active gain medium. Focusing lens with a focal length of 200 mm are used to deliver the laser beam to the work piece. The beam focus is positioned on the bottom surface. This Laser system has following main components: (1) Power supply, (2) Stabilizer, (3) Chiller unit, (4) Control panel, (5) Laser source, (6) Air-conditioner panel, (7) DAQ with PLC, (8) Laser head with beam delivery and focusing lens,

(9) Fume gas extractor, and (10) Shielding gas supply arrangement. The pictorial and schematic view of the experimental setup is shown in Figure 3.6 and 3.7.

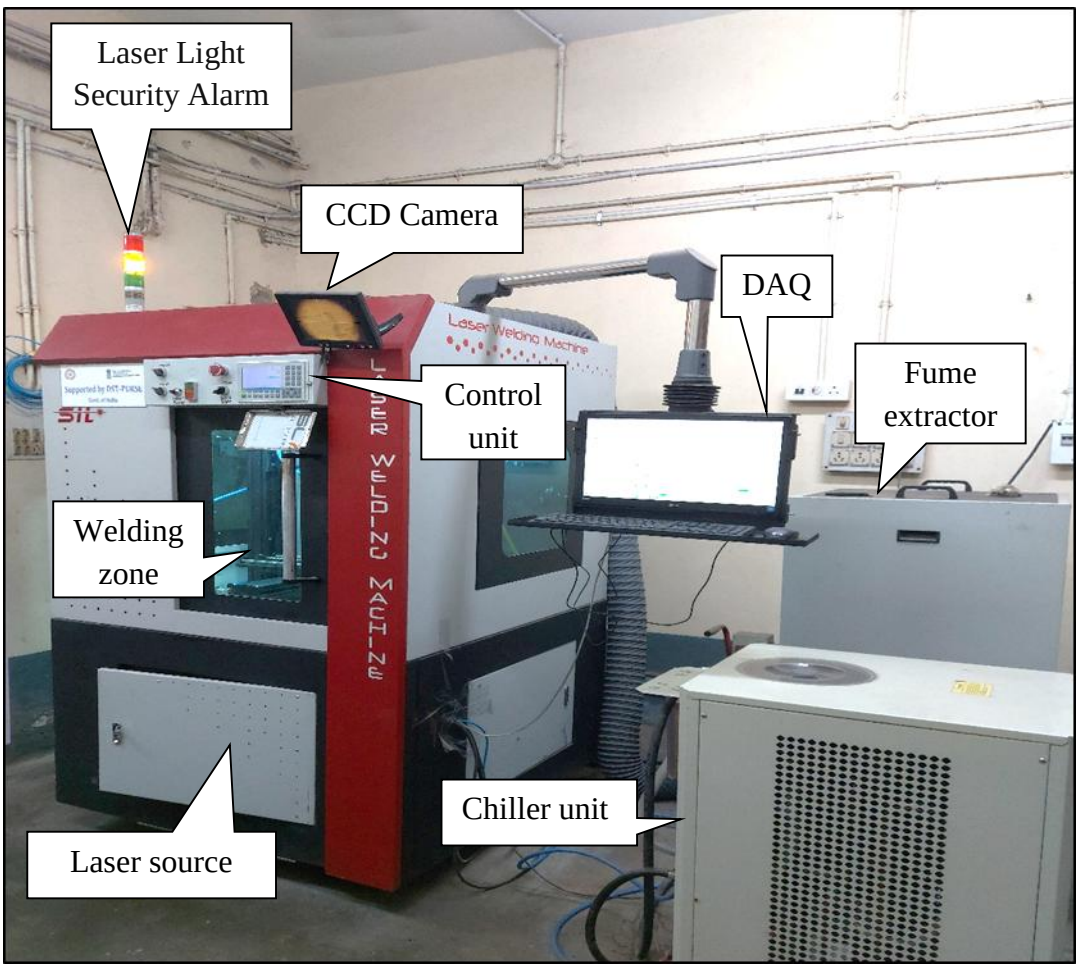

Figure 3.6. Pictorial view of the Laser Welding Machine

3.4.1. Main power supply

A mains power supply must convert the power that is delivered to it at its input by the sinusoidally alternating mains electric supply in order to make power available at its output in the form of a steady and smooth direct voltage. Electronic devices require a range of source voltages to function properly. Although power supplies have significantly increased in reliability in recent years, modern power supplies are incredibly complicated and can deliver output voltages that are tightly controlled by feedback mechanisms. Automatic safety circuits are also present in many power-supply circuits to guard against harmful over-voltages or over-current conditions.

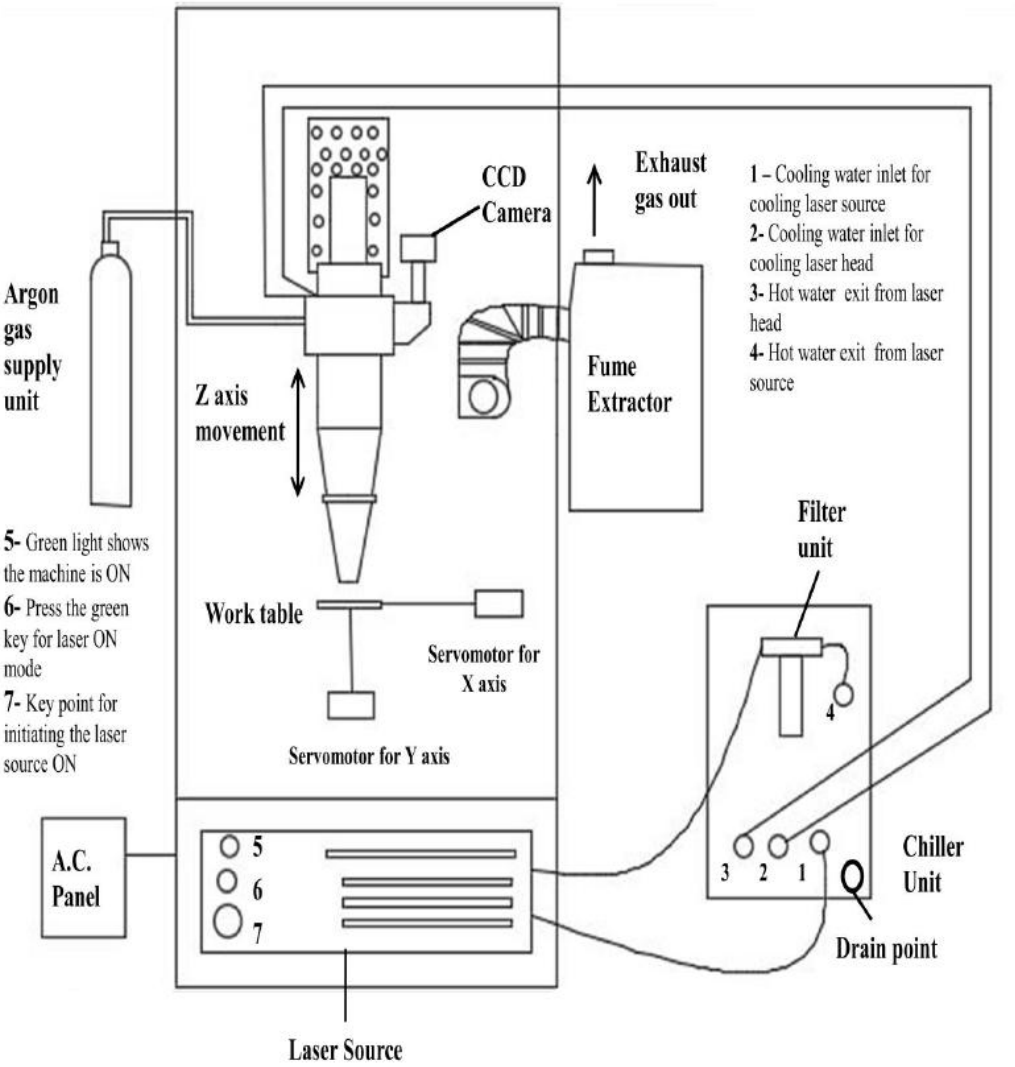

Figure 3.7. Schematic diagram of the Laser Welding Machine

3.4.2. Voltage stabilizer

A voltage stabilizer is a tool that automatically keeps the voltage level constant. Regardless the changes in the input, or incoming supply, it is an electrical device that used to deliver a consistent voltage output to a load at its output terminal. Figure 3.8 shows the photographic view of the voltage stabilizer. Table 3.9 gives the specification of the voltage stabilizer.

Figure 3.8. Voltage stabilizer

Table 3.9. Voltage stabilizer specification

Input voltage	300 to 470 V
Output voltage	415 V
Power	10 KVA
Maximum capacity	139 A

3.4.3. Chiller unit

A laser chiller is the primary element and the most crucial device utilized in managing laser temperature. Table 3.10 gives the specification of the chiller unit.

Table 3.10. Chiller unit specification

Power	220 V/50 Hz
Total input	4080 W
Normal cooling capacity	5200 W
Refrigerant	R 22
Refrigerant charge	1580 g
Maximum water volume	25 L

In order to dissipate heat from laser heat-dissipating components, devices such as laser chillers, portable chillers, rack mounted chillers, water chillers, and heat exchangers are entirely self-contained. De-ionized water is used in chiller. Figure 3.9 shows the photographic view of the chiller unit.

Figure 3.9. Chiller Unit

3.4.4. Control panel

The laser beam system's control panel plays a crucial role. We can control and operate the machine manually from here. Positioning of fixture in X-Y space, firing of laser in Z space as needed are frequently used controls. It also facilitates an emergency button which can be used if any problem occurs during operation. Figure 3.10 shows the photographic view of the control panel.

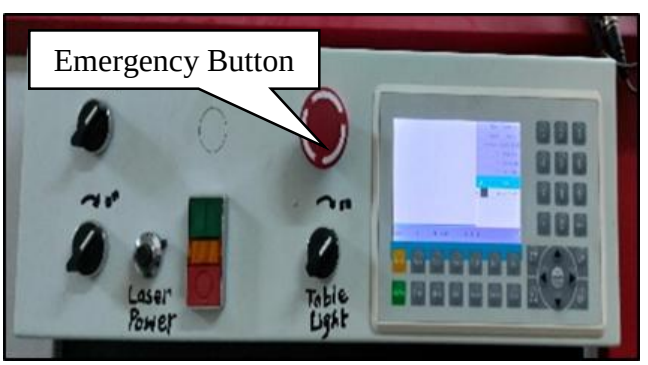

Figure 3.10. Control Panel

3.4.5. Shielding gas (Ar) supply system

Ultra-High Purity (UHP) Ar (99.99%) is non-toxic, tasteless, odorless, and colorless. 0.93% of the earth's atmosphere is made up of the noble gas Argon (Ar). For rolling and annealing

metals and alloys, argon provides an inert, sterile atmosphere, free from nitrogen and oxygen. Argon is used in the casting to remove porosity from molten metals and fix casting flaws. Ar serves the same purpose of providing an inert environment as well in laser welding. Figure 3.11 shows the photographic view of the argon gas cylinder. Table 3.11 gives the specification of the argon gas cylinder.

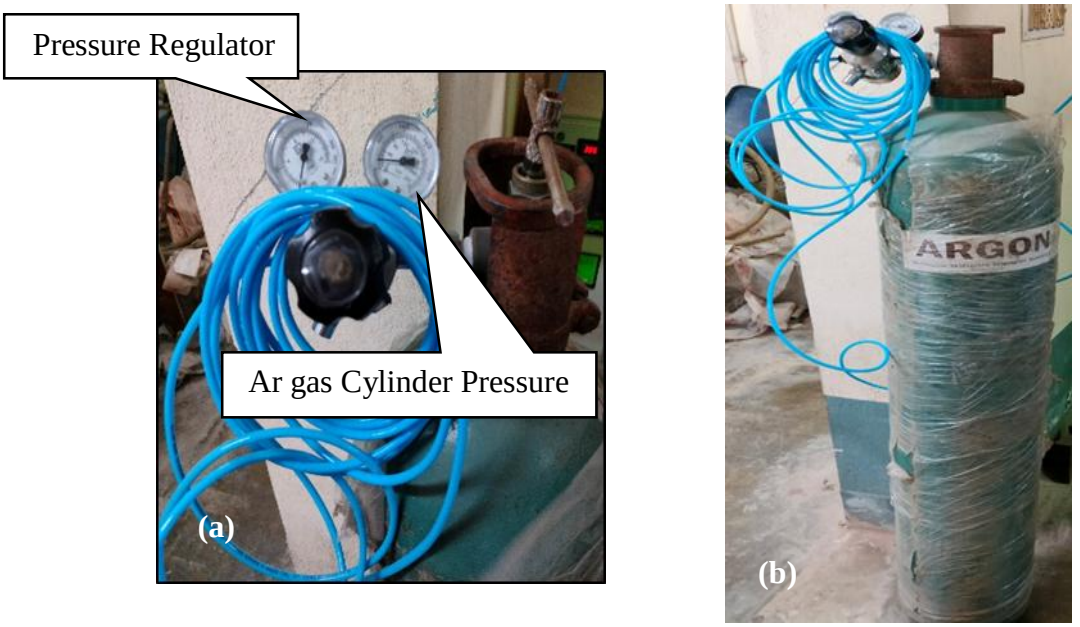

Figure 3.11. (a) Pressure gauges, and (b) Argon gas cylinder

Table 3.11. Argon gas cylinder specification

Total Weight (TW)	51.4 kg
Water Capacity (WC)	46.7 L
TP	250 bar
FP	150 bar

3.4.6. Air-conditioner panel

Air to air heat exchangers is a relatively inexpensive and energy efficient solution, but they won't safeguard equipment in places where the ambient temperature is higher than the electrical components' maximum functioning temperature. A refrigerant, which is akin to a heat pipe, is used in air conditioners for electrical control panels. However, to enhance cooling and lower the enclosure's temperature, a compressor pushes the evaporating refrigerant via a condenser coil and an evaporator coil. Figure 3.12 shows the photographic view of the AC panel. Table 3.12 gives the specification of the AC panel.

Figure 3.12. AC panel

Table 3.12. AC panel specification

Capacity	500 W
Voltage	230 V
Current	2.5 A
Refrigerant	R134a
Ambient temperature	10° C to 45° C
Frequency	50 Hz
Weight	24 Kg

3.4.7. Data acquisition system (DAQ) & programmable logic controller (PLC)

A data acquisition system is a collection of hardware and software that makes it possible to measure or regulate an object's physical characteristics in the actual world. A complete data acquisition system consists of DAQ hardware, sensors, actuators, signal conditioning equipment, and a computer with DAQ software installed. A small computer with inputs for data and outputs for transmitting and receiving commands is called a programmable logic controller. The main aim of a PLC is to use the underlying logic that has been put into it to control a system's functions. Businesses worldwide use PLCs to automate their most important processes. Figure 3.13 shows the photographic view of the data acquisition system and programmable logic controller.

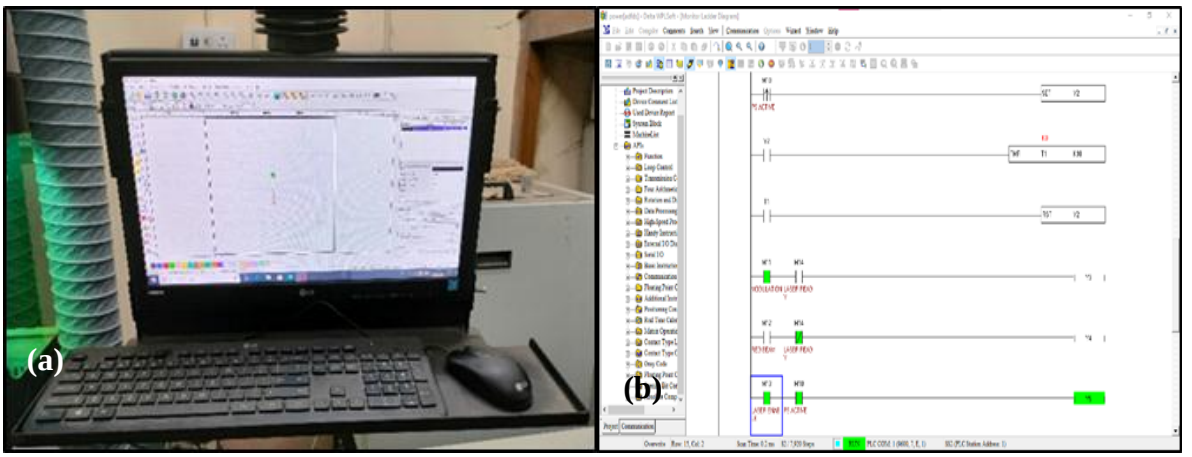

Figure 3.13. (a) DAQ setup, and (b) PLC Interface

3.4.8. Fume extractor and dust collector

In order to improve the safety and quality of the breathable air in commercial and industrial production facilities, dust or fume extraction systems are utilized to remove airborne particulates. Systems for extracting dust operate using the basic principles of capture, transfer, and collection. A difficult part of plant management is maintaining indoor air quality while reducing energy use and enhancing production efficiency. Dust collectors can have an effect in all these areas, whether they are utilized for product recovery or pollution control. Figure 3.14 shows the photographic view of the Fume Extractor. Table 3.13 gives the specification of the Fume Extractor.

Figure 3.14. Fume extractor

Table 3.13. Fume extractor specification

Frequency	50 Hz
Rotor speed	2880 RPM
Power	2 HP
Input	415 V

3.4.9. Laser source

It works on the principle that when an atom absorbs energy, its electrons become excited. A light photon is discharged when it finally returns to its ground state after a period of time. Near-infrared wavelengths, which range from 0.75 nm to 1.4 nm, are used in laser machines. Figure 3.15 shows the photographic view of the laser source.

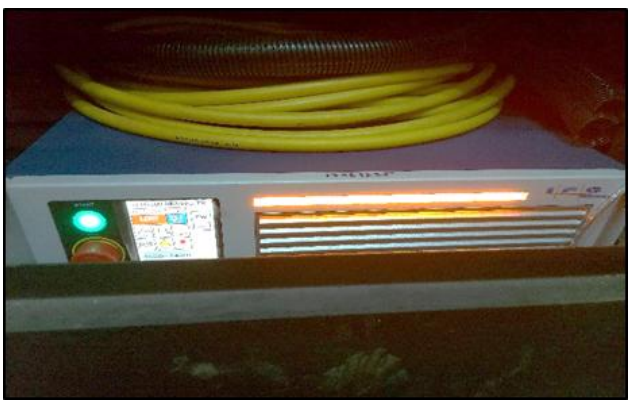

Figure 3.15. Laser source

3.4.10. Laser head and weld fixture

Fiber cable joins into the laser head to supply the beam from laser source. It is also provided with the supply from shielding gas during welding. F-theta lens is also provided in the head to control the defocus distance. Z-axis movement is facilitated by laser head. Figure 3.16 shows the photographic view of the laser head and weld fixture.

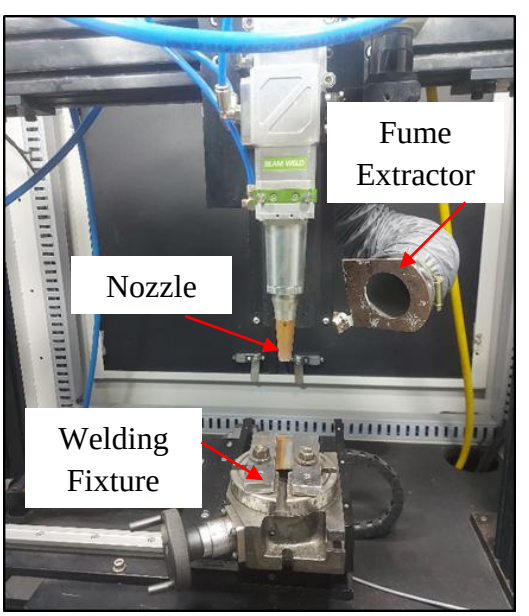

Figure 3.16. Laser head & weld fixture

A copper nozzle is also provided to concentrate the beam more with high speed. Clamping arrangement holds the workpiece during welding to avoid bending of the job. X and Y-axis movements are provided with the weld bed and facilitated with proximity sensors. CCD camera is used for visualization.

3.5. Discussion on Input Parameters

A defect-free, high-strength welds of any type of material require optimum combination of process parameter. Laser welding process needs the most significant parameter like laser power, pulse frequency, scanning speed/welding speed, and defocusing distance, which are elaborated below:

3.5.1. Laser power

Laser power delivery methods are categorized into two modes: continuous wave (CW) and pulsed wave (PW). These modes yield different welding outcomes. In CW laser welding, an increase in welding speed necessitates a corresponding rise in laser power for a given material thickness. Higher welding speeds can be achieved with greater laser power, particularly in systems with high energy density. On the other hand, PW laser welding involves intermittent laser beam application, leading to simultaneous melting and solidification during the process. This mode allows precise control over heating and cooling rates, making it particularly suitable for welding heat-sensitive materials that require controlled heat input at low welding speeds.

3.5.2. Pulse frequency

In laser welding, pulse frequency, which is commonly expressed in Hertz (Hz), is the quantity of laser pulses released per second. It plays a crucial role in determining the heat input, weld penetration, and overall weld quality. Higher pulse frequency leads to increases the number of pulses per second, leading to better fusion of the material. While, lower pulse frequency results in longer intervals between pulses, reducing heat input per unit time.

3.5.3. Scanning speed

Laser power and welding speed are critical factors influencing weld geometry, particularly its depth and width. A decrease in welding speed, while keeping other parameters constant, results in a wider and larger melt pool. Conversely, increasing the welding speed generates a strong flow at the center of the melt pool, restricting material redistribution within the

keyhole. This can lead to the formation of an undercut weld at higher speeds. Moreover, welding speed plays a significant role in determining heat distribution across the weld.

3.5.4. Defocusing

The separation between the focus and the workpiece surface is referred to as defocus. Positive defocus refers to a focus above the workpiece, whereas negative defocus refers to a focus below the workpiece. Due to the excessively high-power density of the spot center at the laser focus, which readily evaporates into holes, laser welding requires a certain degree of defocus. Greater penetration is attained when negative defocus is applied. Positive defocus should be employed when welding thin materials.

3.5.5. Shielding gas

Shielding gas plays a crucial role in determining weld quality during laser welding. It is utilized to prevent oxidation, suppress plasma formation—thereby minimizing laser beam reflection—and protect the optical lens from spatter. Several factors influence its effectiveness, including nozzle geometry, the physical and chemical properties of the gas, and the gas flow rate. In modern laser welding, helium and argon are the most commonly used shielding gases due to their metallurgically neutral behaviour. Helium, with its high ionization potential, effectively breaks down plasma and enhances heat transfer into the weld material, improving weld penetration. However, argon has become the preferred shielding gas in recent applications due to its availability and cost-effectiveness.

3.5.6. Other parameter

In laser welding, there are other parameters that can impact the quality of the weld. Weldability in laser welding is dominated by the physical and chemical characteristics of the welding materials. Thermal conductivity, diffusivity, reflectivity, density, specific heat capacity, thermal expansion coefficient, melting and boiling points, and so on are examples of physical characteristics. Oscillation or wobble width and frequency plays also play very detrimental role in determining weld quality during laser welding. It is a promising technology for welding similar or dissimilar materials and the newest innovation in the field of laser welding. Wobbling solves the drawbacks of laser welding by allowing for micro-welding and enhanced joint strength. Wobble welding is a cutting-edge method that includes oscillating the laser beam longitudinally in several wobbling modes, which causes turbulence inside the weld pool and increases weld strength by boosting material intermixing. In addition

to the standard laser welding process parameters like laser power, pulse frequency, scanning speed, and clamping pressure, wobble amplitude and wobble frequency which regulate the circular overlap, also impact the performance of laser welding. The beam wobbling parameter may be adjusted to control the weld width. Wobbling enhances the strength of welded structure by intermixing the molten pool.

3.6. Methodology used for Experimental Investigation

Experimental design plays a pivotal role in science and industry, facilitating the systematic establishment of relationships between process variables and outcomes. Properly designed experiments, supported by careful observation of processes and operations, are essential for achieving reliable and meaningful results. Researchers must ensure flawless experimental designs to obtain accurate findings. The response surface method (RSM) is a popular statistical technique for establishing empirical correlations between process variables and responses. Experiment is designed on the basis of RSM to determine the potential combination of process parameters in order to achieve better results because of its ease to use and quadratic nature. However, the non-linear relationship between welding parameters and weld quality in laser transmission welding presents a challenging task in predicting appropriate parameter values for desired weld quality attributes. Additionally, the contradicting nature of process outputs necessitates an effective multi-objective optimization approach that can provide trade-off solutions in a single simulation run for optimizing the LTW welding process. To address these challenges, the utilization of nonlinear empirical modeling tools like ANN and metaheuristic optimization algorithms such as GA, PSO, CS, SDCS and TLBO can be advantageous. These tools provide robust frameworks for optimizing the LTW process, ensuring enhanced weld quality and performance.

3.6.1. Response surface methodology

Box and Wilson (1951) were the first to introduce response surface methodology (RSM) in the early 1950s. The primary goal of RSM is to explore the response surface's topography, including identifying maximum, minimum, and target values, as well as the region where desirable responses are located. RSM has become one of the most widely used techniques for modeling and optimizing welding processes to achieve optimal performance. This methodology involves developing response surface models through a series of mathematical steps, which are subsequently validated statistically to ensure their reliability and

applicability. The response surface y is dependent upon the number of process variables or independent input parameters and may be stated as,

$$y = f(x_1, x_2, \ldots\ldots, x_k) \quad \ldots\ldots\ldots\ldots\ldots\ldots\ldots\ldots\ldots\ldots \quad (3.1)$$

It is important to construct an approximate model for the actual response surface using RSM. The approximate model is an empirical model developed by the data collected from the experimental design, defining the relationship between independent process variable and response. This is merely an empirical model that was developed using data from the experiments. The response function with lowest curvature is estimated using the first-order model for a very small range of process variables. As first order model is found unsuitable for evaluating the degree of nonlinearity due to narrow curvature response, second order polynomial is employed. First order model can be expressed as,

$$y = a_0 + a_1 x_1 + a_2 x_2 + \ldots\ldots + a_k x_k \quad \ldots\ldots\ldots\ldots\ldots\ldots\ldots \quad (3.2)$$

A second-order quadratic equation is commonly utilized in RSM, as given in Eq. 3:

$$y = a_0 + \sum_{i-1}^{n} a_i x_i + \sum_{i-1}^{n} a_{ii} x_i^2 + \sum_{i<j}^{n} a_{ij} x_i x_j + \in \quad \ldots\ldots\ldots\ldots \quad (3.3)$$

where, a_0 is a constant; a_i is the linear coefficient; aii is the square coefficient; a_{ij} is interaction between x_i and x_j; x_i, x_j are the design variables; n is number of independent process variables; $\in$ is the response error.

The central composite design (CCD) and Box-Behnken design are among the most commonly used response surface designs. CCD, in particular, is favored for its efficiency, as it requires fewer experiments to achieve accurate modeling. Multiple linear regression techniques are employed to develop response models. CCD or Box-Behnken is typically chosen after conducting several trials, ensuring its suitability for the specific study. The rotatability of a design reflects the consistency of response variation at a fixed distance from the central point of the design space, where all factors are set to their midpoint. Significant parameters are identified using the analysis of variance (ANOVA) technique.

3.6.1.1. RSM-based desirability function approach (DFA) optimization

G. Derringer and R. Suich proposed the modified desirability function analysis (DFA) approach and transform the response variable into desirability function for simultaneous optimization of response variable [123]. DFA is traditional optimization method based on

RSM. DFA has a number of characteristics that make it popular, including orthogonality, rotatability, and uniformity. DFA technique is commonly used for optimization problem due to its simple and easy implementation. In this approach, each response is transformed into associated desirable value di, $0 \leq di \leq 1$.

Desirability (di) may be defined as follows for goal maximization:

$$d_i = \begin{cases} 0 & ;if\ response\ (y_i) \leq (L_i) \\ \left(\frac{y_i - h_i}{H_i - L_i}\right)^{\omega_i} & ;as\ response\ (y_i)\ varies\ from\ low\ (L_i) \rightarrow High\ (H_i) \\ 1 & ;if\ response\ (y_i)\ \geq High\ value\ (H_i) \end{cases} \quad \ldots\ldots (3.4)$$

Desirability (di) may be defined as follows for goal minimization:

$$d_i = \begin{cases} 0 & ;if\ response\ (y_i) \leq (L_i) \\ \left(\frac{H_i - y_i}{H_i - L_i}\right)^{\omega_i} & ;as\ response\ (y_i)\ varies\ from\ low\ (L_i) \rightarrow High\ (H_i) \\ 1 & ;if\ response\ (y_i)\ \geq High\ value\ (H_i) \end{cases} \quad \ldots\ldots (3.5)$$

The weight, ω, can be set anywhere from 0.1 to 10 and is used to highlight the specific desirability function. When the weightage is more than unity, there is more stress on reaching the target value, while when the weightage is less than unity, there is less stress on the target value.

The simultaneous objective function, D, represents the geometric mean of all the transformed responses, where ri is the relative importance assigned to the different responses.

$$D = \left(d_1^{r_1} \times d_2^{r_2} \times \ldots\ldots\ldots\ldots\ldots\ldots \times d_n^{r_n}\right)^{\frac{1}{\Sigma r_i}} = \left(\prod_{i=1}^{n} d_i^{r_i}\right)^{\frac{1}{\Sigma r_i}} \quad \ldots\ldots\ldots\ldots (3.6)$$

Traditional optimization approaches such as grey relational theory, desirability function approach, principal component analysis, and others employ response weights to provide significance to particular output responses that are mainly dependent on the decision makers' choices. This may result in inaccuracy and uncertainty in the optimized value while determining the best solution.

3.6.2. Artificial neural network

Artificial neural networks (ANN) have emerged as one of the most successful empirical modeling tools, particularly for nonlinear systems. ANNs are highly flexible computational models inspired by biological neural networks, which is used to approximate nonlinear functions with several variables. The artificial neural network is a soft computing technique

that simulates the human brain in information processing functions such as reasoning, studying, and remembering. This is made possible by interconnected structures composed of several basic processing neurons capable of doing massive parallel computations for data processing and information representation. Figure 3.17 displays the architecture of an artificial neural network, which has three layers: an input layer, one or more hidden layers, and an output layer.

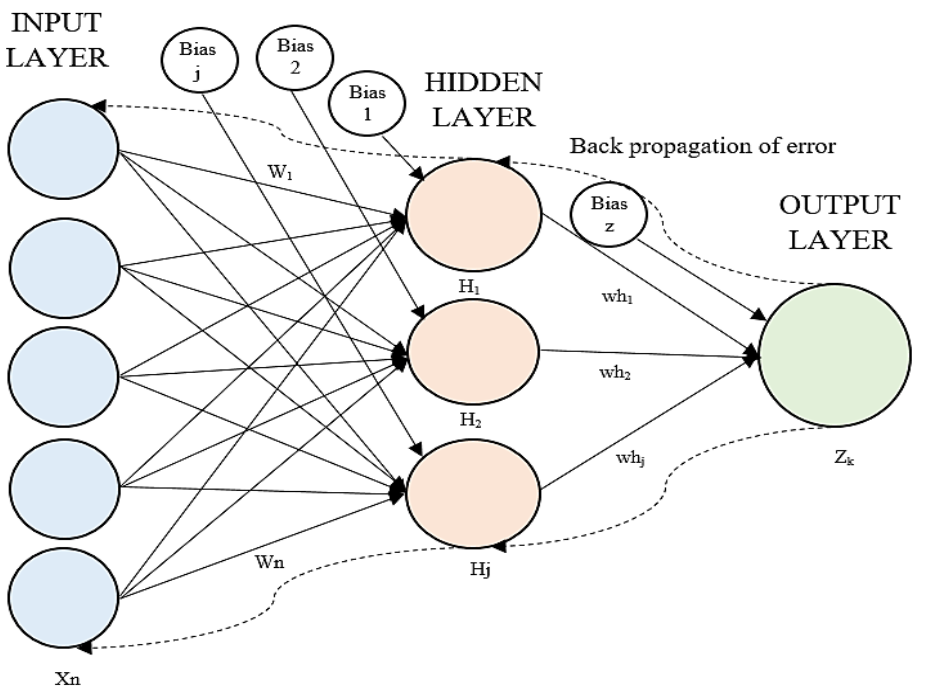

Figure 3.17. An ANN model architecture

The circle symbolizes the neurons that make up each layer, and the lines that link the neurons depict the flow of information. ANNs are taught by using a learning method like back-propagation with an optimization approach like gradient descent. Neurons in one layer are connected to those in the next layer via weighted connections. An activation function in a neuron determines the output of that neuron by introducing nonlinearity into the model. It processes the weighted sum of inputs and bias to decide whether the neuron should be activated, enabling the network to learn complex relationships between inputs and outputs. Using activation functions and weighted connections, the input layer processes information from external sources before adding it to and transmitting it to the neurons of the hidden layer. Eventually, the resulting signals are sent to the output layer, where the training phase assesses the difference between the expected and desired outputs (called targets). There is the same number of output nodes as response parameters. The number of output nodes is equal to the

number of response parameters [32]. Several researchers have defined training as the process where weights and biases of the network are adjusted with the help of a training data set. This helps to minimize the error related to prediction. On the other hand, Testing implies measuring the performance of the trained network on a separate dataset known as testing dataset. This helps to evaluate the models prediction accuracy and generalization power. The phases of ANN modeling are depicted in Figure 3.18, including the steps for initializing the neural network and obtaining the best ANN architecture for this study. ANN emerged as a widely used modeling tool due to its unique characteristics, including non-linearity, adaptability, feature learning, parallel processing, generalization, and the ability to handle high-dimensional and large datasets.

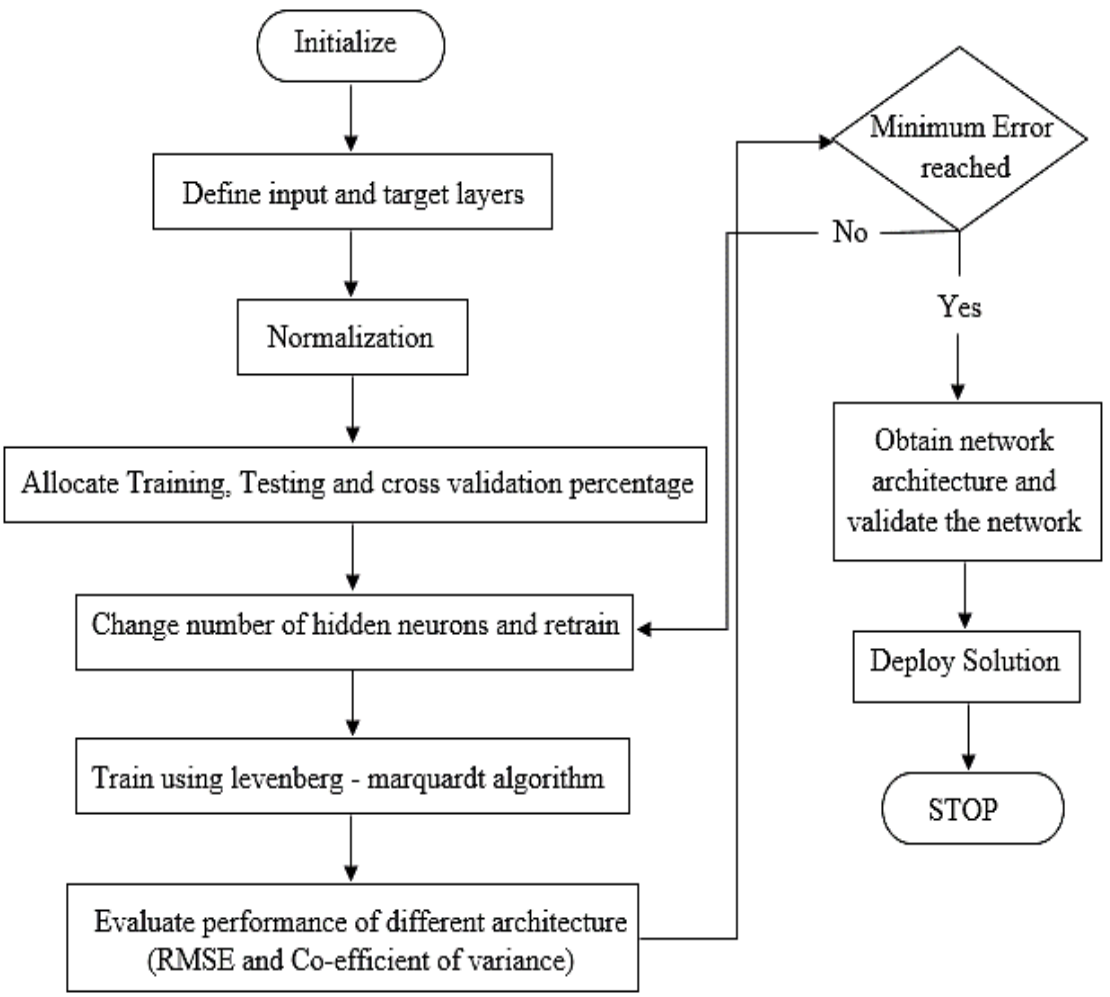

Figure 3.18. Schematic flow diagram of ANN

3.6.3. Artificial intelligence-based optimization technique

The manufacturing sector faces the significant challenge of balancing economic objectives like increased production rates, improved product quality, and lower production costs with environmental concerns by reducing industrial waste, maximizing material utilization, and conserving energy. However, optimizing all these objectives simultaneously is practically unattainable, necessitating trade-offs to determine the overall best solution. Process modeling and optimization have therefore, grown in significance during the past few decades. However, optimizing process performance based on individual process features has limited applicability and impracticality. Furthermore, concurrently optimizing multiple objectives is challenging due to their frequent incompatibilities. This has led to extensive research on determining the ideal process variables for joining processes with conflicting objectives. Consequently, there has been a rise in interest in methods like machine learning and evolutionary algorithms for multi-objective optimization and data-driven process modeling. Figure 3.19 shows the tree diagram of optimization technique.

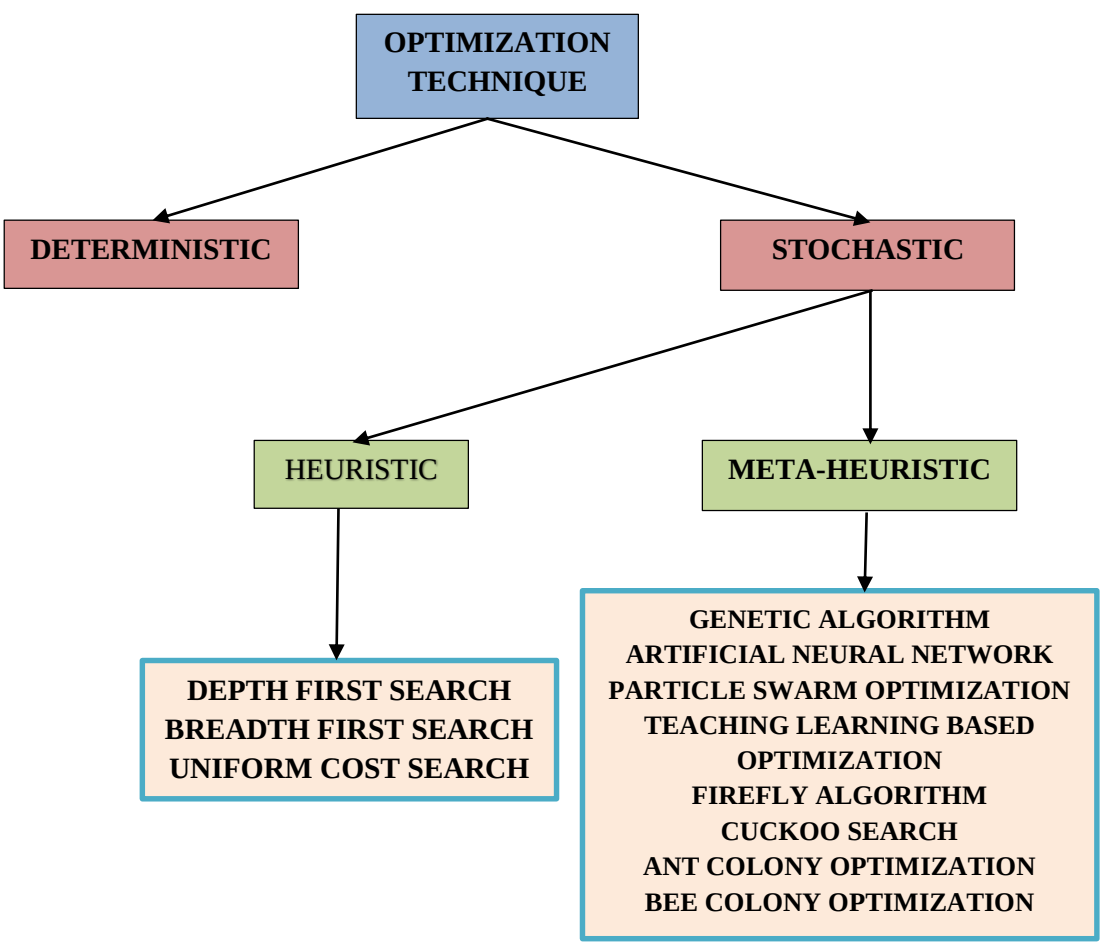

Figure 3.19. Optimization technique

With the progress of technology, optimization plays a significant role in improving quality and lowering operational costs, which benefits both the producer and the consumer [124]. In the context of laser beam welding, optimization plays an important factor for identifying the significant process variables which ensures the high joint quality by minimizing the defects and energy consumption. Further, ANNs are employed to model the nonlinear interactions between input variables and performance characteristics, enabling accurate process prediction. Optimization of process variables is necessary to improve performance of welded structure. Several optimization approaches for manufacturing process optimization have been proposed and used in recent years. The optimization technique based on the desirability function is widely utilized because it is straightforward and easy to apply. However, because one parameter is modified at a time throughout the search in the design space, the RSM-based desirability function optimization technique occasionally clung to local optima. Artificial Intelligence (AI)-based optimization techniques are powerful tools used for solving complex optimization problems by mimicking human-like cognitive processes. Meta-heuristic optimization methods are meant to address the shortcomings of classical optimization techniques. Several researchers are now utilizing metaheuristic optimization algorithms to optimize process parameters because of their superior performance. Various contemporary optimization techniques, such as the artificial bee colony (ABC) algorithm [125], particle swarm optimization (PSO) algorithm [126], cuckoo search algorithm (CSA) [127], ant colony optimization (ACO) algorithm [128], flower pollination algorithm (FPA) [129], firefly algorithm (FA) [129], novel bat algorithm (NBA) [130] and bird swarm algorithm (BSW) [130] among others, have been proven to be successful for engineering optimization problems. Meta-heuristic optimization algorithms such as FPA, FA, NBA, and BSW are found to outperform DFA [129,130].

3.6.3.1. Cuckoo search optimization

Cuckoo search (CS) technique is a global optimization technique based on the behaviour of cuckoos, given by [131]. It mimics the parasitism practiced by certain cuckoo species, in which their eggs are put in other birds' nests and, if the host is not aware of them, hatch into chicks; if not, they are killed. Certain female parasitic cuckoos have evolved to mimic the morphological characteristics of their host, which lowers the likelihood that their eggs will be destroyed and lowers the mortality rate. In the unfortunate event that the host finds the eggs, they are either discarded or the host just alienates the nest and builds a new one. Cuckoo eggs typically hatch before their host eggs, and they are typically laid in nests where host

eggs have previously been laid. On hatching the first action of the newly born cuckoo is to expropriate the host eggs by rolling it down the nest so as to get a better share of the food provided by the host and they also replicate the voices of the host birds to trick them into providing food. Every host egg stands for a solution, and a cuckoo egg, which may be able to take the place of a host egg, represents a new, superior solution. In a simple situation each nest is considered to have only one egg i.e. one solution which can be later extended to nests having multiple eggs.

The following steps are applied: -

i. An initial population of N host nests are generated randomly
ii. An egg is laid in the kth nest (k is a randomly selected) and the parameters of the egg are found by Levy flight technique.
iii. The fitness of the cuckoo egg is compared with the fitness of the host egg and the nest retains the egg with a better fitness value.
iv. If the egg is noticed by the bird then the nest is abandoned and a new nest is built by levy flight with probability p ($0<p<1$).
v. Iterate from step 2 to 4 until the termination criteria is met (mostly number of iterations).

In our case let the three parameters be x_1, x_2 and x_3.

So,

$$\text{New } X_i^k = X_i^k + \text{Random walk (Levy Flight)} \times X_i^k \quad \ldots\ldots\ldots\ldots\ldots (3.7)$$

Where, i denotes the parameter number, K is the nest number and n show the number of nest (60).

One of the disadvantages of Cuckoo search is the unstable convergence which can be solved by a balance between exploration and exploitation as given by [108]. Simply speaking, Snap prevents convergence into a local optima and Drift enables fast convergence. The algorithm can function in two modes which is decided by the performance measure Pm which is,

$$\text{Pm} = \frac{\text{Number of improved solutions}}{\text{Number of evaluated solution}} \quad \ldots\ldots\ldots\ldots\ldots\ldots\ldots\ldots (3.8)$$

If, Pm is between 0 and 0.5, the algorithm functions ins snap mode and is Pm is between 0.5 and 1 the algorithm functions in drift mode.

3.6.3.2. Teaching learning-based optimization

New evolutionary and meta-heuristic algorithms have been developed because of the inefficiency of traditional optimization method. These algorithms are based on natural behavior, and it is observed that they are always the best in terms of performance. Although there is various metaheuristic algorithm, the TLBO method has been shown to be unique and is gaining popularity among scholars. Rao et al. [102] compared the TLBO algorithm with other evolutionary algorithm for parametric optimization, considering the population size, number of iteration and computational time, found that TLBO provides superior result compared to another algorithm. TLBO is a population-based metaheuristic technique influenced by the teacher and learner phase in classroom premises that focuses on the impact of a teacher's influence on the responses of learners in a classroom. In recent years, it has seen widespread usage in a wide range of scientific and engineering applications. A teacher is typically thought to be a highly educated person who shares his or her knowledge with learners. The algorithm that is aided by this teaching-learning technique is referred to as TLBO algorithm. The primary method used in a classroom is the transmission of knowledge from teachers to learners. The two stages of knowledge exchange in this suggested algorithm are the teacher phase and the learner phase. The teacher attempts to disseminate information among learners in order to increase the general knowledge level of the class and assist learners in earning high marks or grades. The learner phase is concerned with the process of conveying knowledge to learners through interaction. It needs to be noted that a best teacher prepares learners to achieve better outcomes in terms of grades or marks. In this optimization process, a population of learners is considered, and different design variables are viewed as different subjects presented to the learners, and the learners' results are equivalent to the optimization problem's 'fitness' value. TLBO searches the population of solutions for the global solution. The design variable is utilized to create the objective function for the optimization problem, and the optimal solution is determined based on the best value of the objective function. Figure 3.20 depicts the operating principle of non-dominated sorted TLBO in the form of a flow diagram employed in this study.

Teacher phase

This phase simulates student (i.e. learner) learning through the teacher. During this phase, a teacher imparts knowledge to students and works to improve the class's mean result. Let M_i be the mean and T_i be the teacher at any iteration i. T_i will aim to get M_i to its level, therefore

T_i will now be labelled as M_{new}, the new mean. The solution is updated based on the difference between the old and new mean as determined by

$$Difference\ Mean_i = r_i\ (M_{new} - T_F\ M_i) \quad \text{..... (3.9)}$$

Where, T_F is a teaching factor that determines the mean value to be altered and r_i is a random number between [0,1]. The value of T_F can be 1 or 2, which is another heuristic step that is determined randomly with equal probability as

$$T_F = round\ [\ 1 + rand\ (0,1)] \quad \text{..... (3.10)}$$

This "Difference Mean" modifies the existing solution with the following expression

$$X_{new,i} = X_{old,i} + DifferenceMean_i \quad \text{..... (3.11)}$$

The new fitness value X_{new} is calculated and greedy selection is applied. Select X_{new} if it gives a better function value.

Learner phase

This phase simulates the learning of the students through interaction among themselves. A learner will learn new information if the other learner has more knowledge than him or her. Mathematically the learning phenomenon of this phase is expressed below. At any iteration i, considering two different learners X_i and X_j where $i \neq j$

$$X_{new,i} = X_{old,i} + r_i(X_i - X_j) \qquad if\ f\ (X_i) < f\ (X_j) \quad \text{..... (3.12)}$$

$$X_{new,i} = X_{old,i} + r_i(X_j - X_i) \qquad if\ f\ (X_j) < f\ (X_i) \quad \text{..... (3.13)}$$

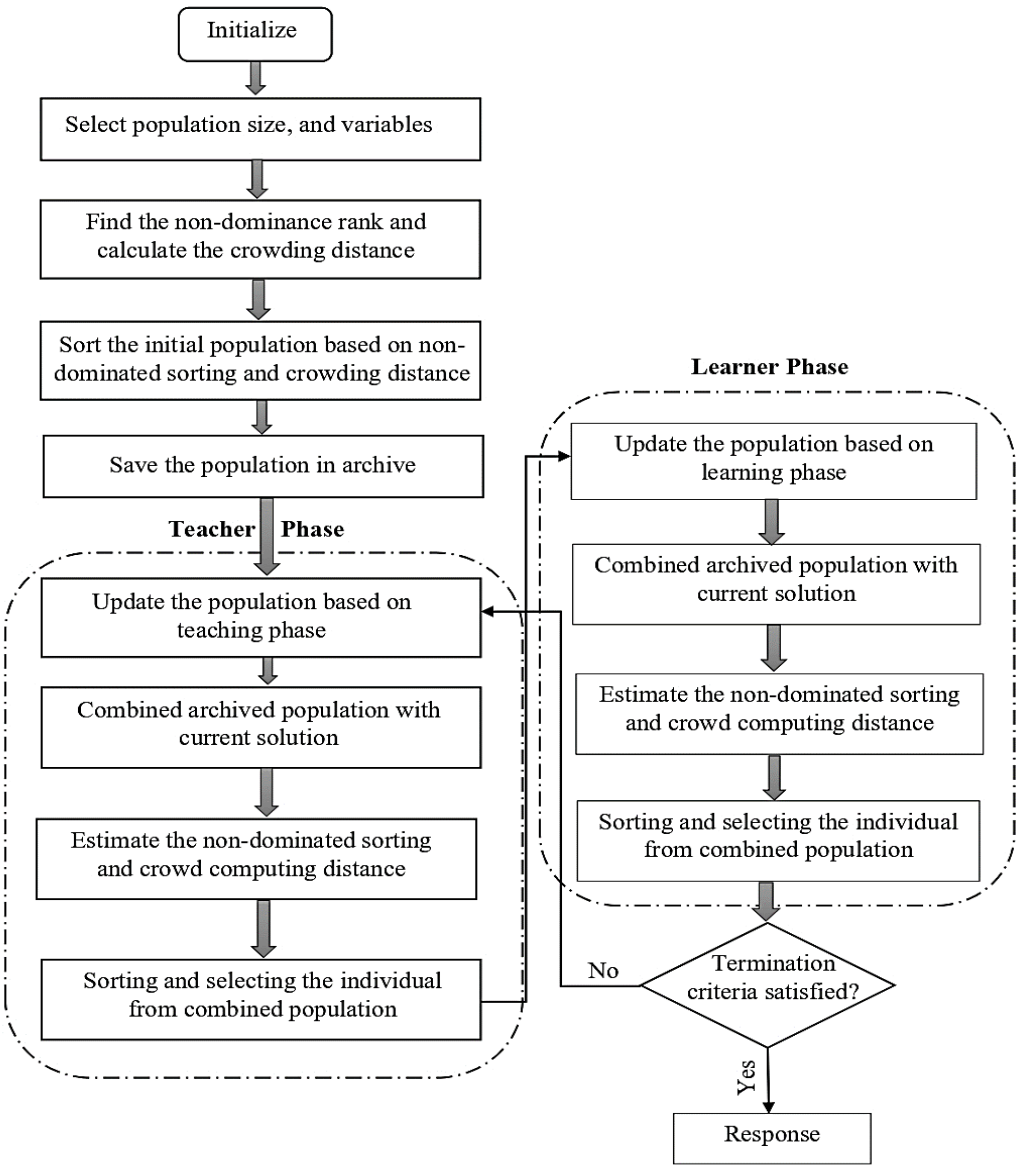

Figure 3.20. Schematic flow diagram of NSTLBO

3.6.3.3. Particle swarm optimization

Particle Swarm Optimization technique is the technique which emulates the pattern in which swarm of birds fly and exude the social behaviour during the same. PSO modifies the paths of individual agents, or particles, to explore the objective function space. This method treats every viable solution as a particle that represents a point in three dimensions. The following equation is used for the purpose of updating the particle position at each stage of the optimization process:

$$X_{i+1} = X_i + V_{i+1} \quad \text{..... (3.14)}$$

Where, V_i indicates the particle's velocity at the *t*th iteration and X_i indicates the particle's position at that time. Two consecutive iterations of the procedure are indicated by the subscripts i and i+1. The main component of position updating is the velocity vector, as shown by above equation. The velocity vectors, which works in three step such as inertia, cognitive and social component, determine how particles travel over the search space. The equation of the velocity vector is:

$$V_{i+1} = \omega V_i + c_1 r_1 (P_i - X_i) + c_2 r_2 (G_i - X_i) \quad \text{..... (3.15)}$$

Where P_i represents that it gives the personal best of individual particle and G_i gives the best performance of the group discovered by swarm. The c_1, c_2 are the cognitive and social coefficient which are in the range of $0 \leq c_1, c_2 \leq 4$. The r_1 and r_2 represent the diagonal matrix obtained from random values in [0, 1] which gives stochastic effect. The velocity vector has three components, as shown in Equation 3.14. For each iteration, the local best is tabulated followed by tabulated of global best. Initially the local best value is taken as the starting position. An initial velocity vector is also assigned and take two random valued components along the direction of global best and local best respectively. The resultant vector from the sum of all three vectors are taken as the velocity vector for next iteration and add this velocity vector to the present position vector to obtain the next position of individual particles and this process continues until the global minimum is found or until the maximum number of iterations allowed is reached, whichever comes first. This implies that all particles drift in the direction of a single point when the swarm's optimal solution is taken into account. It is also possible to modify the influence of this component with the help of c_2. These three components, as illustrated in Figure 3.21, can be used to anticipate a particle's next location.

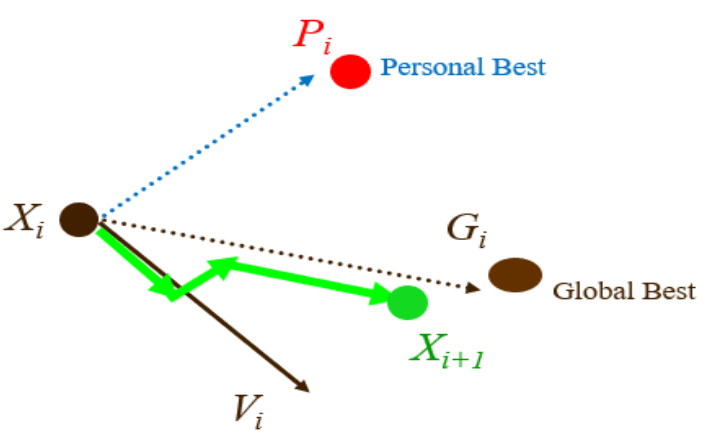

Figure 3.21. Particles updating position

3.6.3.4 Genetic algorithm

Genetic algorithms, originated from John Holland's research at the University of Michigan in the 1960s, surged in popularity during the 1990s owing to advancements in computing power and their effective application to diverse optimization problems. A genetic algorithm is a sort of evolutionary computing and the solutions it provides are subject to recombination and mutation processes, which produce new offspring and continue the process for numerous generations [132]. Consequently, the population's fitness improves over time as people inherit their parent generation's preferred designs. GA is implemented in three stages: selection, crossover, and mutation [133]. The schematic flow diagram of the GA is presented in Figure 3.22, which includes the following operating paradigms. Figure 3.23 is a representative depiction of GA operations.

i. A simulation of the natural genetic process
ii. Randomly generation of an initial population
iii. Exploitation of parent solution
iv. The survival of the fittest for the creation of the next generation
v. Generation of better offspring

Figure 3.22. Schematic flow diagram of GA

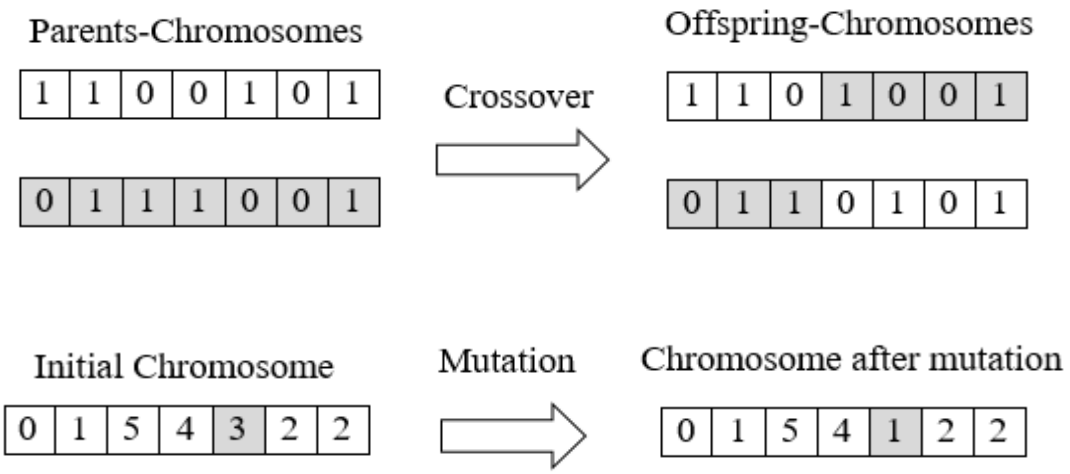

Figure 3.23. Representative depiction of GA operations

CHAPTER: 4

LOW POWER LASER TRANSMISSION WELDING OF ACRYLIC TO POLYPROPYLENE COPOLYMER

4.1. Modelling and Optimization of Laser Transmission Welding of Acrylic to Polypropylene Copolymer

It is always challenging to weld semi crystalline and amorphous thermoplastic polymers by transmission laser welding. The problem occurs due to the different molecular structure, melting point and incompatibility of polymers. Light reflection occurs primarily at the entry and exit of layers of amorphous polymers. The apparent reflection rises in semi-crystalline polymers because of improved back-scattering [3]. Scattering of light happens through single or multiple reflections naturally in the polymer. Semi-crystalline polymer disperses more light as compared to amorphous polymers because of the coexistence of phases as shown in Figure 4.1.

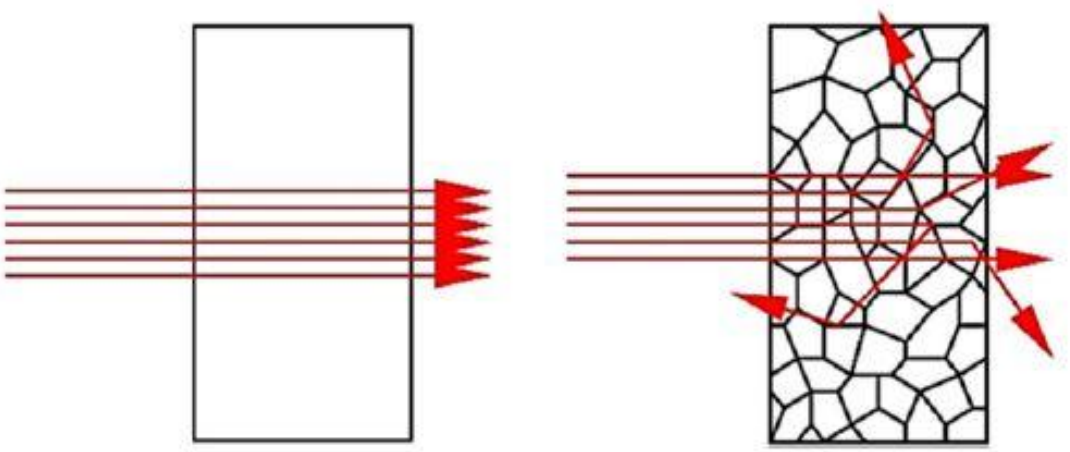

Figure 4.1. Scattering of light in (a) amorphous polymer, and (b) semi-crystalline polymer [12]

Light dispersion in polymers is affected by multiple steps, each with different refractive indices, such as amorphous, crystalline, etc. Laser transmission welding (LTW) between amorphous and semi crystalline polymer presents significant challenges owing to different metallurgical and molecular structure. Excellent mechanical, physical and thermal properties of polypropylene make it suitable for many applications in aerospace, automotive manufacturing and laboratory accessories. However, joining of semi crystalline and amorphous polymers is very difficult due to their poor compatibility or different crystal structure. Here, Acrylic (amorphous) and polypropylene copolymer (semi crystalline) each of 4 mm thickness have been joined by low power diode laser. Experimental analysis of the effect of process parameters such as laser power, scanning speed and pulse frequency on the weld zone has been studied. Greater weld strength is achieved at low scan speed. A novel multi objective snap drift cuckoo search optimization technique has been implemented for betterment of weld strength and weld width. SEM has been used to observe the welded zone morphology. The novelty of this research lies in joining of two dissimilar thermoplastic materials whose molecular structures are different.

4.2. Experimental Planning

Response surface methodology (RSM) is used for the design of experiments (DOE) and to model the output parameters in terms of process parameters. By the use of DOE, the key objective is to enhance the responses which are influenced by many independent variables. The experimentation is planned based on the three continuous factors three level central composite unblocked design. Three independent process parameters namely laser power (P), scanning speed (S) and pulse frequency (F) are varied in this experiment. Beam spot diameter and standoff distance are fixed in this experiment. There is another parameter known as repetition rate which also influence the weld strength. Repetition rate is basically the set of experimental condition applied to a single experiment. So, number of passes is repetition rate plus one. However, it has been fixed at constant value after pilot experiment.

This laser system having three components such as laser, control unit operated with computer system panel and workstation. It contains Neodymium doped yttrium orthovanadate (Nd: YVO_4) having scorpion Rapid and Raptor beam laser. A constant pressure is applied between the work materials to keep the close contact between two work materials. Trial experiments are conducted by changing the one parameter at a time, holding constant other parameters. The experimental work has been carried out on a typical solid state, Nd: YVO_4 (EMS 100;

Electrox Ltd.) system of maximum available laser power 9.28 W with beam diameter of spot 50 µm, wavelength of 1064 nm and laser pulse width of 4.2 ns.

A transparent acrylic and white PPCP each of size 80mm × 35mm × 4mm are used as work materials in this experimentation due to the increasing demand of application in automotive and plastic industry. In this experimentation, transparent acrylic is placed on top layer and white PPCP is used as bottom layer. A lap joint has been performed with an overlap of 20mm and weld center line of about 10mm as shown in Figure 4.2.

Figure 4.2. Acrylic/PPCP welded sample in lap-joint configuration

However, a number of experiments has been performed to weld acrylic and polypropylene copolymer without using any additives, but welding between these two materials is not possible. After that, a whitener ink is applied on the bottom layer of material at the intermediate junction to perform the experiment. Whitener ink contains titanium oxide (TiO_2), organic solvents such as acetone, MEK (Methyl Ethyl Ketone), or hydrocarbons and other acrylic or polymer resins as binding agents which is used to absorb the laser so that heat energy is generated at the interface. This thermal energy is then used to complete the weld. The acrylic surface is softened and slightly melted by the acetone or MEK in the whitener ink, which enables mechanical interlocking. The resin, which is probably acrylic-based, creates a strong bridge between the two surfaces once the whitener ink dries (via solvent evaporation). A welding fixture is prepared, and used for experimental work. A lap area of 20mm × 35mm is ensured during the entire work. The workpiece table can be moved in X-Y direction via CNC (computer numeric control). The workpiece can be placed and aligned in the workstation of laser system. After trial experiment, literature survey and considering machine limitations, the controllable process parameters and their limits have been given in Table 4.1.

Table 4.1. Selected process parameter and their ranges

Parameter	Symbol	Units	Levels		
			-1	0	+1
Laser Power	P	W	8.352	8.584	8.816
Scanning Speed	S	mm/min.	120	180	240
Pulse Frequency	F	kHz	50	60	70

A Universal Tensile Testing Machine (8801; INSTRON) microprocessor controlled has been used for lap-shear strength pull test, for estimation of their joining strength. To overcome the bending moments or eccentricity at weld line, some adjustment has been made to the workpiece to be lap joint strength tested as shown in Figure 4.3. Weld line has to be near to the centerline of the dragging direction. The lap-shear joint strength are estimated as maximum failure load per unit length. A three-dimensional optical measuring microscope (STM-6; OLYMPUS) microscope is utilized to measure the width of weld seam of all welded samples. The weld width of each sample is measured at the center of weld seam length. The average of three results of weld strength and weld width are taken and considered for analysis. Scanning electron microscope (EVO 18 special edition; ZEISS) is used to observe the welded zone morphology.

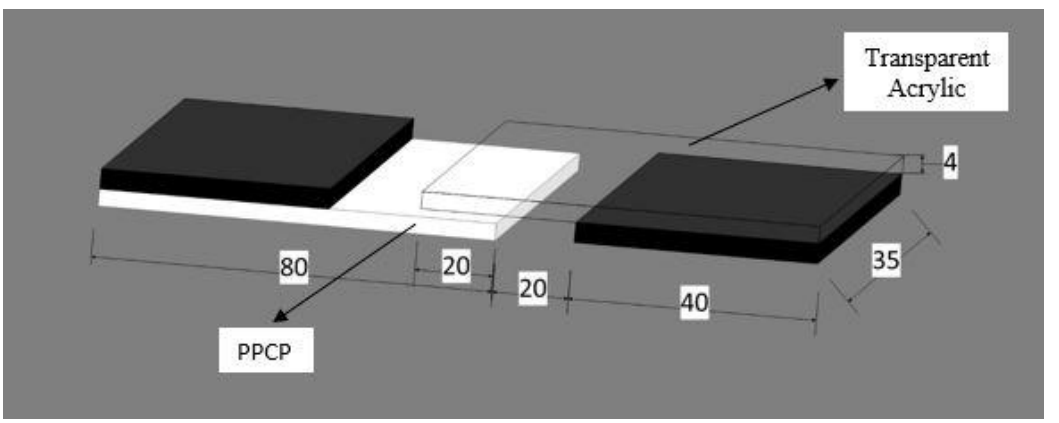

Figure 4.3. Design of weld sample to avoid bending for lap shear testing

4.3. Parametric Analysis Based on RSM Modelling

Table 4.2 presents the experimental plan as well as the measured value of the responses.

Table 4.2 Design matrix and measured experimental result

Experimental Information				Results	
Exp. No.	Welding Parameters			Weld strength (N/mm)	Weld width (μm)
	P (Watt)	F (kHz)	S (mm/min.)		
1	8.584	60	180	8.54	300
2	8.584	70	180	9.852	280
3	8.584	60	240	7.341	242
4	8.352	70	240	6.886	204
5	8.584	60	120	16.438	285
6	8.816	70	120	15.296	218
7	8.584	50	180	7.854	287
8	8.816	60	180	9.134	319
9	8.584	60	180	8.698	293
10	8.816	70	240	11.852	362
11	8.352	70	120	17.835	256
12	8.816	50	120	14.459	250
13	8.584	60	180	8.6	298
14	8.584	60	180	8.5	294
15	8.352	50	120	18.598	397
16	8.584	60	180	8.347	290
17	8.352	60	180	8.122	303
18	8.584	60	180	8.423	298
19	8.352	50	240	3.712	194
20	8.816	50	240	7	246

4.4. Second Order Regression Equation of Responses

Design Expert® software has been used for analysis of the measured output and estimating the model with best fits. The lack-of-fit test, sequential f-test and ANOVA (analysis of variance) technique have been used to check the adequacy of model using the v17 software to get the best fit model. Mathematical models are developed to establish a correlation

between input and output parameters to understand the behaviour of process parameters on responses.

$$WS = 358.4 - 33.62\,P - 1.937\,F - 1.6491\,S + 0.001864\,F \times F + 0.000895\,S \times S + 0.1766\,P \times F + 0.13409\,P \times S + 0.001657\,F \times S \quad \ldots\ldots (4.1)$$

$$WW = 32264 - 6129\,P - 96.30\,F - 31.21\,S + 280.4\,P \times P - 0.1241\,F \times F - 0.009003\,S \times S + 11.584\,P \times F + 3.547\,P \times S + 0.06229\,F \times S \quad \ldots\ldots (4.2)$$

4.5. ANOVA Analysis for Responses

ANOVA is performed to evaluate the significant terms and adequacy measures such as R^2, R^2-adjusted and R^2-predicted of developed model. Model terms with a "Prob > f" <0.05 imply that the model terms are statistically significant at the 95 % confidence level. Since p-value of P×P is 0.793 so it does not add much input to the regression equation of weld strength and does not affect much on response. So, it is removed and final regression equation is generated. Table 4.3 shows the ANOVA table with S, R^2, adjusted R^2, and predicted R^2 of the quadratic model. The model terms are statistically significant if the p-value is less than 0.05 for the model (95% confidence level). The value of lack-of-fit should be insignificant so that the experimental value fits the model accurately.

Table 4.3. ANOVA results for weld shear strength (after backward elimination).

Source	DF	Adj. SS	Adj. MS	F-value	P-value
Model	8	313.782	39.223	1437.30	0.000
Linear	3	220.951	73.650	2698.90	0.000
P	1	0.670	0.670	24.54	0.000
F	1	10.197	10.197	373.66	0.000
S	1	210.085	210.085	7698.48	0.000
Square	2	55.712	27.856	1020.78	0.000
F × F	1	0.111	0.111	4.07	0.069
S × S	1	33.238	33.238	1218.00	0.000
2-way interaction	3	37.118	12.373	453.39	0.000
P × F	1	1.343	1.343	49.22	0.000
P × S	1	27.871	27.871	1021.31	0.000

Source	DF	Adj. SS	Adj. MS	F-value	P-value
F × S	1	7.904	7.904	289.65	0.000
Error	11	0.300	0.027		
Lack-of-fit	6	0.222	0.037	2.37	0.182
Pure error	5	0.078	0.016		
S = 0.165194, R-sq. = 99.90 %, R-sq. (adjusted) = 99.83 %, R-sq. (predicted) = 99.60 %					

ANOVA has been analyzed to see the influence of each parameter on weld seam width. The model having p-value of less than 0.05 (i.e. 95% confidence level) are considered significant parameter. Quadratic relationship has been used to establish the relationship which fit the model well. Table 4.4 shows the ANOVA table with S, R^2, adjusted R^2, and predicted R^2 of the quadratic model. The model terms are statistically significant if the p-value is less than 0.05 for the model (95% confidence level). The value of lack-of-fit should be insignificant so that the experimental value fits the model accurately.

Table 4.4. ANOVA results for weld seam width (after backward elimination).

Source	DF	Adj. SS	Adj. MS	F-value	P-value
Model	9	44927.7	4992.0	247.80	0.000
Linear	3	2956.1	985.4	48.91	0.000
P	1	168.1	168.1	8.34	0.016
F	1	291.6	291.6	14.47	0.003
S	1	2496.4	2496.4	123.92	0.000
Square	3	5515.3	1838.4	91.26	0.000
P × P	1	626.3	626.3	31.09	0.000
F × F	1	423.5	423.5	21.02	0.001
S × S	1	2888.5	2888.5	143.38	0.000
2-way interaction	3	36456.4	12152.1	603.23	0.000
P × F	1	5778.1	5778.1	286.82	0.000
P × S	1	19503.1	19503.1	968.13	0.000
F × S	1	11175.1	11175.1	554.73	0.000
Error	10	201.5	20.1		
Lack-of-fit	5	130.0	26.0	1.82	0.264
Pure error	5	71.5	14.3		

Source	DF	Adj. SS	Adj. MS	F-value	P-value
S = 4.48834, R-sq. = 99.55 %, R-sq. (adjusted) = 99.155 %, R-sq. (predicted) = 97.53 %					

4.6. Parametric Analysis

4.6.1. Weld shear strength

Figure 4.4 signifies the main effect plot of weld strength vs. process parameters. It is observed that weld strength is decreasing with an increase of laser power up to midpoint, and after that weld strength started to incline with an increase of laser power. The same pattern follows the weld strength relative to pulse frequency. Scanning speed is inversely proportional to the heat input, thus, less heat input is delivered into the weld zone. This is because weld strength decreases with an increase of scanning speed.

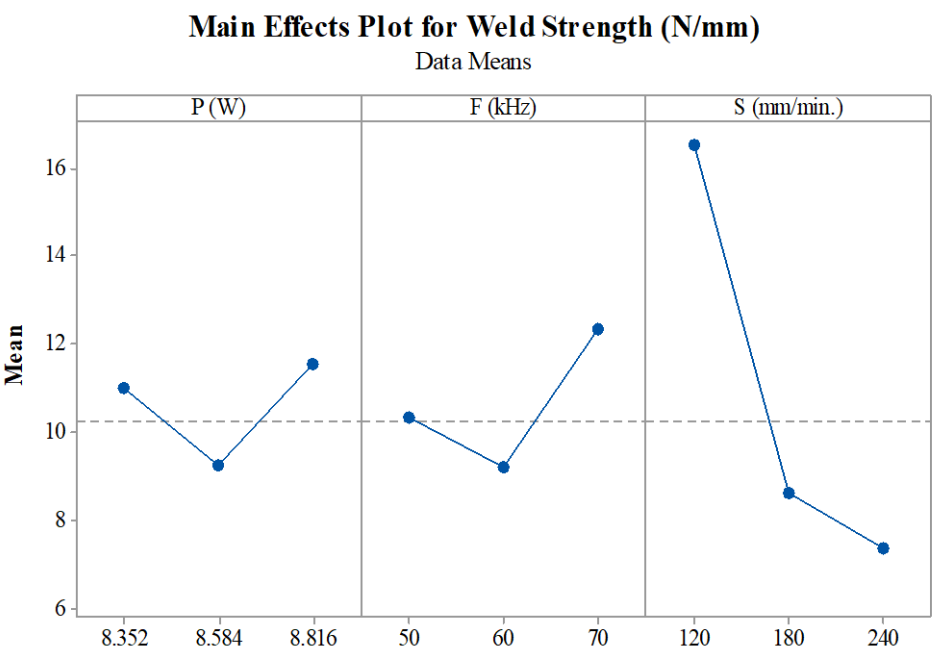

Figure 4.4. Main effects plot of weld strength vs. process parameters

Figure 4.5 shows the surface interaction plot of welding speed (S) and laser power (P) on weld shear strength when frequency (F) is 60 kHz. It is observed from the plot that maximum weld strength is achieved at higher laser power. When the laser power is increasing, the weld shear strength is increasing after a certain level. This happens because laser power increases the weld heat input, results in increased melt volume and weld strength until critical temperature of decomposition is reached. Lower line energy leads to poor heat transfer, lack

of penetration, and poor intermixing of materials that causes an undesirable weld. Line energy (i.e. laser power to welding speed) is defined as the ratio of laser input energy per unit length. Generally, the larger the laser energy input and lower welding speed can cause the greater amount of energy input. It is seen that weld shear strength is higher at low welding speed. This happens due to the fact that energy deposition and heat diffusion into the material in laser transmission welding depends on the laser power density and the irradiation time, and a higher welding speed lowers the irradiation time, causing low- heat input to the weld zone, leading to less volume of base material being melted. Thus, the weld strength decreases. It can be observed that laser power is more dominant parameter than welding speed in the interaction effect of laser power and welding speed on weld shear strength. Optimum value of laser power and welding speed are required to get the optimum Lap-shear weld Strength.

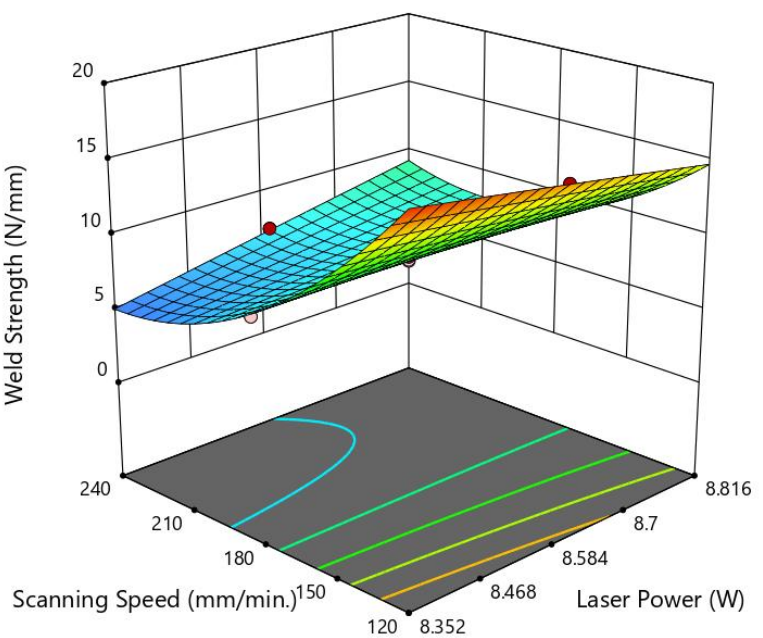

Figure 4.5. Surface plot of weld shear strength vs. laser power and welding speed

Figure 4.6 shows the surface interaction plot of frequency (F) and welding speed (S) on lap shear weld strength when laser power is 8.584 watt. It can be clearly seen that welding speed is increasing, resulting the weld strength decreases.

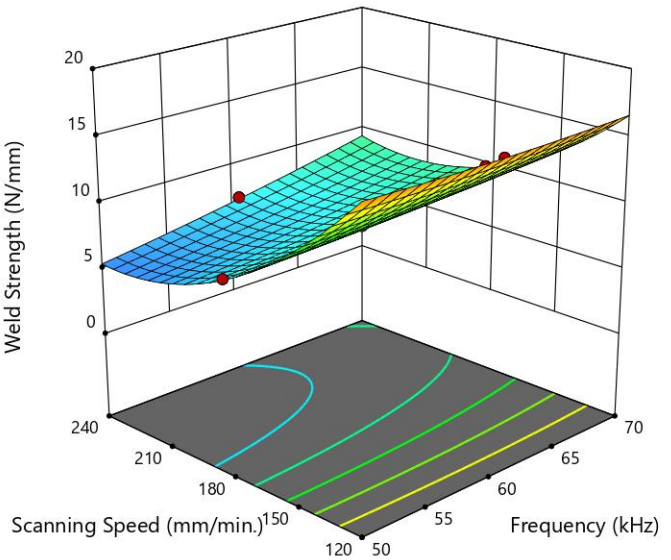

Figure 4.6. Surface plot of weld shear strength vs. welding speed and pulse frequency

In the case of low welding speed, interaction time between the laser and material longer, resulting in a larger heat input to the weld. This enables conduction of significant heat from fusion zone to surrounding base material; this leads to increase in overall heat loss owing to conduction. This results in wider and deeper weld pool. Conversely, the interaction time between laser and material diminishes at higher welding speeds. This results minimization of heat loss by conduction. Consequently, the weld pool becomes narrower and shallower. The laser pulse frequency acts as one of the major determinants of weld strength. It may be noted that at lower pulse frequency, every pulse generates higher energy, which subsequently lead to deeper penetration. On the other hand, more uniform energy distribution and overlapping pulses are produced by higher pulse frequency, which results in consistent melting and solidification. Metallurgical bonding, weld strength and surface finish are improved as a result. Optimum value of welding speed and frequency are required to get the optimum Lap-shear weld Strength.

4.6.2. Weld seam width

Figure 4.7 signifies the main effect plot of weld seam width vs. process parameters. It is observed that weld width is increasing with an increase of laser power up to mid-point, and after that weld width started to decline with an increase of laser power. The same pattern follows the weld width relative to pulse frequency and scanning speed.

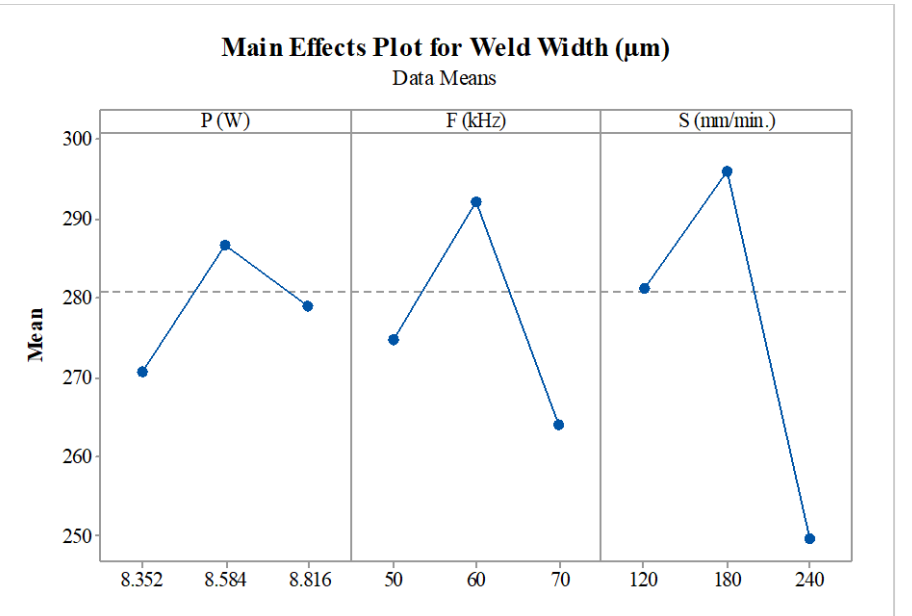

Figure 4.7. Main effects plot of weld strength vs. process parameters

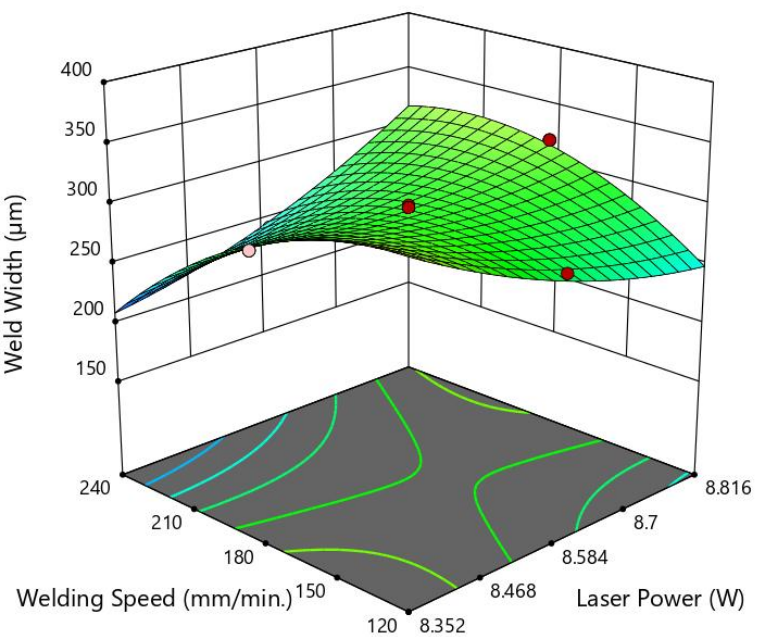

Figure 4.8. Surface plot of weld width vs. laser power and welding speed

Figure 4.8 shows the surface interaction plot of laser power (P) and welding speed (S) on weld width when frequency (F) is 60 kHz. It is observed from the plot that minimum weld width is achieved at lower laser power, higher pulse frequency and higher scanning speed. Larger volume of base material is melted with increased laser power and thus, seam width of the weld zone increases. Increment of weld heat input across the weld line results to greater

bulk of base material being melted, therefore the welded zone width increases. At lower laser power and higher welding speed, the desired minimum weld width is achieved. It may be caused due to the low line energy, which directly varies with laser power and inversely proportional to the welding speed. The surface plot indicates that welding speed has negative effect on weld seam width. This is because, with an increase in welding speed, irradiation time is reduced and less heat is produced, resulting in a decrease in the volume of the molten material resulting in a small and poor weld. Optimum value of Laser power and welding speed are required to get the optimum weld width.

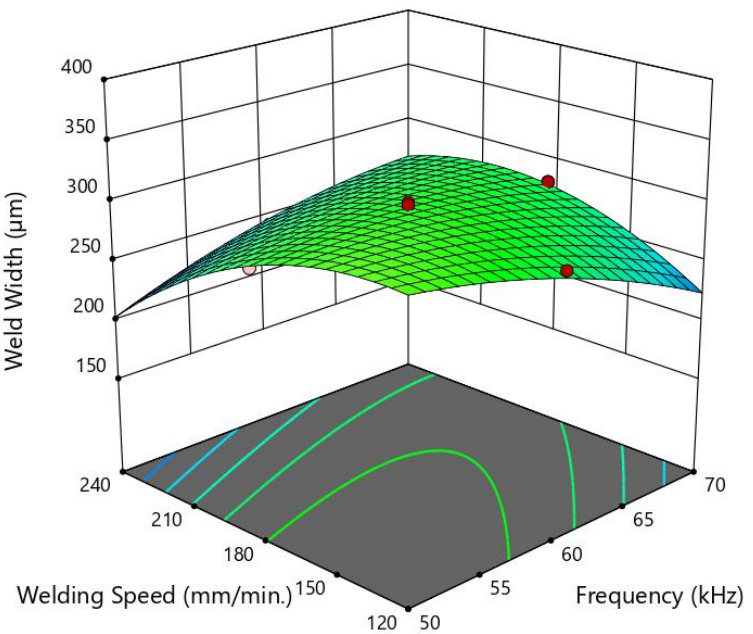

Figure 4.9. Surface plot of weld width vs. welding speed and pulse frequency

Figure 4.9 shows the surface interaction plot of frequency (F) and welding speed (S) on weld width when laser power is 8.584 watt. It is clear from the graph that weld width is minimum at higher frequency (F) and higher welding speed (S). This happens due to the fact that line energy (i.e. laser power to welding speed) varies inversely to the welding speed. Welding speed is most dominant factor on weld width followed by frequency. This dominance is attributed to the direct effect of welding speed on the heat input of the weld. At low welding speed, the line energy maximizes the laser heat input to the weld region leading to greater amount of material being melted, resulting in a wider weld width. At higher welding speed, interaction time reduces between laser and materials, leading to lower heat input and lesser weld width. In comparison, frequency affects the weld width by determining the number of

overlapping pulses within a given length of weld. Increase of frequency tends to decrease the interaction time, results in low line energy. Optimum value of frequency and welding speed are required to get the optimum weld width.

4.7. Optimization Based on SDCS Technique

One of the disadvantages of Cuckoo search is the unstable convergence which can be solved by a balance between exploration and exploitation as given by [108]. Snap prevents convergence into a local optima and drift enables fast convergence. The algorithm can function in two modes which is decided by the performance measure P_m which is,

$$P_m = \frac{\text{Number of improved solutions}}{\text{Number of evaluated solution}} \quad \ldots\ldots\ldots\ldots\ldots\ldots\ldots\ldots\ldots\ldots \quad (4.3)$$

If, P_m is between 0 and 0.5, the algorithm functions ins snap mode and is P_m is between 0.5 and 1 the algorithm functions in drift mode.

Here, the main goal is to maximize the weld strength (WS) and minimize the weld seam width (WW) concurrently even if both the objective functions are inversely proportional to each other. Maximizing one function causes minimization of the other and vice versa. Here, the priori method (among the two standard methods) of multi-objective optimization with equal weights given to both the functions and obtaining a single minimization objective function by adding the normalized inverse of the WS function to the normalized WW function.

The values of the two function are normalized using equation (4.4) and (4.5) at each iteration and then use those normalized values in the singular minimization function to obtain the single objective function value given in equation (4.6) at each iteration and then rank them from low to high and the singular function with lowest value has the component functions with optimal values and their parameters as the optimal parameters.

$$\text{Norm}_{(1/WS)} = \frac{(1/WS) - \text{Min}(1/WS)}{\text{Max}(1/WS) - \text{Min}(1/WS)} \quad \ldots\ldots\ldots\ldots\ldots\ldots\ldots \quad (4.4)$$

$$\text{Norm}_{(WW)} = \frac{(WW) - \text{Min}(WW)}{\text{Max}(WW) - \text{Min}(WW)} \quad \ldots\ldots\ldots\ldots\ldots\ldots\ldots \quad (4.5)$$

$$\text{Theta}\ (X_i) = \text{Norm}_{(1/WS)} + \text{Norm}_{(WW)} \quad \ldots\ldots\ldots\ldots\ldots\ldots\ldots \quad (4.6)$$

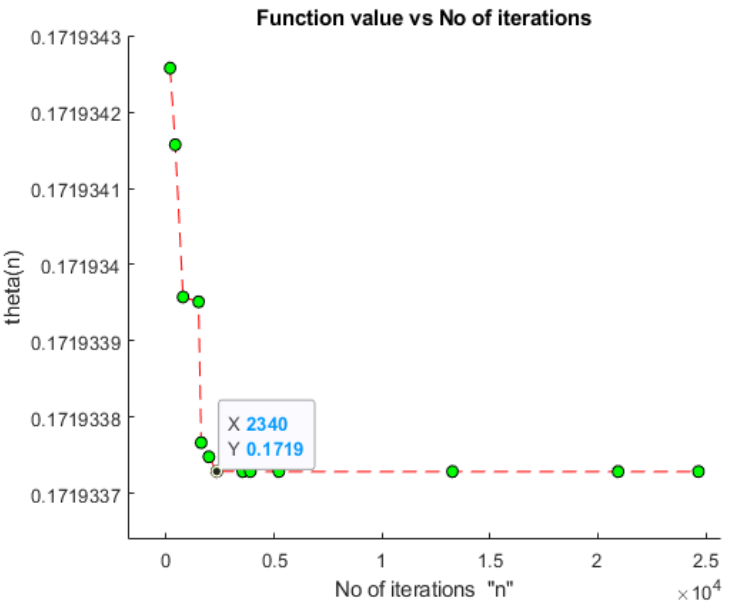

Figure 4.10. Pareto front obtained between theta and number of iteration in CS technique

To compare the speed and find out the advantages of SDCS over CS in our experiment, Theta (n) versuss number of iterations is plotted firstly in case of Cuckoo Search followed by that in Snap Drift Cuckoo Search. Figure 4.10 represents plot of Cuckoo Search Algorithm and Figure 4.11 represents the plot of Snap Drift Cuckoo Search (SDCS) algorithm. Two parameters are used such as Time and No. of Iterations, till optimal value is reached. As we can notice in the plot of Cuckoo Search, the function reaches the minimum value after 2340 iterations whereas in Snap Drift Cuckoo Search, the function reaches the minimum value after 300 iterations only thereby proving that in this case the SDCS has a convergence rate almost 8 times that of CS.

Now, coming to the time to optimal value, it has been found out that in case of SDCS it is 0.2309 seconds and in case of CS it is 0.4148 seconds which is almost twice that in case of SDCS. This analysis has been conducted using MATLAB 9.8 under Windows 10 on a hardware platform using i5 9400F processor and 16 GB of RAM. Conclusion can be drawn from the aforementioned data points that SDCS is more computationally efficient compared to CS in our experiment. Now, L shaped Pareto front is obtained of the function Theta (X_i) against the number of iterations (n) as shown in Figure 4.11 and can easily see that the snap-drift implementation within the cuckoo search model increased the initial convergence rate manifold by operating in the DRIFT mode initially and then switching to SNAP mode later as it exudes slow convergence to global optima.

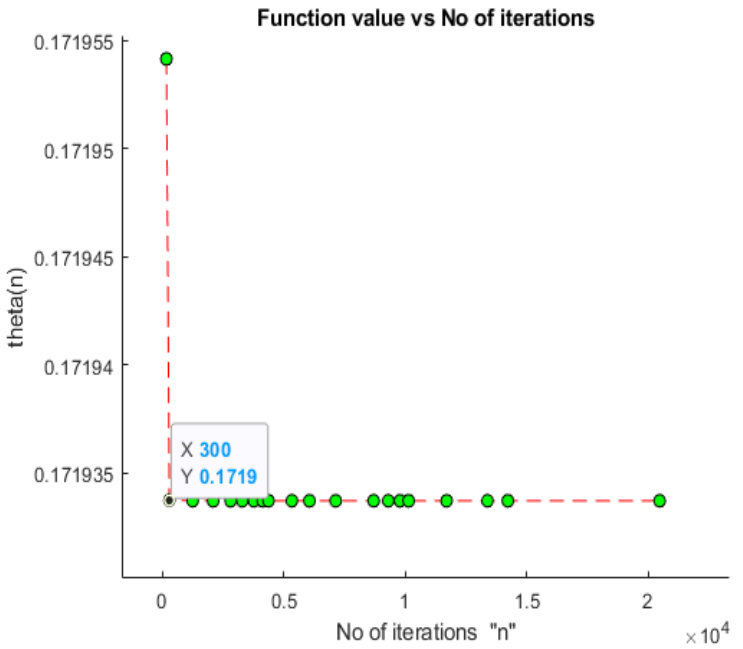

Figure 4.11. Pareto front obtained between theta and number of iteration in SDCS technique

4.8. Validation Experiments

The optimal values of weld strength (WS) is 15.949 N/mm and weld width (WW) is 222.225 µm at optimum parameter settings. A confirmation test has been conducted to calculate the percentage error as shown in Table 4.5.

Table 4.5 WS and WW values after confirmation test

Optimized value from SDCS			Confirmation test	%Error
Process Parameters	P (W)	8.69	8.69	
	F (kHz)	70	70	
	S (mm/min.)	120	120	
Performance Parameters	WS (N/mm)	15.949	15.607	2.144
	WW (µm)	222.225	229.713	3.369

4.9. Morphological Analysis

Weld zone surface has been analysed through scanning electron microscope (SEM) for their morphological characterization as shown in Fig. 4.12-4.13 at different magnification. SEM image has been taken of the top surface of weld bead. Fig. 4.12 shows the welded zone surface

between PPCP and acrylic. It can be clearly said from Fig. 4.13 that fibrillation in PPCP phase is more than acrylic phase. This may happen due to the semicrystalline nature of PPCP [7].

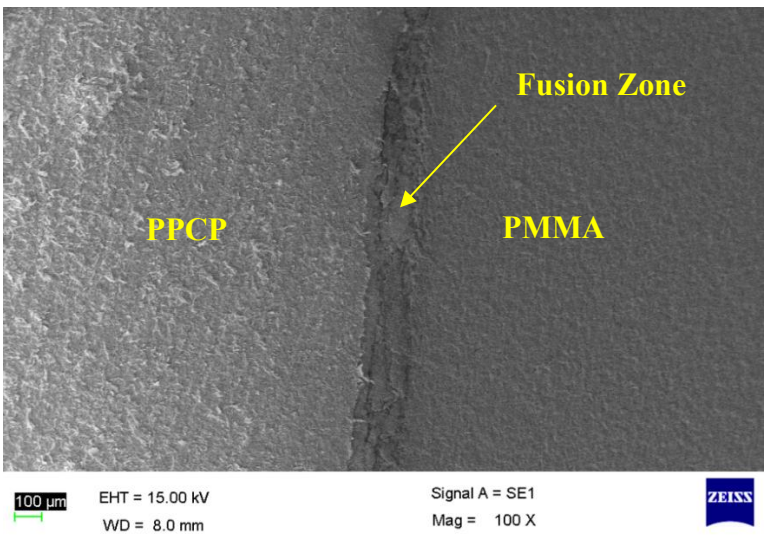

Figure 4.12. SEM micrograph of the weld zone of PPCP-Acrylic at 100X

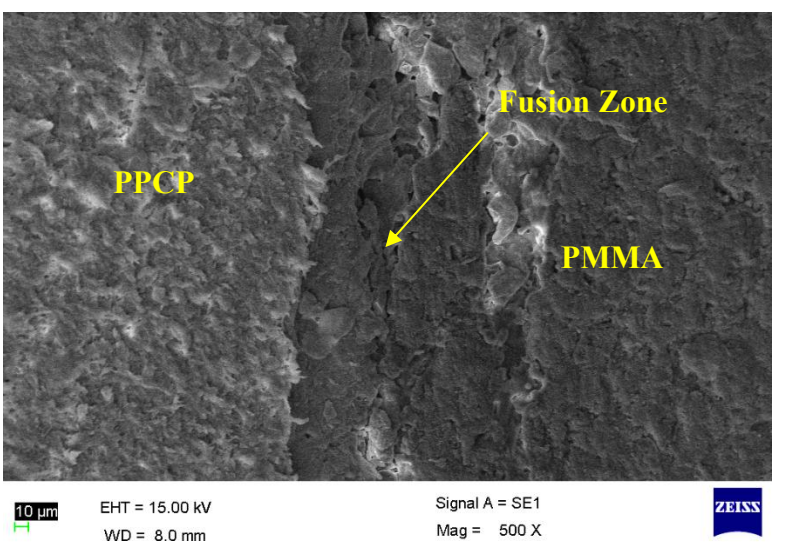

Figure 4.13. SEM micrograph of the weld zone of PPCP-Acrylic at 500X

White ink absorbent seems to be effective for inducing fibrillation in to amorphous and thereby mechanical interlocking. It is observed that intermixing of these two polymers happens through white ink and molecular chain interfuse in molten state. The weld quality between amorphous and semi crystalline polymers depends on mechanical interlocking rather than on interfacial bonding. This happens because of the different glass transition temperature of semi crystalline and amorphous polymers [134]. The weld quality affects the lap shear strength. Better interlocking between the layers leads to good adhesion at the joint.

4.10. Outcomes of the Present Research Work

An attempt has been made here to weld the two 4mm thick semi crystalline and amorphous thermoplastic materials by low power diode laser welding. An attempt has been made here to weld the two 4 mm thick semi crystalline and amorphous thermoplastic materials by low power diode laser welding. The following conclusion can be said from the experimental study and investigation within the selected range of parameters considered in the present study. The following conclusion can be said from the experimental study and investigation within the selected range of parameters considered in the present study.

1. White ink has applied at the weld interface, which increases the solubility and retain the laser heat.
2. The laser welding between semi crystalline and amorphous polymers seems to be ineffective without the use of white ink.
3. The developed response surface models estimate the responses effectively within the range of welding process parameters.
4. Laser power, frequency and scanning speed have a better interaction effect on weld shear strength and width of weld seam. These parameters control the heat input of laser to the weld area.
5. It is revealed that weld shear strength is higher when laser power and welding speed are smaller. This happens due to the fact that higher laser energy input may cause degradation of base material.
6. It has been found out that scanning speed is more dominant parameter followed by frequency and laser power based on ANOVA.
7. Multi objective snap drift cuckoo search optimization technique is applied to achieve the optimum weld strength of 15.949 N/mm and weld width of 222.225 μm.
8. It has been observed from the SEM that fibrillation in PPCP phase is more than acrylic phase due to semi crystalline nature of PPCP and thereby mechanical anchorage.

CHAPTER: 5

LOW POWER LASER TRANSMISSION WELDING OF POLYCARBONATE TO ACRYLIC

5.1. Modelling and Optimization of Laser Transmission Welding of Polycarbonate to Acrylic without Beam Wobbling Technique

It is well known fact that LTW requires laser transparent polymers and laser absorbent polymers for performing successful welding. Carbon black is generally considered as pigmentation due to its cost effectiveness. Natural polycarbonate and carbon black filled acrylic are used as work material for performing LTW using statistical method. It is always challenging to join two dissimilar thermoplastic materials. The problem happens such as that the materials to be joined must have similar melting temperatures, joining member must be soluble with each other in order to permit diffusion of melts. Response surface methodology is applied to develop the mathematical model between the laser welding process parameters and the responses of weld joint. The developed mathematical model is tested for its adequacy using analysis of variance and other adequacy measures. In the present experimental work, an attempt has been made to join polycarbonate and acrylic. The effect of process parameter such as laser power, pulse frequency and welding speed on responses has been described elaborately. Confirmation experiment has also been performed for validation of experiment within certain limits.

5.1.1. Experimental Planning

A transparent polycarbonate and black carbon filled acrylic plates each of size 70 mm x 35 mm x 2.8 mm are used in this experimental work. A transparent polycarbonate is used as upper part while black carbon filled acrylic is placed on bottom part to perform the transmission laser welding. Black carbon filled acrylic absorbs the laser and after that melting and vaporization happens. A lap joint is created with an overlap area of 20 mm. Laser beam is scanned the middle of the overlap length as shown in Figure 5.1.1.

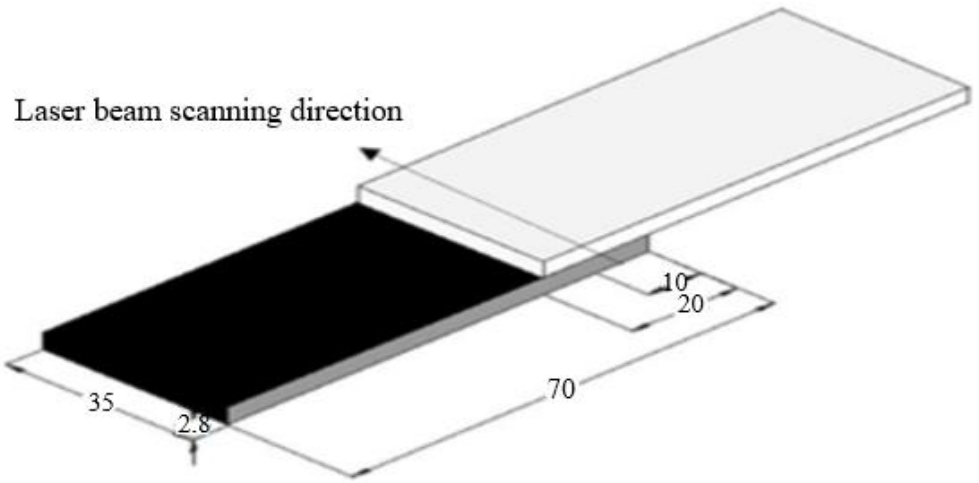

Figure 5.1.1. Weld joint configuration

Central composite unblocked design based on response surface method is used for design of experiment. Based on the literature survey and the specifications of the laser system utilized, a series of trial tests are carried out to establish the possible ranges of process parameters, as shown in Table 5.1.1.

Table 5.1.1. Process control parameters and their levels

Parameter	Notations	Units	Levels				
			-1.68179	-1	0	+1	+1.68179
Laser Power	P	W	4.787	5.104	5.568	6.032	6.348
Welding Speed	S	mm/s	0.159	0.5	1	1.5	1.840
Frequency	F	kHz	18.295	20	22.5	25	26.704

An Instron universal tensile testing machine is used for lap shear test of laser welded sample. It is performed to determine the joint strength. The specimen is labelled approximately 25 mm from the weld centre line before pulling test and the end of the grips is matched with these markings. There is some adjustment to the sample. To avoid bending moments, as shown in the Figure 5.1.2, two polymer sheets measuring 35mm×35mm×2.8mm are pasted with each specimen, thus, the weld is close to the pulling path centreline. After that, each specimen is roughened to avoid slip during the lap-shear test on both sides of two ends. A three-dimensional optical measuring microscope (STM6, OLYMPUS) is used to measure the weld width of all the welded samples. The average weld strength and weld width of at least three tests are taken are considered for analysis.

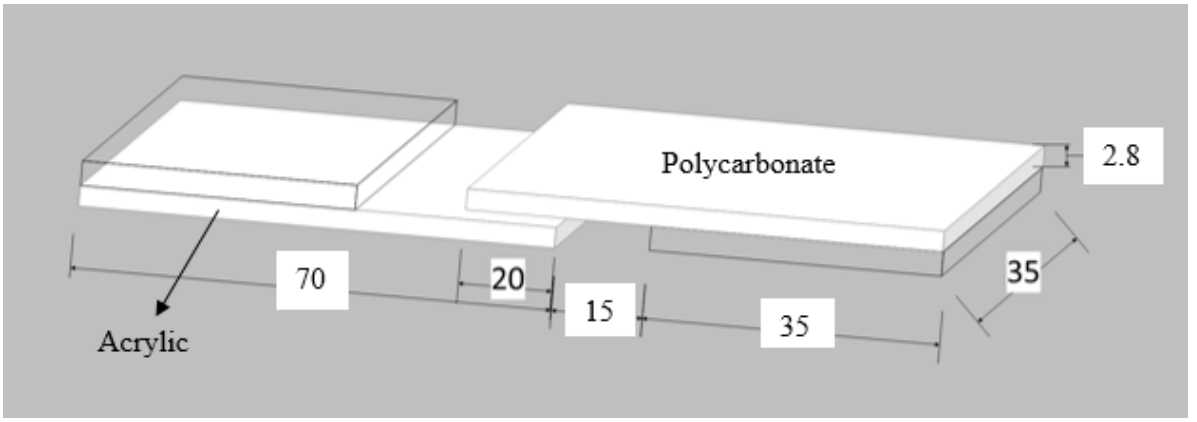

Figure 5.1.2. Schematic diagram of the tensile test specimen

5.1.2. Parametric Analysis Based on RSM Modelling

Table 5.1.2 presents the experimental plan as well as the measured value of the responses.

Table 5.1.2 Design matrix and measured experimental result

Experimental Information				Results	
Exp. No.	Welding Parameters			Weld strength (N/mm)	Weld width (mm)
	P (Watt)	F (kHz)	S (mm/s)		
1	5.104	20	0.5	18.534	2.828
2	6.032	20	0.5	34.016	3.929
3	5.104	25	0.5	19.105	2.705
4	6.032	25	0.5	34.534	4.082
5	5.104	20	1.5	15.392	1.650
6	6.032	20	1.5	22.345	2.250
7	5.104	25	1.5	15.138	1.661
8	6.032	25	1.5	21.938	2.452
9	4.787	22.5	1	17.425	1.354
10	6.348	22.5	1	36.644	2.825
11	5.568	18.295	1	16.059	2.331
12	5.568	26.704	1	16.803	2.447
13	5.568	22.5	0.159	31.158	4.700
14	5.568	22.5	1.84	17.608	2.301
15	5.568	22.5	1	21.5	2.580
16	5.568	22.5	1	21.732	2.466

17	5.568	22.5	1	21.468	2.492
18	5.568	22.5	1	21.808	2.584
19	5.568	22.5	1	21.882	2.484
20	5.568	22.5	1	21.533	2.517

5.1.3. Second Order Regression Equation of Responses

Mathematical models are developed to establish a correlation between input and output parameters to understand the behaviour of process parameters on responses. Design Expert® software is employed for mathematical modelling and parametric analysis. The adequacy of the derived model is tested using the analysis of variance (ANOVA), the F-test, and the lack of fit test.

$$WS = 31.41 - 76.52\,P + 13.596\,F + 39.85\,S + 8.793\,P \times P - 0.29714\,F \times F + 3.815\,S \times S - 9.245\,P \times S - 0.1750\,F \times S \quad \text{(5.1.1)}$$

$$WW = -21.92 + 8.037\,P + 0.028\,F - 0.956\,S - 0.6809\,P \times P - 0.00655\,F \times F + 1.4084\,S \times S + 0.0503\,P \times F - 0.5857\,P \times S \quad \text{(5.1.2)}$$

5.1.4 ANOVA Analysis for Responses

ANOVA is performed to evaluate the significant terms and adequacy measures such as R^2, R^2-adjusted and R^2-predicted of developed model. Model terms with a "Prob > f" <0.05 imply that the model terms are statistically significant at the 95 % confidence level. The fit for weld strength proposes the quadratic model and the model is not aliased. Since p-value of interaction of power on frequency is 0.705, thus, it is considered insignificant parameter and it does not impact much on weld strength. Therefore, in order to improve model accuracy, it is eliminated by the backward elimination process. P-value of lack of fit shows its insignificance model, which is desirable. ANOVA results for weld shear strength is shown in Table 5.1.3.

Table 5.1.3 ANOVA results for weld shear strength (after backward elimination).

Source	DF	Adj. SS	Adj. MS	F-value	P-value
Model	8	811.921	101.490	3113.19	0.000

Source	DF	Adj. SS	Adj. MS	F-value	P-value
Linear	3	648.844	216.487	6634.41	0.000
P	1	434.317	434.317	13311.34	0.000
F	1	0.209	0.209	6.40	0.028
S	1	214.936	214.936	6585.4	0.000
Square	3	125.693	41.898	1296.48	0.000
P × P	1	51.593	51.593	1596.48	0.000
F × F	1	49.690	49.690	1537.62	0.000
S × S	1	13.100	13.100	405.38	0.000
2-way interaction	2	37.182	18.591	575.29	0.000
P × S	1	36.800	36.800	1138.73	0.000
F × S	1	0.383	0.383	11.85	0.006
Error	11	0.355	0.032	-	-
Lack-of-fit	6	0.201	0.033	1.08	0.469
Pure error	5	0.155	0.031	-	-
Total	19	812.277	-	-	--
S = 0.180555, R-sq = 99.96%, R-sq (adjusted) = 99.92%, R-sq (predicted) = 99.83%					

ANOVA has been analyzed to see the influence of each parameter on weld seam width. The model having p-value of less than 0.05 (i.e. 95% confidence level) are considered significant parameter. Since p-value of interaction of frequency on scanning speed is 0.219, thus, it is considered insignificant parameter and it does not impact much on weld width. Therefore, in order to improve model accuracy, it is eliminated by the backward elimination process. P-value of lack of fit shows its insignificance model, which is desirable. ANOVA results for weld seam width is shown in Table 5.1.4.

Table 5.1.4 ANOVA results for weld seam width (after backward elimination).

Source	DF	Adj. SS	Adj. MS	F-value	P-value
Model	8	12.1525	1.51906	580.99	0.000
Linear	3	9.6669	3.22230	1232.42	0.000
P	1	2.9463	2.94631	1126.87	0.000
F	1	0.0141	0.01410	5.39	0.040
S	1	6.7065	6.70649	2565.01	0.000

Source	DF	Adj. SS	Adj. MS	F-value	P-value
Square	3	2.3176	0.77253	295.47	0.000
P × P	1	0.3109	0.31094	118.93	0.000
F × F	1	0.0240	0.02403	9.19	0.011
S × S	1	1.7851	1.78513	682.75	0.000
2-way interaction	2	0.1750	0.08751	33.47	0.000
P × F	1	0.0272	0.02721	10.41	0.008
P × S	1	0.1478	0.14781	56.53	0.000
Error	11	0.0288	0.00261	-	-
Lack-of-fit	6	0.0160	0.00267	1.05	0.486
Pure error	5	0.0127	0.00255	-	-
Total	19	12.1813	-	-	-
S = 0.0511603, R-sq = 99.76%, R-sq (adjusted) = 99.59%, R-sq (predicted) = 99.13%					

5.1.5. Parametric Analysis from the Surface Plot

5.1.5.1. Weld shear strength

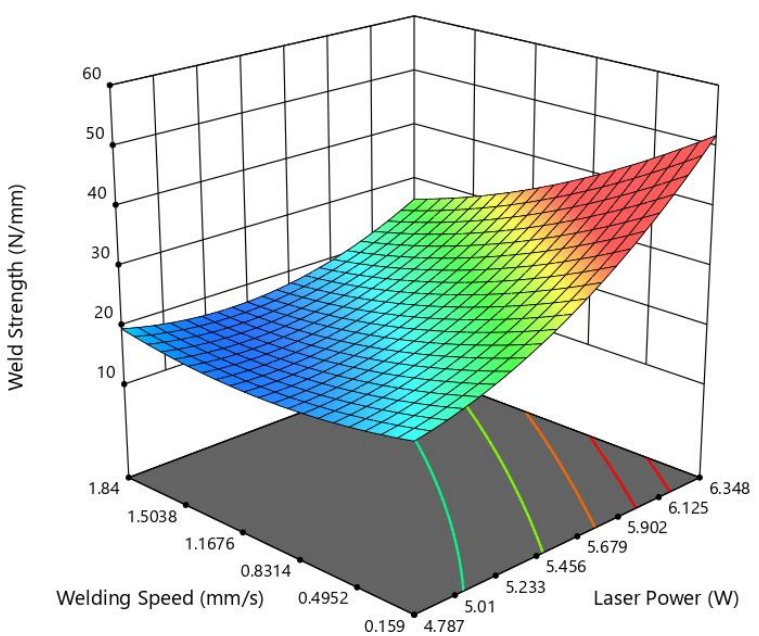

Figure 5.1.3. Surface plot of weld shear strength vs. laser power and welding speed

Figure 5.1.3 shows surface plot of weld shear strength versus laser power and scanning speed. It is evident from the figure that welding or scanning speed has a negative effect on weld shear strength. This happens because heat diffusion and deposition of energy into the material depends on the time of irradiation and the density of power. Higher scanning speed decreases the irradiation time, causes less heat input to the weld zone, resulting in less material being melted, resulting in decreased weld strength. Laser power has also been found to have a positive impact on the weld strength. The reason for the positive effect is that higher laser power increases the input of laser heat to the material, increases the melting area and increases the weld shear strength. It can be clearly observed from the figure that weld strength tends to maximum when laser power is maximum and scanning speed is minimum. This is due to the increased laser power and lower scanning speed that increases the line energy and thus increases the bond strength. Line energy, described as laser heat energy per unit length, is basically defined as the ratio of laser power to the scanning speed.

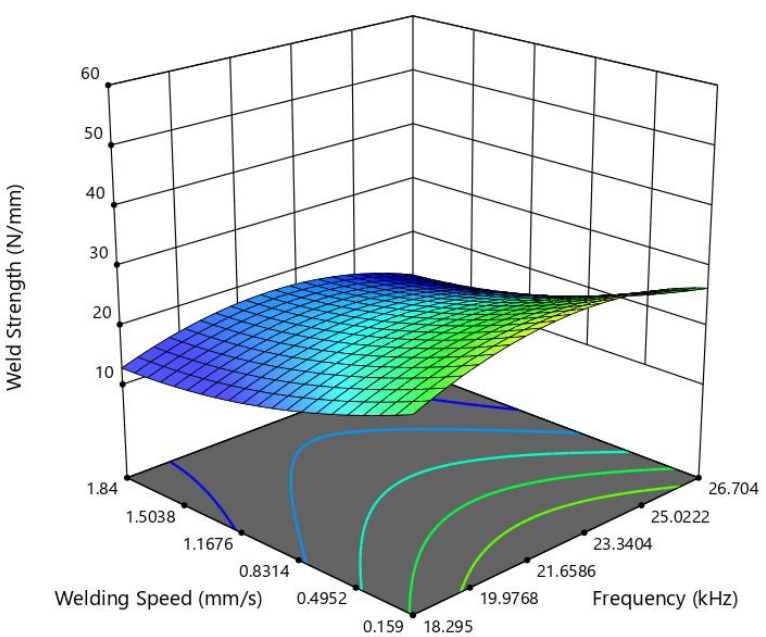

Figure 5.1.4. Surface plot of weld shear strength vs. welding speed and frequency

Figure 5.1.4 shows surface plot of weld shear strength versus welding speed and frequency. It is evident from the figure that weld shear strength is maximum at low scanning speed and at F = 22 kHz. This happens due to the fact that losses in heat conduction have a higher impact at low speed. At high value of welding speed, the heat loss is minimal because there is less heat dissipation time available. Higher scanning speed decreases the irradiation time, causes

less heat input to the weld zone, and thus weld shear strength decreases. Too low frequency tends to narrow the laser beam, causing less amount of laser energy deposition whereas too high frequency spread the laser beam. Here welding speed is most dominant parameter.

5.1.5.2. Weld seam width

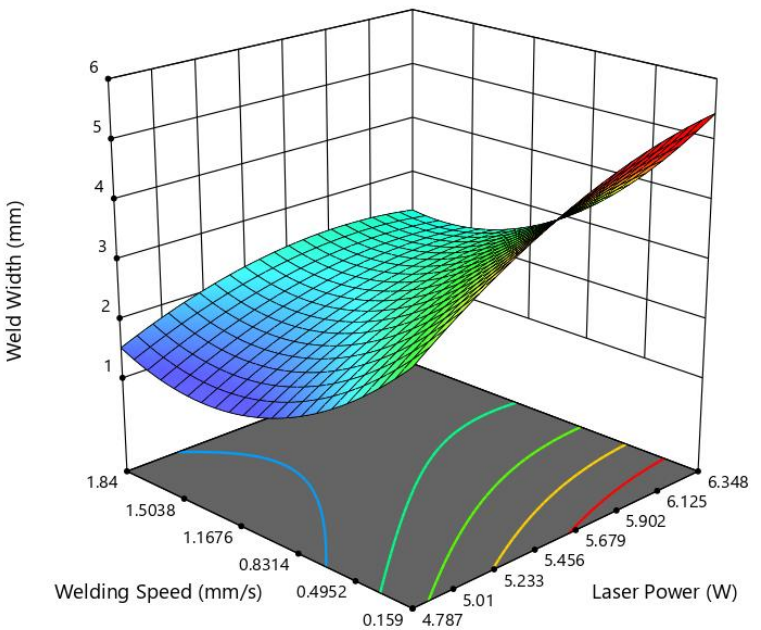

Figure 5.1.5. Surface plot of weld seam width vs. laser power and welding speed

Figure 5.1.5 shows the surface plot of weld seam width versus laser power and welding speed. The weld width is maximum at high value of laser power and low value of welding speed. It is evident from the result that welding speed has a negative effect on weld seam width. This is because increased welding speed decreases irradiation time and allows less heat to be supplied with reduced molten volume resulting in narrow and weak weld formation. It can also be observed that weld width increases with laser power, as higher laser power melts the large amount of base material, thus increasing the weld zone width.

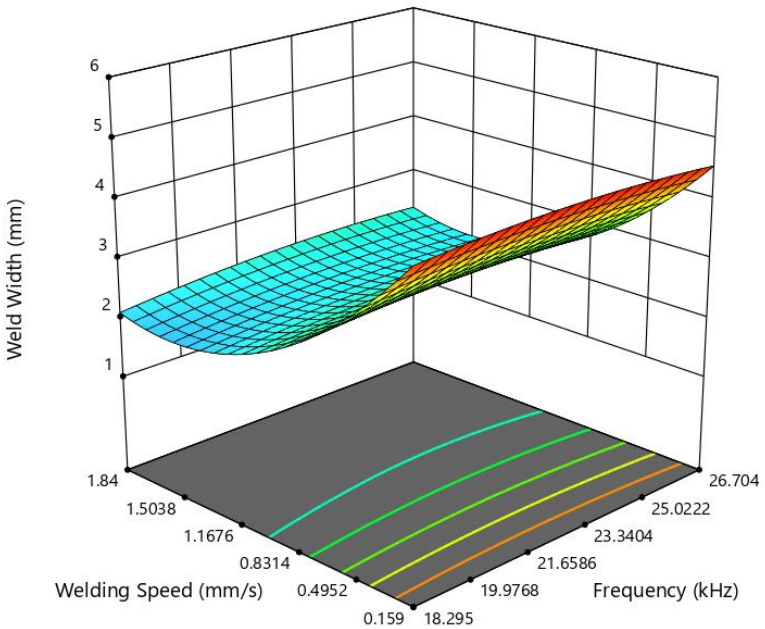

Figure 5.1.6 Surface plot of weld seam width vs. welding speed and frequency

Figure 5.1.6 shows surface plot of weld seam width versus welding speed and frequency. It is revealed from the figure that weld width tends to maximum at low value of welding speed and F = 22 kHz. This is because increment of welding speed reduces the irradiation time, causes less heat is delivered with reduction in molten volume resulting in formation of narrow and weak weld. Too low frequency tends to narrow the laser beam, causing less amount of laser energy deposition whereas too high frequency spread the laser beam. Optimum value of welding speed and frequency are required to get the optimum weld seam width.

5.1.6. Optimization Based on RSM

Desirability function-based optimization technique is used to determine the optimum process parameter which simultaneously maximize the weld shear strength and minimizes weld seam width. Multi-objective optimization technique is carried out numerically by choosing the desired objectives for each response using desirable function.

Table 5.1.5 Optimal value of weld shear strength and weld seam width

P (W)	F (kHz)	S (mm/s)	Weld shear strength (N/mm)	Weld seam width (mm)
6.348	21.437	1.1268	34.3173	2.61547

Table 5.1.5 represents the optimum welding process parameter which gives the optimized value of response. Figure 5.1.7 shows the optimization plot between process parameter and response. Figure 5.1.8 shows the overlaid contour plot of weld strength and weld seam width. Maximum weld strength and minimum weld width is found at higher laser power and mid value of scanning speed.

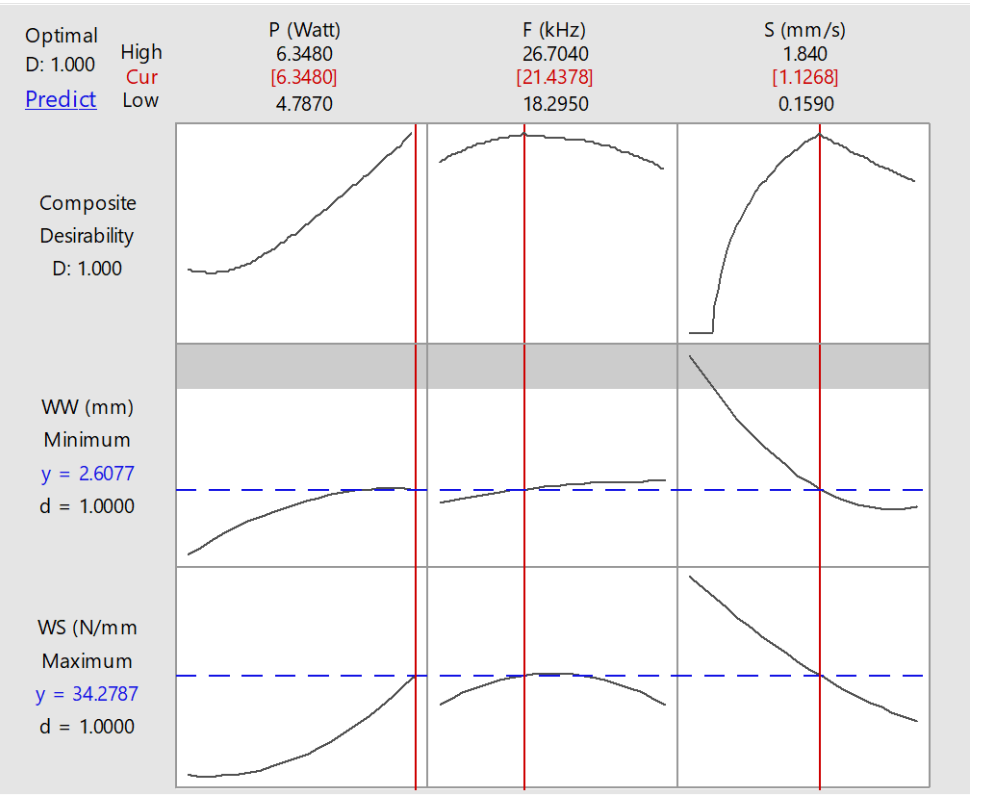

Figure 5.1.7 Multi-objective Optimization

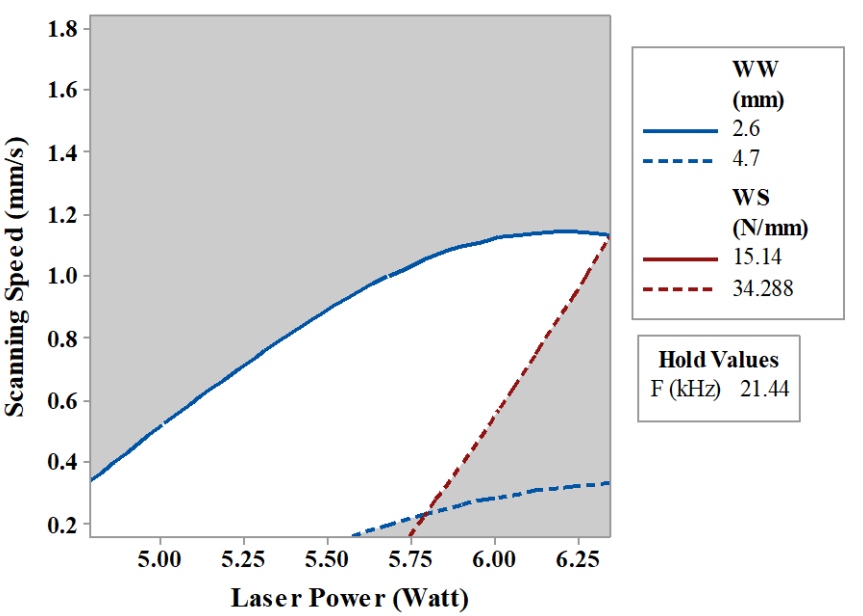

Figure 5.1.8 Overlaid contour plot of WS and WW

5.1.7. Validation Experiments

The optimal solutions thus obtained are as given in Table 5.1.6. Finally, a confirmation experiment has been conducted at optimum parameter setting to find the generated error, and it has been found that weld strength has an error of 3.491% whereas weld seam width has an error of 3.726% (Table 5.1.6) which is very minimal and acceptable.

Table 5.1.6 Confirmation Test

Optimized value from Desirability analysis			**Confirmation test**	**%Error**
Process Parameters	P	6.348	6.348	
	F	21.437	21.437	
	S	1.1268	1.1268	
Performance Parameters	WS	34.278	33.119	3.491
	WW	2.61	2.518	3.726

5.2. Modelling and Optimization of Laser Transmission Welding of Polycarbonate and Acrylic with Beam Wobbling Technique

It can be said from the literature survey that a good amount of research has been carried out in the area of laser transmission welding of similar or dissimilar thermoplastic materials. There are very few literatures covering the multi objective optimization of process parameters in laser transmission welding of thermoplastic materials by Particle swarm optimization technique. To the best knowledge of authors, scant amount of investigation has been done in the area of joining of dissimilar thermoplastic material by laser beam wobbling approach. In the current research work, transparent polycarbonate and black carbon filled acrylic is joined by low power laser with beam wobbling technique to improve the responses of weld joint. PSO has also been used to optimize the process parameters to improve the effectiveness of responses. Here, effect of wobble frequency and wobble width are studied along with other process parameters. Response surface methodology has been used to model the laser welding process parameters and responses of welding through regression analysis. The results of ANOVA reveal that the models formed appropriately predict the responses within the range of process parameters. A confirmation experiment has also been conducted to validate the results. A multi objective optimization has been used to find the optimum solution by Particle swarm optimization technique.

5.2.1. Experimental Planning

The experimental work has been performed on Electrox EMS 100 Raptor laser system. The Nd: YVO_4 (Neodymium doped Yttrium Orthovanadate) diode laser with available laser power of 9.28 W and 1064 nm wavelength have been used for laser transmission welding of thermoplastic materials. A COMSOL marker software is used to control the operation of laser. Stand-off distance, beam spot diameter and number of passes are fixed in this experimentation. A constant pressure is applied between two workpiece materials. The workpiece material for laser transmission welding is as shown in Figure 5.2.1. Here, central composite unblocked design with five continuous factors P (laser power), F (welding frequency), S (scanning speed), W (wobble width) and L (wobble frequency) are used for design of experiment. It contains 32 sets of coded conditions comprising of sixteen factorial designs plus six center points and ten-star points. Thus, the total 32 number of experiments has to be performed.

If all process parameters are measurable, controllable and continuous throughout experiments, the response surface y may be represented by:

$$y = f(P, F, S, W, L)$$

Where y is the response and it depends on P, F, S, W and L.

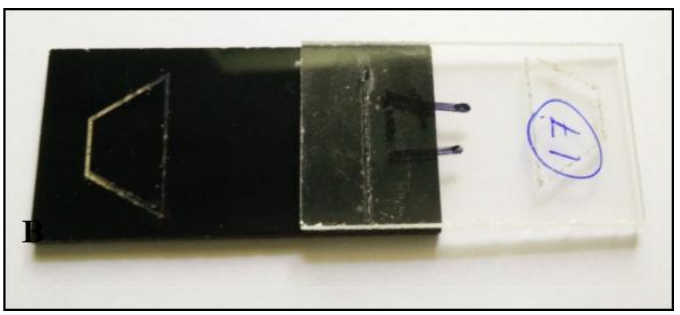

Figure 5.2.1 Welding Specimen

A polycarbonate and acrylic each of size 70 mm x 35 mm x 2.8 mm are chosen as workpiece material during experimentation. In this experimental work, transparent acrylic are placed on top surface and black carbon filled acrylic is used in a bottom layer to absorb the laser radiation properly. No extra absorbent are used. A lap joint is created with a 20 mm overlap area and 10 mm weld centre line. The limit of the input parameters and their levels are decided based on the trial experiment, literature review and machine limitations as given in Table 4.7.

Table 5.2.1 Selected range of process parameters and their levels

Parameters	Symbol	Units	Level				
			-2	-1	0	+1	+2
Laser Power	P	Watt	5.48	5.75	6.03	6.31	6.59
Welding frequency	F	kHz	20	22	24	26	28
Welding speed	S	mm/sec	1.5	2	2.5	3	3.5
Wobble width	W	mm	1	2	3	4	5
Wobble frequency	L	kHz	1	2	3	4	5

To assess the relative strength of weld joint, a microprocessor-controlled Instron universal tester with an accuracy of ±0.4% is used for lap shear pull test. Some adjustments are made (two plastic sheets measuring 35mm×35mm×2.8mm are pasted) to the welded samples to be shear tested to mitigate the bending moment, so the weld is similar to the pulling path centre line. The shear strength is measured as the total failure load per weld unit length. A three-

dimensional optical measuring microscope (STM-6, OLYMPUS) is used to measure the weld width of all welded samples. For experimental analysis, the average of at least three measurements of both lap-shear tests and weld width is determined.

5.2.2. Parametric Analysis Based on RSM Modelling

The result of experiment has been collected after thirty-two experiments conducted using the design of experiment as shown in Table 5.2.2.

Table 5.2.2 Design matrix and measured experimental result

S. No.	P (W)	F (kHz)	S (mm/s)	W (mm)	L (kHz)	WS (N/mm)	WW (mm)
1	5.75	22	2	2	4	15.235	1.9309
2	6.31	22	2	2	2	17.502	2.0918
3	5.75	26	2	2	2	20.167	2.0178
4	6.31	26	2	2	4	14.523	2.1314
5	5.75	22	3	2	2	16.857	1.7490
6	6.31	22	3	2	4	12.608	1.8210
7	5.75	26	3	2	4	21.524	1.7041
8	6.31	26	3	2	2	16.726	1.8510
9	5.75	22	2	4	2	14.912	2.7712
10	6.31	22	2	4	4	24.283	2.7014
11	6.31	26	2	4	4	23.394	2.7282
12	6.31	26	2	4	2	21.902	2.8905
13	5.75	22	3	4	4	13.342	2.5741
14	6.31	22	3	4	2	15.026	2.7003
15	5.75	26	3	4	2	11.194	2.6511
16	6.31	26	3	4	4	19.138	2.6470
17	5.48	24	2.5	3	3	18.679	2.1722
18	6.59	24	2.5	3	3	20.958	2.3393
19	6.03	20	2.5	3	3	18.568	2.2704
20	6.03	28	2.5	3	3	22.327	2.2986
21	6.03	24	1.5	3	3	21.241	2.5013
22	6.03	24	3.5	3	3	16.112	2.1378

S. No.	P (W)	F (kHz)	S (mm/s)	W (mm)	L (kHz)	WS (N/mm)	WW (mm)
23	6.03	24	2.5	1	3	10.316	1.6492
24	6.03	24	2.5	5	3	10.997	3.2014
25	6.03	24	2.5	3	1	19.594	2.3148
26	6.03	24	2.5	3	5	20.965	2.1921
27	6.03	24	2.5	3	3	20.987	2.2659
28	6.03	24	2.5	3	3	21.117	2.3008
29	6.03	24	2.5	3	3	20.883	2.2879
30	6.03	24	2.5	3	3	21.020	2.2936
31	6.03	24	2.5	3	3	21.110	2.2701
32	6.03	24	2.5	3	3	20.942	2.3043

5.2.3. Second Order Regression Equation of Responses

Mathematical models are developed to establish a correlation between input and output parameters to understand the behaviour of process parameters on responses. Design Expert® software is employed for mathematical modelling and parametric analysis. The adequacy of the derived model is tested using the analysis of variance (ANOVA), the F-test, and the lack of fit test.

$$Weld\ Strength = -278.4 + 65.91 \times P + 7.438 \times F + 25.84 \times S - 21.974 \times W + 1.847 \times L - 4.149 \times P \times P - 0.03983 \times F \times F - 2.4123 \times S \times S - 2.4083 \times W \times W - 0.2013 \times L \times L - 0.9611 \times P \times F - 3.738 \times P \times S + 7.675 \times P \times W - 1.455 \times P \times L + 0.4584 \times F \times S - 0.2285 \times F \times W + 0.0689 \times F \times L - 2.68 \times S \times W + 1.062 \times S \times L + 1.2404 \times W \times L \quad \text{(5.2.1)}$$

$$Weld\ Width = -1.03 + 1.33 \times P - 0.1282 \times F - 0.4779 \times S + 0.346 \times W + 0.0376 \times L - 0.1288 \times P \times P + 0.03272 \times W \times W - 0.01024 \times L \times L + 0.02210 \times P \times F - 0.0469 \times P \times W + 0.0775 \times S \times W + 0.0207 \times S \times L - 0.02074 \times W \times L \quad \text{(5.2.2)}$$

5.2.4. ANOVA Analysis for Responses

ANOVA is performed to evaluate the significant terms and adequacy measures such as R^2, R^2-adjusted and R^2-predicted of developed model. Model terms with a "Prob > f" <0.05

imply that the model terms are statistically significant at the 95 % confidence level. ANOVA is applied to the outcome obtained during experimentation to visualize the influence of individual process parameter on weld strength. A confidence interval of 95% has been used to check the level of significance. It can be seen that all factors have significant value. Table 5.2.3 shows the finding of ANOVA for weld shear strength.

Table 5.2.3 ANOVA results for weld shear strength (after backward elimination).

Source	DF	Adj. SS	Adj. MS	F-value	P-value
P	1	6.148	6.148	510.34	0.000
F	1	16.794	16.794	1394.07	0.000
S	1	35.861	35.861	2976.81	0.000
W	1	1.183	1.183	98.18	0.000
L	1	2.158	2.158	179.12	0.000
P × P	1	2.965	2.965	246.09	0.000
F × F	1	0.744	0.744	60.98	0.000
S × S	1	10.521	10.521	870.88	0.000
W × W	1	196.766	196.766	16329.32	0.000
L × L	1	1.183	1.183	97.37	0.000
P × F	1	3.205	3.205	262.03	0.000
P × S	1	2.947	2.947	226.28	0.000
P × W	1	50.231	50.231	4177.26	0.000
P × L	1	1.844	1.844	150.09	0.000
F × S	1	2.696	2.696	207.01	0.000
F × W	1	2.680	2.680	205.76	0.000
F × L	1	0.405	0.405	31.11	0.000
S × W	1	23.428	23.428	1934.50	0.000
S × L	1	3.624	3.624	303.79	0.000
W × L	1	20.081	20.081	1657.54	0.000
Error	11	0.143	0.013	-	-
Lack of fit	6	0.090	0.015	1.74	0.279
Pure Error	5	0.043	0.009	-	-
Total	31	454.657	-	-	-
S = 0.109758, R-sq = 99.97%, R-sq (adjusted) = 99.92%, R-sq (predicted) = 99.48%					

ANOVA is applied to the outcome obtained during experimentation to visualize the influence of individual process parameter on weld width. A confidence interval of 95% has been used to check the level of significance. It is seen from ANOVA that squared interaction of frequency, squared interaction of speed, interaction of power on speed, interaction of power on wobble frequency, interaction of frequency on speed, interaction of frequency on wobble width and interaction of frequency on wobble frequency are insignificant parameter. Since the p- value of these parameters are greater than 0.05 which is undesirable. Thus, these parameters does not add much impact on weld width. Hence, it is removed by backward elimination process and new regression equation is generated. Table 5.2.4 shows the finding of ANOVA.

Table 5.2.4 ANOVA results for weld seam width (after backward elimination).

Source	DF	Adj. SS	Adj. MS	F-value	P-value
P	1	0.04677	0.04677	114.24	0.000
F	1	0.00255	0.00255	6.24	0.035
S	1	0.19451	0.19451	475.13	0.000
W	1	3.54696	3.54696	8664.29	0.000
L	1	0.02710	0.02710	66.21	0.000
P × P	1	0.00293	0.00293	7.16	0.009
W × W	1	0.03076	0.03076	109.66	0.000
L × L	1	0.00310	0.00310	11.05	0.013
P × F	1	0.00216	0.00216	5.28	0.034
P × W	1	0.00244	0.00244	5.95	0.039
S × W	1	0.02271	0.02271	55.47	0.000
S × L	1	0.00203	0.00203	7.24	0.021
W × L	1	0.00681	0.00681	24.26	0.000
Error	18	0.00737	0.00041		
Lack of fit	13	0.00617	0.00047	1.88	0.252
Pure Error	5	0.00126	0.00025		
Total	31	4.10660			
S = 0.0202331, R-sq = 99.82%, R-sq (adjusted) = 99.69%, R-sq (predicted) = 99.34%					

5.2.5. Parametric Analysis from the Surface Plot

5.2.5.1. Weld Shear Strength

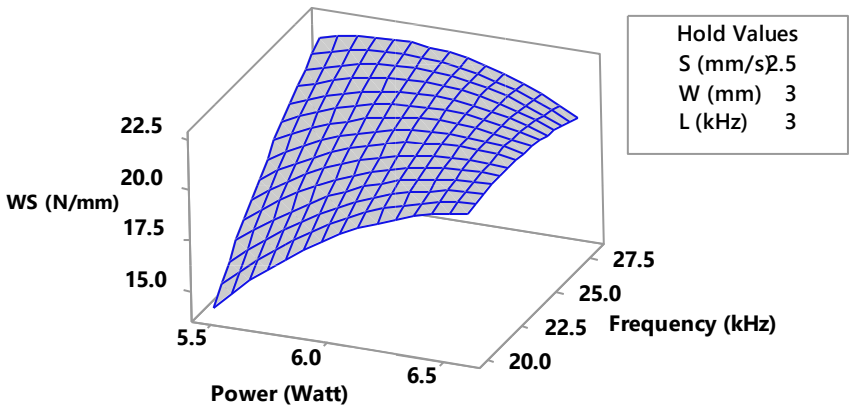

Figure 5.2.2 Surface plot of weld shear strength vs. laser power and frequency

Figure 5.2.2 shows the interaction effect of laser power and frequency on weld strength. Welding speed, wobble width and wobble frequency are taken as constant at 2.5 mm/s, 3mm and 3 kHz, respectively. It has been found out that weld strength is higher at low laser power and high frequency. At low power the depth of penetration is higher for high weld frequency and the weld strength is much greater. At high power the melt zone is high but depth of penetration is low, thus the weld strength is weak.

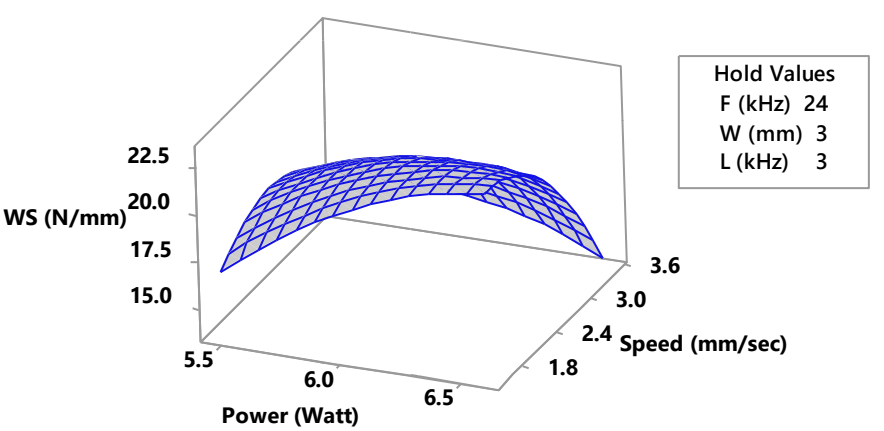

Figure 5.2.3 Surface plot of weld shear strength vs. laser power and speed

Figure 5.2.3 shows the interaction effect of laser power and frequency on weld strength. Pulse frequency, wobble width and wobble frequency are taken as constant at 24 kHz, 3mm and 3

kHz, respectively. It is observed from the response surface plot in Figure 5.2.3 that at high laser power and lower welding speed, weld shear strength is higher. This is because of the fact that heat input or line energy is directly proportional to laser power and inversely proportional to welding speed.

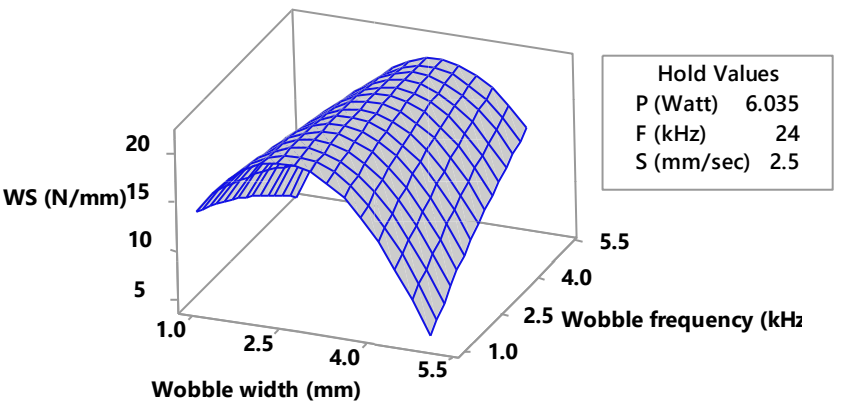

Figure 5.2.4 Surface plot of weld shear strength vs. wobble width and wobble frequency

The combination of the result of the important process parameters, wobble width and wobble frequency, on weld shear strength is shown in Figure 5.2.4. Laser power, pulse frequency and welding speed are taken as constant at 6.035 watt, 24 kHz and 2.5 mm/s, respectively. Weld strength is increasing with an increment of wobble width at a certain point and after that it declines.

5.2.5.2 Weld Seam Width

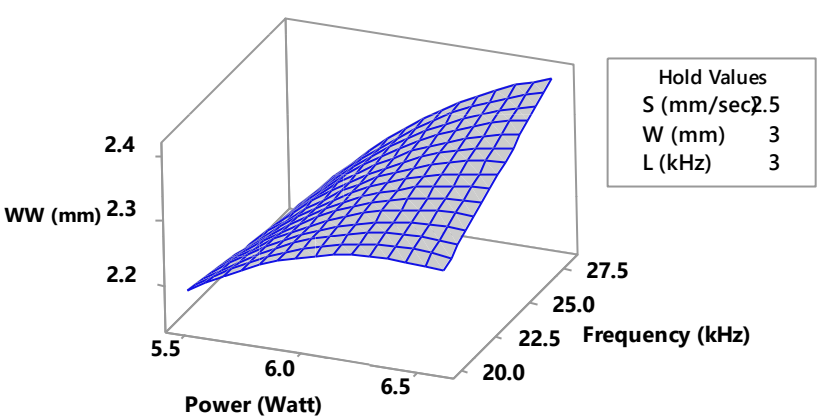

Figure 5.2.5 Surface plot of weld seam width vs. laser power and frequency

The combination of the result of the important process parameters, laser power and pulse frequency, on weld seam width is shown in Figure 5.2.5. Welding speed, wobble width and wobble frequency are taken as constant at 2.5 mm/s, 3 mm and 3 kHz, respectively.

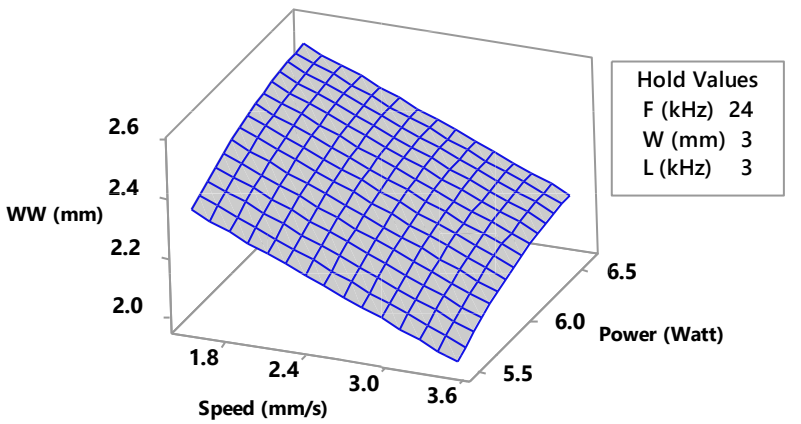

Figure 5.2.6 Surface plot of weld seam width vs. laser power and welding speed

The combination of the result of the important process parameters, laser power and welding speed, on weld seam width is shown in Figure 5.2.6. Frequency, wobble width and wobble frequency are taken as constant at 24 kHz, 3 mm and 3 kHz, respectively. It is observed from the Figure 5.2.6, that increasing the laser power and decreasing the weld speed increases the weld-seam width. The effect is due to the increase of the line energy, which is directly proportional to the laser power and inversely proportional to the welding speed. Therefore, the heat input to the weld zone increases leading to more volume of base material being melted, consequently the width of the welded zone increases.

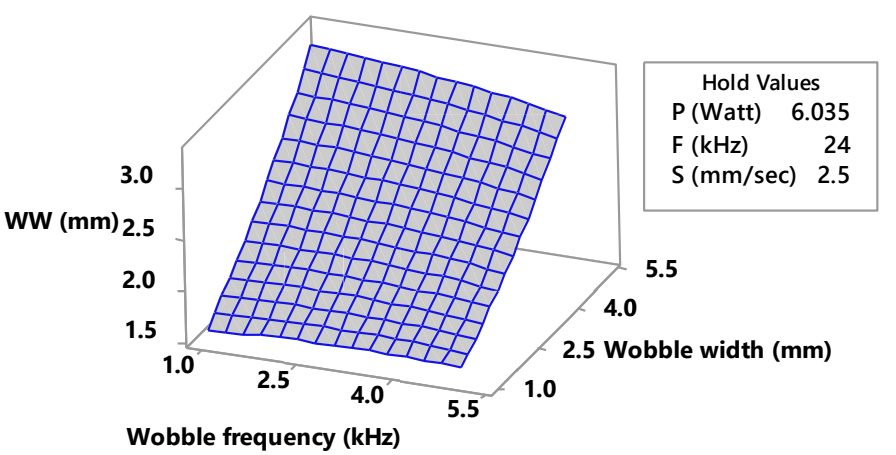

Figure 5.2.7 Surface plot of weld seam width vs. wobble frequency and wobble width

The combination of the result of the important process parameters, wobble width and wobble frequency, on weld seam width is shown in Figure 5.2.7. Laser power, pulse frequency and welding speed are taken as constant at 6.035-watt, 24 kHz and 2.5 mm/s, respectively. It is observed from the Figure 5.2.7, that increasing the wobble width and decreasing the wobble frequency increases the weld-seam width. The effect is due to the increase of the line energy, which is inversely proportional to the wobble frequency and width of the heat affected zone which is directly proportional to the wobble width. Therefore, the heat input to the weld zone and heat affected zone both are increases leading to more volume of base material being melted, consequently the width of the welded zone increases. According to the result presented in the Figure 5.2.7, the maximum weld width is achieved at higher level i.e at 4 mm wobble width level and wobble frequency at lower level, i.e, 2, when remaining parameters are at their center value.

5.2.6 Multi-objective optimization by PSO

Multi-objective PSO algorithm have been proposed by Coello [14, 15]. Here, the objective is to maximize the weld strength (WS) while at the same time minimizing the weld width (WW). Now, maximizing one comes at the cost of minimizing the other and vice versa. So those values of features are chosen which are better than the values of other features in terms of both the objectives. The set of such values are called pareto front and the remaining set of values inferior to this set is called the dominated set. Pareto front is generated between weld width and square of inverse of weld strength as shown in Figure 5.2.8.

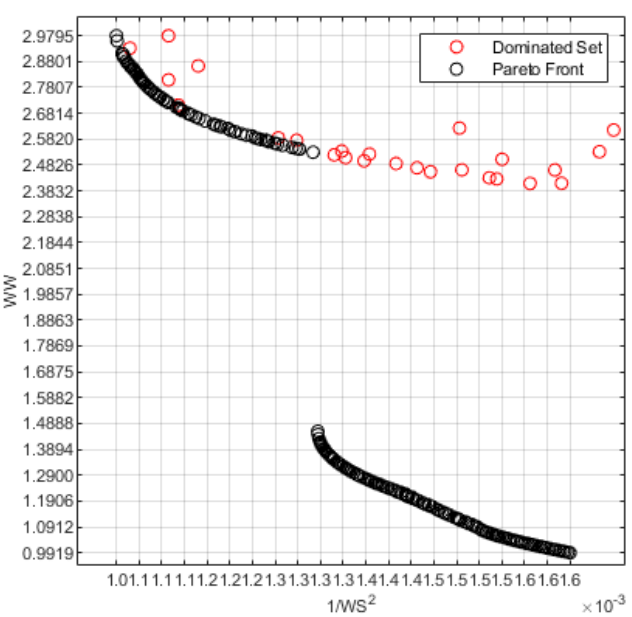

Figure 5.2.8. Pareto front obtained between WW and $1/WS^2$ values

Here, the objective is set up for minimization of the both functions by taking the square of inverse of weld strength and weld width. Now, among the many non-dominated optimized solutions obtained in the Pareto front, only one value are chosen for further optimization. Hence, Pareto values of both the functions are normalized using equations 5.2.3 and 5.2.4 and then find the composite rank of both the functions by adding each pair of normalized values and then ranking the pair from lowest to highest sum and whichever pair has the minimum rank is our optimized output and the corresponding parameters are our optimal parameters.

$$\text{Norm}_{(1/WS^2)} = \frac{(1/WS^2) - \text{Min}(1/WS^2)}{\text{Max}(1/WS^2) - \text{Min}(1/WS^2)} \quad \ldots\ldots\ldots\ldots\ldots\ldots \text{(5.2.3)}$$

$$\text{Norm}_{(WW)} = \frac{(WW^2) - \text{Min}(WW^2)}{\text{Max}(WW^2) - \text{Min}(WW^2)} \quad \ldots\ldots\ldots\ldots\ldots\ldots \text{(5.2.4)}$$

The optimal value thus obtained from the best rank solution are given in Table 5.2.5. Confirmation test is also performed at optimal welding process parameter to see the percentage error (Table 5.2.5) and validation.

Table 5.2.5 Confirmation Test

Optimized value from PSO			Confirmation test	% Error
Process Parameters	P	5.48	5.48	
	F	28	28	
	S	3.5	3.5	
	W	1.7714	1.771	
	L	5	5	
Performance Parameters	WS	27.735	26.826	3.276
	WW	1.3718	1.3321	2.891

5.3 Outcomes of the Present Research Work

An attempt has been made here to join polycarbonate and black carbon filled acrylic with or without beam wobbling by using low power laser. Beam wobbling can be used to control the seam width and it also provides the high-speed laser welding. Based on the experimental study and research within the specified set of parameters considered in the present study, the following inference can be said.

1. Increasing laser power increases the weld shear strength and weld width; while, welding speed has a negative impact on both responses.

2. The developed surface response models estimate the responses within the limit of process parameters for laser welding
3. Laser power, frequency and speed have a better interaction effect on weld shear strength and weld width. Such parameters regulate the laser heat input to the weld area.
4. The weld strength is limited by very high laser heat input, which causes the material to overheat and decompose. On the other hand, very low laser heat input results in lack of fusion.
5. Beam wobbling is found to have a substantial effect on weld shear strength when beam wobbling parameters such as wobble width and wobble frequency are used. It has been observed that beam wobbling gives the greater joint strength at a certain level after that it declines, as beam wobbling enhances the better intermixing of molten material and heat distribution across the weld interface. However, excessive oscillation width or frequency cause uneven heating or insufficient overlap of melt pools, resulting in reduced weld strength.
6. It can be seen from the ANOVA table that wobble width is the most dominant parameter on weld seam width and weld width increases with an increase in wobble width.
7. It is observed that laser power, welding frequency, scanning speed, wobble width and wobble frequency have a strong interaction effect on both weld strength and width. These parameters control the laser energy input.
8. It has been observed that at low laser power, the depth of penetration is higher for high welding frequency and thus weld strength is greater.
9. It is also observed from the results that maximum weld strength and minimum seam width can be achieved at optimal parameter setting with beam wobbling because of greater intermixing of the material at the weld interface.

CHAPTER: 6

LOW POWER LASER TRANSMISSION WELDING OF CLEAR TRANSPARENT POLYMERS

6.1. Modelling and optimization of laser transmission welding of clear acrylic transparent polymers without beam wobbling technique

Joining of two transparent polymer components requires special laser-absorbing medium in between them. Welding of same transparent thermoplastic polymers has become essential due to growing number of applications in microfluidic devices. Few researchers have tried to join different combination of clear to clear thermoplastic materials without the use of additive. Generally, two techniques are used for LTW of transparent polymer (a) use of colorless dyes comprise non infrared-absorbent materials with 0.78–1.1 μm laser wavelengths (b) use of lasers with wavelength spectrum range in between 1.4 μm and 2.2 μm. Laser transmission welding at 1940 nm wavelength has been proven to be a superior technique as compared to present technique such as thermal, adhesive and solvent bonding. Most of the authors reported the laser transmission welding by making the lower part fully absorbent using black carbon filled or by applying some absorbent to the bottom part. But there is a lack of uniformity of absorbent. In this research, black marker is used to draw a line along the weld interface to increase the absorptivity of lower part. Black marker contain resin, solvent, glyceride and pyrrolidone. Black marker is very cheap as compared to other absorbent and easily available to use. It is observed that higher weld strength is achieved using black marker. New technique has been implemented to weld two transparent polymers by using black marker as an absorbing agent on the top surface of lower part.

6.1.1 Experimental Planning

Central composite design is used to design the experiment based on a three factor five level with full replication. Twenty number of experiment has to be performed. Laser power (LP), pulse frequency (PF) and scanning speed (SS) are selected as controllable process parameter

in this design. Laser spot diameter has been fixed throughout this experimental work. Generally, a faster welding speed will get less interaction time with the material may results low weld width and or less depth of penetration of the laser beam. Hence, keeping the spot diameter remains constant, various weld width can be achieved by controlling the welding speed. Standoff distance and number of passes are also fixed in this experiment. A mechanical clamping device is used to keep the close contact between materials. The experimental work is performed on Neodymium doped yttrium orthovanadate (Nd: YVO_4) having raptor beam laser. Nd: YVO_4 (EMS 100; Electrox Ltd.) laser comprises 50 µm spot diameter, maximum power 9.28 W, pulse width 4.2 ns and 1064 nm wavelength. Laser crystals are used to generate laser radiation. Nd: YVO_4 is one of the most efficient laser host crystal for diode laser- pumped solid-state lasers.

Two of the same transparent acrylic each of size 80mm × 35mm × 4mm are considered as work material for performing experimental work. Acrylic is extensively used in household, medical and optical applications due to its high strength, heat resistance and excellent dimensional stability. Laser transmission welding is performed to create lap joint with an overlap of 20 mm and weld center line of 10 mm as shown in Figure 6.1.1.

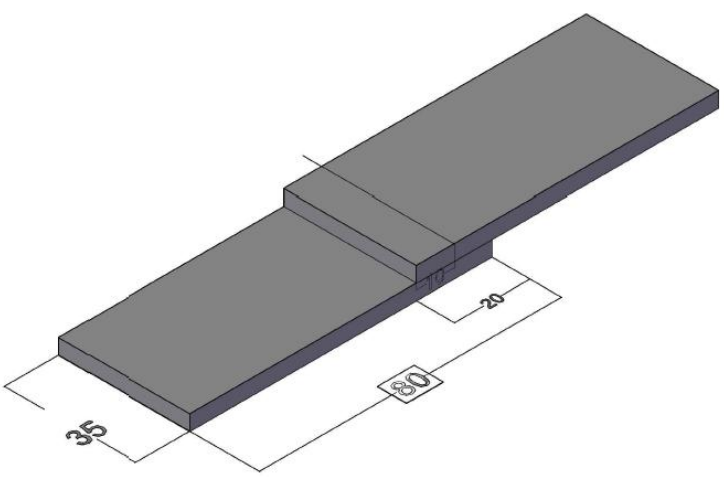

Figure 6.1.1 Configuration of weld joint

A black marker is used to draw a line across weld center line on the lower part at the weld interface. This black line at the interface absorbs the laser energy and it converts in to thermal energy. Melting and vaporization of both part occurs and joining happens. Black marker contain resin, solvent, glyceride and pyrrolidone. A fixture is also prepared to hold the workpiece. Lap area of 20mm × 35mm is considered during experimentation. The worktable

is controlled by CNC in X and Y direction. After considering literature survey and feasibility of machine, trial experiment has been conducted and based on that, process parameter and their ranges are decided as given in Table 6.1.1.

Table 6.1.1 Selected process parameter and their ranges

Parameter	Symbol	Units	Levels				
			-1.682	-1	0	+1	+1.682
Laser Power	LP	Watt	7.107	7.424	7.888	8.352	8.668
Pulse Frequency	PF	kHz	19.773	30	45	60	70.226
Scanning Speed	SS	mm/min.	8.185	90	210	330	411.815

As the melting temperature of the work piece materials are very low (160°C), the maximum available power of laser has been set to 9.28 watt (material degrade at higher laser power). Also at very low laser power, joining did not happen due to insufficient of laser heat absorption at the weld interface thus, range selected for laser power was varied within narrow range.

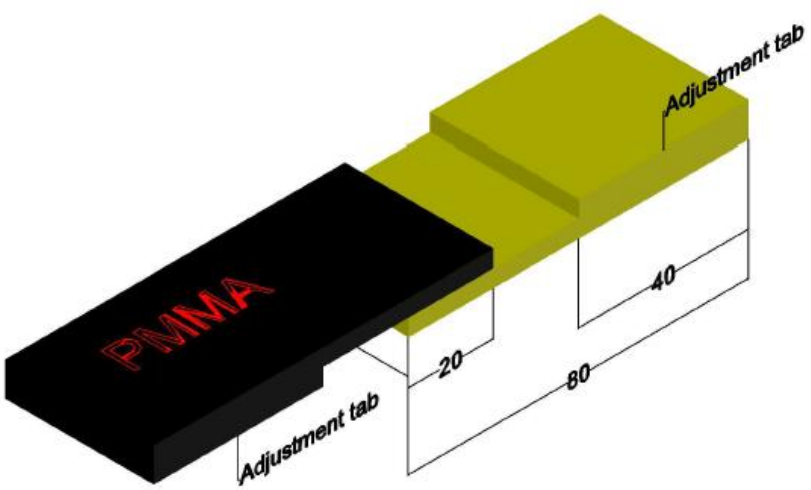

Figure 6.1.2. Design of welded sample for lap-shear testing

A universal tensile testing machine (8801; INSTRON) has been used to measure the lap shear pull test, for estimation of joint strength. A plaque of dimension 40 mm × 35 mm are attached

at each corner to avoid the bending moment while testing of material as shown in Figure 6.1.2. Weld strength is calculated as maximum load at break per unit length. A three-dimensional optical measuring microscope (STM-6; OLYMPUS) has been used to measure the seam width of all welded samples. Three measurements are taken to each welded samples and average of them are considered for further analysis. Scanning electron microscope (EVO 18 special edition; ZEISS) is used to observe the welded zone morphology.

6.1.2 Parametric Analysis Based on RSM Modelling

Table 6.1.2 presents the experimental plan as well as the measured value of the responses.

Table 6.1.2 Design matrix and measured experimental result

Experimental Information				Results	
Exp. No.	Welding Parameters			Weld strength (N/mm)	Weld width (μm)
	LP (Watt)	PF (kHz)	SS (mm/min.)		
1	7.424	30.000	90.000	23.0460	287
2	8.352	30.000	90.000	25.9000	285
3	7.424	30.000	330.000	5.9836	331
4	8.352	30.000	330.000	6.1712	285
5	7.424	60.000	90.000	26.5872	256
6	8.352	60.000	90.000	26.7852	317
7	7.424	60.000	330.000	9.8251	259
8	8.352	60.000	330.000	9.1261	290
9	7.107	45.000	210.000	13.9510	293
10	8.668	45.0000	210.000	15.8130	319
11	7.888	45.000	8.185	34.5140	204
12	7.888	45.000	411.815	6.1583	218
13	7.888	19.773	210.000	10.0000	352
14	7.888	70.226	210.000	16.1130	342

15	7.888	45.000	210.000	12.0000	287
16	7.888	45.000	210.000	11.5376	280
17	7.888	45.000	210.000	12.6394	298
18	7.888	45.000	210.000	12.2132	294
19	7.888	45.000	210.000	12.9174	298
20	7.888	45.000	210.000	12.9217	284

6.1.3 Second Order Regression Equation of Responses

Design Expert® software has been used for analysis of the measured output and estimating the model with best fits. The lack-of-fit test, sequential f-test and ANOVA (analysis of variance) technique have been used to check the adequacy of model using the v17 software to get the best fit model. Mathematical models are developed to establish a correlation between input and output parameters to understand the behavior of process parameters on responses.

$$WS = 271.8 - 65.2\,LP + 0.445\,PF - 0.1012\,SS + 4.476\,LP \times LP + 0.001415\,PF \times PF + 0.000201\,SS \times SS - 0.0636\,LP \times PF - 0.0080\,LP \times SS + 0.000165 PF \times SS \quad (6.1)$$

$$WW = 2535 - 488\,LP - 27.36\,PF + 2.360\,SS + 26.87\,LP \times LP + 0.09013\,PF \times PF - 0.001931\,SS \times SS + 2.514\,LP \times PF - 0.1661\,LP \times SS - 0.00472\,PF \times SS \quad \text{..... (6.2)}$$

6.1.4 ANOVA Analysis for Responses

ANOVA is performed to evaluate the significant terms and adequacy measures such as R^2, R^2-adjusted and R^2-predicted of developed model. Model terms with a "Prob > f" <0.05 imply that the model terms are statistically significant at the 95 % confidence level. Table 6.1.3 shows the ANOVA results with S, R^2, adjusted R^2, and predicted R^2 of the quadratic model. The model terms are statistically significant if the p-value is less than 0.05 for the model (95% confidence level). The value of lack-of-fit should be insignificant so that the experimental value fits the model accurately.

Table 6.1.3 ANOVA results for weld shear strength (after backward elimination).

Source	DF	Adj. SS	Adj. MS	F-value	P-value
Model	9	1202.47	133.61	348.99	0.000
Linear	3	1071.40	357.13	932.85	0.000
LP	1	2.36	2.36	6.15	0.033
PF	1	33.86	33.86	88.44	0.000
SS	1	1035.19	1035.19	2703.96	0.000
Square	3	127.21	42.40	110.76	0.000
LP × LP	1	13.38	13.38	34.96	0.000
PF × PF	1	1.46	1.46	3.81	0.079
SS × SS	1	120.54	120.54	314.85	0.000
2-way interaction	3	3.86	1.29	3.36	0.063
LP × PF	1	1.57	1.57	4.10	0.070
LP × SS	1	1.59	1.59	4.15	0.069
PF × SS	1	0.70	0.70	1.83	0.205
Error	10	3.83	0.38		
Lack-of-fit	5	2.30	0.46	1.50	0.333
Pure Error	5	1.53	0.31		
S = 0.618741, R-sq. = 99.68%, R-sq. (adj.) = 99.40%, R-sq. (pred.) = 98.32%					

ANOVA has been analyzed to see the influence of each parameter on weld seam width. The model having p-value of less than 0.05 (i.e. 95% confidence level) are considered significant parameter. Quadratic relationship has been used to establish the relationship which fit the model well. Table 6.4 shows the ANOVA table with S, R^2, adjusted R^2, and predicted R^2 of the quadratic model. The model terms are statistically significant if the p-value is less than 0.05 for the model (95% confidence level). The value of lack-of-fit should be insignificant so that the experimental value fits the model accurately.

Table 6.1.4 ANOVA results for weld seam width (after backward elimination).

Source	DF	Adj. SS	Adj. MS	F-value	P-value
Model	9	24397.2	2710.8	62.50	0.000
Linear	3	1204.6	401.5	9.26	0.003
LP	1	563.5	563.5	12.99	0.005

Source	DF	Adj. SS	Adj. MS	F-value	P-value
Model	9	24397.2	2710.8	62.50	0.000
Linear	3	1204.6	401.5	9.26	0.003
PF	1	502.2	502.2	11.58	0.007
SS	1	138.8	138.8	3.20	0.104
Square	3	19480.1	6493.4	149.71	0.000
LP × LP	1	482.1	482.1	11.12	0.008
PF × PF	1	5926.8	5926.8	136.65	0.000
SS × SS	1	11140.5	11140.5	256.86	0.000
2-way interaction	3	3712.5	1237.5	28.53	0.000
LP × PF	1	2450.0	2450.0	56.49	0.000
LP × SS	1	684.5	684.5	15.78	0.003
PF× SS	1	578.0	578.0	13.33	0.004
Error	10	433.7	43.4		
Lack-of-fit	5	144.9	29.0	0.50	0.766
Pure Error	5	288.8	57.8		
S = 6.58576, R-sq. = 98.25%, R-sq. (adj.) = 96.68%, R-sq. (pred.) = 93.74%					

6.1.5 Validation of the developed models

In order to validate the developed response surface equations, obtained from regression analysis, three validation experiments are carried out under randomly selected welding conditions for which the regression equations are generated. The actual results are estimated and average of three results are considered. The predicted results, experimental results and percentage error are given in Table 6.1.5. It is seen from the validation experiment that there is small percentage error between predicted and the experimental values, which show that the established models can produce almost precise results. Figure 6.1.3 and 6.1.4, respectively, reflect the relation between experimental and predicated values of weld shear strength and weld width. These figures also specify that the developed models are acceptable and estimated results are compatible with measured value.

Table 6.1.5 Validation test results

Exp. No.	LP (Watt)	PF (kHz)	SS (mm/min.)		Weld-shear strength (N/mm)	Weld-shear width (μm)
1.	7.424	45	210	Actual	11.873	276.052
				Predicted	12.795	291.121
				% Error	7.765	5.458
2. .	7.107	30	90	Actual	21.959	312.753
				Predicted	23.413	298.042
				% Error	6.621	4.703
3. .	7.888	60	8	Actual	35.176	244.355
				Predicted	36.472	236.225
				% Error	3.684	3.327

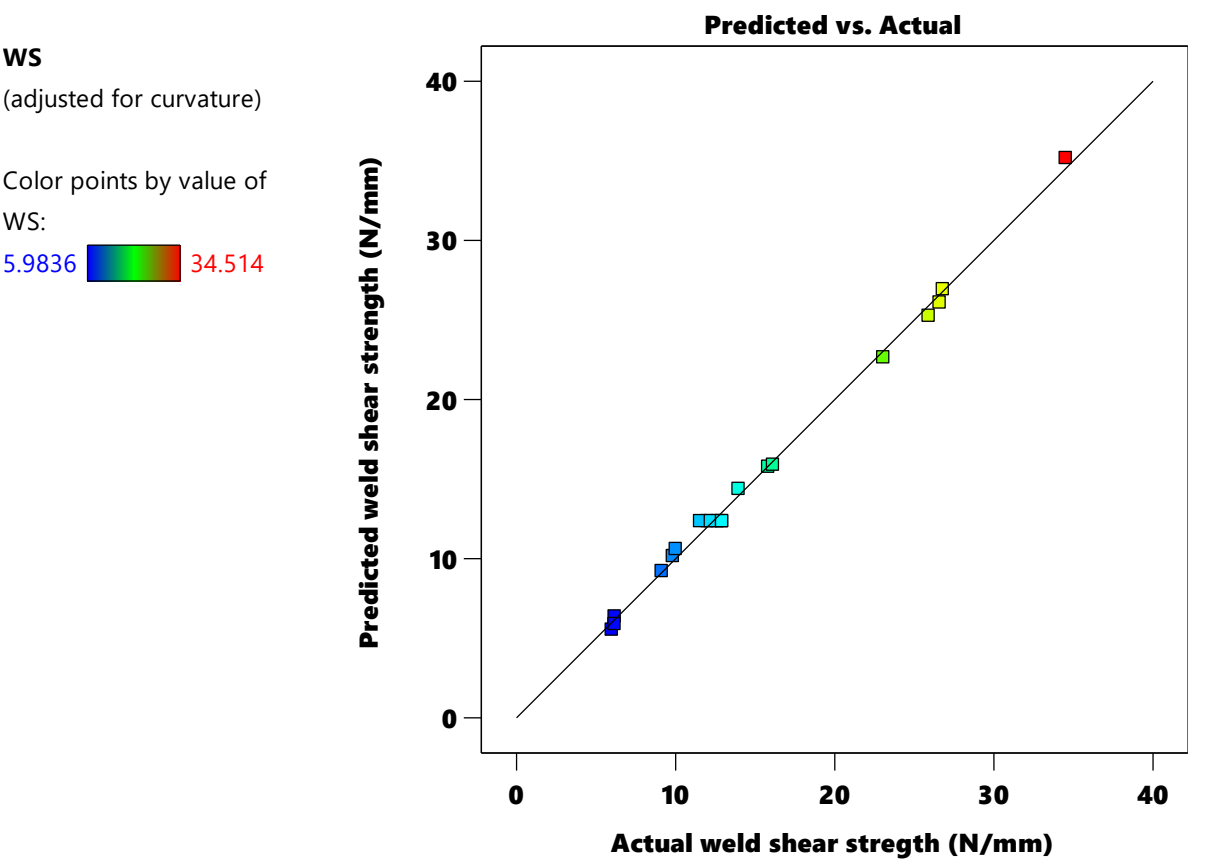

Figure 6.1.3 Plot of actual vs. predicted weld shear strength

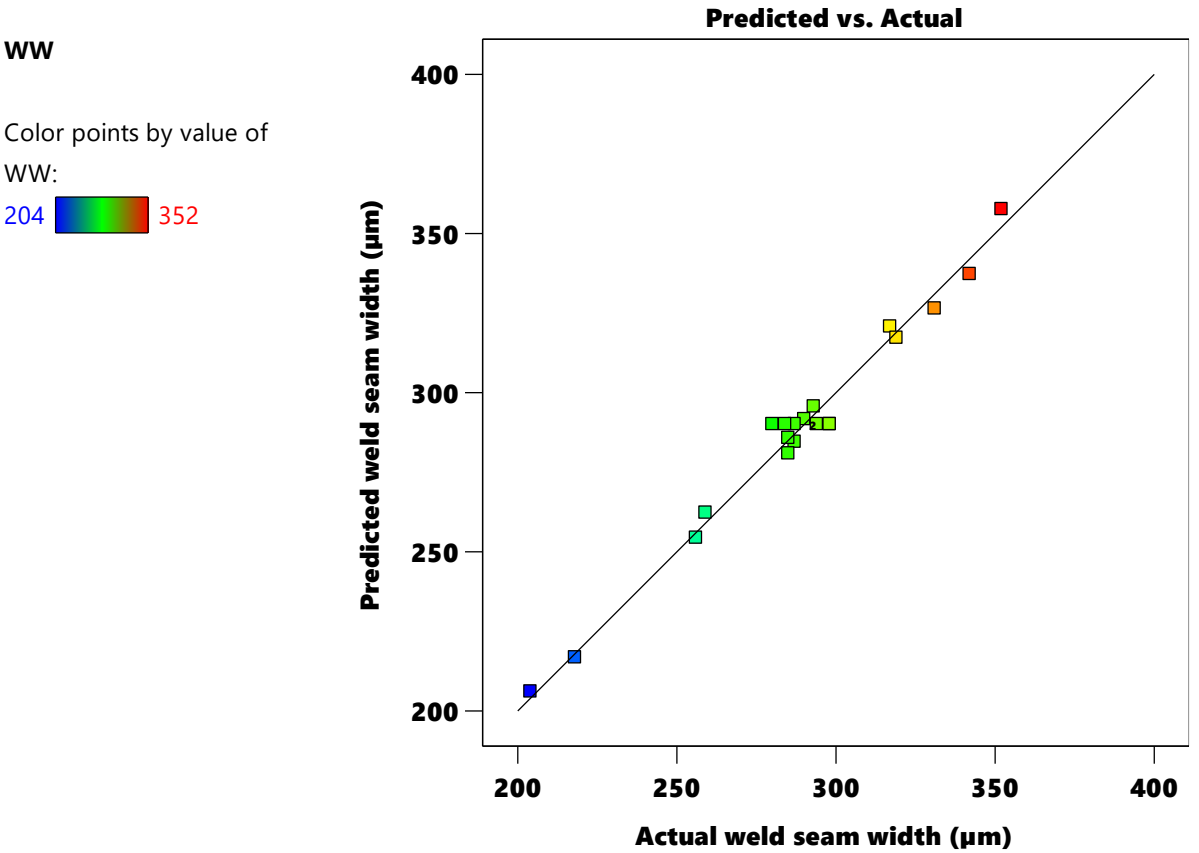

Figure 6.1.4 Plot of actual vs. predicted weld-seam width

6.1.6 Parametric Analysis

6.1.6.1 Weld Shear Strength

Figure 6.1.5 shows the surface plot of laser power and scanning speed on weld shear strength (WS). Weld strength is found to be higher at lower scanning speed. This is due to the fact that lower scanning speed increases the laser interaction time and therefore, increase the total energy input. Thus, greater volume of base material is melted and weld strength is higher. However, heat conduction losses are greater at low scanning speed. Here, scanning speed is most dominating factor. This can also be seen that weld strength is reducing with an increase of scanning speed, because a higher scanning speed lowers the irradiation time, which causes the less heat input, resulting in less volume of material being melted. But, heat conduction losses are minimum at higher scanning speed because of less time available for heat dissipation. Figure 6.1.6 shows the surface plot of laser power and pulse frequency on weld shear strength (WS). At lower pulse frequency, weld strength is found to be lower because of lack of penetration [16]. Laser power is found to be less dominant parameter as compared to scanning speed, the same can also be confirmed by the ANOVA results.

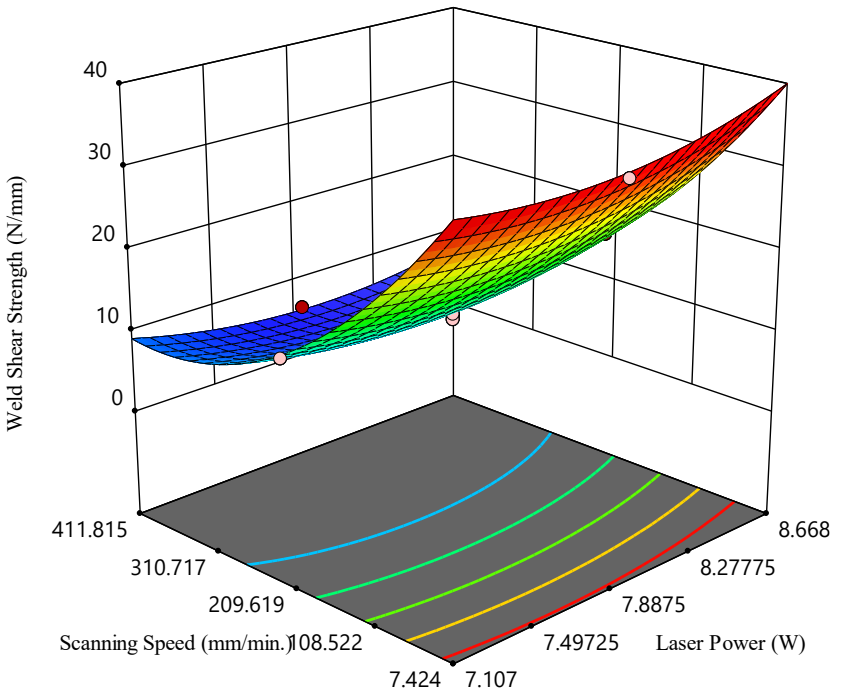

Fig. 6.1.5 Surface plot showing the interaction effect of laser power and scanning speed on weld shear strength, when all other parameters are at their central values

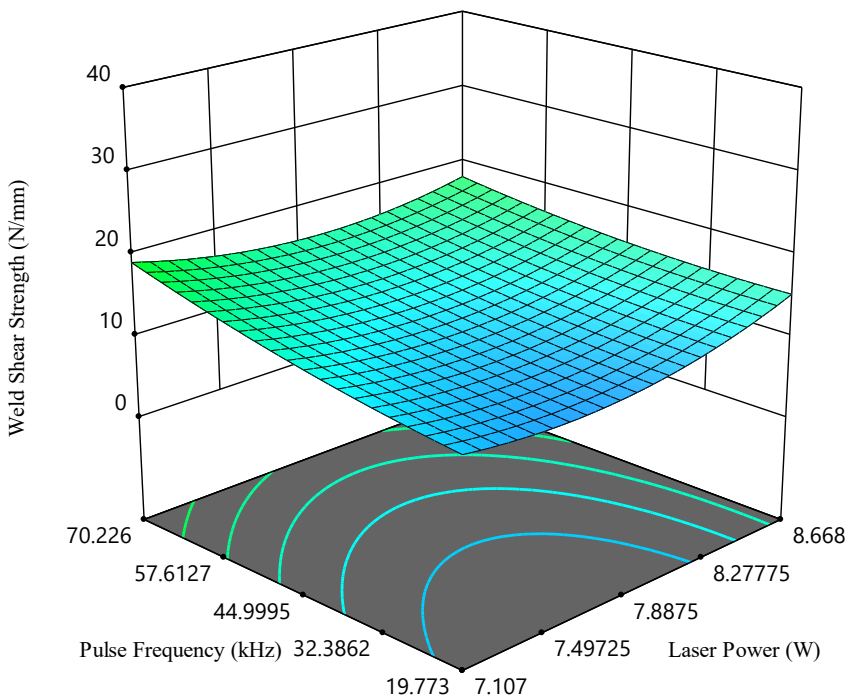

Fig. 6.1.6 Surface plot showing the interaction effect of laser power and pulse frequency on weld shear strength, when all other parameters are at their central values

Figure 6.1.7 shows the interaction plot of laser power (LP) and pulse frequency (PF) on weld shear strength (WS). Weld strength is found to be higher at certain range of laser power. This happens because low line energy leads to lack of penetration, poor heat transfer and poor mixing of materials, therefore, weld strength is weak. High-line energy, on the other hand, may cause degradation of base material. Line energy is defined as the ratio of laser power to scanning speed i.e. laser energy input per unit length. At lower pulse frequency, the number of laser pulses per unit time decreases, which leads to reduction of heat input to weld. As a result, heat accumulation is insufficient to achieve complete melting, resulting in lack of penetration and lower weld strength [16]. The optimum welding strength is therefore found at a desirable value of laser power and pulse frequency.

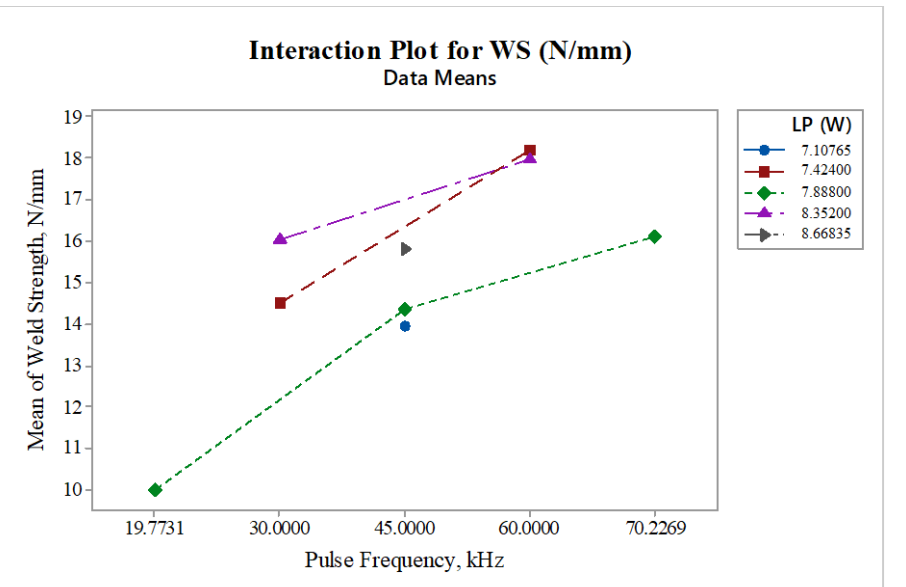

Figure 6.1.7 Interaction plot of weld shear strength vs. laser power and pulse frequency

6.1.6.2 Weld Seam Width

Figure 6.1.8 shows the surface plot of laser power and scanning speed on weld-seam width (WW). It is observed that weld width is minimum at certain value of laser power (7.4-8.2 watt) until the critical temperature of decomposition is reached. Weld width is maximum at higher laser power because more amount of base material is melted with increased laser power and consequently the seam width increases. Weld width is also found to be minimum at higher scanning speed and laser power (7.4-8.2 watt). This is because irradiation time reduces at higher scanning speed and low heat input is supplied, consequently narrow weak weld is

formed. Optimum value of laser power and scanning speed are required to achieve the significant seam width.

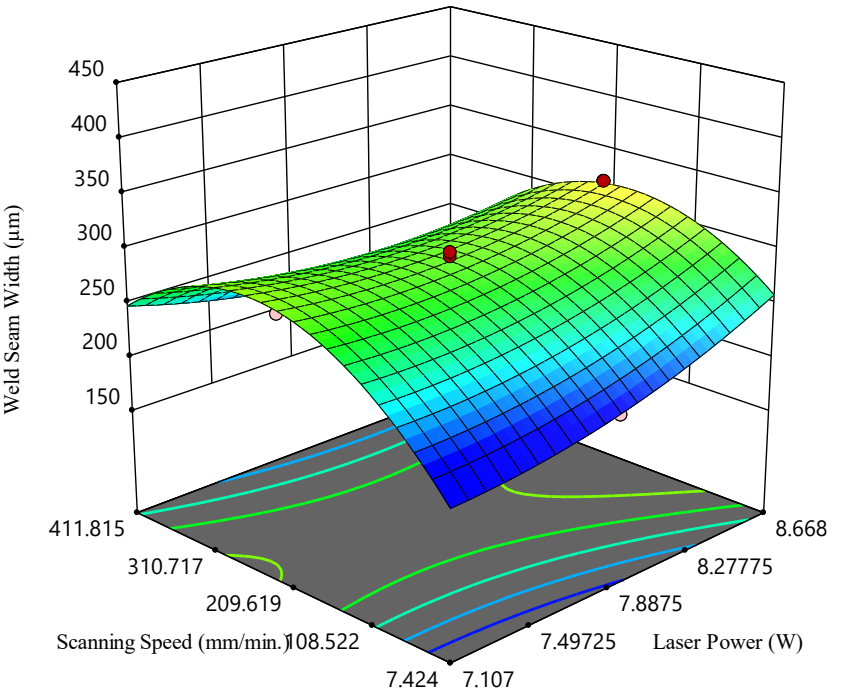

Fig. 6.1.8 Surface plot showing the interaction effect of laser power and scanning speed on weld seam width, when all other parameters are at their central values

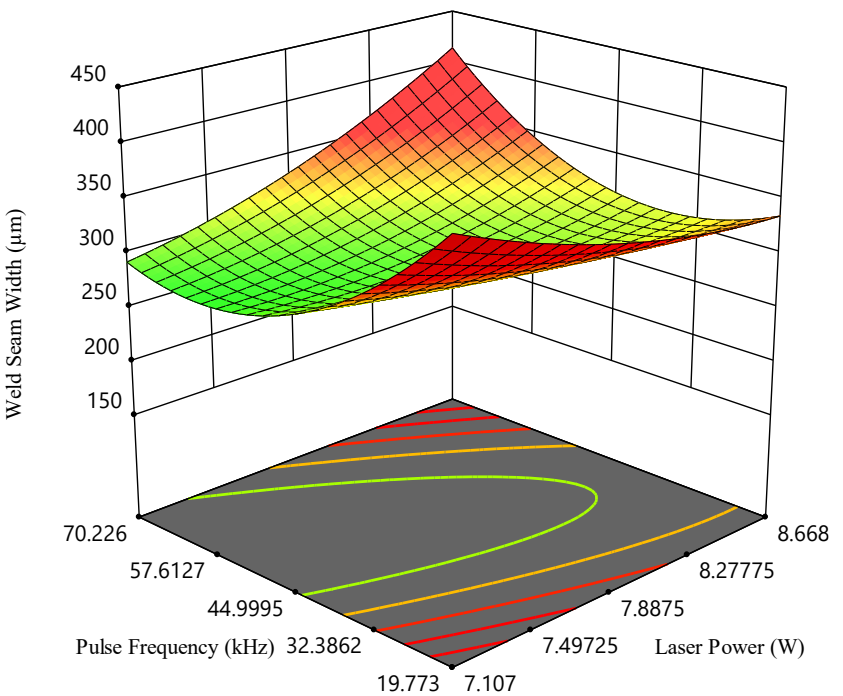

Fig. 6.1.9 Surface plot showing the interaction effect of laser power and pulse frequency on weld seam width, when all other parameters are at their central values

Figure 6.1.9 shows the surface plot of laser power and pulse frequency on weld-seam width (WW). It can be clearly seen from fig. 6.1.9 that weld seam width is decreasing with an increment of pulse frequency at low laser power. This is because increment of pulse frequency at low laser power decreases peak power and the interaction time; therefore, low heat input is delivered to the weld zone which leads to formation of a narrow weld. Figure 6.1.10 shows the interaction plot of laser power and pulse frequency on weld seam width. Weld seam width is found to be minimum at pulse frequency of 45 kHz. At high laser power, weld seam width is increasing very insignificant way with an increment of pulse frequency. This happens due to long gap pulses at low pulse frequency resulting poor heat transfer and poor intermixing at weld zone. Desirable value of weld seam width is achieved at medium laser power and medium pulse frequency. That is why a favourable value of laser power and pulse frequency are required to obtain optimum weld seam width.

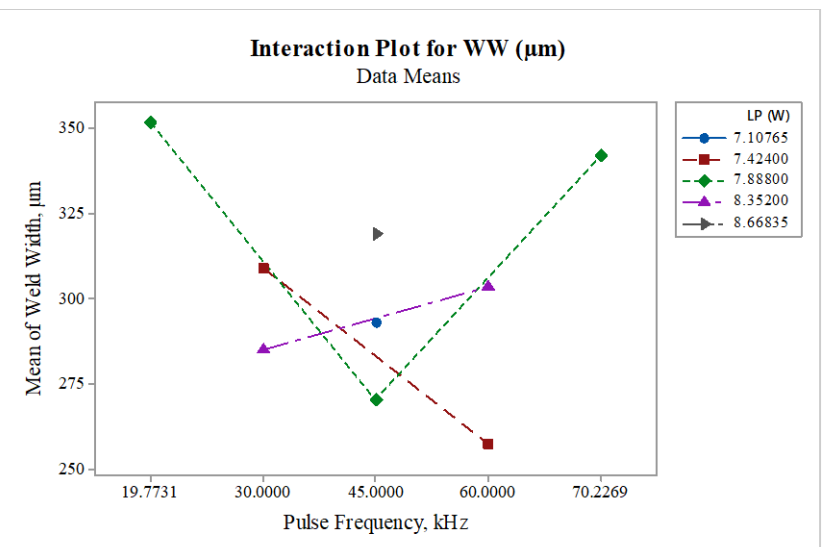

Fig. 6.1.10 Interaction plot of weld shear strength vs. laser power and pulse frequency

6.1.7 Microstructure Analysis

In LTW the absorbent element of the lower polymer absorbs energy and transforms in to heat. Thus, upper and lower part melts at the interface and mix to create a weld. Figure 6.1.11 and Figure 6.1.12 show the morphology of weld zone between the alike transparent acrylic parts

at different magnification. A number of small bubbles can be seen in Figure 6.1.11 and a small number of larger bubbles is observed in Figure 6.1.12.

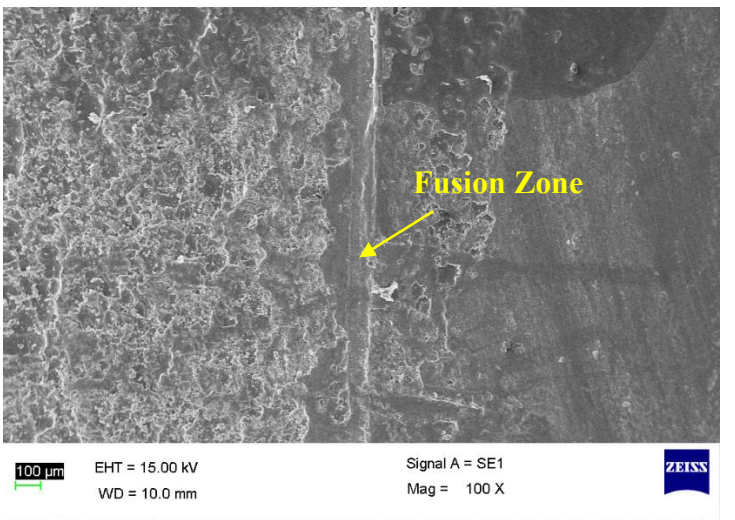

Fig. 6.1.11 SEM micrograph of the weld zone of Acrylic-Acrylic at 100X

Due to different welding conditions, the heating zone in weld area often generates bubbles and ablation which influence the appearance and welding quality. Degradation and bubbles for the high laser energy intensity can appear in the welding region. These small bubbles cause pits and cracks to be created on the material surface which can activate the micro-anchor mechanism and enhance the joining strength. It can be explained by the fact that bubbles create high pressure and make the fused plastic float to the surface pits or holes, in order to provide more mechanical binding for a close contact; therefore, the bubbles have some benefits to increase the welding performance to a certain point.

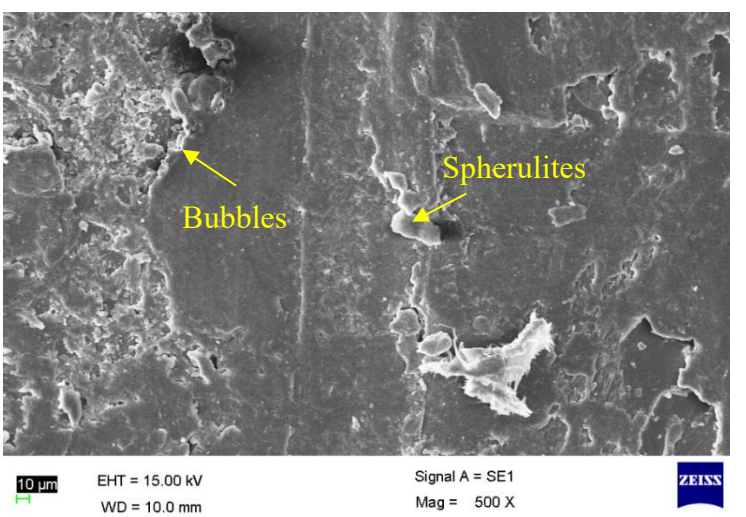

Fig. 6.1.12 SEM micrograph of the weld zone of Acrylic-Acrylic at 500X

6.1.8 Multi-objective optimization using desirability function based technique

Desirability function based optimization technique is used to determine the optimum process parameter for maximizing the weld shear strength and at the same time minimizing the weld width. It works by translating the responses in to corresponding value of desirability. Desirability value depends upon range and target response. When response reach its goal, then desired unity value is assigned. Desirability value is considered zero outside certain limit.

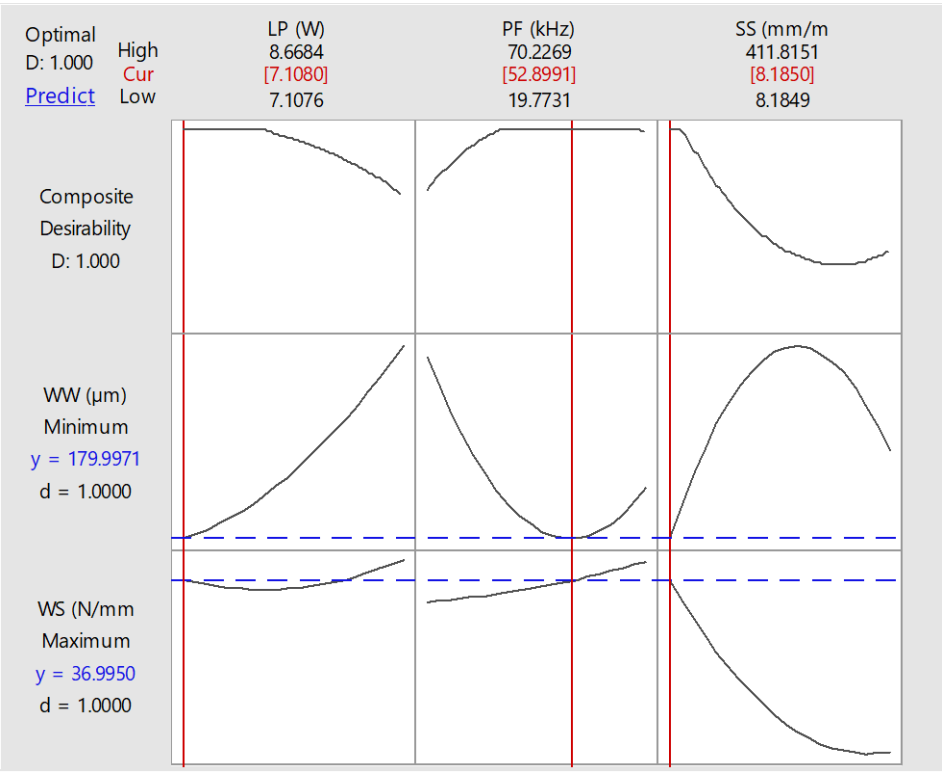

Fig. 6.1.11 Optimization plot of responses

The single value of D derives the overall desirability of combined responses. Composite desirability varies from 0 to 1. If any individual desirability becomes zero then overall desirability will also be zero, since overall desirability is geometric mean of individual response. Figure 6.1.11 shows the optimization plot between input and output parameter.

6.1.9 Validation Experiment

A confirmation experiment has been performed at the optimal welding process parameter setting to find the error, and it is estimated that weld strength has an error of 4.003% and weld seam width has an error of 3.334% (Table 6.1.6), which is very minimum and less than 5%; thus it is acceptable.

Table 6.1.6 Confirmation test at optimal process parameter

Optimum value from Desirability function technique			Confirmation test	%Error
Process Parameters	LP (Watt)	7.108	7.108	
	PF (kHz)	52.8991	52.8991	
	SS (mm/min.)	8.185	8.185	
Response Parameters	WS (N/mm)	36.995	35.514	4.003
	WW (μm)	179.997	186	3.334

6.2. Beam wobbling effects on laser transmission welding of dissimilar polymers: Experiments, modeling, and process optimization

Wobble laser welding has emerged as a cutting-edge technology in the field of laser welding. Wobble welding is performed by oscillating the laser beam longitudinally at a high wobble frequency, resulting in a stirring action inside the molten weld pool. As a consequence, the weld pool is controlled by the oscillating beam, which affects the critical features of the weld. The wobbling mode might be circular, linear, eight, or infinite. When compared to welding without beam oscillation, wobble welding expands the weld fusion area. TWIST (Transmission welding using incremental scanning method), is an effective technology for performing micro and macro welding in polymers. However, the wobble LTW of polymers is one of the least studied LTW study topics. The wobble amplitude and frequency both have a direct influence on laser material interaction time. The wobbling scanners, such as galvanometers, polygons, and resonance, allow modify the required weld seam without changing the optical configuration of the laser head. A detailed investigation of the wobble LTW of dissimilar polymers has been carried out using experimental study, empirical modelling, and process optimization. An Nd:YVO_4 laser with beam wobbling facility is utilized to conduct the LTW between transparent acrylic and polycarbonate, with a black ink line acting as laser absorber applied at the interface. A morphological analysis of the fusion zone is carried out in order to determine the process of joining and the influence of beam wobbling action. This research also addresses the existing research gap in the utilization of advanced optimization techniques for TWIST welding, considering the highly non-linear nature of the process and conflicting objectives. The outcomes of this study will provide insights into the effectiveness and comparative performance of ANN-NSGA-II and ANN-NSTLBO, facilitating the selection of an appropriate optimization strategy for TWIST welding in industrial applications.

6.2.1 Experimental Planning

Transparent acrylic and polycarbonate plaques, each of size 80 mm × 40 mm × 4 mm, are selected as workpiece materials. An Nd:YVO_4 laser (EMS 100; Electrox Ltd.) with beam wobbling feature is employed to perform the wobble LTW of dissimilar transparent polymers. The top half of the assembly is transparent acrylic plaque, while the bottom part is transparent polycarbonate plaque in a lap joint configuration. A narrow strip of transparent polymer is marked with a black marker along the desired weld line to serve as the laser absorber. Laser

spot diameter and the stand-off distance are kept constant throughout the experimentation. The stand-off distance between the laser optic and the top polymer surface is fixed at 185 mm. A welding fixture is utilized to hold the workpieces in the correct position during the experiments. Mechanical clamping is used to maintain a consistent pressure during the experiment. The pictorial view of the mechanical clamping is shown in Figure 6.2.1.

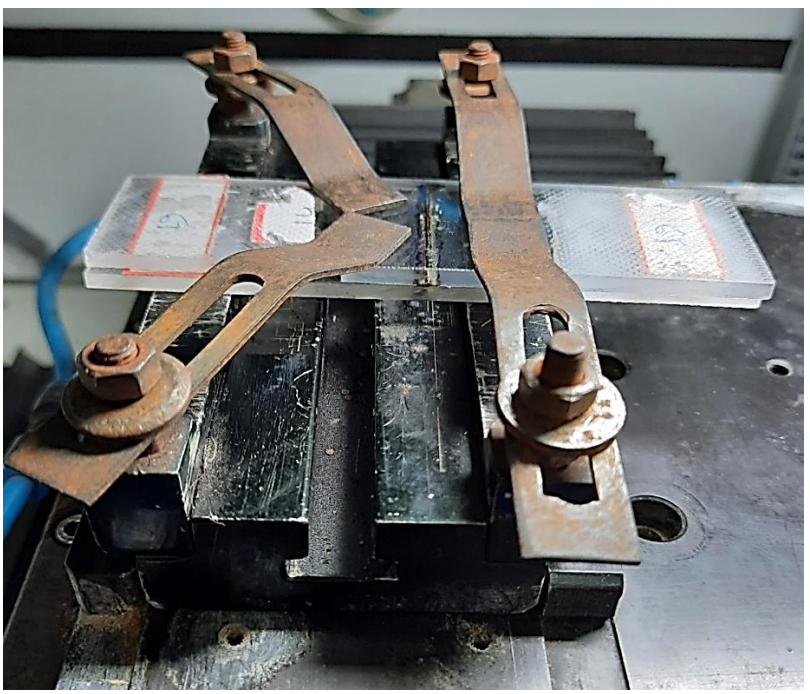

Figure 6.2.1: Pictorial view of welding fixture used for experimental work

Bolted connections are used in this clamping to provide sufficient pressure to produce intimate contact at the interface, ensuring enhanced heat conduction from the absorbent part to the top transparent part. The fixture is used for repetitive operations in order to keep the lapping area consistent during each run and to avoid misalignment of the components to be welded. Lap welding is conducted with a 30 mm overlap of the plaques, and the laser beam is directed on the intended weld line, the center line of the overlap. Figure 6.2.2 (a) & (b) presents the schematic and pictorial view of the welded sample. Laser power (LP), pulse frequency (PF), scanning speed (SS), wobble width (WO) and wobble frequency (WF) are considered as the process parameters while weld shear strength (WS) and weld seam width (WW) are the process responses.

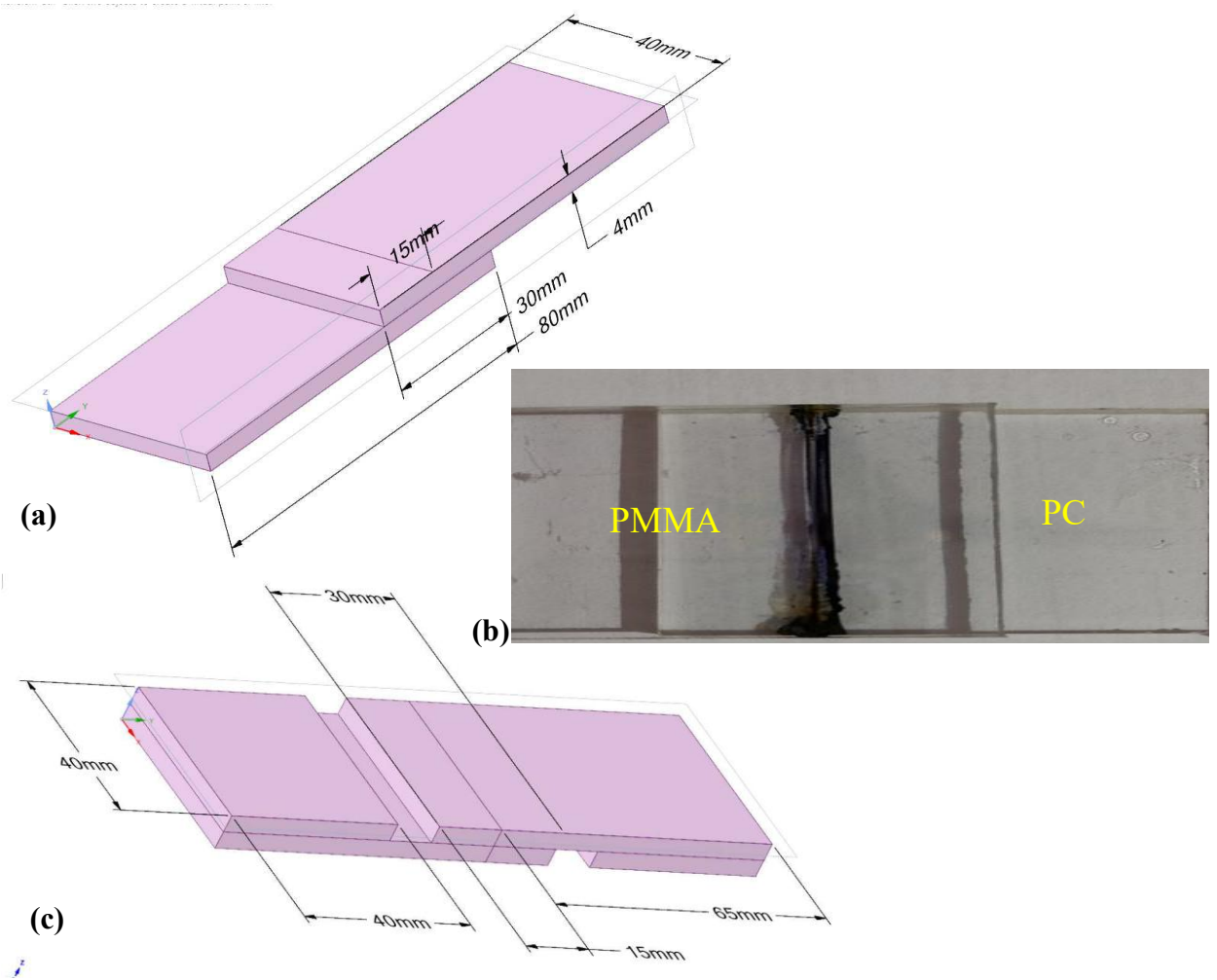

Figure 6.2.2: (a) Schematic, and (b) pictorial view of the welded sample, and (c) the schematic view of the tensile test specimen

A universal tensile testing machine (Model 8801, Instron) has been utilized for the lap shear test of the welded sample. The maximum breaking-load that a welded sample can withstand during a lap shear test before failing is considered the joint strength and is referred to as weld shear strength in this study. The test sample is marked about 35 mm from the weld centerline before pulling, and the grip ends are aligned with these marks. As illustrated in Figure 6.2.2 (c), a square plaque 40 mm^2 is affixed at each free ends of the test sample to prevent bending during lap shear test of the welded sample. Super glue is used to paste the square plaque on the test sample. Furthermore, to avoid slipping during the lap-shear test, each specimen is roughened on both sides of two ends. The schematic diagram of test specimen along with fixture is shown in Figure 6.2.3. The seam width of the welded sample is measured using a 3-dimensional optical measuring microscope (STM-6, OLYMPUS). Each sample is measured three times, and the average of these readings is used for analysis. A metallurgical scanning electron microscope (EVO 18 Special Edition, ZEISS) is used to study the weld

morphology. Figure 6.2.4 (a) & (b) compare the irradiation strategies of contour laser welding and wobble laser welding. Figure 6.2.4 (b) also depicts the beam oscillation mode and irradiation strategy utilized in this investigation.

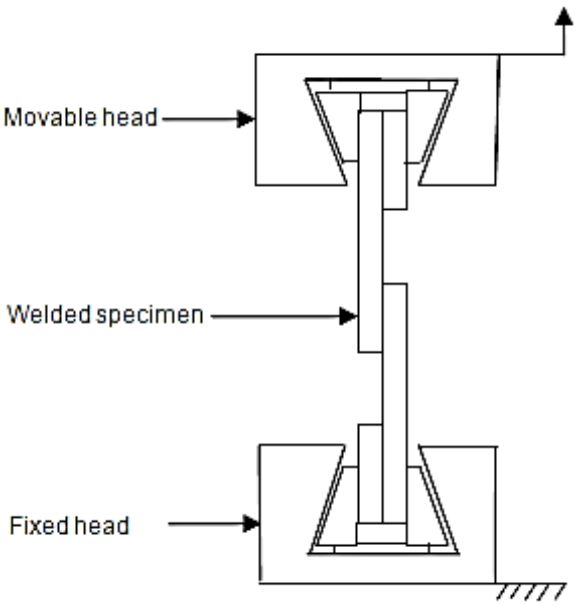

Figure 6.2.3: Schematic diagram of tensile testing of sample for the lap shear test

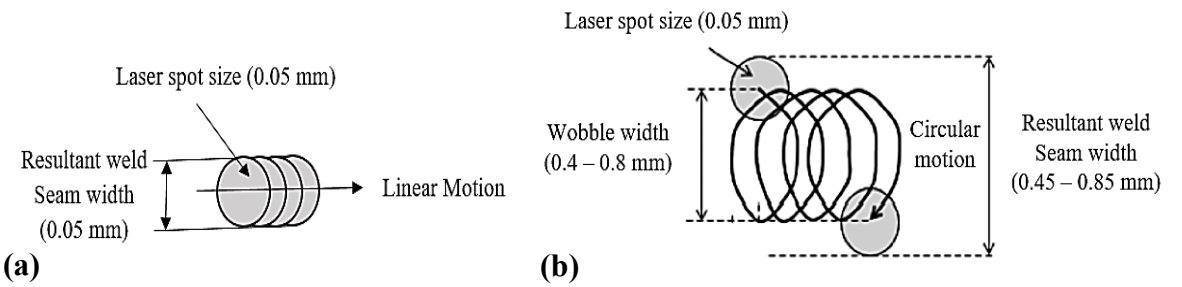

Figure 6.2.4: Schematic diagram of (a) contour laser welding, and (b) wobble laser welding

The five-factor three-level face centered cubic (FCC) variant of central composite design of RSM is utilized for executing the experimental plan. The FCC design is one of the well-organized experimental design techniques used for fitting second order regression models. On the basis of this design, fifty experiments with three replications need to be carried out, using 32 factorial points, ten star points, and eight center points. Based on the literature survey and the specifications of the laser system utilized, a series of trial tests are carried out to establish the possible ranges of process parameters, as shown in Table 6.2.1.

Table 6.2.1: Process control parameters and their levels

Controllable Parameters	Units	Notations	Levels		
			-1	0	+1
Laser Power (*A*)	W	LP	7.89	8.12	8.35
Pulse Frequency (*B*)	kHz	PF	25	30	35
Scanning Speed (*C*)	mm/s	SS	2	3	4
Wobble width (*D*)	mm	WO	0.4	0.6	0.8
Wobble frequency (*E*)	kHz	WF	1	3	5

6.2.2. Parametric Analysis Based on RSM Modelling

Table 6.2.2 presents the experimental plan as well as the measured value of the responses.

Table 6.2.2: Design matrix and measured experimental result

Experimental information						Results	
Exp. No.	Welding parameters					Weld shear strength (N)	Weld seam width (mm)
	LP (W)	PF (kHz)	SS (mm/s)	WO (mm)	WF (kHz)		
1	7.89	25	2	0.4	1	471.24	0.479
2	8.35	25	2	0.4	1	487.23	0.619
3	7.89	35	2	0.4	1	474.38	0.403
4	8.35	35	2	0.4	1	488.87	0.589
5	7.89	25	4	0.4	1	446.08	0.443
6	8.35	25	4	0.4	1	462.18	0.507
7	7.89	35	4	0.4	1	461.72	0.359
8	8.35	35	4	0.4	1	476.22	0.515
9	7.89	25	2	0.8	1	475.44	0.543
10	8.35	25	2	0.8	1	487.43	0.643
11	7.89	35	2	0.8	1	465.08	0.546
12	8.35	35	2	0.8	1	483.57	0.710
13	7.89	25	4	0.8	1	429.78	0.519
14	8.35	25	4	0.8	1	439.77	0.602
15	7.89	35	4	0.8	1	431.92	0.509

16	8.35	35	4	0.8	1	445.41	0.654
17	7.89	25	2	0.4	5	543.24	0.634
18	8.35	25	2	0.4	5	562.98	0.681
19	7.89	35	2	0.4	5	552.13	0.586
20	8.35	35	2	0.4	5	572.37	0.668
21	7.89	25	4	0.4	5	495.33	0.529
22	8.35	25	4	0.4	5	513.08	0.495
23	7.89	35	4	0.4	5	522.72	0.453
24	8.35	35	4	0.4	5	539.97	0.508
25	7.89	25	2	0.8	5	479.69	0.577
26	8.35	25	2	0.8	5	500.00	0.548
27	7.89	35	2	0.8	5	477.03	0.587
28	8.35	35	2	0.8	5	497.32	0.682
29	7.89	25	4	0.8	5	402.28	0.493
30	8.35	25	4	0.8	5	419.03	0.422
31	7.89	35	4	0.8	5	417.17	0.526
32	8.35	35	4	0.8	5	434.41	0.553
33	7.89	30	3	0.6	3	497.65	0.531
34	8.35	30	3	0.6	3	517.77	0.642
35	8.12	25	3	0.6	3	616.82	0.618
36	8.12	35	3	0.6	3	646.59	0.587
37	8.12	30	2	0.6	3	607.47	0.613
38	8.12	30	4	0.6	3	566.94	0.487
39	8.12	30	3	0.4	3	541.29	0.452
40	8.12	30	3	0.8	3	498.12	0.475
41	8.12	30	3	0.6	1	507.71	0.682
42	8.12	30	3	0.6	5	524.71	0.739
43	8.12	30	3	0.6	3	582.43	0.591
44	8.12	30	3	0.6	3	577.43	0.602
45	8.12	30	3	0.6	3	580.12	0.579
46	8.12	30	3	0.6	3	574.43	0.574
47	8.12	30	3	0.6	3	579.23	0.613

48	8.12	30	3	0.6	3	582.58	0.598
49	8.12	30	3	0.6	3	578.57	0.585
50	8.12	30	3	0.6	3	572.41	0.583

6.2.3. Second Order Regression Equation of Responses

Mathematical models are developed to establish a correlation between input and output parameters to understand the behaviour of process parameters on responses. Design Expert® software is employed for mathematical modelling and parametric analysis. The adequacy of the derived model is tested using the analysis of variance (ANOVA), the F-test, and the lack of fit test.

The developed mathematical models for lap shear strength (Y_{ws}) in terms of coded and actual factors are given as follows:

(a) In terms of coded factors,

$$Y_{ws} = 574.99 + 8.37\,A + 4.57\,B - 21.22\,C - 24.34\,D + 15.28\,E + 3.70\,BC - 2.77\,BD + 2.17\,BE - 6.58\,CD - 6.27\,CE - 17.67\,DE - 63.87\,A^2 + 60.13\,B^2 + 15.63\,C^2 - 51.87\,D^2 - 55.37\,E^2 \quad \text{..... (6.2.1)}$$

(b) In terms of actual factors,

$$Y_{ws} = -76287.02 + 19306.65\,A - 144.60\,B - 108.05\,C + 1748.73\,D + 120.08\,E + 0.74\,BC - 2.76\,BD + 0.21\,BE - 32.91\,CD - 3.13\,CE - 44.17\,DE - 1186.61\,A^2 + 2.40\,B^2 + 15.62\,C^2 - 1296.82\,D^2 - 13.84\,E^2 \quad \text{..... (6.2.2)}$$

The developed mathematical models for weld seam width (Y_{ww}) in terms of coded and actual factors are given as follows:

(a) In terms of coded factors,

$$Y_{ww} = 0.59 + 0.039\,A + 0.0024\,B - 0.045\,C + 0.02\,D + 0.011\,E + 0.019\,AB - 0.011\,AC - 0.0056\,AD - 0.027\,AE + 0.023\,BD + 0.0079\,BE + 0.0091\,CD - 0.017\,CE - 0.031\,DE - 0.039\,C^2 - 0.13\,D^2 + 0.012\,E^2 \quad \text{.....(6.2.3)}$$

(b) In terms of actual factors,

$$Y_{ww} = -0.772 + 0.068\,A - 0.148\,B + 0.579\,C + 4.258\,D + 0.344\,E + 0.016\,AB - 0.048\,AC - 0.122\,AD - 0.058\,AE + 0.022\,BD + 0.00079\,BE + 0.045\,CD - 0.00875\,CE - 0.076\,DE - 0.038\,C^2 - 3.127\,D^2 + 0.03\,E^2 \quad \text{..... (6.2.4)}$$

6.2.4. ANOVA Analysis for Responses

ANOVA is performed to evaluate the significant terms and adequacy measures such as R^2, R^2-adjusted and R^2-predicted of developed model. Model terms with a "Prob>f" less than 0.05 imply that the model terms are statistically significant at the 95 % confidence level. The remaining terms are non-significant terms that are eliminated using a backward elimination method to improve the adequacy of the model. Table 6.2.3 furnishes the results of ANOVA for the reduced quadratic model (after backward elimination of non-significant model terms) of weld shear strength. The reduced model has a "Prob>f" value of less than 0.05, suggesting that the model is significant. The R^2-predicted of 0.9871 agrees with the R^2-adjusted of 0.993 and is close to unity, indicating that the model is adequate. The adequate precision compares the signal-to-noise ratio, and a ratio larger than 4 is preferred. The adequate precision ratio of 83.957 suggests a good signal for navigating the design space. The lack-of-fit f-value of 2.043 indicates that the lack-of-fit is not significant in comparison to the pure error, which is desired.

Table 6.2.3: ANOVA results for weld shear strength (after backward elimination)

Source	Sum of squares	df	Mean squares	F-value	Prob>f	
Model	168082.68	16	10505.17	448.598	< 0.0001	significant
A-LP	2384.56	1	2384.56	101.827	< 0.0001	
B-PF	709.11	1	709.11	30.281	< 0.0001	
C-SS	15308.57	1	15308.57	653.716	< 0.0001	
D-WO	20143.35	1	20143.35	860.173	< 0.0001	
E-WF	7935.18	1	7935.18	338.853	< 0.0001	
BC	438.92	1	438.92	18.743	0.0001	
BD	244.91	1	244.91	10.458	0.0028	
BE	150.81	1	150.81	6.440	0.0161	
CD	1386.42	1	1386.42	59.204	< 0.0001	
CE	1257.90	1	1257.90	53.716	< 0.0001	

DE	9989.59	1	9989.59	426.582	< 0.0001	
A^2	10089.13	1	10089.13	430.832	< 0.0001	
B^2	8941.74	1	8941.74	381.836	< 0.0001	
C^2	603.99	1	603.99	25.792	< 0.0001	
D^2	6655.34	1	6655.34	284.200	< 0.0001	
E^2	7582.37	1	7582.37	323.787	< 0.0001	
Residual	772.79	33	23.42			
Lack of Fit	682.82	26	26.26	2.043	0.1665	Not significant
Pure Error	89.97	7	12.85			
Cor Total	168855.47	49				
Standard deviation = 4.839				R^2 = 0.995		
Mean = 510.147				Adjusted R^2 = 0.993		
Coefficient of variation = 0.949				Predicted R^2 = 0.987		
Predicted residual error of sum of square = 2179.689				Adequate precision = 83.957		

ANOVA is used to analyse the significant model terms and adequacy measures of the developed model for weld seam width, such as R^2, R^2-adjusted and R^2-predicted. The non-significant model terms are removed using the backward elimination approach to improve the model's adequacy; nevertheless, the primary effect of pulse frequency is added to the support hierarchy. The ANOVA results for the reduced quadratic model of weld seam width are furnished in Table 6.2.4. The reduced model is statistically significant since it has a "Prob>f" value less than 0.05. R^2-predicted, R^2-adjusted, adequate precision ratio, and lack-of-fit f-value of 0.942, 0.965, 41.209, and 1.499, respectively, all indicate that the developed model is adequate.

Table 6.2.4: ANOVA results for weld seam width (after backward elimination)

Source	Sum of squares	df	Mean squares	F-value	Prob>f	
Model	0.3182	17	0.0187	79.4955	< 0.0001	significant
A-LP	0.0513	1	0.0513	217.9789	< 0.0001	
B-PF	0.0002	1	0.0002	0.8605	0.3605	
C-SS	0.0692	1	0.0692	293.9405	< 0.0001	

D-WO	0.0132	1	0.0132	55.9063	< 0.0001	
E-WF	0.0038	1	0.0038	16.0990	0.0003	
AB	0.0116	1	0.0116	49.3853	< 0.0001	
AC	0.0040	1	0.0040	17.2006	0.0002	
AD	0.0010	1	0.0010	4.3962	0.0440	
AE	0.0234	1	0.0234	99.5345	< 0.0001	
BD	0.0165	1	0.0165	69.9537	< 0.0001	
BE	0.0020	1	0.0020	8.5626	0.0063	
CD	0.0027	1	0.0027	11.3163	0.0020	
CE	0.0098	1	0.0098	41.6211	< 0.0001	
DE	0.0299	1	0.0299	126.9449	< 0.0001	
C^2	0.0043	1	0.0043	18.3452	0.0002	
D^2	0.0454	1	0.0454	192.6779	< 0.0001	
E^2	0.0431	1	0.0431	182.9352	< 0.0001	
Residual	0.0075	32	0.0002			
Lack of Fit	0.0063	25	0.0003	1.4990	0.3025	Not significant
Pure Error	0.0012	7	0.0002			
Cor Total	0.3257	49				
Standard deviation = 0.0153				R^2 = 0.977		
Mean = 0.5627				Adjusted R^2 = 0.965		
Coefficient of variation = 2.7272				Predicted R^2 = 0.942		
Predicted residual error of sum of square = 0.0188				Adequate precision = 41.209		

6.2.5. Validation of the developed models

The mathematical models developed using RSM are validated via a confirmation experiments. Three confirmation tests are carried out by selecting three different process parameter settings at random within the specified design space. The actual results are calculated by averaging three measured values for each response. The percentage error of the confirmation experiment is calculated by comparing the actual results to the predicted values derived from the mathematical models, and is shown in Table 6.2.5. The validation experiment reveals a small percentage of error between experimental and predicted results,

confirming that the developed model produces reliable results. The relationship between the actual and predicted results for weld shear strength and weld seam width is displayed in Figure 6.2.5 (a) & (b).

Table 6.2.5: Validation test results

Exp. No.	LP (W)	PF (kHz)	SS (mm/s)	WO (mm)	WF (kHz)		Weld shear strength (N)	Weld seam width (mm)
1	7.89	27	3	0.5	4	Actual	498.24	0.487
						Predicted	514.45	0.520
						|Error| %	3.25	6.77
2	8.12	30	2	0.4	3	Actual	546.37	0.407
						Predicted	572.68	0.387
						|Error| %	4.81	4.91
3	8.35	33	4	0.6	2	Actual	543	0.493
						Predicted	516.65	0.517
						|Error| %	4.85	4.86

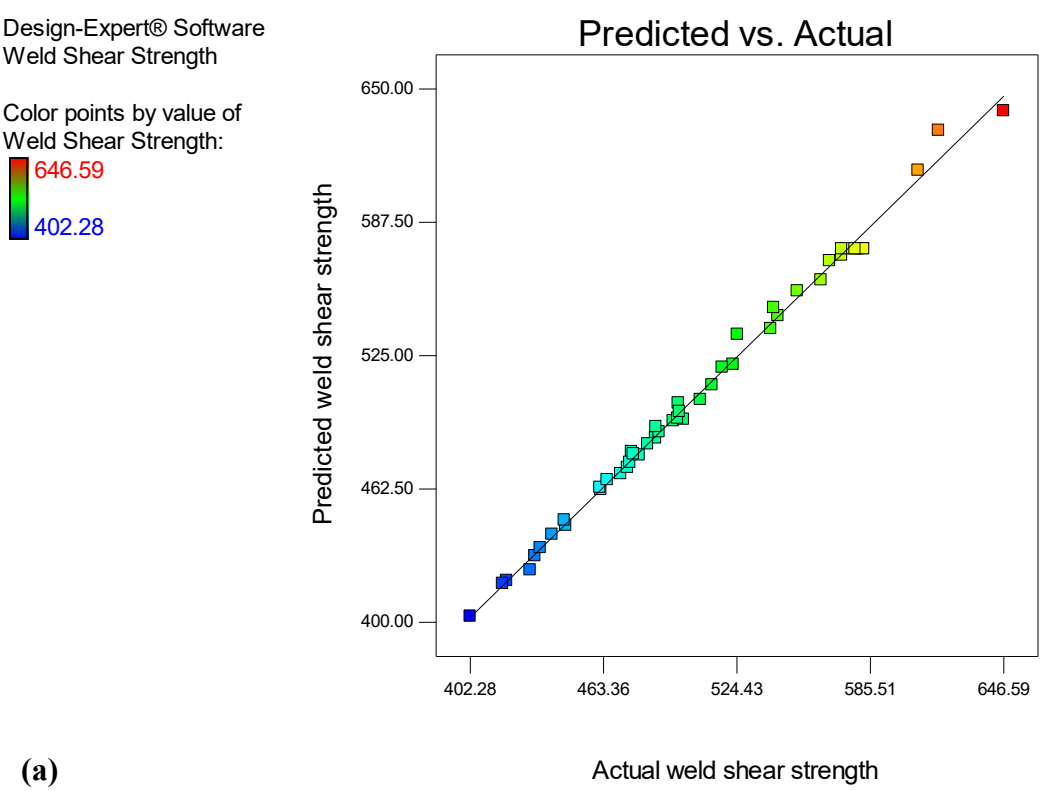

(a)

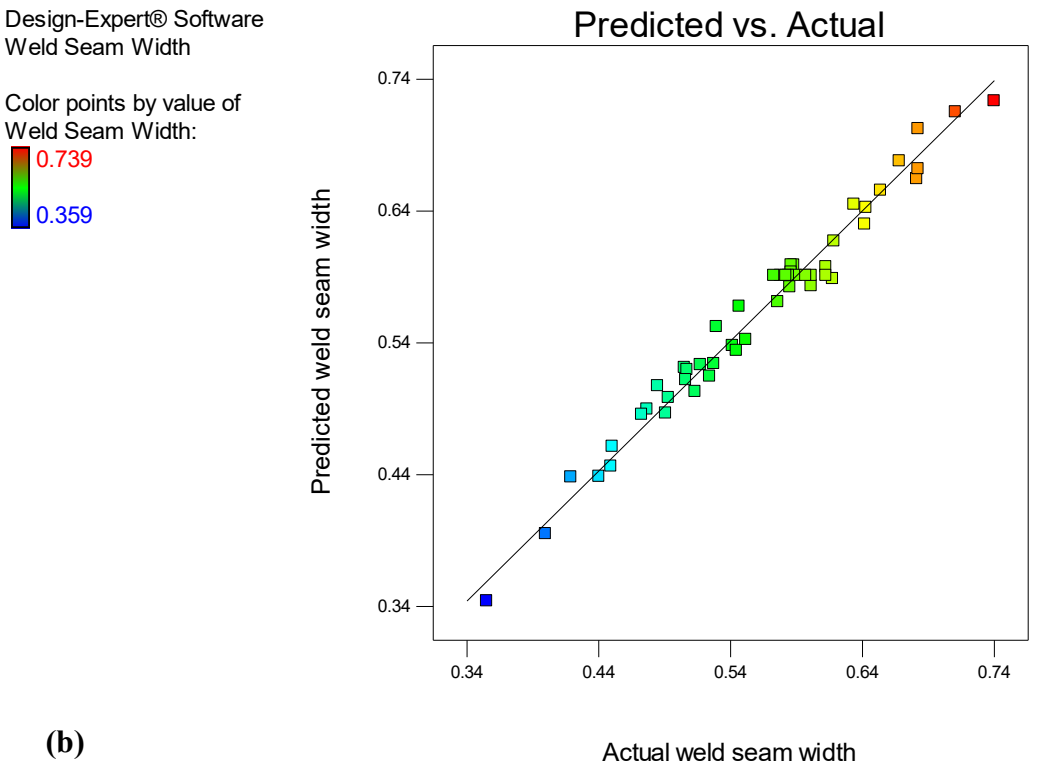

(b)

Figure 6.2.5: Plot of actual vs. predicted response of (a) weld shear strength, and (b) weld seam width

6.2.6. Parametric Analysis

The effects of process variables on weld quality characteristics such as weld shear strength and weld seam width, within the specified range, are thoroughly investigated. The surface interaction plot depicts the behaviour of responses as the value of the process variable changes; the rationale for this is discussed in detail.

6.2.6.1 Weld Shear Strength

The perturbation plot (Figure 6.2.6) depicts the effects of all process variables on weld shear strength at the center point of the specified design space. The perturbation plot shows that weld shear strength increases with laser power, wobble width, and wobble frequency up to the center point, then begins to decline with further increase of corresponding parameter. This may happen for a variety of causes, including those listed below. Heat input increases with laser power since it directly varies with line energy; hence, higher energy leads to optimal material interfusion. However, ablation of base material occurs with higher laser power, which weakens the joint. Wobble width increases the width of the seam and improves material

intermixing through an expanded turbulence zone in the weld pool, which increases weld shear strength. A wider wobbling width, on the other hand, scatters the line energy, resulting in a decreased heat input to the fusion zone. Spatter development causes weld strength to be reduced at higher wobbling frequencies. The scanning speed has an inverse relationship with weld shear strength. Laser interaction time decreases as scanning speed increases. It can also be observed that weld shear strength reduces with increasing pulse frequency up to the center point, then begins to rise with increasing pulse frequency. At increasing pulse frequency, the laser interaction time increases.

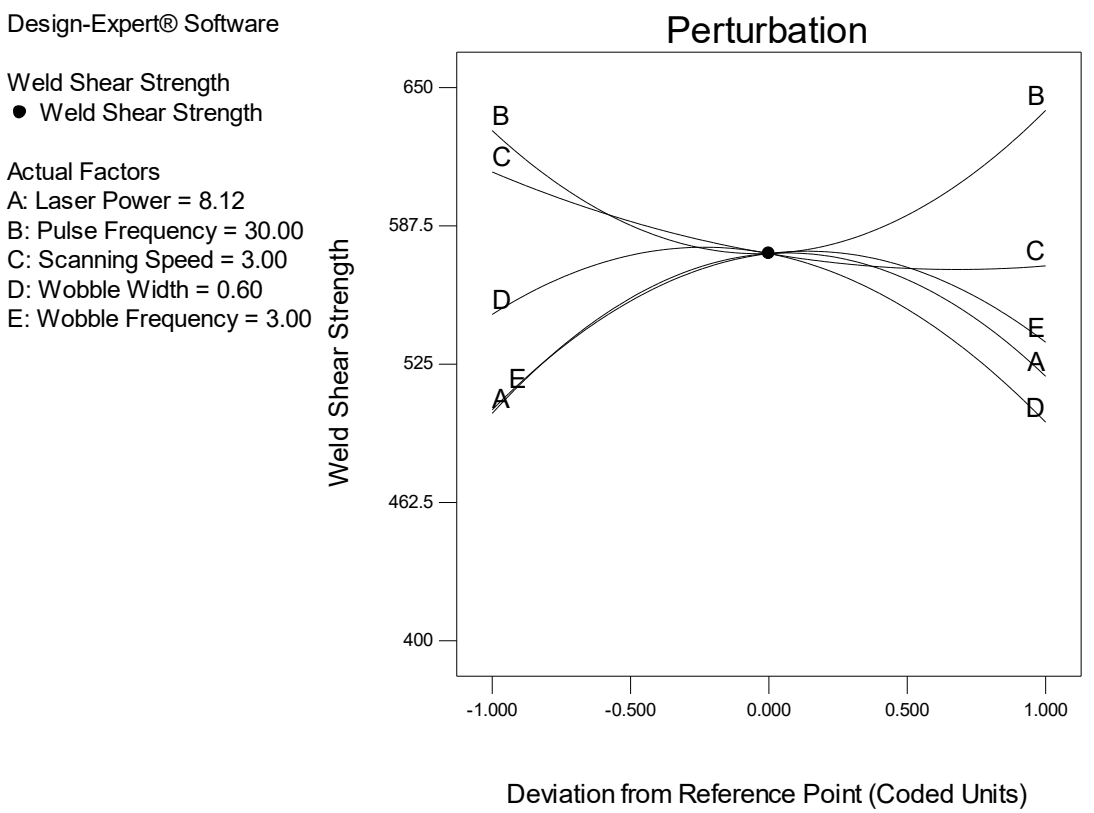

Figure 6.2.6: Perturbation plot showing the effect of all the factors on weld shear strength

The surface interaction plot of laser power and pulse frequency on weld shear strength is shown in Figure 6.2.7 (a). Weld shear strength is shown to be greater with higher pulse frequency and laser power of 8.12 watts. This is due to the fact that at low laser power, less energy is supplied to the weld, resulting in improper material fusing. The maximum weld shear strength is found to be at 8.12 watts of laser power, since adequate line energy enhanced the melt volume and weld strength. Ablation and material degradation may occur beyond this

range owing to the high laser heat input, which may have a detrimental effect on weld shear strength. At lower pulse frequencies, the less interaction time results in reduced energy dissipation and poor polymer intermixing. As the pulse frequency increases, the long laser pulse interactions improve the weld shear strength. To achieve higher weld shear strength, the laser power and pulse frequency must be precisely adjusted. Figure 6.2.7 (b) depicts the interaction plot of laser power and scanning speed on weld shear strength. Weld strength is shown to be higher at low scanning speeds and medium laser power level. At lower scanning speeds, the laser contact duration increases, increasing the energy input to the weld zone and causing more base material melted and improved fusion. Higher scanning speed, on the other hand, reduces the laser material interaction time, resulting in less energy input to the weld zone, which reduces weld shear strength. Heat loss can be minimized with faster scanning speeds due to less time for heat conduction. However, it is feasible to achieve adequate weld shear strength using low power laser by keeping the scanning speed low.

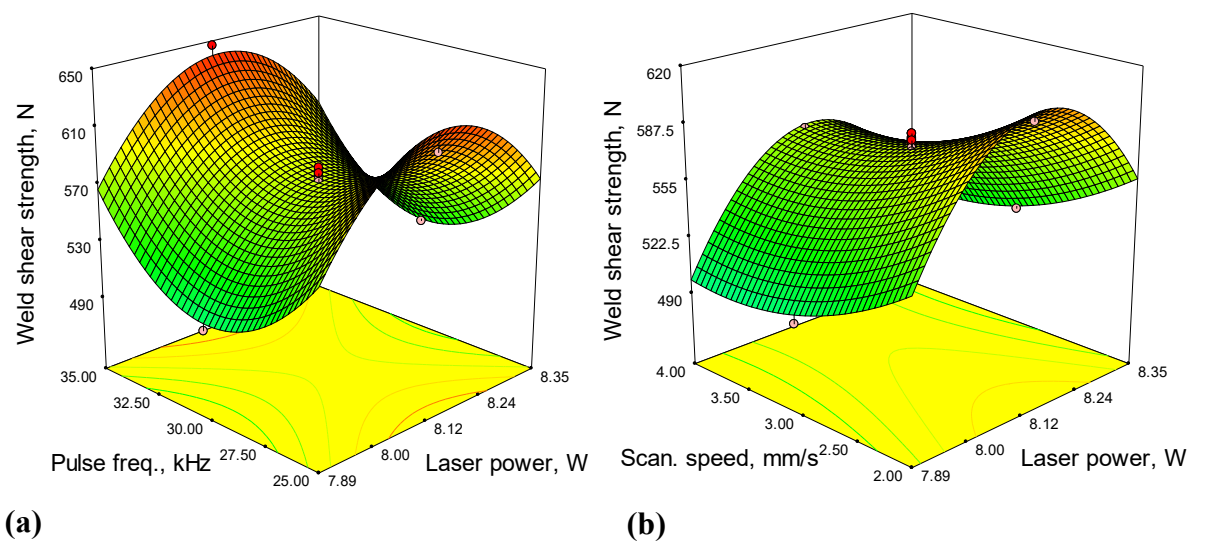

Figure 6.2.7: Surface plot showing the interaction effects of (a) laser power and pulse frequency, and (b) laser power and scanning speed on weld shear strength, when all other parameters are at their central values

The surface interaction plot of wobbling frequency and scanning speed on weld shear strength is shown in Figure 6.2.8 (a). Higher weld strength is found at lower scanning speeds with the middle of the wobbling frequency range. Laser interaction time is expected to be higher at lower scanning speed. Weld strength begins to deteriorate when the wobbling diameter is either small or too large. This is due to the fact that the distances between two subsequent laser loops is directly linked to the frequency of oscillation or wobble, thus more

homogenized distribution of laser energy is found at mid value of wobble frequency which increases the material fusing with less heat affected zone. Figure 6.2.8 (b) depicts the interaction plot of wobbling width and frequency on weld shear strength. The wobbling parameter is critical in the welding of dissimilar materials. It is worth noting that maximum weld strength is attained around the mid value of the wobble width, where the difference between theoretical weld width (wobble width + laser spot diameter) and actual weld width is nearly zero. This occurs because wobbling causes melt pool turbulence, allows for good heat transfer, and allows polymers to mix properly. Weld shear strength improves with an increase in wobbling frequency up to a mid-value, then decreases. Wobble frequency expands the overlap region, reducing penetration for high oscillation frequencies. Higher weld strength necessitates the use of the optimal value of wobbling frequency. Circular oscillation mode is employed to achieve better weld quality. A wobbling frequency of 3 kHz resulted in the highest weld shear strength.

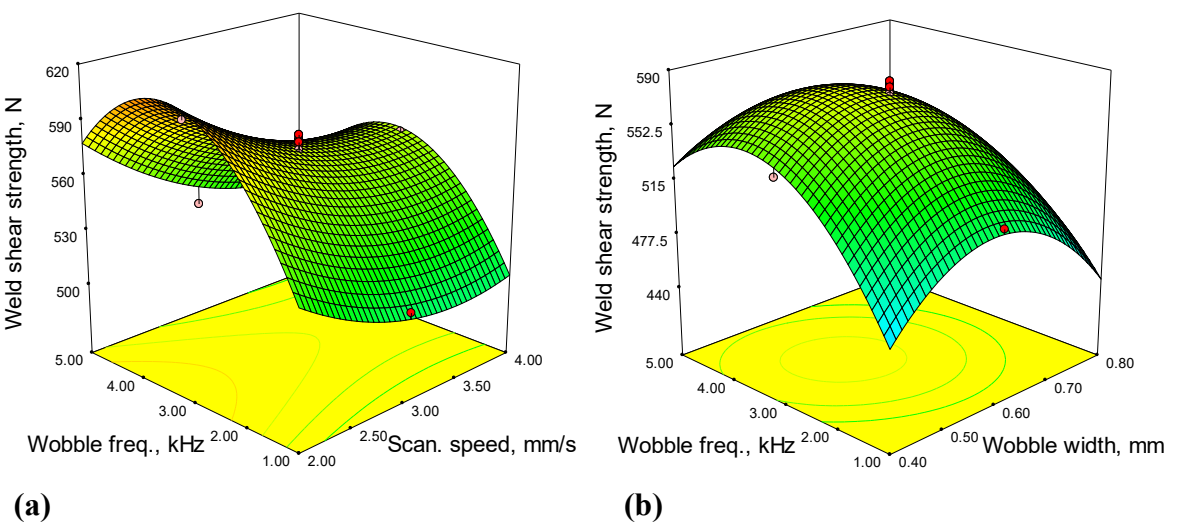

Figure 6.2.8: Surface plot showing the interaction effects of (a) scanning speed and wobble frequency, and (b) wobble width and wobble frequency on weld shear strength, when all other parameters are at their central values

6.2.6.2 Weld Seam Width

The perturbation plot (Figure 6.2.9) depicts the effects of all process variables on the weld seam width at the centre point of the specified design space. The power of the laser appears to have a positive influence on weld seam width. This is due to the fact that increasing laser power increases power density, which increases melt volume and hence the seam width. Within the parameter range utilized, the effect of pulse frequency on weld seam width is

shown to be insignificant. Weld seam width rises as an increment of wobbling width up to its center value, and then begins to decrease. Wobble width increases oscillation amplitude, which increases seam width, however larger oscillation width has an unfavourable effect on weld fusion. Weld seam width is inversely related to scanning speed. This is due to the fact that line energy reduces with increasing scanning speed, resulting in less heat input and a lower amount of material melted. The plot shows that as the wobbling frequency increases, the weld width decreases until it hits the center value, at which point it begins to expand. As wobble frequency is directly related to overlap area, and most laser overlap occurs at higher wobble frequency, and it is not affected by heat. Furthermore, when the wobbling frequency rises, the volume of the melt pool expands and the lower temperature gradient causes the enlargement of weld seam width.

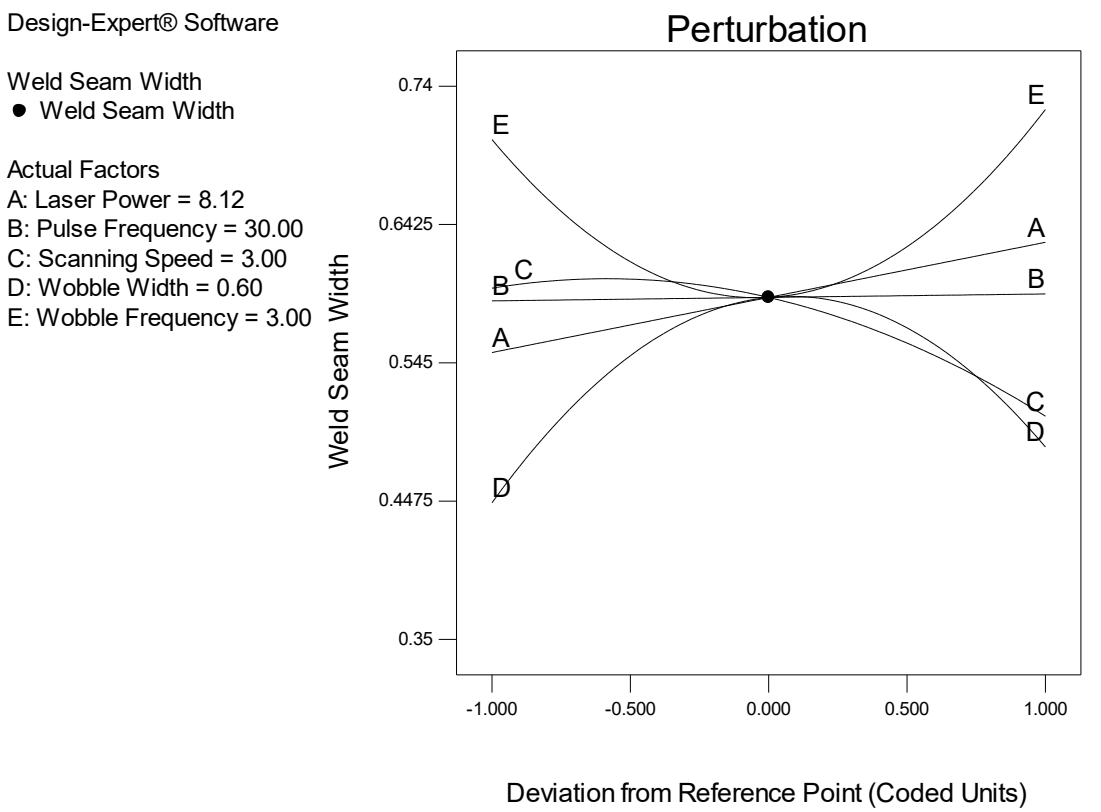

Figure 6.2.9: Perturbation plot showing the effect of all factors on weld seam width

The surface interaction plot of laser power and pulse frequency on weld seam width is shown in Figure 6.2.10 (a). Weld seam width increases considerably with an increase in laser power up to 8.12 watt; additional increases in laser power only minimally enhance weld width. This is due to the fact that increasing the laser power promotes the melting of a larger volume of

base material, resulting in an increase in weld width. A very high laser power may degrade the base material and increase penetration depth. At higher laser power and pulse frequency, maximum weld width is attained. This might occur because increasing the pulse frequency extends the irradiation time by triggering more pulses, and with greater laser power, more energy is supplied, resulting in more energy transferred to the weld fusion zone. To accomplish the desired weld seam width, the optimum combination of laser power and pulse frequency is required. Figure 6.2.10 (b) depicts the surface interaction plot of laser power and scanning speed on weld seam width. Lower scanning speeds increase laser interaction time, which causes higher melt volume of material, increasing the weld width. Weld width gradually decreases until it reaches the midpoint of scanning speed, at which point it rapidly decreases. This is due to the fact that when the scanning speed increases; the irradiation time reduces, resulting in less heat input and a narrow weak weld width. Penetration depth reduces as scanning speed increases; therefore a slower scanning speed is preferred for greater seam width and penetration depth.

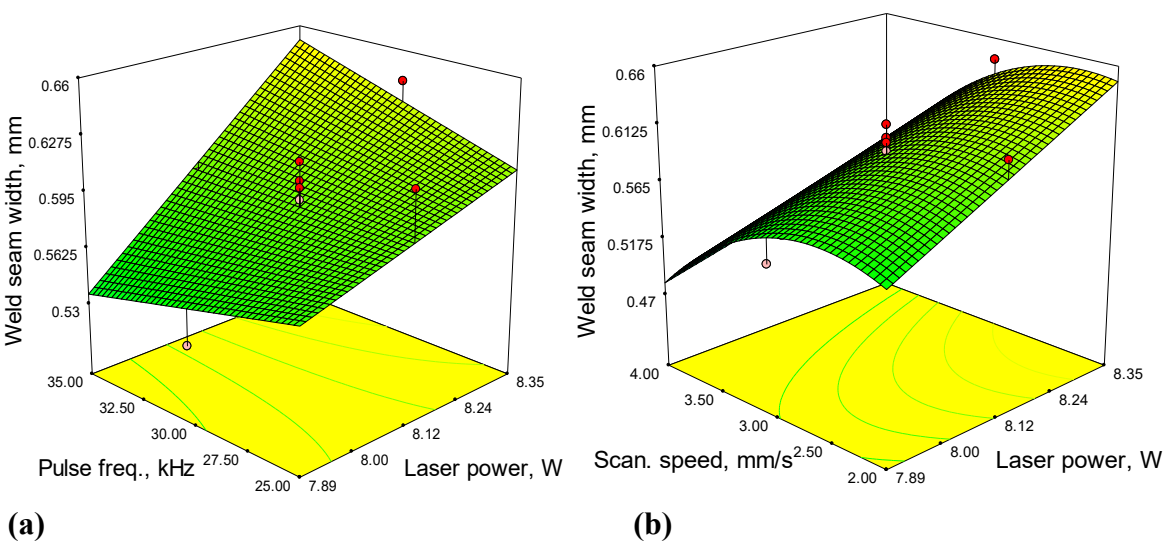

Figure 6.2.10: Surface plot showing the interaction effects of (a) laser power and pulse frequency, and (b) laser power and scanning speed on weld seam width, when all other parameters are at their central values

The surface interaction plot of scanning speed and wobbling frequency on weld seam width is shown in Figure 6.2.11 (a). Weld width is found to be maximum at the highest wobbling frequency and slowest scanning speed. The greater the wobbling frequency, the more overlaps there are, and the slower the scanning speed, the longer the interaction periods, and therefore the wider the weld. Figure 6.2.11 (b) depicts the interaction plot of wobble width

and wobbling frequency on weld seam width. Beam wobbling increases seam width while improving joint quality and weld width. It is observed that the maximum weld seam width is obtained at 0.6 mm wobble width, where the theoretical weld width (wobble width + laser spot diameter) is nearly equal to actual (experimental) weld seam width. The maximum weld seam width is obtained at the highest wobble frequency and the intermediate wobble width. Beam oscillation creates turbulence in the weld pool, which enhances polymer intermixing, accelerates solidification, and increases weld width. For improved intermixing and weld quality, the wobbling parameter must be set to their optimum values.

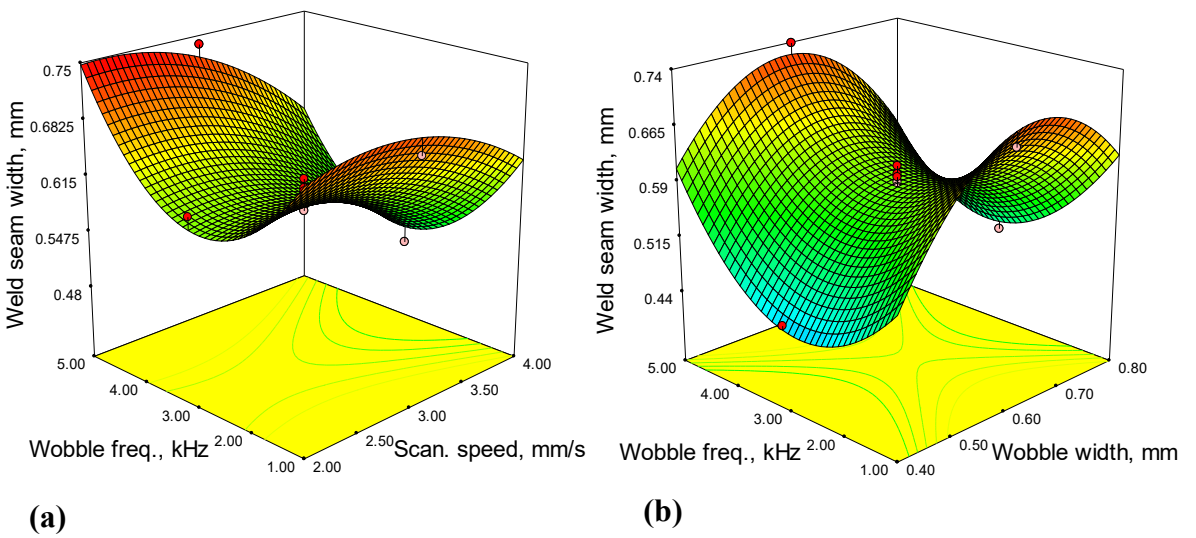

Figure 6.2.11: Surface plot showing the interaction effects of (a) scanning speed and wobble frequency, and (b) wobble width and wobble frequency on weld seam width, when all other parameters are at their central values

6.2.7. Performance evaluation of TWIST welding

Weld strength and weld width are critical performance metrics in TWIST welding, where their significance is underlined by their direct influence on joint reliability and load-carrying capacity. These metrics are intricately tied to the selection of process variables and experimental setup, further emphasizing the need for precise control and optimization to achieve superior weld quality. The graphs are plotted which serves as a visual representation of the intricate relationship between process variables and their impact on desired performance parameters in TWIST welding. It emphasizes the necessity for identifying the optimal range of process variables to ensure a defect-free seam with maximum weld strength, providing essential insights for achieving superior weld quality and mechanical integrity. Figure 6.2.12 depicts the influence of laser power on weld strength and weld seam width, as

the scanning speed is varied. The dotted line showcases the behaviour of weld strength, while the solid line captures the trends in weld seam width, providing insights into the complex interplay between laser power, scanning speed, and the resulting weld characteristics. It is evident that weld strength exhibits a discernible pattern with respect to the variation in laser power. Initially, as laser power increases, weld strength shows a progressive trend until reaching a mid-point. Beyond this critical threshold, however, weld strength begins to decline. The rationale behind this trend lies in the intricacies of heat input during TWIST welding. At the mid-range of laser power, the material experiences sufficient heat input, enabling proper interfusion and resulting in higher weld strength. Deviating from this mid-value, either towards lower or higher laser power, leads to adverse effects on the joint. Insufficient heat input at lower laser powers hampers proper material bonding, while excessively high laser powers degrade the material, leading to weakened joints. The observed phenomenon of weld width increasing with higher laser power can be attributed to the substantial increase in line energy delivered to the material. As the laser power is raised, a greater amount of energy is imparted to the material, resulting in increased heat input and a wider weld seam. The results reveal a decline in both weld strength and weld width as the scanning speed increases. These results can be attributed to the inverse relationship between line energy and scanning speed; higher scanning speeds result in reduced line energy, leading to insufficient heat input during the welding process. Consequently, inadequate heat input adversely affects material fusion, contributing to diminished weld strength and narrower weld seams.

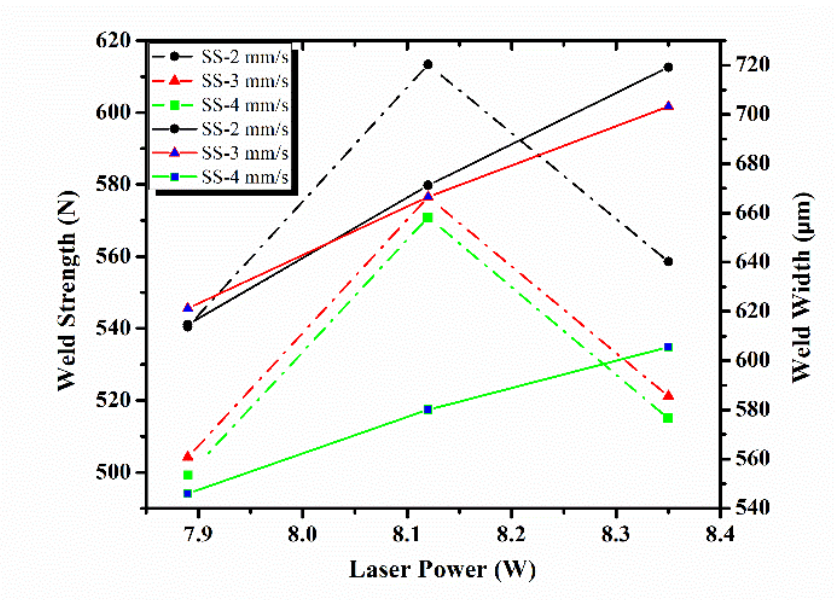

Figure 6.2.12 Effect of laser power on performance parameter at varying scan speed

Figure 6.2.13 shows the impact of varying pulse frequency on weld strength and weld seam width. The dotted line illustrates the variation in weld strength, while the solid line represents the changes in weld seam width, presenting insights into the interplay of pulse frequency and its effects on the mechanical properties and dimensions of the weld joint. A striking resemblance is observed between the trends of weld strength concerning the change in pulse frequency and laser power. In both cases, weld strength demonstrates an initial increase, reaching a critical threshold, beyond which it starts to decline. This intriguing similarity suggests a potential connection between pulse frequency and laser power in influencing the welding process and its impact on weld strength. Initially, as pulse frequency and laser power increase, the heat input to the material intensifies, resulting in improved material fusion and interfacial bonding, which contributes to higher weld strength. However, beyond a certain point, excessively high pulse frequency and laser power can lead to an overabundance of heat, causing adverse effects like increased material degradation, porosity, or overheating. These unfavourable conditions weaken the joint, leading to a decline in weld strength. The observed trend shows that at lower laser power, low pulse frequency results in higher weld width, while at higher laser power, higher pulse frequency leads to higher weld width. At lower laser power settings, low pulse frequencies provide longer pulse durations, resulting in greater heat input to the material, leading to a wider weld. Conversely, at higher laser power settings, higher pulse frequencies deliver shorter pulse durations but with higher energy per pulse. This concentrated and intense heat input facilitates more material melting, leading to wider welds.

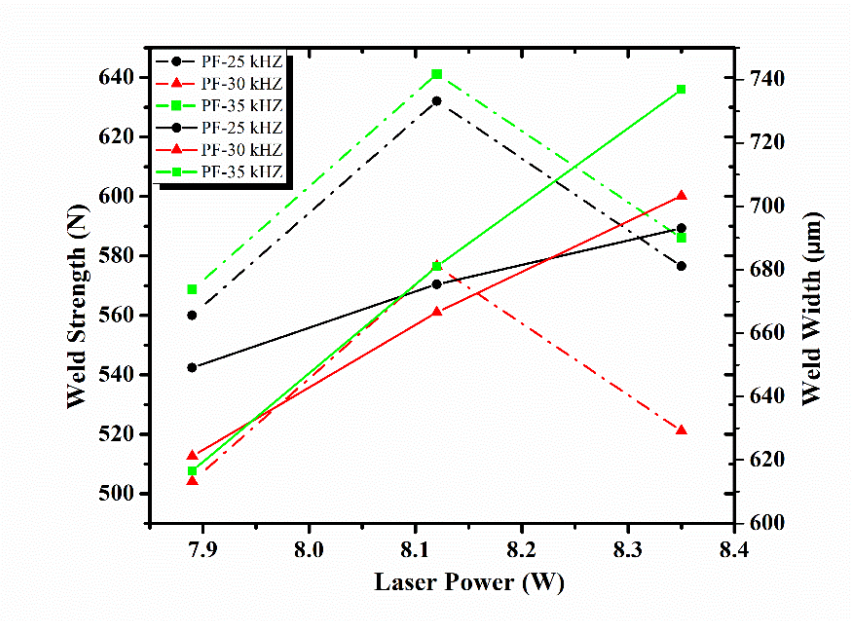

Figure 6.2.13 Effect of laser power on performance parameter at varying pulse frequency

In Figure 6.2.14, the impact of scanning speed on weld quality characteristics in TWIST welding is investigated by varying the pulse frequency. The dotted line represents the weld strength, while the solid line represents the weld seam width The trends for both weld strength and weld width exhibit a similar pattern, indicating a decrease in values with increasing scanning speed. This consistent behavior suggests that higher scanning speeds are associated with reduced weld strength and narrower weld seams in TWIST welding. The observed decrease in weld strength and weld width with increasing scanning speed can be attributed to the inverse relationship between scanning speed and laser heat input. The observed effect of increasing welding speed with higher pulse frequency is a reduction in weld strength. The combination of higher pulse frequency and faster welding speed leads to insufficient heat input, resulting in inadequate material fusion and weaker bonding at the weld interface. On the other hand, the impact on weld width varies when welding speed is combined with a higher pulse frequency. At lower welding speeds, increasing the pulse frequency results in wider welds due to a longer heat exposure time and more thorough material melting. However, at very high welding speeds, the heat input becomes insufficient to produce a wider weld, leading to a decrease in weld width.

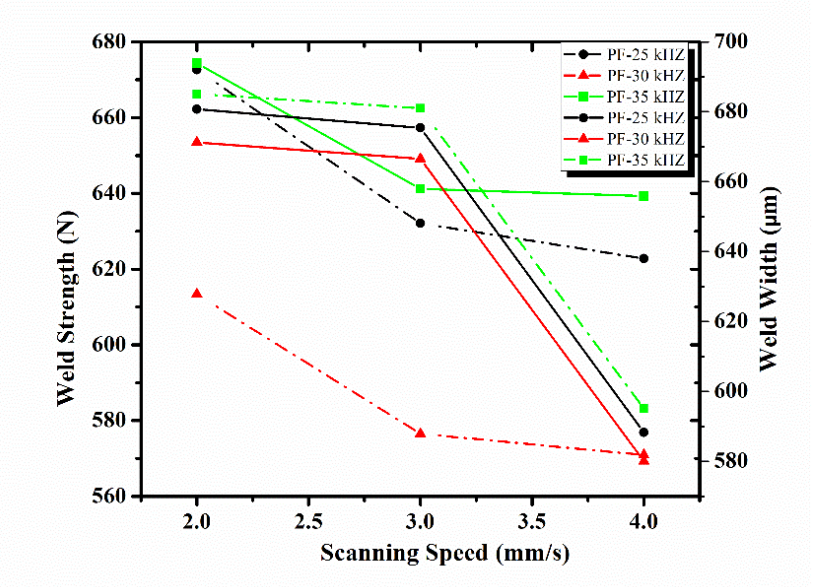

Figure 6.2.14 Effect of scanning speed on performance parameter at varying pulse frequency

In Figure 6.2.15, the relationship between wobble width and weld quality characteristics in TWIST welding is depicted through the variation of wobble frequency. The study explores how changes in wobble width and wobble frequency influence weld quality and provides

valuable insights into the impact of these TWIST welding parameters on weld strength and weld width. The observed trend in the effect of wobble width on weld strength and weld width follows a consistent pattern: an increase with wobble width up to a mid-point, beyond which both metrics decline. Wobble width contributes to widening the seam through the circular oscillation of the beam, promoting better material intermixing within an expanded turbulence zone in the weld pool, thereby enhancing weld shear strength. However, when the wobble width becomes too wide, it scatters the line energy, leading to a reduced heat input to the fusion zone, which subsequently affects both weld strength and width negatively. The observed trend where the mid value of wobble frequency consistently yields higher weld strength across the entire range of wobble width can be attributed to the synergistic effect of these parameters on the welding process. The mid value of wobble frequency ensures that the heat input to the fusion zone remains balanced and sufficient for proper material fusion without excessive scattering of line energy. This precise balance between heat input and material mixing at the mid-range of wobble frequency contributes to higher weld strength compared to both lower and higher wobble frequency values. The observations indicate that, at lower wobble width settings, increasing the wobble frequency results in more frequent oscillations of the laser beam, which in turn leads to a wider weld seam. On the other hand, at higher wobble width settings, lowering the wobble frequency allows for extended and spaced-out circular oscillations, providing sufficient time for the material to spread out and flow, resulting in a wider weld seam.

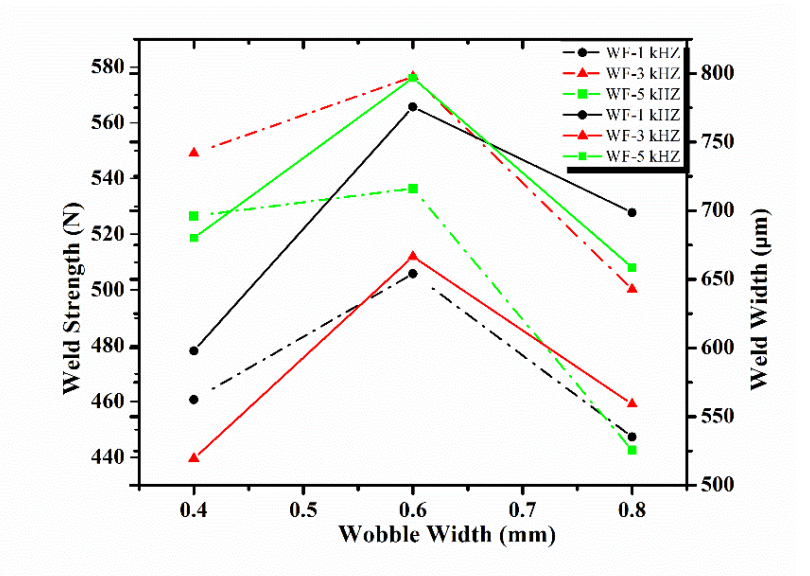

Figure 6.2.16 Effect of wobble width on performance parameter at varying wobble frequency

6.2.8. Morphological Analysis

The analysis of changes in microstructure/crystal structure at and around the weld bead is critical for understanding the process of dissimilar polymer joining. The weld zone morphology of the welded acrylic/polycarbonate sample is examined at different magnification, as shown in Figure 6.2.17 (a) & (b). Acrylic and polycarbonate are both amorphous polymers. Amorphous polymer weld morphology is exceedingly difficult to define through microscopic observations due to its non-crystalline and random nature. Crystallinity and crystalline morphology are linked to semi-crystalline polymers. A number of bubbles and voids can be observed on the top surface of the weld in Figure 6.2.17 (a) and (b), as well as tiny pieces of polymer debris on the margins of the bubbles. An essential aspect is that bubbles push the molten material to flow and enter the voids or pits present on the contacting surface of the polymer, which strengthens the micromechanical jointing at the interface and increases weld strength. A number of tiny bubbles can also form fractures and pits, as seen in Figure 6.2.17 (a), triggering the micro-anchor process. Bubbles form as a result of the laser-polymer interaction, however they must be restricted at the weld interface or else they will degrade the material. The bubbles offer certain advantages in terms of improving welding performance to a certain extent. Kumar et al. [55] conducted the morphological study of conventional LTW of two transparent acrylic polymers, as shown in Figure 6.2.18. A number of voids, spherulites and bubbles can be seen at the weld or fusion zone. In this case, beam wobbling can minimize the voids and porosity at weld zone by controlling the fusion and solidification process. Figure 6.2.17 (a) reveals the improved weld quality as compared to Figure 6.2.18 because of dispersion of laser power over the whole radiation zone. The beam wobbling is important because it creates turbulence and intermixing in the weld pool and also induces the development of bubbles at the weld bead boundary, as illustrated in Figure 6.2.17 (b). Because the laser beam oscillates while traveling, it has numerous encounters in the welding zone. Following the first oscillation, the polymers are preheated, which increases the laser absorptivity of polymer in the subsequent oscillation. The molten area in the weld zone is significantly larger than the laser spot diameter of 50 μm. It has been observed that equally distributed small bubbles are favorable for high weld strength.

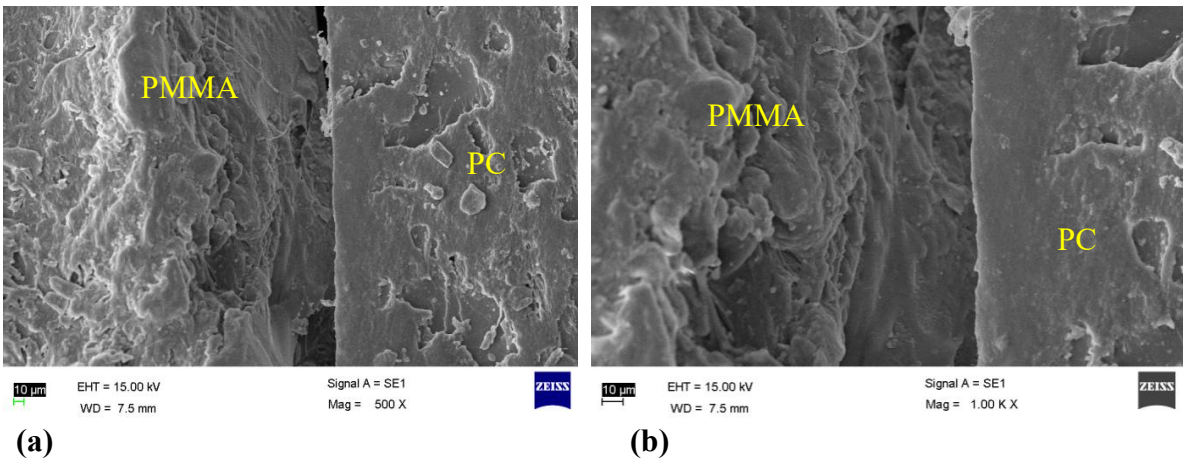

Figure 6.2.17: SEM micrograph of PMMA/PC weld zone at (a) 500 X magnification, and (b) 1000 X magnification

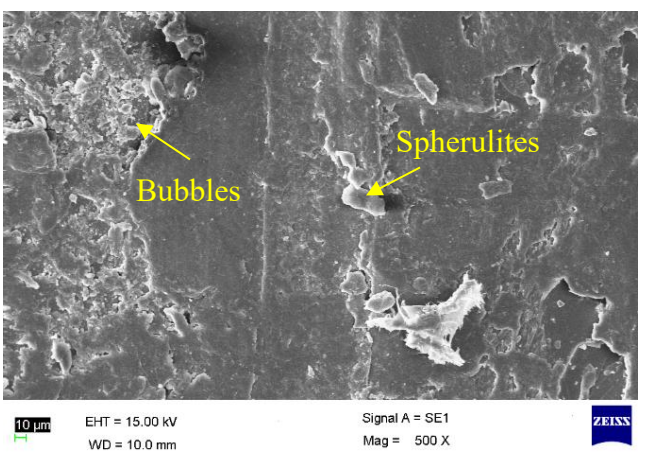

Figure 6.2.18: SEM micrograph of conventional LTW of PMMA/PMMA weld zone at 500 X magnification

6.2.9. Modelling of TWIST process using ANN

The TWIST welding process is modeled using a multilayer feed-forward neural network with a back-propagation algorithm. In this study, a network with an input layer with five neurons, one or two hidden layers with varying numbers of neurons in each hidden layer, and an output layer with two neurons is employed. The number of hidden layers and the number of neurons in each layer both affect how well a neural network performs. As a result, several combinations are tested to select an optimum architecture, as shown in Table 3. The majority of the researchers utilized RMSE (Root mean square error) as a neural network performance metric to choose the optimum architecture.

$$RMSE_i = \sqrt{\frac{\sum_{k=1}^{n}(Target_{i,k} - Output_{i,k})^2}{n}} \quad \ldots\ldots\ldots\ldots\ldots\ldots \quad (6.2.5)$$

However, as the output distribution values are completely different in terms of magnitude order and unit of measurement, a direct comparison of the RMSE values is inadequate. Because of this, the coefficient of variance (CV) is employed as a statistical indicator parameter for evaluating the error, which is independent of the distribution [48]. It is defined as the ratio of the standard deviation (σ_{RMSE_i}) to the distribution's average value (μ_{RMSE_i}) multiplied by 100.

$$CV_i = \frac{\sigma_{RMSE_i}}{\mu_{RMSE_i}} \times 100 \quad \ldots\ldots\ldots\ldots\ldots\ldots\ldots\ldots\ldots \quad (6.2.6)$$

The lower total CV that results in the lowest error when comparing targets and outputs determines the best ANN architecture.

6.2.9.1 Definition of input and output layers

The number of input nodes is the same as the number of process parameters. Using activation functions and weighted connections, the input layer processes information from external sources before adding it to and transmitting it to the neurons of the hidden layer. Eventually, the resulting signals are sent to the output layer, where the training phase assesses the difference between the expected and desired outputs (called targets). There is the same number of output nodes as response parameters. The number of output nodes is equal to the number of response parameters. Five process parameters are considered inputs, while weld shear strength and weld seam width are considered outputs in a single network to create the logical link between inputs and outputs.

6.2.9.2 Definition of hidden layers

Unlike input and output layers, the number of neurons and hidden layers may be changed. In ANNs, one or two hidden layers are often used to compute the best approximation. Given that having too many or too few hidden neurons might result in over-fitting or under-fitting problems, the number of hidden neurons needs to be determined with caution. This is achieved by changing the number of neurons in a range, with the upper and lower numbers chosen via a heuristic method. Here, four heuristic approaches are applied in order to define the upper and lower threshold.

The lower bound of hidden neurons is heuristically defined by Her Majesty's Department of Trade and Industry (MTI) [49]:

$$MTI = \frac{IN+ON}{2} = 3.5, \text{ this can be taken as 3 (Lower Bound)} \ldots\ldots (6.2.7)$$

Where, IN and ON denotes the input and output nodes. Furthermore, a hidden neuron (HN) is added in the hidden layer until the upper threshold of HN is reached. For this purpose, three alternative heuristic approaches are considered for determining the maximum number of HN.

The upper bound of hidden neurons is heuristically defined by Kolmogorov (KOL) [50]:

$$KOL = 2(IN) + 1 = 11 \ldots\ldots\ldots\ldots\ldots\ldots (6.2.8)$$

The upper bound of hidden neurons is heuristically defined by Lippmann (LIP) [51]:

$$LIP = ON \times (IN + 1) = 12 \ldots\ldots\ldots\ldots\ldots\ldots (6.2.9)$$

The upper bound of hidden neurons is heuristically defined by Kudrycky (KUD) [52]:

$$KUD = 3 \times ON = 6 \ldots\ldots\ldots\ldots\ldots\ldots (6.2.10)$$

Max (11, 12, 6) = 12 (Upper Bound)

The CV is determined by taking the lower (MTI = 3 nodes) and upper bounds (LIP = 12 nodes) into account in order to produce the optimal configuration, as shown in Table 6.2.6. The ANN model with 11 hidden neurons in the first hidden layer and 6 hidden neurons in the second hidden layer is found to produce the least error. The chosen architectural model is shown in bold, and it has the lowest CV of any architecture.

Table 6.2.6: Comparing CVs for ANNs with different architectures

Sl. No.	Network architecture	CV_{WS}	CV_{WW}	CV_{total}
1	5-3-2	1.1825	1.3137	2.4961
2	5-4-2	1.2078	1.8539	3.0616
3	5-5-2	0.9542	1.6897	2.6439
4	5-6-2	0.4474	1.6640	2.1113
5	5-7-2	0.5613	0.5614	1.1227
6	5-8-2	0.6893	0.7435	1.4328
7	5-9-2	0.9715	0.5508	1.5222

8	5-10-2	0.8721	0.4270	1.2991
9	5-11-2	1.5634	0.6070	2.1704
10	5-12-2	1.5506	0.5891	2.1396
11	5-3-3-2	0.5049	1.1135	1.6184
12	5-3-4-2	1.1567	0.5236	1.6803
13	5-3-5-2	0.7261	2.6386	3.3647
14	5-3-6-2	0.6882	0.7098	1.3980
15	5-3-7-2	1.6153	2.4195	4.0348
16	5-3-8-2	1.3118	1.7937	3.1055
17	5-3-9-2	1.7717	1.5561	3.3278
18	5-3-10-2	1.0723	2.1253	3.1976
19	5-3-11-2	1.0982	2.0738	3.1720
20	5-3-12-2	1.4883	1.1486	2.6370
21	5-4-3-2	0.7244	1.0519	1.7764
22	5-4-4-2	0.6379	1.0487	1.6865
23	5-4-5-2	1.0888	0.8291	1.9179
24	5-4-6-2	1.3218	0.8324	2.1543
25	5-4-7-2	1.0169	0.8226	1.8395
26	5-4-8-2	1.6664	0.6814	2.3478
27	5-4-9-2	0.7696	1.9954	2.7649
28	5-4-10-2	1.5619	1.1803	2.7423
29	5-4-11-2	0.8066	1.0700	1.8766
30	5-4-12-2	1.1394	2.2526	3.3919
31	5-5-3-2	1.2995	1.7011	3.0006
32	5-5-4-2	1.6345	1.8346	3.4690
33	5-5-5-2	0.8369	0.8691	1.7059
34	5-5-6-2	1.2410	1.1727	2.4137
35	5-5-7-2	1.0579	1.0487	2.1067
36	5-5-8-2	1.0162	2.4857	3.5019
37	5-5-9-2	0.9632	1.2237	2.1870
38	5-5-10-2	0.8803	0.6236	1.5039
39	5-5-11-2	0.8026	0.6467	1.4493

40	5-5-12-2	1.0040	0.8730	1.8770
41	5-6-3-2	0.6215	0.6644	1.2859
42	5-6-4-2	1.3828	1.3705	2.7533
43	5-6-5-2	0.6140	0.8084	1.4224
44	5-6-6-2	1.2248	0.5245	1.7493
45	5-6-7-2	0.5217	2.2500	2.7717
46	5-6-8-2	1.1985	1.3182	2.5167
47	5-6-9-2	0.9505	1.0382	1.9886
48	5-6-10-2	1.3501	0.7427	2.0927
49	5-6-11-2	1.3439	0.6632	2.0071
50	5-6-12-2	0.8336	0.5503	1.3839
51	5-7-3-2	1.9447	1.3359	3.2806
52	5-7-4-2	1.1872	2.4746	3.6618
53	5-7-5-2	0.7056	0.5280	1.2336
54	5-7-6-2	0.9607	0.7376	1.6983
55	5-7-7-2	1.2958	1.9017	3.1976
56	5-7-8-2	1.6699	0.4835	2.1534
57	5-7-9-2	0.6598	0.6305	1.2904
58	5-7-10-2	0.6037	0.7946	1.3983
59	5-7-11-2	1.0523	1.1255	2.1778
60	5-7-12-2	1.0180	0.5691	1.5871
61	5-8-3-2	0.4619	0.6636	1.1255
62	5-8-4-2	1.2374	0.8585	2.0959
63	5-8-5-2	0.5985	1.6165	2.2150
64	5-8-6-2	1.6142	0.7142	2.3284
65	5-8-7-2	0.6727	0.7994	1.4722
66	5-8-8-2	0.9088	0.4907	1.3995
67	5-8-9-2	1.1113	0.6009	1.7122
68	5-8-10-2	0.8152	0.5807	1.3959
69	5-8-11-2	0.7992	0.9211	1.7203
70	5-8-12-2	1.1163	0.4967	1.6130
71	5-9-3-2	0.6821	0.9234	1.6055

72	5-9-4-2	0.7604	1.0380	1.7983
73	5-9-5-2	0.8286	1.1999	2.0285
74	5-9-6-2	1.6480	0.5834	2.2314
75	5-9-7-2	0.7446	0.5664	1.3110
76	5-9-8-2	0.6780	0.6906	1.3686
77	5-9-9-2	1.0211	0.6261	1.6472
78	5-9-10-2	0.5834	0.3598	0.9433
79	5-9-11-2	0.7266	0.5265	1.2531
80	5-9-12-2	1.3567	0.7417	2.0984
81	5-10-3-2	1.3052	0.6117	1.9169
82	5-10-4-2	0.9865	1.8162	2.8027
83	5-10-5-2	1.2469	0.5521	1.7990
84	5-10-6-2	0.9133	0.8587	1.7720
85	5-10-7-2	0.5127	0.5025	1.0152
86	5-10-8-2	0.7371	0.5179	1.2549
87	5-10-9-2	1.2460	0.5637	1.8097
88	5-10-10-2	0.6239	0.4193	1.0433
89	5-10-11-2	0.7981	0.4607	1.2587
90	5-10-12-2	0.5605	1.0780	1.6385
91	5-11-3-2	1.4104	1.0206	2.4311
92	5-11-4-2	0.6891	1.1584	1.8474
93	5-11-5-2	0.5770	0.5483	1.1253
94	**5-11-6-2**	**0.5111**	**0.4319**	**0.9429**
95	5-11-7-2	0.9266	1.5998	2.5264
96	5-11-8-2	0.7156	0.8613	1.5769
97	5-11-9-2	0.7583	0.4120	1.1703
98	5-11-10-2	1.5884	1.4558	3.0442
99	5-11-11-2	1.0725	0.5930	1.6654
100	5-11-12-2	1.1589	0.8543	2.0131
101	5-12-3-2	0.7518	1.0201	1.7720
102	5-12-4-2	0.9498	0.8136	1.7634
103	5-12-5-2	0.4875	0.9490	1.4365

104	5-12-6-2	1.1584	0.6122	1.7706
105	5-12-7-2	0.7175	0.8238	1.5413
106	5-12-8-2	1.2633	1.0428	2.3061
107	5-12-9-2	1.0933	0.7268	1.8202
108	5-12-10-2	0.7999	0.4680	1.2678
109	5-12-11-2	0.9129	0.5110	1.4239
110	5-12-12-2	1.1202	0.8612	1.9814

6.2.9.3 Training, validation, and test of the ANN model

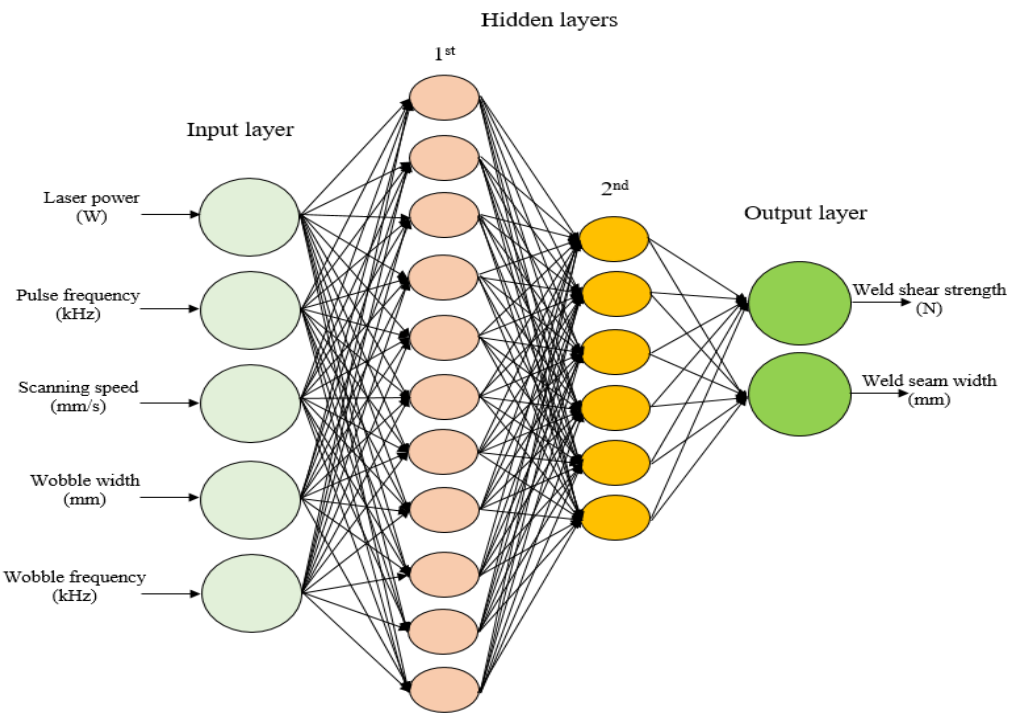

Figure 6.2.19. ANN architecture used for predicting weld shear strength and weld seam width

The experimental data is used to train the ANN for predicting weld shear strength and weld seam width. The ANN employs the Levenberg-Marquardt Learning Algorithm along with a feed-forward and back-propagation network. The architecture of the ANN model is shown in Figure 6.2.19. The MATLAB 2019 platform is used for ANN modeling, training, validation, and testing. During training, the fifty experimental input-output datasets are divided into three sets: 70% for training, 15% for cross-validation, and 15% for testing. This division allows the network to learn from the majority of the data and evaluate its performance on separate validation and testing sets to assess its generalization abilities. A normalization technique is

applied to standardize the input and output variables by scaling them between 0 and 1. This ensures that all variables fall within a consistent range, aiding in the convergence and stability of the training process.

The ANN architecture consists of different layers, including the input layer, hidden layers, and output layer. Neurons in the input layer do not use a transfer function, while neurons in the hidden layers and output layer employ a log-sigmoid transfer function. This choice of transfer function allows the neurons to produce outputs ranging from 0 to 1, which is appropriate for the prediction task. Figure 6.2.20 shows the performance convergence diagram of the ANN architecture after training. This diagram illustrates the progress of the network's performance during training epochs. The best validation performance achieved is 335.0634 at epoch 14, indicating that the network's performance, as evaluated on the validation set, is optimal at this stage of training. The utilization of the Levenberg-Marquardt Learning Algorithm, along with the specific ANN architecture and training methodology, enables the accurate prediction of weld shear strength and weld seam width.

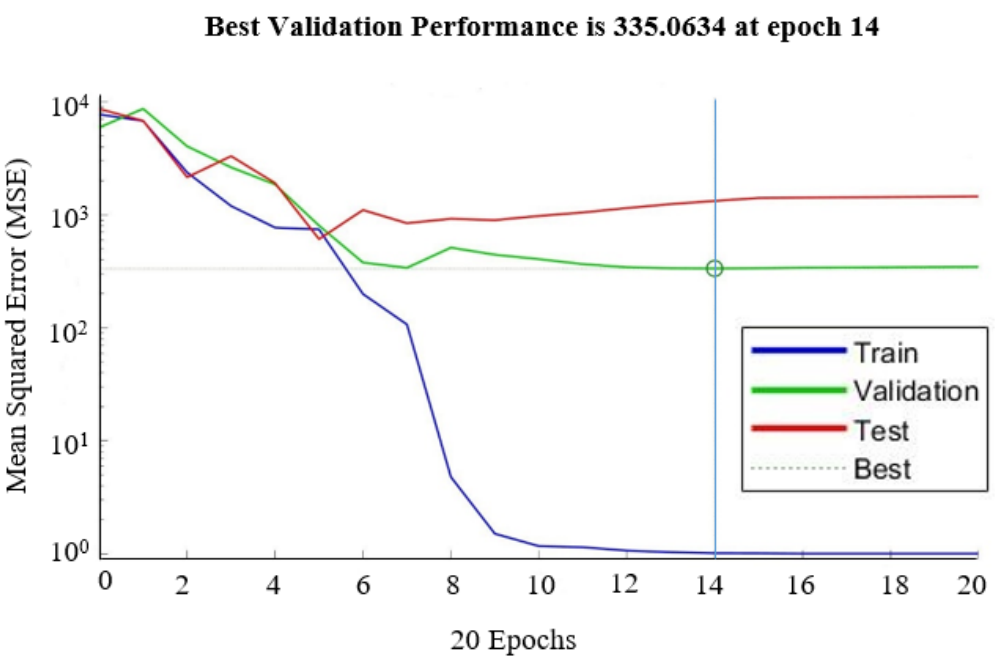

Figure 6.2.20. Convergence diagram of the 5-11-6-2 network architecture

The regression plots shown in Figure 6.2.21 are used to evaluate the fitness of the ANN model. Figure 6.2.21(a) shows a comparison of anticipated and actual data for the training patterns. It is evident from this figure that the predicted values have little error, demonstrating a remarkable level of accuracy in capturing the underlying patterns in the training dataset.

Figures. 6.2.21(b) and 6.2.21(c) present the comparison of actual and predicted data for the validation and testing patterns, respectively. These plots reveal a close agreement between the ANN predictions and the actual response values. The close agreement of the data points in both the validation and testing plots indicates the model's exceptional ability to generalize and yield precise predictions.

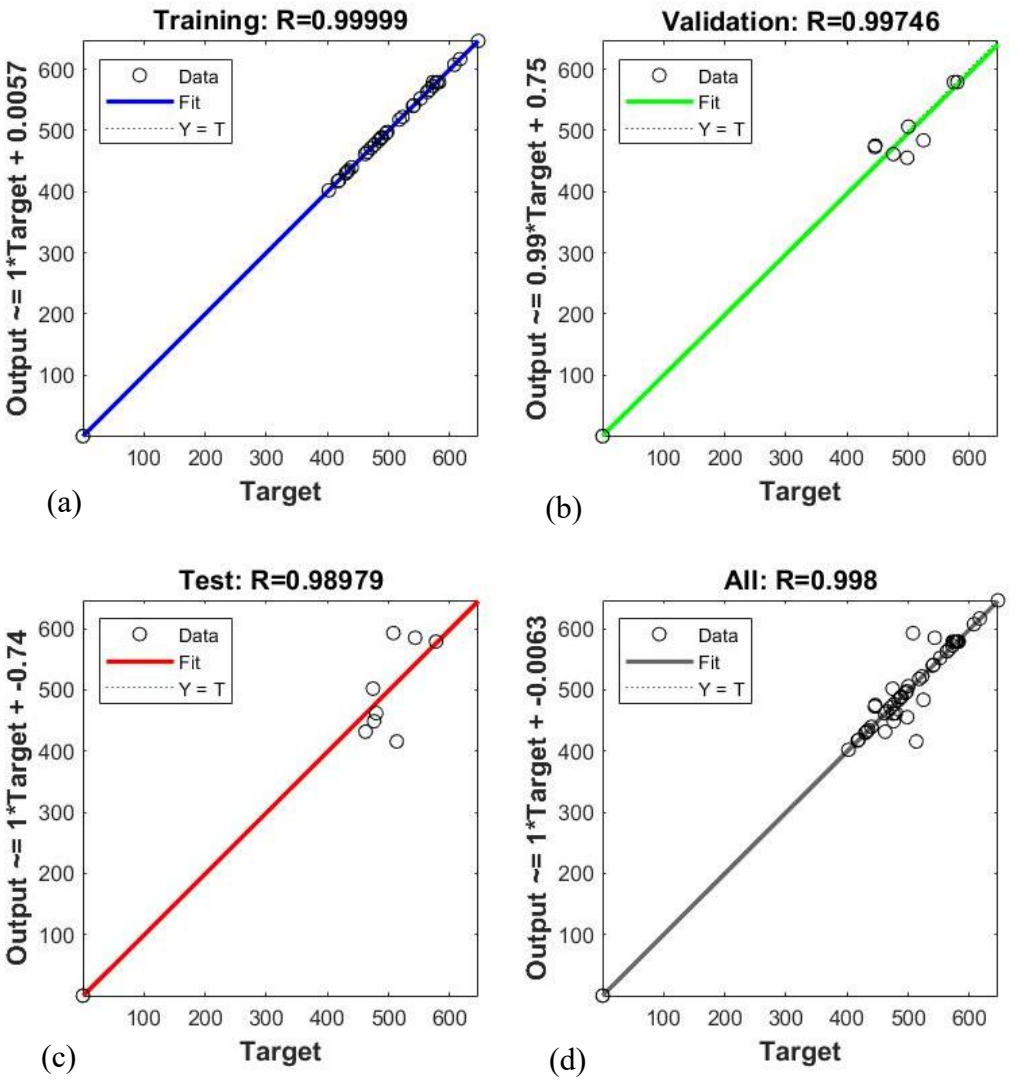

Fiure 6.2.21. Actual and predicted data regression plots for weld shear strength and weld seam width

The efficacy of the developed ANN model is further assessed by an impressive R-squared value of 0.99, as shown in Figure 6.2.21(d). This confirms the predictability and robustness of the developed ANN, putting confidence in its capability to deliver precise predictions for both weld shear strength and weld seam width. Tables 4 and 5 supplement the regression plots by displaying the prediction error percentages for the chosen ANN architecture across all test samples. These tables give a summary of the prediction errors

pertaining to weld shear strength and weld seam width, allowing for a thorough inspection of the model's performance. Together, the regression graphs, R-squared value, and prediction error percentages highlight the excellent prediction ability of the developed ANN model.

Table 6.2.7: Comparison of actual and predicted outputs for test data of weld shear strength

Sl. No.	Welding parameter					Weld shear strength (N)			
	LP (W)	PF (kHz)	SS (mm/s)	WO (mm)	WF (kHz)	Actual	ANN output	Error	Error %
1	7.89	35	2	0.8	1	465.08	465.12	0.04	0.0087
2	7.89	35	2	0.8	5	477.03	477.02	0.01	0.0017
3	8.35	35	4	0.8	5	434.41	434.59	0.18	0.0419
4	8.35	30	3	0.6	3	517.77	517.94	0.17	0.0329
5	8.12	30	4	0.6	3	566.94	566.78	0.16	0.0289
6	8.12	30	3	0.6	5	524.71	483.88	40.82	7.7807
7	8.12	30	3	0.6	3	577.43	579.01	1.58	0.2743
8	8.12	30	3	0.6	3	574.43	579.01	4.58	0.7979

Table 6.2.8: Comparison of actual and predicted outputs for test data of weld seam width

Sl. No.	Welding parameter					Weld seam width (mm)			
	LP (W)	PF (kHz)	SS (mm/s)	WO (mm)	WF (kHz)	Actual	ANN output	Error	Error %
1	7.89	35	2	0.8	1	0.546	0.577	0.031	5.681
2	7.89	35	2	0.8	5	0.587	0.567	0.019	3.351
3	8.35	35	4	0.8	5	0.553	0.491	0.061	11.164
4	8.35	30	3	0.6	3	0.642	0.617	0.025	3.940

5	8.12	30	4	0.6	3	0.487	0.506	0.019	3.914
6	8.12	30	3	0.6	5	0.739	0.656	0.083	11.231
7	8.12	30	3	0.6	3	0.602	0.587	0.015	2.544
8	8.12	30	3	0.6	3	0.574	0.587	0.012	2.210

Figures. 6.2.22 (a) and (b) provide a comparison of actual and predicted weld shear strength and weld seam width for test data, respectively, and show that they are in good agreement.

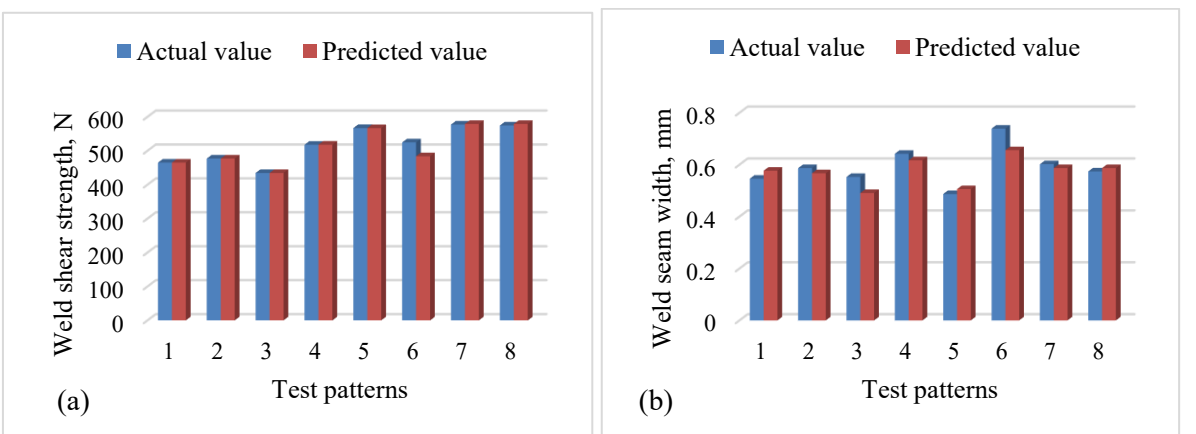

Figure 6.2.22. Actual and ANN prediction of (a) weld shear strength and (b) weld seam width for test data

Figure 6.2.23 (a) & (b) presents the comparison of actual and predicted weld shear strength, and actual and predicted weld seam width, respectively, for training patterns. It can be clearly observed from the line diagram that most of the predicted data points match with the actual fitted data points, which confirms the adequacy of the developed model.

The weights and biases are now extracted from the trained model, and the predicted values are obtained. The inputs are normalized and fed into the mathematical equation for ANN. The outputs are then de-normalized to get the predicted values.

$$Y = b_0 + \sum_{k=1}^{h}[w_k \times f_{sig}(b_{hk} + \sum_{i=1}^{m} w_{ik} X_i)] \quad \ldots\ldots\ldots\ldots (6.2.11)$$

Where, b_o is the output bias; w_k is the weight of the connection between the k_{th} of the hidden layer and the single output neuron; b_{hk} is the bias in the k_{th} neuron of the hidden layer; n is the number of neurons in the hidden layer; w_{ik} is the weight of connection between the i_{th} input parameter and the hidden layer; X_i is the input variable, while Y is the response.

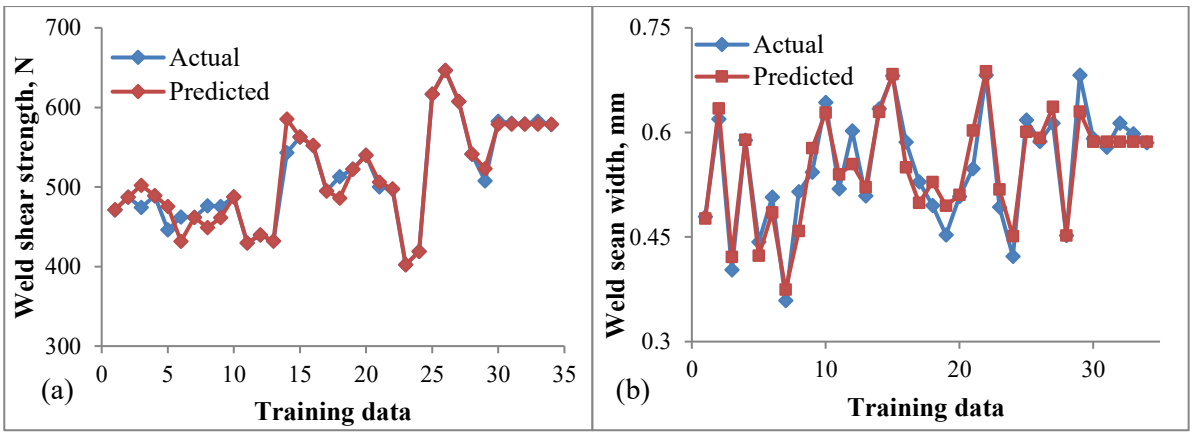

Figure 6.2.23. Line diagram with best fit of actual and ANN prediction of (a) weld shear strength and (b) weld seam width, for training patterns

The de-normalized ANN value is plotted against the experimental value to perform a comparison analysis for weld shear strength and weld seam width, as illustrated in Figure 6.2.24 (a) & (b).

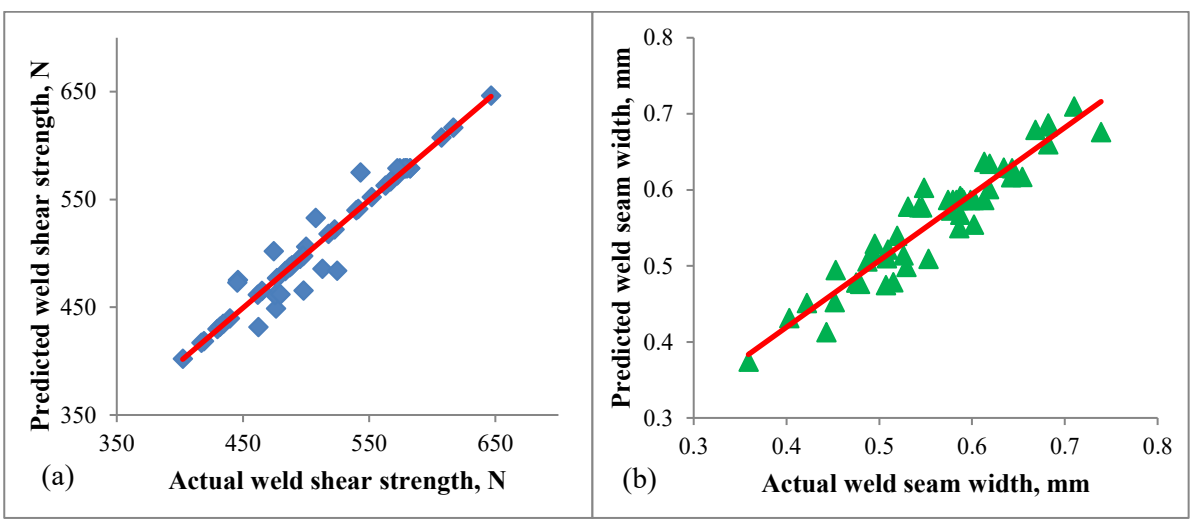

Figure 6.2.24. Scatter diagram with the best fit of ANN prediction (de-normalized value) vs. actual (a) weld shear strength and (b) weld seam width

Linear regression analysis is applied to find the correlation coefficient (CC) of the developed ANN model. CC is utilized to establish the relationship between actual and predicted output values. The developed ANN model for weld shear strength and weld seam width has a correlation coefficient near 1, which yields minimal error as shown in Figure 6.2.24 (a) & (b). As a result, the developed neural network is found to be suitable for predicting the outputs of the TWIST process with significant accuracy.

6.2.10. Multi-objective Optimization of the TWIST process

The selection of appropriate process parameters is critical in any welding process since it impacts weld quality, associated costs, and productivity. Multi-objective optimization of process parameters is pertinent to achieve overall desirability by simultaneously optimizing desired responses to produce better quality, enhanced productivity, and reduced costs. Both priori and posteriori methods can be used to solve a multi-objective optimization problem. In the priori method, a multi-objective problem is reduced to a single objective problem by weighting each goal, and then solved as a single objective optimization problem, yielding a unique optimum solution. The disadvantage of the priori technique is likewise solved by the posterior approach since the multi-objective problem is not reduced to a single objective problem, and hence no weighting is used. In this case, the Pareto optimum solution is obtained, which allows the freedom to choose one solution from the collection of Pareto points depending on the objective criterion. Due to its adaptability, the posteriori strategy is therefore considered to be more suited for tackling multi-objective optimization problems. Several optimization techniques based on genetic algorithms have been developed over the years. The non-dominated sorting algorithm, NSGA-II, is one of the finest genetic algorithm-based optimization algorithms ever developed. The non-dominated sorting TLBO algorithm has also emerged as a popular metaheuristic algorithm for multi-objective optimization due to its low computing cost and freedom from any algorithm parameters. The produced ANN model expression serves as the fitness function for the optimization algorithms. The hyper-parameter values for both algorithms used are presented in Table 6.2.9.

$$Weld\ shear\ strength\ =\ bs0\ +\ \{lws21 \times tanh\ (a21)\}\ +\ \{lws22 \times tanh\ (a22)\}\ +\ \{lws23 \times tanh\ (a23)\}\ +\ \{lws24 \times tanh\ (a24)\}\ +\ \{lws25 \times tanh\ (a25)\}\ +\ \{lws26 \times tanh\ (a26)\} \quad (6.2.12)$$

$$Weld\ seam\ width\ =\ bw0\ +\ \{lww21 \times tanh\ (a21)\}\ +\ \{lww22 \times tanh\ (a22)\}\ +\ \{lww23 \times tanh\ (a23)\}\ +\ \{lww24 \times tanh\ (a24)\}\ +\ \{lww25 \times tanh\ (a25)\}\ +\ \{lww26 \times tanh\ (a26)\} \quad (6.2.13)$$

Table 6.2.9 Hyper-parameter values of NSGA-II and NSTLBO algorithms

Constant Parameters	Laser Power (lower bound – upper bound)	7.89 - 8.35
	Pulse Frequency (lower bound – upper bound)	25 - 35
	Scanning Speed (lower bound – upper bound)	2 - 4
	Wobble Width (lower bound – upper bound)	0.4 - 0.8
	Wobble Frequency (lower bound – upper bound)	1-5
NSGA-II	Population Size	50
	Maximum Number of Generations	100
	Crossover Rate	0.8
	Mutation Rate	0.01
	Selection Function	Tournament
	Mutation Function	Adaptive Feasible
NSTLBO	Population Size	50
	Maximum Number of Generations	100
	Teaching Factor	1 to 2

6.2.10.1 Optimization using NSGA–II

Deb et al. initially presented NSGA-II, which is frequently used to solve optimization problems because of its excellent performance and low computing cost [53]. Initially, multi-objective evolutionary algorithms based on non-dominated sorting lack computational complexity and a non-elitism approach. However, Multi-objective optimization based on NSGA-II overcomes the drawback associated with evolutionary algorithms. The Posteriori method is used for multi-objective optimization based on NSGA-II, which optimizes each objective simultaneously without being dominated by another solution. For most situations, NSGA-II can identify a significantly wider range of solutions and better convergence at the actual Pareto optimum front.

Objective function definition and NSGA–II application

When employed as objectives in multi-objective optimization, the performance characteristics of the TWIST welding process, the weld shear strength and the weld seam width, are in conflict with one another. Weld shear strength must be increased while weld seam width must be reduced to achieve better weld quality. For the multi-objective NSGA-II, a posteriori strategy is employed to provide a collection of Pareto optimum solutions. The

fitness function is derived from an artificial neural network [Eq. (8) & (9)] using five process variables. The problem space must be constrained by establishing upper and lower limits on each process variable, specified as inputs from Table 6.2.1. The bounds are defined in normalized units ranging from 0 to 1, and the population size is fixed at 50. The selection function is set to *Tournament*, with a reasonable crossover percentage of 0.8, and the mutation function is set to *Adaptive Feasible*. The NSGA-II algorithm is implemented in the MATLAB code to maximize and minimize the fitness function, which is derived based on the output values from the ANN. Table 6.2.10 shows the collection of Pareto optimum solutions produced by the NSGA-II algorithm. Among the obtained set of solutions, solutions no. 4 and 5 represent the maximum weld strength of 678.2 N at higher line energy (ratio of laser power to welding speed). Whereas, solution no. 1 and 2 represent the minimum weld seam width of 0.36 mm at lower heat input. Higher line energy can degrade the material and lower line energy leads to insufficient penetration. It is observed that better weld quality is achieved at the mid value of heat input (solution no. 7). The optimal parameter settings at which the highest weld shear strength and the minimum weld seam width are attained simultaneously are shown in bold. Depending on the proportional relevance of responses, the decision-maker can use any optimum option.

Table 6.2.10. Non-dominated set of solutions obtained using the NSGA-II algorithm

S. No.	LP (W)	PF (kHz)	SS (mm/s)	WO (mm)	WF (kHz)	WS (N)	WW (mm)
1	8.07	34.97	3.94	0.47	1.05	450.07	0.360
2	8.07	34.97	3.94	0.47	1.05	450.07	0.360
3	8.13	34.16	3.20	0.55	2.40	654.74	0.573
4	8.21	34.72	2.88	0.53	3.43	678.21	0.592
5	8.21	34.72	2.88	0.53	3.43	678.21	0.592
6	8.10	33.83	3.40	0.50	1.81	541.30	0.456
7	**8.09**	**33.14**	**3.33**	**0.49**	**2.05**	**581.46**	**0.498**
8	8.08	33.60	3.45	0.51	1.80	549.14	0.465
9	8.10	33.74	3.31	0.50	1.80	567.27	0.486
10	8.08	34.31	3.65	0.49	1.30	468.99	0.381
11	8.08	34.66	3.75	0.48	1.35	458.22	0.369
12	8.26	33.66	3.64	0.51	1.83	519.42	0.429

13	8.22	33.53	3.17	0.54	2.14	616.07	0.530
14	8.18	34.11	3.31	0.60	1.90	602.40	0.522
15	8.13	34.86	3.44	0.50	2.16	537.42	0.448
16	8.13	34.06	3.20	0.52	2.44	651.03	0.566
17	8.28	33.64	3.09	0.58	2.22	618.45	0.540
18	8.09	33.68	3.42	0.52	1.77	561.85	0.479

The collection of Pareto optimum solutions is depicted in Figure 6.2.25. The graphic depicts several optimal points from which weld shear strength and weld seam width can be obtained based on the decision-maker's desired relevance of the response.

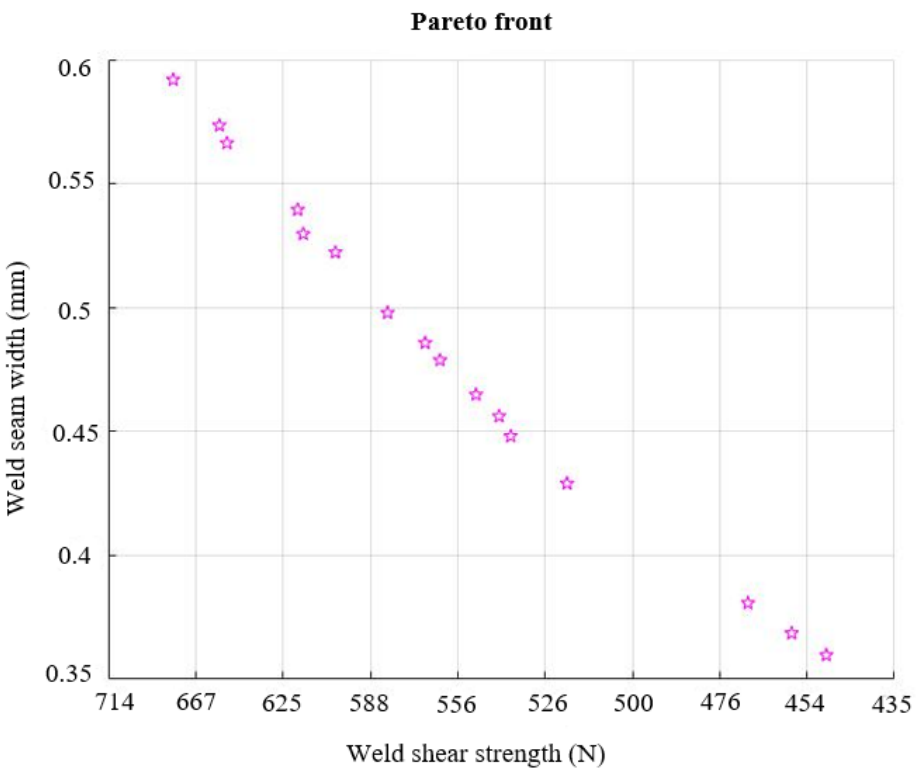

Figure 6.2.25. Pareto front obtained from NSGA-II

Validation experiment

The confirmation experiment has been conducted at optimal parameter settings (solution no. 7) in order to validate the optimal solution obtained from the NSGA-II algorithm. Table 6.2.11 presents the confirmation test and shows that very minimal error has been found out.

Table 6.2.11: Confirmation tests

Experiment	Actual value	Weld shear strength (N)	Weld seam width (mm)
At NSGA-II optimal parameter (Sol. No. 7)	Actual value	606.27	0.523
	NSGA-II results	581.45	0.477
	|Error| %	4.09	8.79

6.2.10.2 Optimization using the NSTLBO algorithm

The NSTLBO algorithm is an extension of the TLBO algorithm, which solves multi-objective optimization problems using the posteriori method, yielding a diversified range of Pareto optimum solutions. The NSTLBO algorithm functions similarly to the TLBO algorithm and includes both a teacher and a learner phase. To solve multi-objective problems effectively, Rao et al. [14] presented the NSTLBO method, which employs a non-sorting technique and crowd distance computation. The NSTLBO algorithm's teacher and learner phases enable extensive exploration and exploitation of the search space, and the non-dominated sorting strategy assures that the selection process is always toward the best solutions and that the population is driven to the Pareto-front in each generation.

Objective function definition and the NSTLBO algorithm application

The fitness function for the NSTLBO algorithm is derived from the ANN model [Eq. (6.2.12) & (6.2.13)], and the lower and upper ranges of process variables in the design space act as constraints. A MATLAB code has been constructed to solve the optimization problem using the NSTLBO algorithm, with the learner population set to 50, with the number of subjects set to the number of input variables. The teaching factor can vary from one to two, and the number of iterations is decided to be 100. Table 6.2.12 shows the collection of Pareto optimum solutions obtained using the NSTLBO algorithm.

Table 6.2.12. Non-dominated set of solutions obtained using the NSTLBO algorithm

S. No.	LP (W)	PF (kHz)	SS (mm/s)	WO (mm)	WF (kHz)	WS (N)	WW (mm)
1	8.32	35.00	3.82	0.40	1.00	466.40	0.689
2	8.28	33.08	3.82	0.40	1.47	466.40	0.689

3	**8.35**	**35.00**	**3.83**	**0.40**	**1.00**	**466.40**	**0.689**
4	8.35	35.00	4.00	0.40	1.00	466.40	0.689
5	8.30	35.00	3.71	0.40	1.00	466.40	0.689
6	8.35	35.00	4.00	0.40	1.00	466.40	0.689
7	8.35	35.00	4.00	0.40	1.00	466.40	0.689
8	8.35	35.00	3.82	0.40	1.00	466.40	0.689
9	8.35	35.00	4.00	0.40	1.00	466.40	0.689
10	8.35	35.00	3.93	0.40	1.00	466.40	0.689
11	8.35	35.00	3.98	0.40	1.00	466.40	0.689
12	8.35	35.00	4.00	0.40	1.00	466.40	0.689
13	8.35	35.00	3.94	0.40	1.00	466.40	0.689
14	8.35	35.00	3.94	0.40	1.00	466.40	0.689
15	8.35	35.00	3.95	0.40	1.00	466.40	0.689
16	8.35	35.00	4.00	0.40	1.00	466.40	0.689
17	8.32	35.00	3.75	0.40	1.00	466.40	0.689
18	8.34	35.00	3.83	0.40	1.00	466.40	0.689
19	8.35	35.00	3.82	0.40	1.00	466.40	0.689
20	8.34	35.00	4.00	0.40	1.00	466.40	0.689
21	8.34	35.00	3.82	0.40	1.00	466.40	0.689
22	8.34	35.00	3.82	0.40	1.00	466.40	0.689
23	8.31	35.00	3.81	0.40	1.00	466.40	0.689
24	8.33	35.00	3.82	0.40	1.00	466.40	0.689
25	8.33	35.00	3.83	0.40	1.00	466.40	0.689
26	8.32	35.00	3.82	0.40	1.00	466.40	0.689
27	8.33	35.00	3.83	0.40	1.00	466.40	0.689
28	8.30	35.00	3.82	0.40	1.00	466.40	0.689
29	8.32	35.00	3.82	0.40	1.00	466.40	0.689
30	8.32	35.00	3.82	0.40	1.00	466.40	0.689

Among the obtained non-dominated set of solutions, all pareto optimal point represent the almost same response, such as maximum weld shear strength of 466.4 N and minimum weld seam width of 0.689 mm. Although, Solution no. 3 is selected because correct amount of heat input is required in order to obtain simultaneously the maximum weld shear strength and

minimum weld seam width. The optimal parameter setting at which the maximum weld shear strength and the minimum weld seam width are attained simultaneously is shown in bold. The collection of Pareto-optimal solutions found by the NSTLBO algorithm is shown in Fig. 6.2.26. It is obvious that the majority of the optimum points converge at one value, and that value represents the most favorable result.

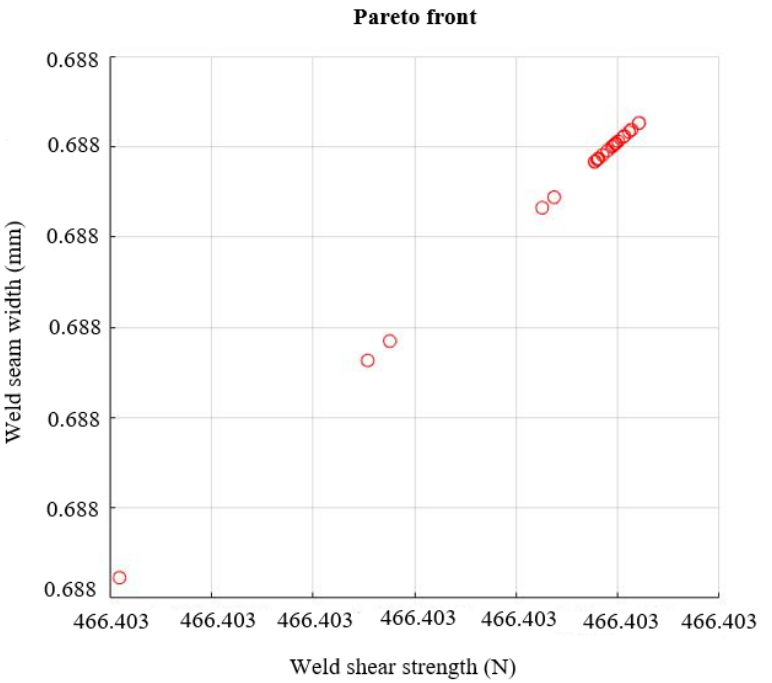

Figure 6.2.26. Pareto front obtained from NSTLBO

Validation experiment

The confirmation experiment has been conducted at optimal parameter settings (solution no. 7) in order to validate the optimal solution obtained from the NSGA-II algorithm. Table 6.2.13 presents the confirmation test and shows that very minimal error has been found out.

Table 6.2.13: Confirmation tests

Experiment	Actual value	Weld shear strength (N)	Weld seam width (mm)
At NSTLBO optimal parameter (Sol. No. 3)	Actual value	497.49	0.617
	NSTLBO results	466.4	0.689
	|Error| %	6.25	11.67

The multi-objective optimization algorithms, NSGA-II and NSTLBO, are put to the test to evaluate their effectiveness using a range of performance metrics. These metrics, namely computational time (CT), uniform distribution (UD), error ratio (ER), overall non-dominated vector generation (ONVG), maximum spread (MS), generational distance (GD), and maximum Pareto front error (MPFE) [54, 55], are carefully considered for the comparison. The comparisons are conducted across five independent trials, and the average values are used for the comparative study.

Computational time metric, which measures the time required by each algorithm to perform a computational process. In Figure 6.2.27, it becomes evident that the NSGA-II algorithm takes more computational time compared to NSTLBO. This can be attributed to the intricate nature of NSGA-II's evolutionary process, which demands greater computational resources. However, lower CT generally indicates better performance when this is used as a metric for the evaluation of algorithm performance.

The uniform distribution metric evaluates how solutions are distributed along the approximation front within a predetermined parameter range. A higher UD value signifies a more evenly distributed set of solutions, indicating better algorithm performance. Figure 6.2.28 presents the comparison between NSGA-II and NSTLBO in terms of UD. Notably, NSGA-II exhibits a greater UD compared to NSTLBO. This suggests that NSGA-II is capable of generating a more uniformly distributed set of solutions across the Pareto front, enabling it to explore a broader range of trade-off solutions.

The error ratio metric assesses the quality of the approximation front by considering the proportion of non-true Pareto points relative to the population size. A lower ER value indicates a superior non-dominated set, implying that a larger portion of the solutions in the front are truly Pareto-optimal. In Figure 6.2.29, it becomes evident that NSGA-II boasts a lower ER value compared to NSTLBO, underscoring its superior performance in generating a higher proportion of non-dominated solutions. This showcases NSGA-II's ability to provide a more accurate representation of the Pareto front.

The overall non-dominated vector generation metric refers to the number of non-dominated individuals found in the approximation front. It is crucial to strike a balance, avoiding an excessive or inadequate number of non-dominated solutions based on the specific problem and context. Figure 6.2.30 showcases an intriguing finding: while NSGA-II managed to discover a non-dominated set, NSTLBO failed to find any non-dominated individuals during its evolution. While ONVG alone does not guarantee algorithm performance, this

outcome highlights NSGA-II's superiority in generating a diverse and well-balanced set of non-dominated solutions.

The maximum spread metric evaluates how well the approximation set covers the true Pareto front. A higher MS value indicates better performance, as it signifies a broader coverage of the true Pareto front by the approximation set. Figure 6.2.31 presents the comparison between NSGA-II and NSTLBO in terms of MS, unveiling NSGA-II's achievement of a higher MS value relative to NSTLBO. This suggests that NSGA-II can cover a larger area of the true Pareto front, thereby providing a more comprehensive set of trade-off solutions.

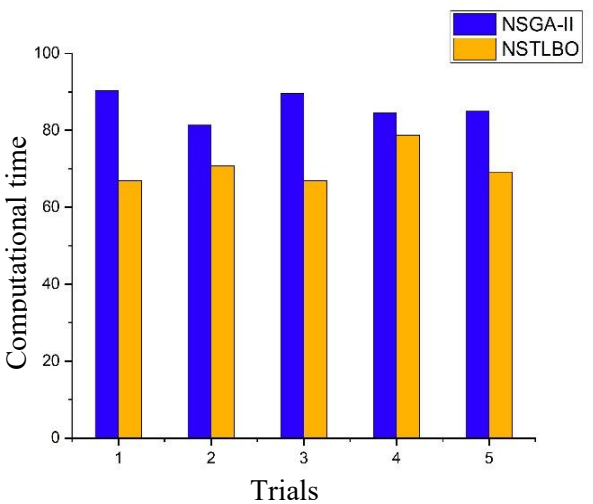

Fig. 6.2.27. Comparison of NSGA-II and NSTLBO in terms of computational time

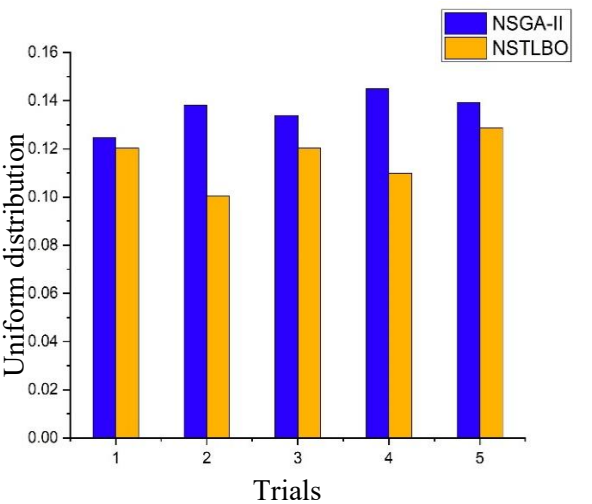

Fig. 6.2.28. Comparison of NSGA-II and NSTLBO in terms of uniform distribution

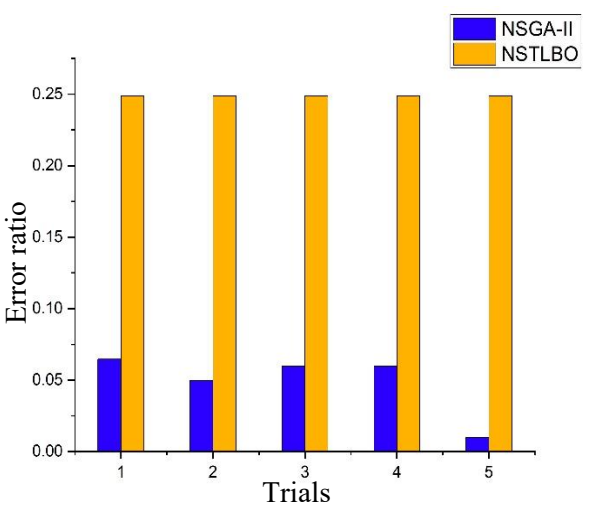

Fig. 6.2.29. Comparison of NSGA-II and NSTLBO in terms of error ratio

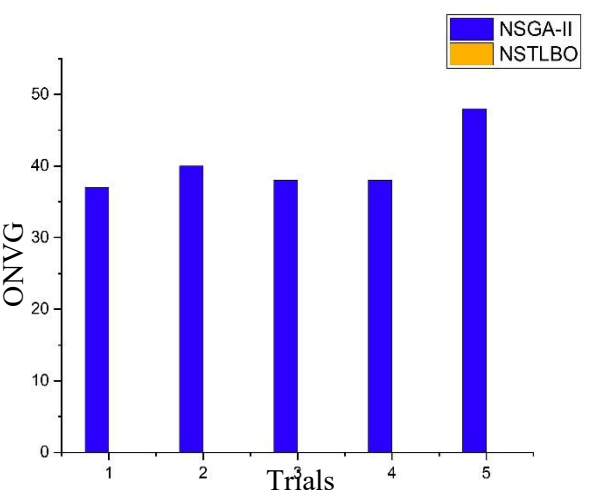

Fig. 6.2.30. Comparison of NSGA-II and NSTLBO in terms of ONVG

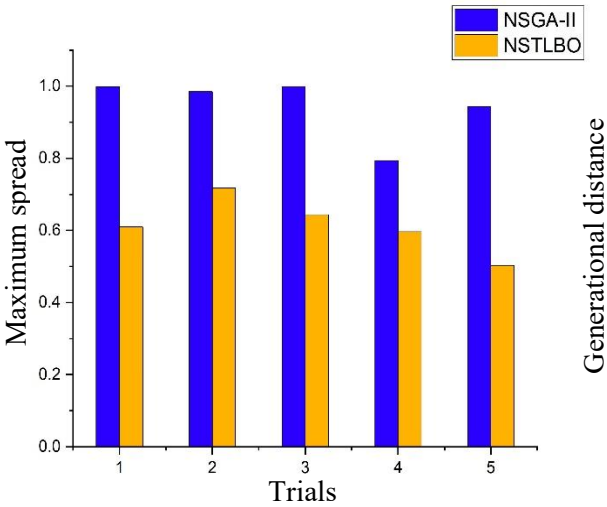

Figure 6.2.31. Comparison of NSGA-II and NSTLBO in terms of maximum

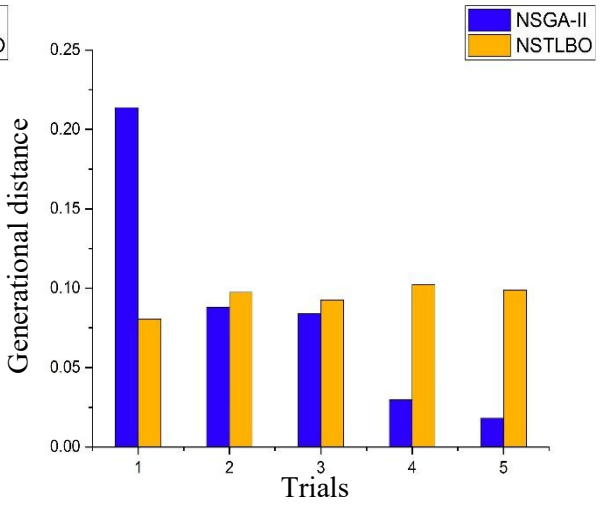

Figure 6.2.32. Comparison of NSGA-II and NSTLBO in terms of generational distance

The generational distance metric measures the distance between the evolved solution set and the true Pareto front. A lower GD value implies a closer approximation to the true front. As depicted in Fig. 6.2.32, NSGA-II outperforms NSTLBO with a lower GD value. This indicates NSGA-II's superior performance in terms of proximity to the true Pareto front. Consequently, NSGA-II excels at finding solutions that closely resemble the optimal solutions on the Pareto front.

Lastly, we consider the maximum Pareto front error metric, which focuses on the largest distance between individuals on the evolved solution set from the true Pareto front. In Figure 6.2.33, it becomes evident that NSGA-II exhibits a lesser MPFE compared to NSTLBO. This finding suggests that NSGA-II surpasses NSTLBO in terms of minimizing the error between the approximation front and the true Pareto front.

The comprehensive analysis of multiple performance metrics highlights NSGA-II's superior performance over NSTLBO. NSGA-II excels in various aspects, including uniform distribution, error ratio, overall non-dominated vector generation, maximum spread, generational distance, and maximum Pareto front error. The only area where NSTLBO outperforms NSGA-II is computational time, with NSGA-II requiring more time to obtain optimal solutions. NSGA-II emerges as the stronger algorithm based on this thorough examination of performance metrics.

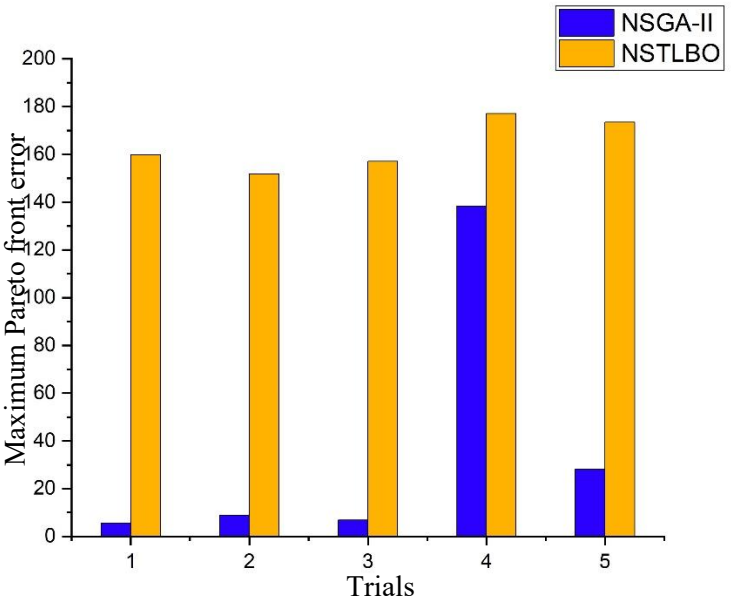

Fig. 6.2.33 Comparison of NSGA-II and NSTLBO in terms of maximum Pareto front error

The study has limitations regarding the accuracy of model predictions and the confined search range within the experimental design space, which may result in errors when predicting beyond this space. Additionally, the employed modeling and optimization techniques, such as ANN, NSGA-II, and NSTLBO, have their inherent limitations. ANNs require a significant amount of labeled training data, are susceptible to overfitting, and can be computationally expensive. Selecting appropriate architecture and parameters for ANNs can be challenging and time-consuming. NSGA-II requires setting various parameters, and its reliance on Pareto dominance may not accurately capture the preferences of decision-makers. NSTLBO faces challenges in balancing exploration and exploitation of the search space, which may lead to premature convergence or inadequate exploration. However, the study mitigated these limitations by employing proper validation techniques and rigorous testing. Despite the limitations, the results obtained from the ANN, NSGA-II, and NSTLBO algorithms are excellent in terms of accuracy and precision, providing reliable outcomes.

6.2.11 Outcomes of the Present Research Work

The efficacy of welding of alike transparent acrylic materials using low power laser transmission welding (LTW) with or without beam wobbling technique has been demonstrated. This research also addresses the challenges of predicting appropriate parameter values and optimizing conflicting objectives in TWIST welding. The effects of wobble LTW parameters on weld quality and weld morphology are investigated through experimental work

and statistical analyses. Based on microstructure, A number of voids, spherulites and bubbles can be seen at the weld or fusion zone in conventional LTW. In the case of wobble LTW, beam wobbling can minimize the voids and porosity at weld zone by controlling the fusion and solidification process. The outcomes of the study provide insights into the effectiveness and comparative performance of ANN-NSGA-II and ANN-NSTLBO, aiding the selection of an appropriate optimization strategy for TWIST welding in industrial applications. The following conclusions are drawn from the current study within the scope of the chosen design space:

1. Transparent dissimilar thermoplastic polymers such as acrylic and polycarbonate can be conveniently and efficiently welded together utilizing LTW with a black ink line serving as a laser absorber applied at the interface.
2. The developed mathematical models can accurately predict the responses within the boundaries of the welding settings being utilized, as verified by additional experiments.
3. The depth of penetration at low scanning speed is greater and the deposition of heat energy in the melt zone is lower, and so the joining strength of the weld is greater.
4. Beam wobbling is found to have a substantial effect on weld shear strength when beam wobbling parameters such as wobble width and wobble frequency are used.
5. The beneficial effects of beam wobbling on weld shear strength are attributed to homogenized heat input, melt pool turbulence, and improved polymer intermixing in the weld pool. Beam wobbling is also found to have a significant effect on weld seam width.
6. The morphological analysis indicates the formation of bubbles near the fusion zone, as well as small bits of polymer debris on the bubbles' edges. The small bubbles create cracks and pits on the contacting surfaces, pushing the molten polymer into cavities and activating the micro-anchoring process.
7. The optimum results derived by the TLBO algorithm are found to be in good agreement with the experimental results, as verified by the confirmation tests.
8. ANN with double hidden layers yields lower variance and better predictability than single hidden layer.
9. Graphical representation of actual vs. predicted weld shear strength and weld-seam width results shows good agreement between actual and predicted weld quality.

10. NSGA-II achieves a wide range of optimal solutions, while NSTLBO converges at one point.
11. NSGA-II outperforms NSTLBO in simultaneously maximizing weld strength and minimizing seam width.
12. NSGA-II has better performance in terms of various metrics (uniform distribution, error ratio, overall non-dominated vector generation, maximum spread, generational distance, and maximum Pareto front error) despite slightly longer computational time.
13. The implemented optimization approaches optimized process parameters effectively within specified constraints, improving quality and performance.

At the conclusion of **Chapter 6**, the feasibility and performance of **laser welding of polymers** using a **low-power diode laser (10 W)** have been investigated. In this study, the laser weldability of polymeric materials was evaluated. These materials present significant challenges in welding due to their **inherent incompatibility**, as well as the difficulty in welding of **clear transparent polymers** without the use of additives. To address these challenges, some new techniques were employed to improve weldability and joint quality. The influence of **laser processing parameters** such as power, scanning speed, frequency, and beam wobbling was systematically studied in relation to **weld shear strength** and **weld seam width**. Furthermore, morphological characterization of the welded joints was conducted to understand the internal structure and behavior of the weld pool. A **multi-objective optimization technique** was also implemented to determine the most suitable process parameters that yield optimal weld quality with desired mechanical performance.

With the successful completion of polymer welding investigations, this research work is further extended to investigate the laser welding of metals and alloys. In the **following chapter**, the laser welding of titanium and NiTinol alloys have been explored, focusing on how laser parameters influence key weld responses. Although polymers and titanium based alloys are fundamentally different materials but they share similar challenge in laser welding such as material specific challenges (i.e. optical properties, heat sensitivity, morphology changes in polymers whereas high reflectivity, oxidation and microstructural transformation in titanium based alloys), defect formation (i.e. voids, bubbles, poor seam strength due to heat degradation in polymers, whereas porosity, cracks, oxidation affecting mechanical properties in titanium based alloys) and process parameter optimization (Both materials require careful selection of process parameters to ensure optimal weld quality).

CHAPTER: 7

HIGH POWER LASER BEAM WELDING OF NITINOL ALLOYS

The present research work is **further extended** to investigate the laser welding of metals and alloys with higher laser power. While some studies on laser welding have been carried out on polymers and metals separately, there is limited comprehensive study on the simultaneous investigation of both material classes, their process parameters, and performance optimization. Addressing these gaps is essential for improving weld quality, durability, and industrial applicability. A moderately **high-power fiber laser (500 W) is used for welding of metals and alloys**. The use of a high-power laser is necessitated by the **higher melting temperatures and thermal conductivities** of metallic materials compared to polymers. Titanium and NiTinol alloys are considered as material for investigation, these materials also faces several challenges such as high melting points, reflectivity, and sensitivity to oxidation, necessitating inert gas shielding and precise energy control to achieve defect-free welds. Both polymers and titanium alloys are utilized in aerospace structures where weight reduction and high-strength joints are critical. In this chapter, we will explore the laser welding of **Titanium and NiTinol** alloys, focusing on how laser parameters influence key weld responses. Special emphasis will be placed on studying the impact of laser heat input on the morphological features of the weld zone, microhardness variation across the weld bead, and the welding challenges associated with these high-performance materials. The main objective is to study the effect of heat input, laser power, and scanning speed on weld quality and advance the understanding of laser welding behavior across diverse material classes, ultimately contributing toward the development of optimized welding strategies for both low-melting polymers and high-melting-point metal alloys.

Nitinol, an equiatomic Ni–Ti system, having the trade name of NiTinol, was first discovered by Buehler and Wiley in Naval Ordnance Laboratory in the year 1960. Since its invention, it is the most popular shape memory alloy (SMA) among designers and product developers.

Due to its exceptional qualities, such as shape memory effect (SME), great corrosion resistant behavior, extremely good biocompatibility, and super elasticity (SE), this alloy has been widely used in the biomedical and medical industries for the past 10 years. These days, the automobile sector, power plants, civil engineering, aerospace, and micro electro-mechanical systems (MEMS) all heavily utilize these materials. In many different industries, nitinol shows promise as a material. Its uses include micro-electromechanical systems, the aerospace sector, and heat-recoverable couplings in shipyards. However, obstacles including low machinability, a lack of connecting methods, and expensive material prices prevent it from being fully utilized in real-world applications. One could argue that the mechanical characteristics of NiTinol must be impacted by any fusion welding system. Getting good quality joints in NiTinol without significantly compromising the outstanding features is primarily wanted, despite all the restrictions in fabricating NiTinol components using standard methods. According to earlier studies, the most popular production method for this material is laser welding. This work used a high power Yb-fiber laser operating continuously to examine the impacts of welding on the bead shape, microstructure, and micro-hardness variation for laser welding of 2-mm thick NiTinol sheet in butt joint arrangement.

7.1. Experimental Planning

In this study, commercially available Nitinol sheets (1.7 mm thick, composed of 50 atomic% Ni and 50 atomic% Ti) are cut into dimensions of 20 mm × 50 mm. Prior to experimentation, acid cleaning is performed on the Nitinol samples to remove any oxide layers from their surfaces. A 500 W ytterbium-doped CW fiber laser (SILFLDP004, Suresh Indu Lasers Pvt. Ltd.), operating at a wavelength of 1.064 μm with a 200 mm focal length, is utilized as the welding power source. The laser system is configured in continuous wave mode, with a spot diameter of 500 μm at the focal plane during welding. Ultra-high-purity argon gas is employed to provide the shielding environment. A butt joint is created on the 1.7 mm thick Nitinol plates using the fiber laser at a maximum power of 500 W. The process parameters, including Laser Power (LP), Scanning Speed (SS), Defocus Distance (DF), and Argon Gas Pressure (GP), are selected based on a review of literature, machine limitations, and trial experiments, as outlined in Table 7.1. The weld quality assessment focuses on factors such as weld seam width or fusion zone width and the heat-affected zone (HAZ) to ensure optimal weld quality. Thirty-one Nitinol samples are prepared, cleaned, and edge-treated to minimize gaps at the welding interface. The welding process is initiated with all parameters precisely

set, and at focus, the laser beam spot diameter is measured at 500 µm, increasing with defocus distance. A central composite unblocked design, based on the response surface method (RSM), is applied for the experimental design. Figure 7.1 provides a visual representation of the ongoing laser welding on the workpiece.

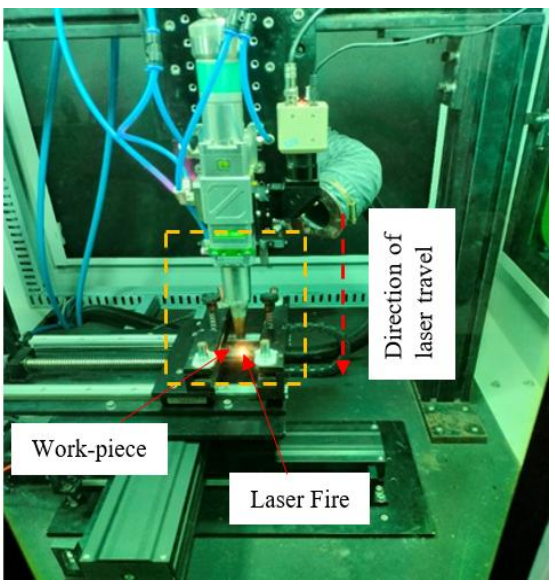

Figure 7.1. Laser welding setup used for experimental work

Table 7.1. Process control parameters and their levels

Controllable Parameters	Units	Notations	Levels				
			-2	-1	0	+1	+2
Laser Power	W	LP	330	360	390	420	450
Scanning Speed	mm/s	SS	1	2	3	4	5
Defocussing Distance	mm	DF	-1	2	5	8	11
Gas Pressure	Bar	GP	0	1	2	3	4

After completion of welding, the fusion zone width and heat-affected zone are initially measured using an optical microscope (STM 6 OLYMPUS). To avoid the edge effect and provide a regular cross section of the weld-bead, the tracks were cut a certain distance from the plate's edge, and the cut cross section was manually polished by mechanical means. Etching was carried out in an acid solution of HF: HNO_3: H2O = 3:7:21 for 30 s to expose the weld-bead profile. The metallographic samples were analysed using optical microscope (Model: Leica DM 2700M) for obtaining the microstructural information. Using a Vickers micro hardness tester (model: S. Auto) from Omnitech, India, a microhardness test was

performed on the etched cross section of the base material and bead. A diamond pyramid indenter is used to measure the variance in microhardness across various zones. A typical load of 100 gf and a dwell period of 10 s are applied. The base material, HAZ, and fusion zone (FZ) are the three zones in which the hardness of the welded sample is evaluated. Using an energy dispersive X-ray spectrometer and scanning electron microscope, the morphological analysis and elemental composition of the weld bead are examined (Model: JEOL JSM IT500).

Tensile test samples were cut utilizing the wire electrical discharge machining (wire-EDM) method in accordance with ASTM E8/E8M standards. Figure 7.2 shows a representation of a typical tensile sample with measurements. A standard gauge length of 32 mm was selected for mechanical tests, and a load cell-type universal testing equipment (Instron 8862) was used to execute the tensile test at a traverse head speed of 1 mm/min. The room temperature tensile tests were conducted using the 50 KN tensile testing device. Initially, a single loading cycle was used for the uniaxial tensile test until the rupture occurred.

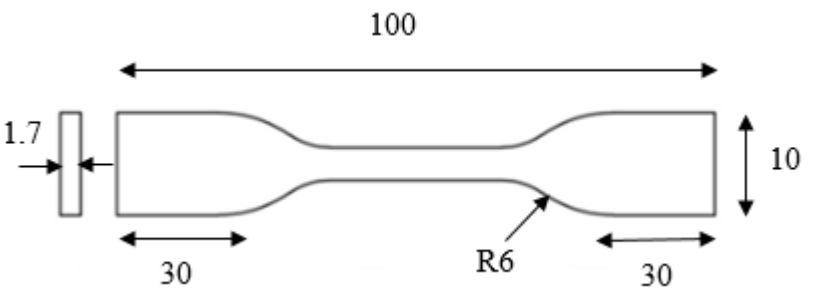

Figure 7.2. Tensile test sample with measurements

7.2 Parametric Analysis Based on RSM Modelling

Table 7.2 presents the experimental plan as well as the measured value of the responses. The Central Composite Design (CCD) of the RSM is employed to design the experiments, facilitating a systematic investigation of the variables influencing the welding process. The FZ and HAZ widths are precisely measured using an STM 6 OLYMPUS microscope, as shown in Fig. 7.3. The welded specimen's surface macrograph shows that proper shielding gas and process parameter selection successfully reduce crack formation along the weld interface, allaying oxygen embrittlement fears. Additionally, different colours along the weld interface show varied thicknesses of the oxidized layer, which gives information on the chemical and thermal processes that take place during welding.

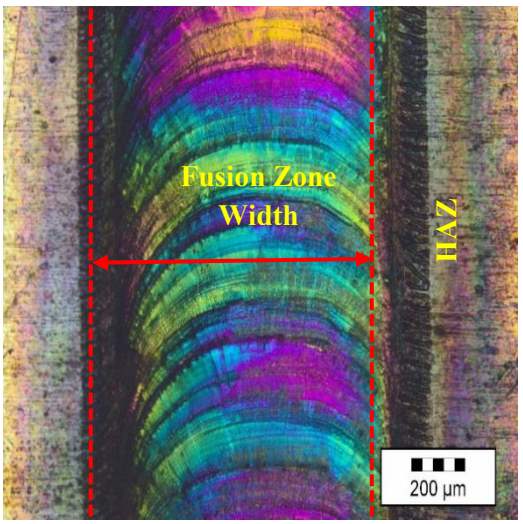

Figure 7.3. Microscopic measurement of the fusion zone and heat-affected zone

Table 7.2 Design matrix and measured experimental result

Experimental Information					Results	
Exp. No.	Welding Parameters				FZ width (µm)	HAZ width (µm)
	LP (Watt)	SS (mm/s)	DF(mm)	GP (Bar)		
1	360	2	2	1	1180.2	937.9
2	420	2	2	1	1253.34	1082.54
3	360	4	2	1	1037.78	563.56
4	420	4	2	1	1063.56	695.94
5	360	2	8	1	1173.04	741.7
6	420	2	8	1	1308.36	874.3
7	360	4	8	1	1093.4	394.72
8	420	4	8	1	1205.4	498.23
9	360	2	2	3	1153.84	1048.26
10	420	2	2	3	1214.57	1209.86
11	360	4	2	3	1012.36	627.38
12	420	4	2	3	1027.5	778.32
13	360	2	8	3	1097.62	819.91
14	420	2	8	3	1237.66	951.66
15	360	4	8	3	1000.94	413.92
16	420	4	8	3	1107.47	524.38
17	330	3	5	2	932.66	456.4

18	450	3	5	2	1103.63	726.58
19	390	1	5	2	1292.12	1302.12
20	390	5	5	2	1009.06	482.34
21	390	3	-1	2	1078.6	945.4
22	390	3	11	2	1147.96	523.94
23	390	3	5	0	1346.06	753.49
24	390	3	5	4	1219.36	922.48
25	390	3	5	2	980.9	1136.72
26	390	3	5	2	983.6	1143.66
27	390	3	5	2	987.74	1149.5
28	390	3	5	2	978.08	1145
29	390	3	5	2	970.6	1147
30	390	3	5	2	975.4	1140
31	390	3	5	2	972.5	1137

7.3 Second Order Regression Equation of Responses

The model with the best fits has been estimated and the measured output has been analysed using Design Expert® software. To determine the best fit model, the v17 program has employed the lack-of-fit test, sequential f-test, and ANOVA (analysis of variance) techniques to assess the model's adequacy. In order to comprehend how process factors affect responses, mathematical models are created to establish a correlation between input and output parameters.

$$FZ = 3056 - 6.55\,LP - 225.2\,SS - 123.96\,DF - 308.47\,GP + 0.00998\,LP \times LP + 42.09\,SS \times SS + 3.64\,DF \times DF + 75.12\,GP \times GP - 0.312\,LP \times SS + 0.2216\,LP \times DF + 5.235\,SS \times DF - 4.373\,DF \times GP \quad \text{..... (7.1)}$$

$$HAZ = -23945 + 122.9\,LP + 258.1\,SS + 112.59\,DF + 368.8\,GP - 0.15384\,LP \times LP - 63.27\,SS \times SS - 11.407\,DF \times DF - 76.83\,GP \times GP - 0.1527\,LP \times SS - 0.0773\,LP \times DF + 0.0867\,LP \times GP + 1.188\,SS \times DF - 12.61\,SS \times GP - 3.812\,DF \times GP \quad \text{..... (7.2)}$$

7.4 ANOVA Analysis for Responses

ANOVA is performed to evaluate the significant terms and adequacy measures such as R^2, R^2-adjusted and R^2-predicted of developed model. Model terms with a "Prob > f" <0.05 imply that the model terms are statistically significant at the 95 % confidence level. Since p-value of interaction of laser power and gas pressure, interaction of scanning speed and gas pressure is more than 0.05, so it does not add much input to the regression equation of weld strength and does not affect much on response. So, it is removed and final regression equation is generated. Table 7.3 shows the ANOVA table with S, R^2, adjusted R^2, and predicted R^2 of the quadratic model. The model terms are statistically significant if the p-value is less than 0.05 for the model (95% confidence level). The value of lack-of-fit should be insignificant so that the experimental value fits the model accurately.

Table 7.3 ANOVA results for fusion zone width (after backward elimination).

Source	DF	Adj. SS	Adj. MS	F-value	P-value
Model	12	406305	33859	652.5	0.000
Linear	4	182846	45712	880.91	0.000
LP	1	42556	42556	820.11	0.000
SS	1	111567	111567	2150.03	0.000
DF	1	7331	7331	141.28	0.000
GP	1	21392	21392	412.24	0.000
Square	4	208993	52248	1006.88	0.000
LP × LP	1	2305	2305	44.43	0.000
SS × SS	1	50659	50659	976.26	0.000
DF × DF	1	30694	30694	591.51	0.000
GP × GP	1	161366	161366	3109.71	0.000
2-way interaction	4	14466	3617	69.69	0.000
LP × SS	1	1402	1402	27.02	0.000
LP × DF	1	6364	6364	122.64	0.000
SS × DF	1	3946	3946	76.05	0.000
DF × GP	1	2754	2754	53.07	0.000
Error	18	934	52	-	-
Lack-of-fit	12	709	59	1.57	0.300
Pure error	6	225	38	-	-

Source	DF	Adj. SS	Adj. MS	F-value	P-value
S = 7.20345, R-sq. = 99.77 %, R-sq. (adjusted) = 99.62 %, R-sq. (predicted) = 99.22 %					

To determine how each parameter affects weld seam width, an ANOVA analysis was conducted. Models with a 95% confidence level (p-value) of less than 0.05 are deemed to have significant parameters. The relationship that best fits the model has been established using the quadratic relationship. The ANOVA findings with S, R^2, adjusted R^2, and anticipated R^2 for the quadratic model are displayed in Table 7.4. If the model's 95% confidence level p-value is less than 0.05, the model terms are considered statistically significant. To ensure that the experimental result appropriately fits the model, the lack-of-fit value should be negligible.

Table 7.4 ANOVA results for heat affected zone width (after backward elimination).

Source	DF	Adj. SS	Adj. MS	F-value	P-value
Model	14	2280431	162888	3186.10	0.000
Linear	4	1381694	345423	6756.50	0.000
LP	1	107768	107768	2107.95	0.000
SS	1	963700	963700	18850.00	0.000
DF	1	274746	274746	5374.04	0.000
GP	1	35480	35480	693.99	0.000
Square	4	893682	223170	4365.22	0.000
LP × LP	1	548192	548192	10722.65	0.000
SS × SS	1	114479	114479	2239.22	0.000
DF × DF	1	301386	301386	5895.12	0.000
GP × GP	1	168812	168812	3301.96	0.000
2-way interaction	6	6056	1009	19.74	0.000
LP × SS	1	336	336	6.57	0.021
LP × DF	1	773	773	15.13	0.001
LP × GP	1	108	108	2.12	0.165
SS × DF	1	203	203	3.98	0.063
SS × GP	1	2543	2543	49.73	0.000
DF × GP	1	2092	2092	40.92	0.000
Error	16	818	51	-	-
Lack-of-fit	10	672	67	2.75	0.114

Source	DF	Adj. SS	Adj. MS	F-value	P-value
Pure error	6	146	24	-	-
S = 7.15015, R-sq. = 99.96 %, R-sq. (adjusted) = 99.93 %, R-sq. (predicted) = 99.82 %					

7.5 Validation of the developed model

Fig. 7.4 and 7.5 represent the correlation between the measured and predicted values of the width of fusion zone and heat affected zone, respectively. Since the predicted outcomes closely match the measured data, these figures show that the generated models are satisfactory. The generated models can produce extremely accurate results, which show a small percentage difference between the estimated and experimental results.

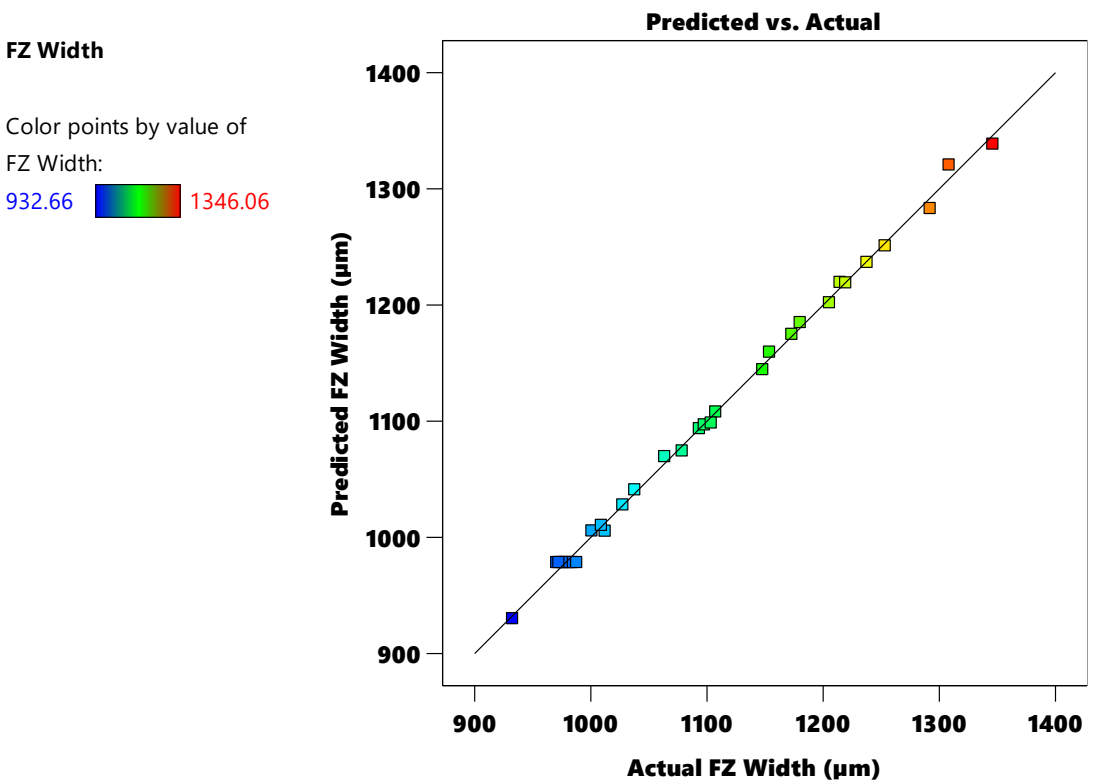

Figure 7.4 Plot of actual vs. predicted Fusion Zone Width

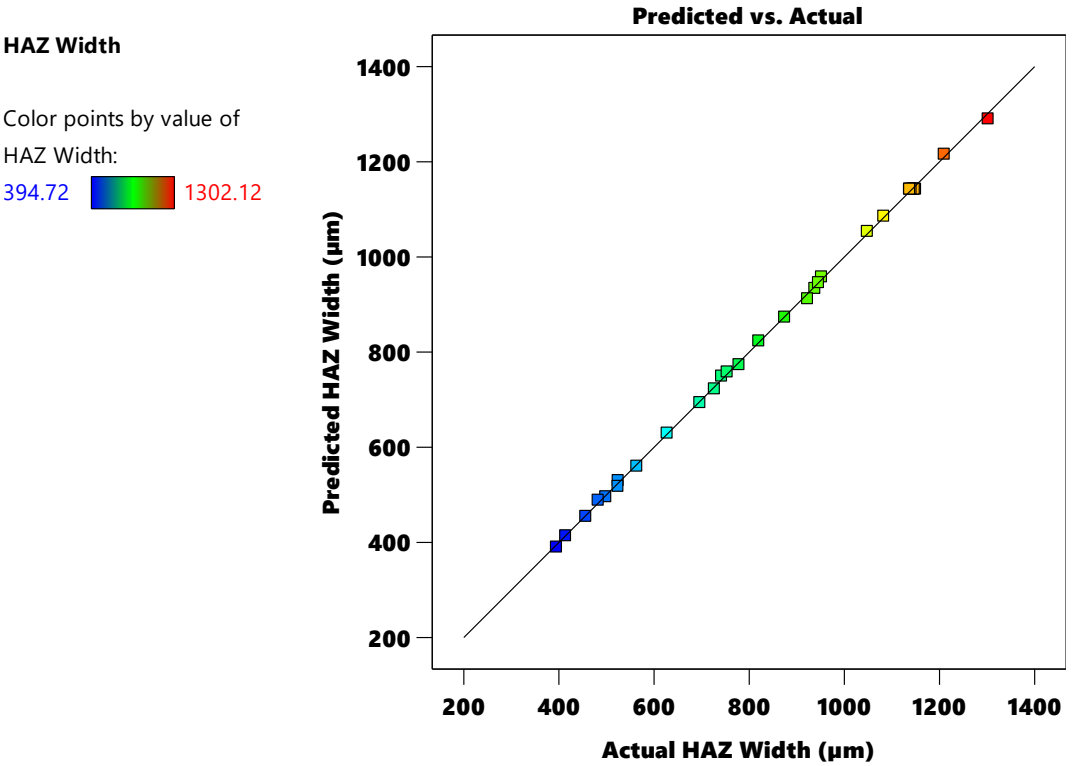

Figure 7.5 Plot of actual vs. predicted Heat Affected Zone Width

7.6 Parametric Analysis

The effects of process variables on weld quality characteristics such as weld shear strength and weld seam width, within the specified range, are thoroughly investigated. The surface interaction plot depicts the behaviour of responses as the value of the process variable changes; the rationale for this is discussed in detail.

7.6.1 Fusion Zone Width

The surface interaction plot of laser power and scanning speed on fusion zone width is shown in Fig. 7.6. It can be observed from Fig.7.6 that the FZ width increases with the applied laser power, as laser power is directly proportional to the heat input. The FZ width expands with increased laser power due to more material being melted. It is also found out from the figure that FZ width decreases with an increase of scanning speed. This reduction is attributed to the shorter interaction times between the laser and the material at higher scanning speeds, which results in less heat input. As the laser moves rapidly, the weld pool's size is minimized. Furthermore, the rapid cooling of the molten metal contributes to the narrowing of both the FZ.

.

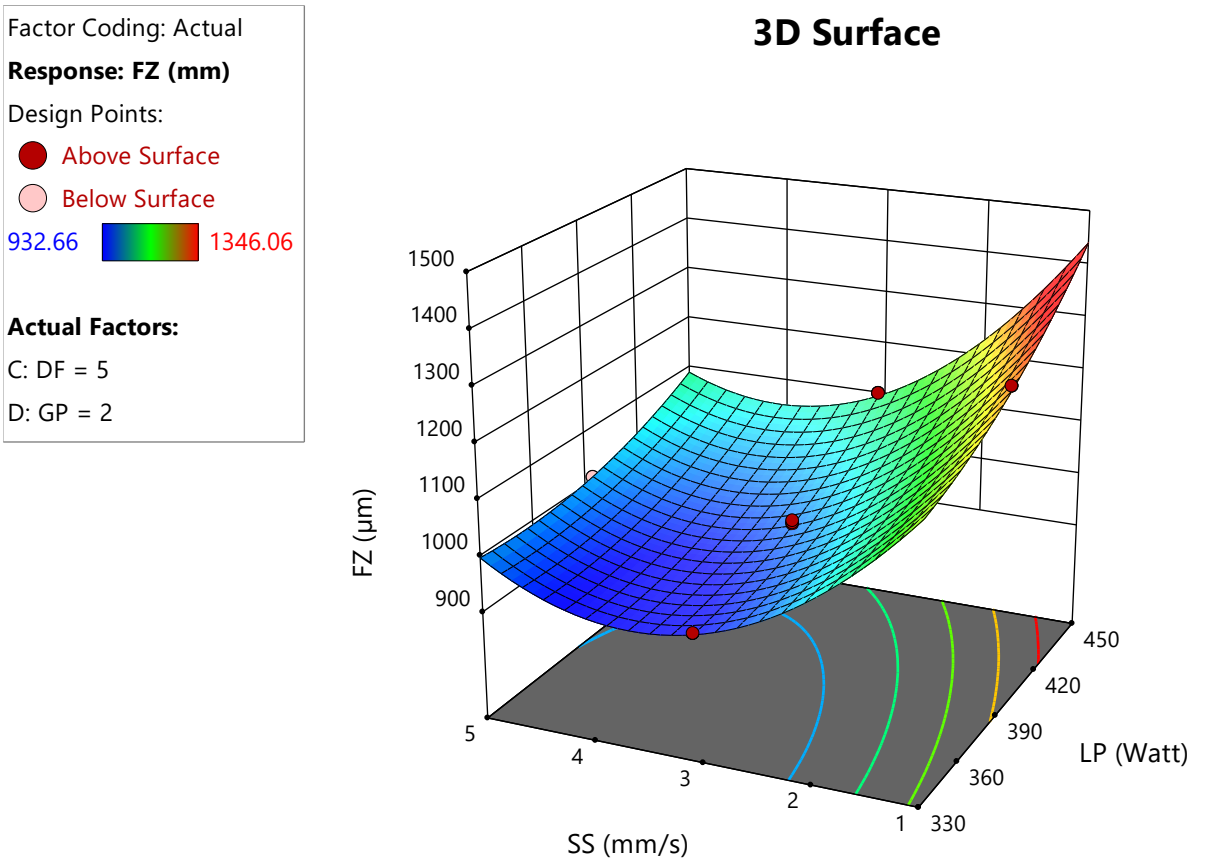

Figure 7.6: Surface plot showing the interaction effects of laser power and scanning speed on fusion zone width, when all other parameters are at their central values

The surface interaction plot of laser power and gas pressure on fusion zone width is shown in Fig. 7.7. It is observed that gas pressure plays detrimental role on weld quality. Based on Fig. 7.7, fusion zone width decreases with an increase of gas pressure up to mid-point and thereafter it increases. This is because lower gas pressure causes a broader distribution of heat, enlarging these zones. However, it is essential to balance gas pressure to avoid excessive cooling, which might cause incomplete fusion or affect weld quality.

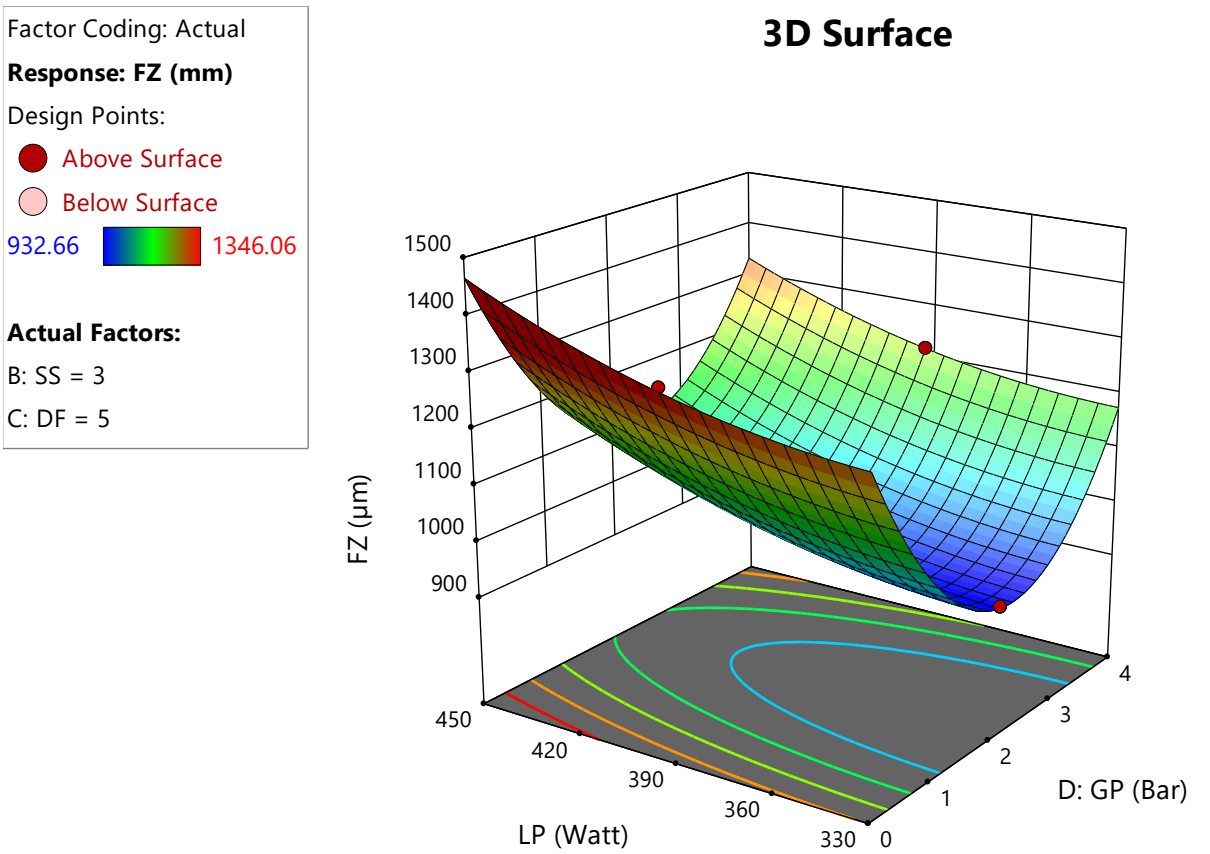

Fig. 7.7: Surface plot showing the interaction effects of laser power and gas pressure on fusion zone width, when all other parameters are at their central values

The surface interaction plot of laser power and defocussing distance on fusion zone width is shown in Fig. 7.8. It can be observed from the Fig. that fusion zone width decreases with an increase of defocusing distance. This behaviour may result from the changes in energy density and heat distribution as the defocusing distance affects the focal spot size and energy concentration on the workpiece. As the defocussing distance continues to increase, the reduction in effective heat input may contribute to a decrease in FZ size.

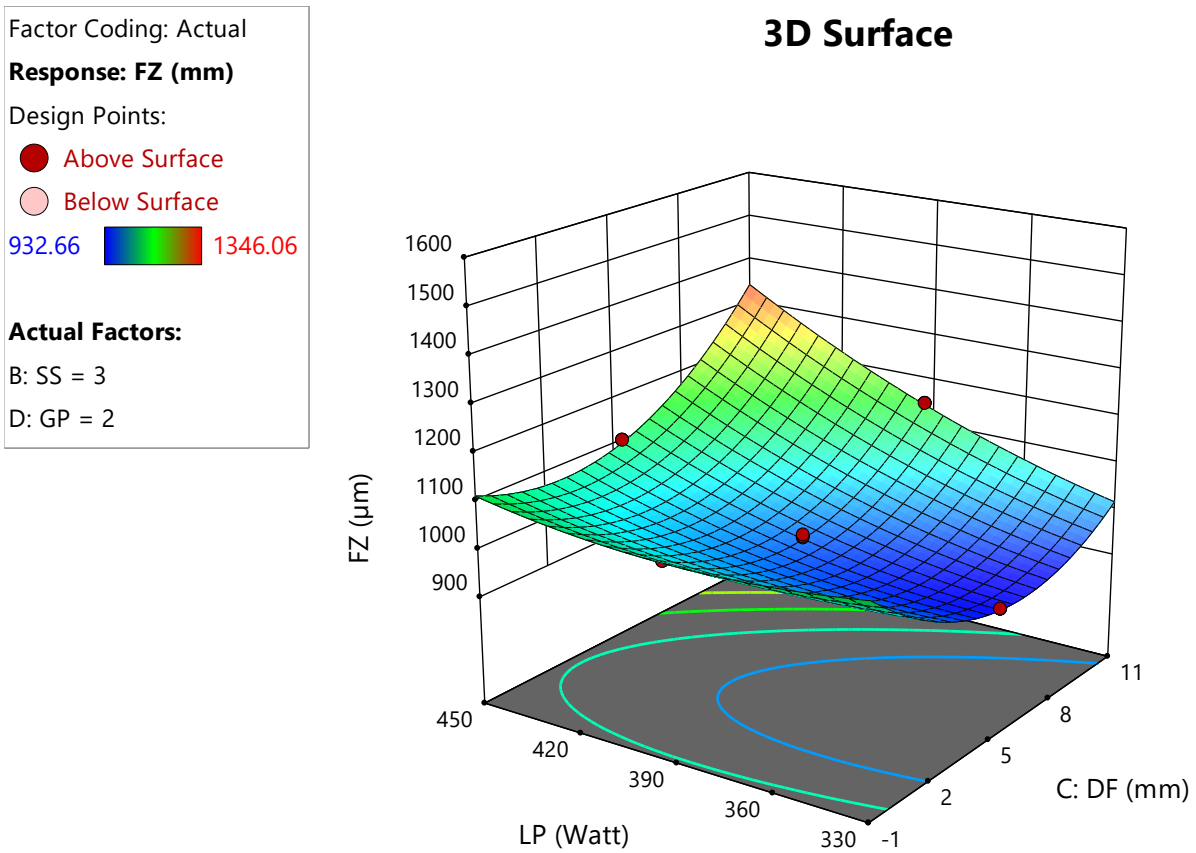

Figure 7.8: Surface plot showing the interaction effects of laser power and defocussing distance on fusion zone width, when all other parameters are at their central values

7.6.2 Heat Affected Zone Width

The surface interaction plot of laser power and scanning speed on heat affected zone width is shown in Fig. 7.9. It is seen from Fig.7.9 that the up to a certain threshold, the HAZ width increases with laser intensity; beyond that, a drop is observed. The HAZ width initially increases with laser power until it reaches a peak, after which it decreases due to the dominant effects of melting and rapid cooling surrounding the weld area. Figure 7.10 displays the surface interaction plot of gas pressure and laser power on heat-affected zone width. It has been found that the HAZ width rises with increasing laser power until the halfway mark, at which point it starts to fall. This is because lower laser power gives less heat input into weld zone, and higher laser power may provide more penetration into weld zone. Higher gas pressure helps in achieving a more concentrated heat input, resulting in a narrower HAZ, while lower gas pressure causes a broader distribution of heat, enlarging these zones.

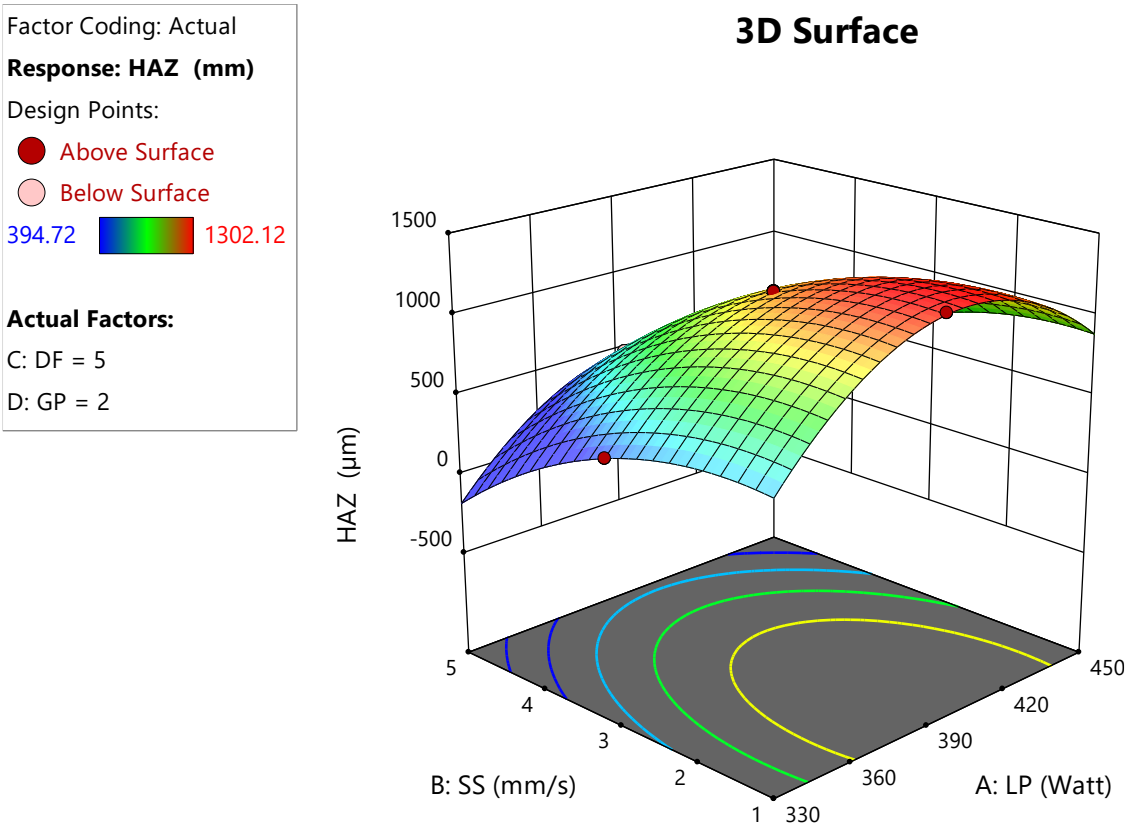

Figure 7.9: Surface plot showing the interaction effects of laser power and scanning speed on heat affected zone width, when all other parameters are at their central values

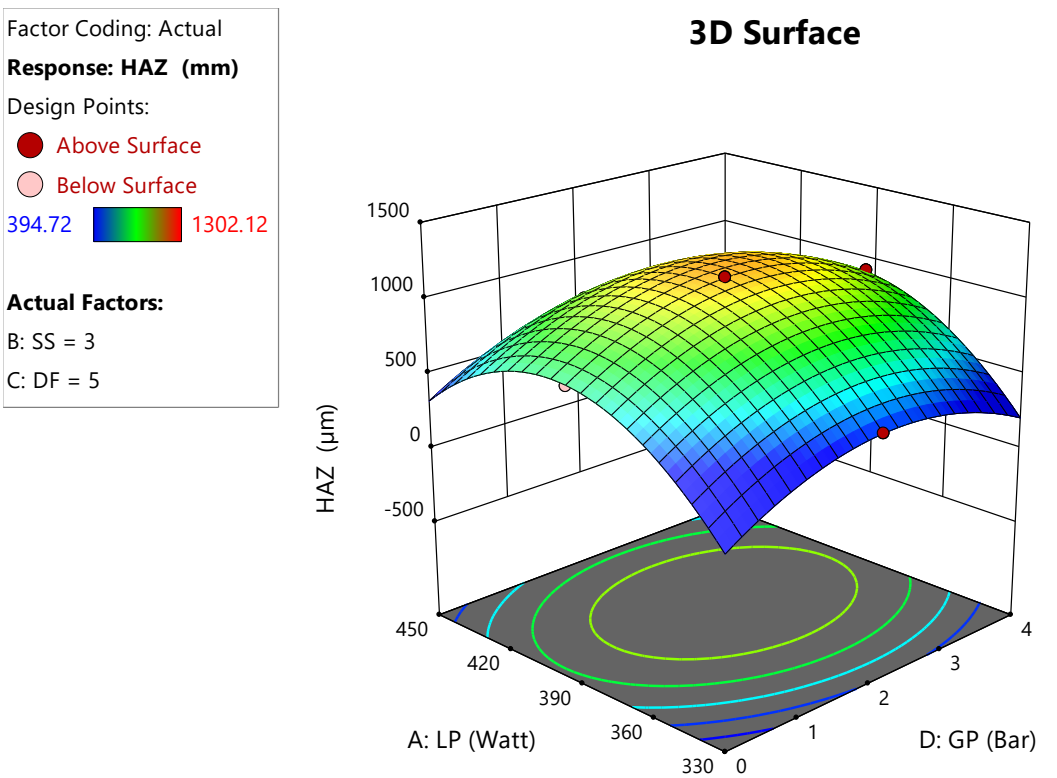

Figure 7.10: Surface plot showing the interaction effects of laser power and gas pressure on heat affected zone width, when all other parameters are at their central values

The surface interaction plot of laser power and defocussing distance on heat affected zone width is shown in Fig. 7.11. The HAZ width initially increases before subsequently decreasing with the rising defocusing distance. This behavior may result from the changes in energy density and heat distribution as the defocusing distance affects the focal spot size and energy concentration on the workpiece. Initially, a larger defocusing distance can lead to more heat being dispersed, increasing the HAZ. However, as the distance continues to increase, the reduction in effective heat input may contribute to a decrease in HAZ width.

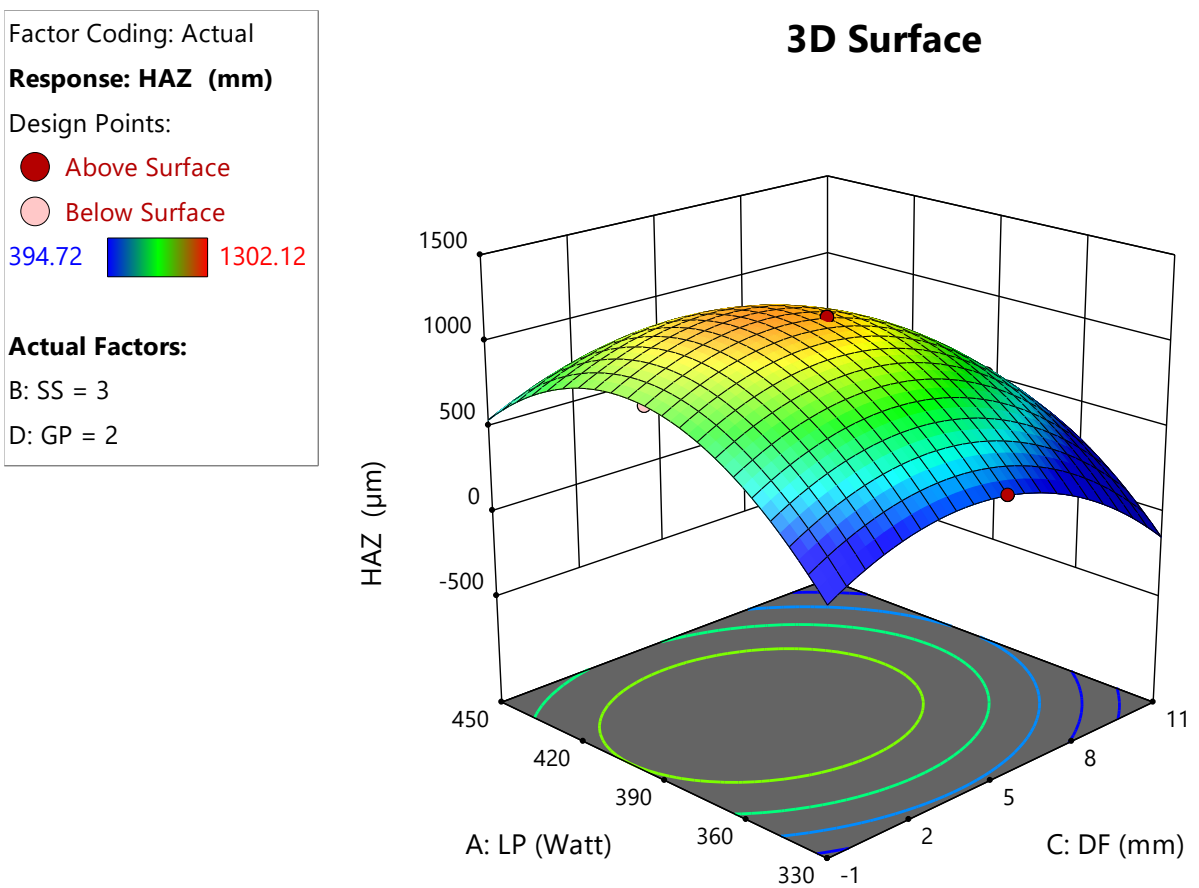

Figure 7.11: Surface plot showing the interaction effects of laser power and defocussing distance on heat affected zone width, when all other parameters are at their central values

7.7. Weld bead microstructure

The microstructure of the Nitinol weldment, as shown in Fig.7.12 (a-c), provides a detailed insight into the distinct zones formed during the welding process. Fig. 7.12(a) highlights three critical zones: the base material, the fusion zone (FZ), and the heat-affected zone (HAZ). These zones exhibit different microstructural characteristics due to variations in thermal exposure during welding. Fig. 7.12(b) presents a high-magnification view of the FZ, revealing

a pronounced columnar dendritic structure. This structure results from the molten metal rapidly cooling and solidifying as soon as the laser power is cut off. In cases of full penetration welding, columnar dendritic grains are observed to orient almost perpendicular to the weld centerline (as shown in Fig. 7.12(b)), indicating uniform heat flow and solidification throughout the weld thickness. In contrast, during partial penetration welding, the dendritic grains are oriented at acute angles from the interface toward the center of the bead. This difference in orientation reflects the non-uniform heat distribution in partial penetration welds, where the solidification front progresses differently based on localized heat accumulation. Additionally, Fig. 7.12(c) reveals the presence of black precipitates inside the weld bead. These precipitates are more pronounced with increased heat input, suggesting that higher heat inputs contribute to the segregation of alloying elements or the development of secondary stages of the solidification process. The increased amount of precipitation with higher heat input could negatively impact the mechanical properties of the weld, including strength and corrosion resistance, making heat input a critical parameter in controlling weld quality in Nitinol.

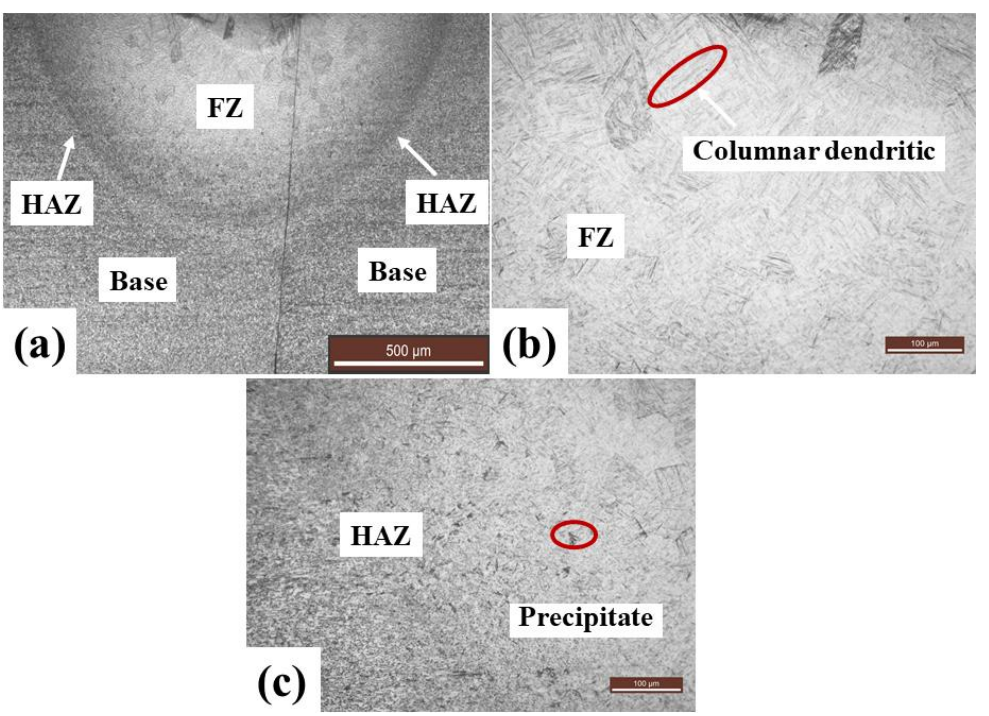

Figure 7.12. Microstructure of welded sample (a) weld bead (b) fusion zone (c) heat affected zone

7.8. SEM microstructure and EDX analysis

The SEM (Scanning Electron Microscopy) and EDX (Energy Dispersive X-ray) analysis of the welded specimens, depicted in Fig. 7.13 and 7.14, reveal significant insights into the microstructural characteristics influenced by shielding gas pressure during the laser welding of Nitinol. Fig. 7.13(a) illustrates the development of a cellular structure in the weld zone, a direct result of the rapid solidification of the molten pool. This cellular structure is crucial as it influences the mechanical properties, particularly strength and ductility. Additionally, the presence of carbides on the surface of the weld specimen suggests potential alloying effects that could enhance hardness but may also lead to embrittlement if not carefully controlled.

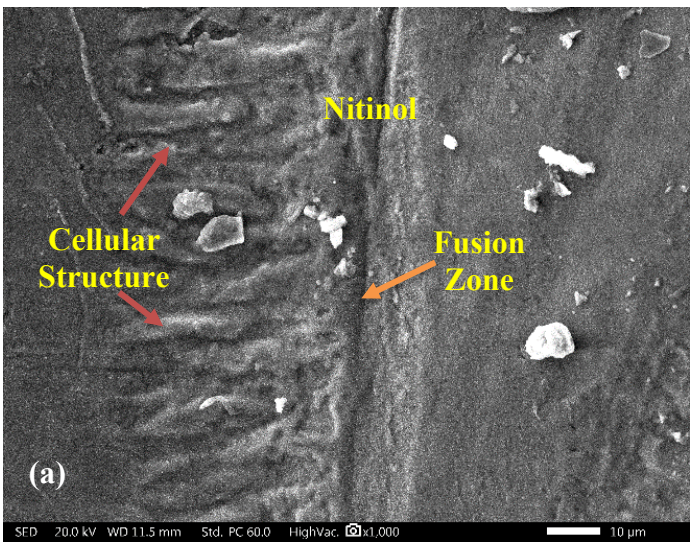

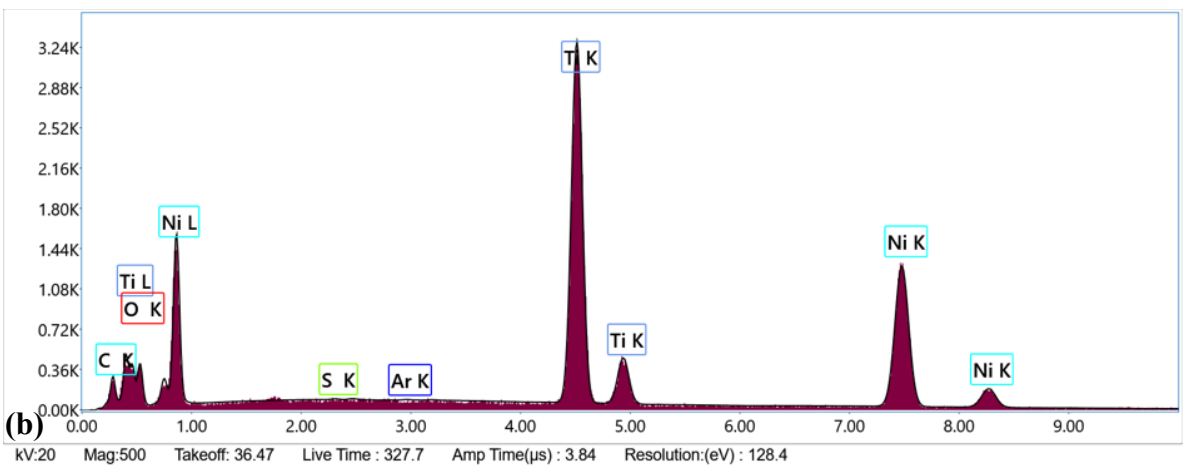

Figure 7.13. (a) SEM micrograph of weld zone at 1000x magnification, and (b) EDX analysis of weld zone, with shielding gas environment

EDX analysis, presented in Fig. 7.13(b), indicates the development of a passive titanium oxide layer on the welded specimen. The minimal oxide layer observed highlights the

effectiveness of shielding gas in protecting the weld from atmospheric contamination, thereby maintaining weld integrity and strength. In contrast, Fig. 7.14(a) and 7.14(b) demonstrate the detrimental effects of welding without shielding gas. The increased oxidation in these specimens is evident, resulting in a thicker oxide layer that can significantly impair weld quality. The absence of shielding gas not only contributes to a larger oxide layer but also correlates with the formation of cracks within the weldment. The EDX analysis reinforces this observation by indicating increased oxidation in the fusion zone, as shown in Fig. 7.14(b), which can adversely affect penetration and overall weld strength.

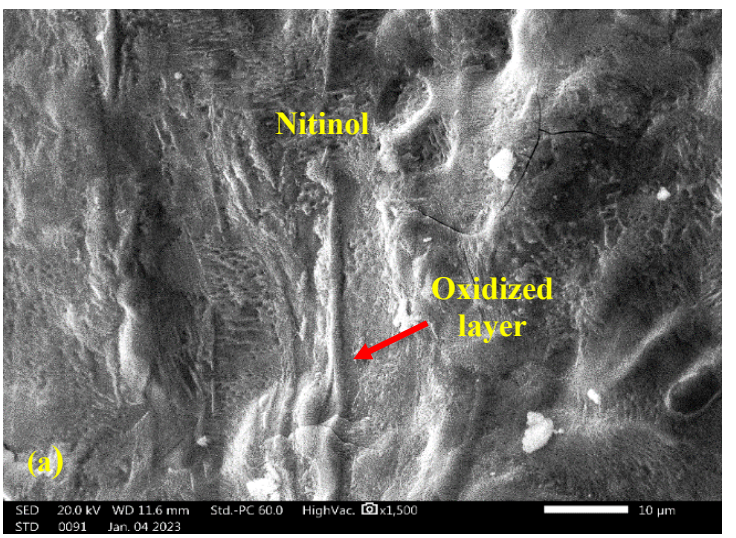

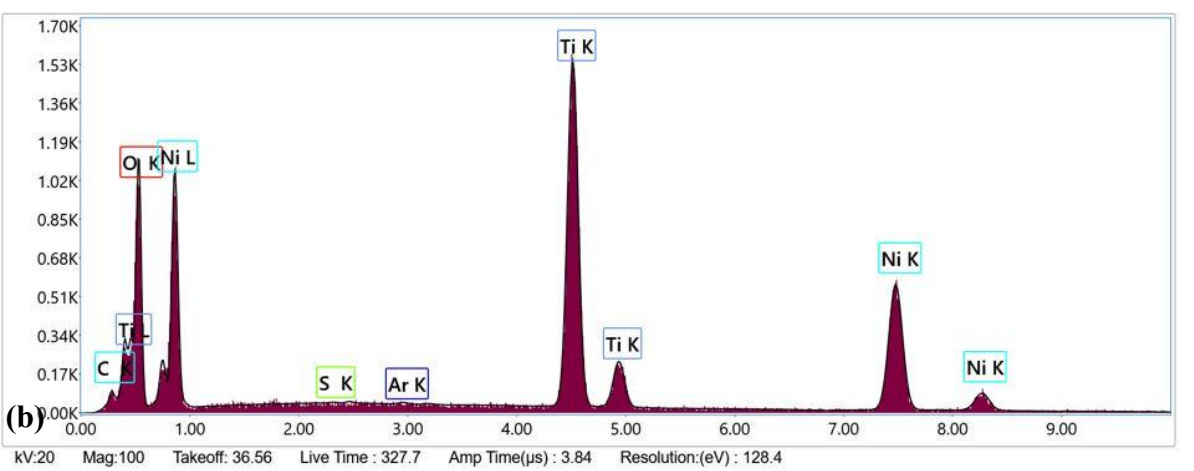

Figure 7.14. (a) SEM micrograph of weld zone at 1000x magnification, and (b) EDX analysis of weld zone, without shielding gas environment

7.9. Micro-hardness variation

The variations in microhardness across the weld bead, illustrated in Fig. 7.15, reveal critical insights into the mechanical properties of the laser-welded Nitinol. The plot distinctly outlines

three hardness zones: the base material, FZ and HAZ. Notably, the maximum micro hardness is recorded in the fusion zone, measuring 420 $HV_{0.1}$, compared to 340 $HV_{0.1}$ in the HAZ and 310 $HV_{0.1}$ in the base material. Rapid cooling rates during solidification and the ensuing refining of the grain structure are two of the reasons for the observed rise in microhardness within the FZ. In the FZ, the intense heat from the laser welding process leads to the formation of fine, equiaxed grains, which enhance hardness due to the Hall-Petch relationship, where smaller grains hinder dislocation movement, increasing strength. Conversely, the microhardness decreases toward the base material, indicating coarser grains and a more homogeneous composition that does not support similar mechanical enhancement. The inhomogeneous chemical composition also contributes to the variation in hardness across the weld zones. Different zones exhibit distinct microstructural characteristics, influenced by the thermal cycles experienced during welding. The HAZ experiences heating and subsequent recrystallization, altering its hardness relative to both the FZ and the base material. This analysis underscores the importance of understanding microhardness distribution in welded joints, as it directly correlates with performance characteristics such as wear resistance and overall structural integrity, which are critical for applications in demanding environments.

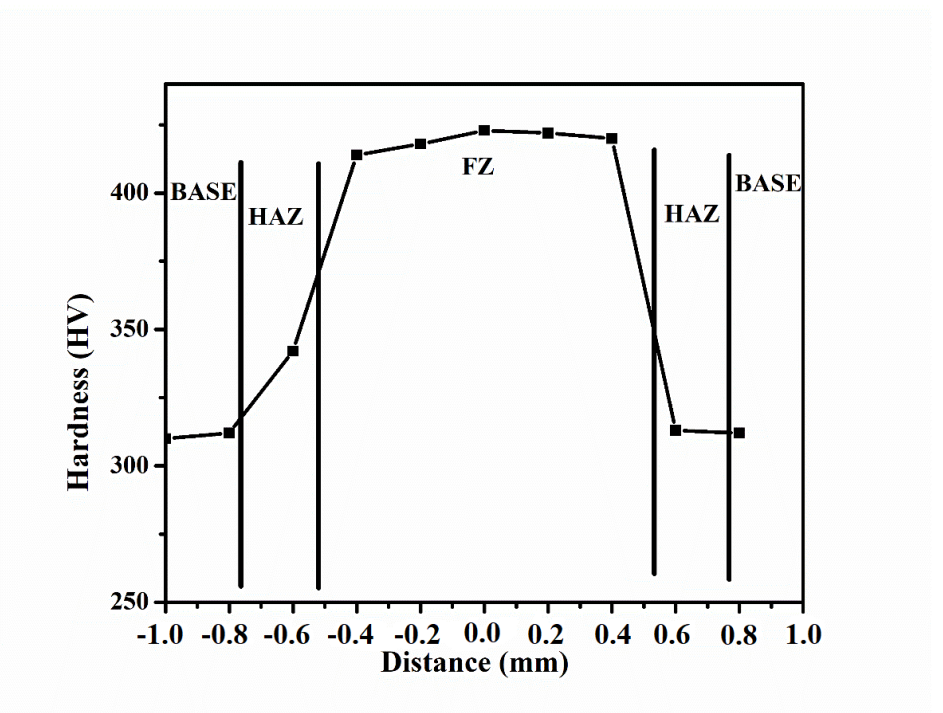

Figure 7.15 Variation of micro-hardness across the weld bead

7.10 Multi-objective optimization using desirability function based technique

The optimal process parameter for minimizing the fusion zone width and simultaneously minimizing the heat impacted zone width is found using an optimization technique based on DFA method. It works by translating the responses in to corresponding value of desirability. Desirability value depends upon range and target response. When response reach its goal, then desired unity value is assigned. Desirability value is considered zero outside certain limit. Minimum fusion zone width of 926.32 µm and minimum heat affected zone width of 190.92 µm has been achieved at 330 watt laser power, 3.9 mm/s scanning speed, 5.67 mm defocussing distance and 2.56 bar gas pressure as shown in Fig. 7.16.

Fig. 7.17 shows the overlaid contour plot fusion zone width as well as heat affected zone width. Minimum seam width or fusion zone and minimum HAZ is achieved at lower laser power and higher scanning speed.

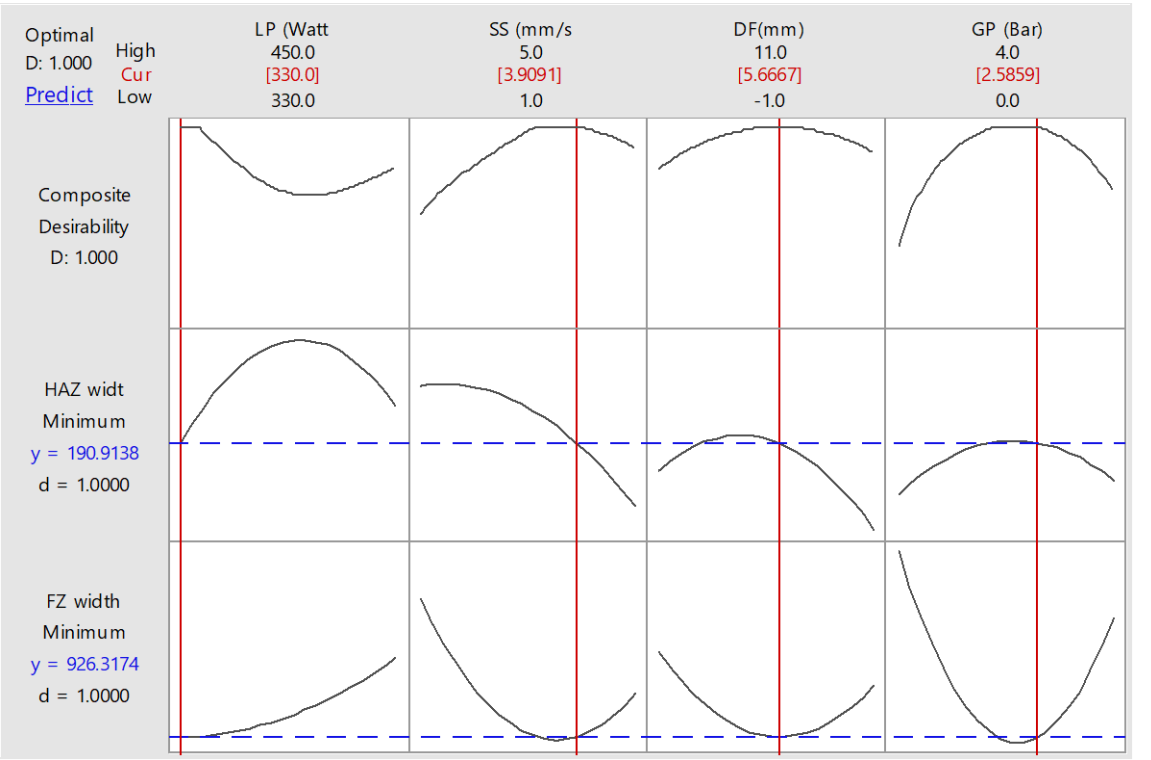

Figure 7.16. Optimization results for minimum FZ and minimum HAZ

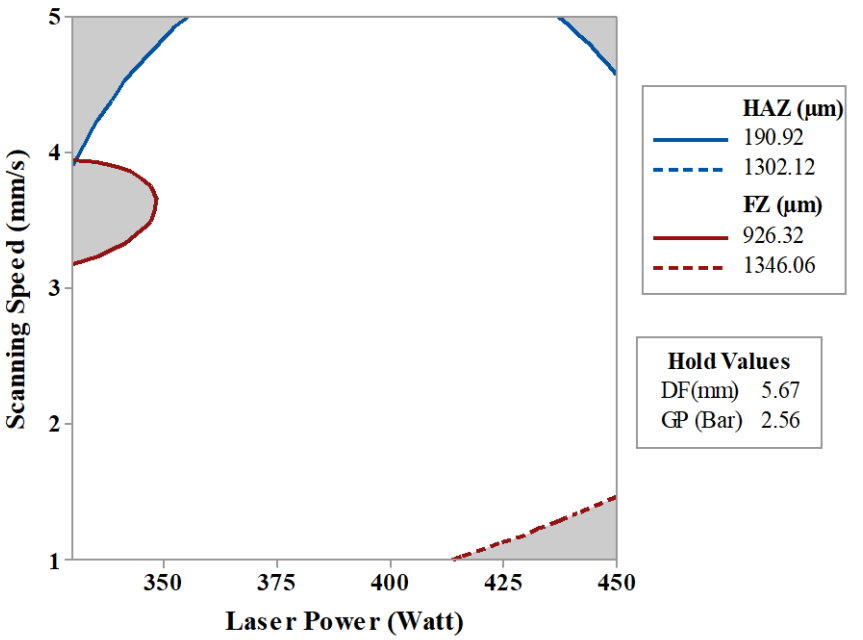

Figure 7.17 Overlaid contour plot of FZ and HAZ

7.11. Tensile test

Tensile test is performed at optimal process parameter settings obtained by RSM based DFA technique to assess the weld strength. The welded samples undergo tensile testing to examine the relation between applied stress and strain, as seen in Fig. 7.18.

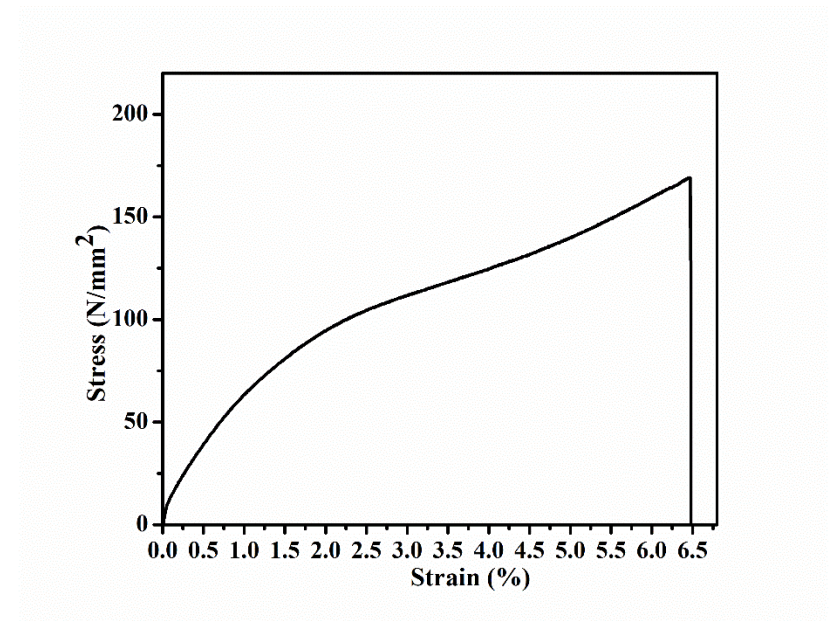

Figure 7.18. Graphs showing the tensile test results of welded samples

The welded specimens had an elongation to fracture of roughly 6.56% and ultimate tensile values of 169.1 MPa. Additionally, the welded sample exhibits a yield strength of 106.9 MPa. It is observed that for the welded samples, the fracture occurred in the welding zone. It can be said that the welded sample's tensile strength is significantly lower than that of the base material. The decrease in tensile strength suggested that welding causes the material to become more brittle. The ductility of the welded samples began to decline because of the growth of fine dendritic structures in the weld pool as confirmed by microstructure.

7.12 Validation Experiment

A confirmation experiment has been performed at the optimal welding process parameter setting to find the error, and it is estimated that fusion zone width has an error of 4.39% and heat affected zone width has an error of 3.7% (Table 7.5), which is very minimum and less than 5%; thus it is acceptable.

Table 7.5 Confirmation test at optimal process parameter

Optimum value from Desirability function technique			Confirmation test	% Error
Process Parameters	LP (Watt)	330	330	
	SS (mm/s)	3.9	3.9	
	DF (mm)	5.67	5.67	
	GP (bar)	2.59	2.59	
Response Parameters	FZ (µm)	926.32	967	4.39
	HAZ (µm)	190.92	198	3.70

7.13 Outcomes of the present research work

From this study bead on plate laser welding of 1.7 mm thick NiTinol plate, the following outcomes could be drawn from the present research work:

1. Laser butt welding of 2 mm thick Nitinol using a continuous-wave fiber laser successfully produced smooth, uniform weld beads with shiny surfaces and no defects.

2. Weld-bead consisted of the columnar dendritic structure. Columnar dendritic grains are observed to orient almost perpendicular to the weld centerline, indicating uniform heat flow and solidification throughout the weld thickness.

3. The fusion zone width increases with laser power while scanning speed and defocusing distance effectively reduce both widths of fusion as well as heat-affected zone.

4. Based on ANOVA results, scanning speed is found to be the most dominant parameter on widths of fusion as well as heat-affected zone, as it governs the heat input and laser material interaction time. Higher scanning speed reduces the interaction time, which leads to narrower fusion and HAZ width, conversely, lower scanning speeds cause greater heat input and wider width.

5. Optimal gas pressure concentration narrows the fusion as well as heat-affected zones, whereas very high gas pressure can result in excessive turbulence in the fusion zone and compromised weld quality.

6. Microhardness value was gradually increased from the base material to weld center. This increase in micro-hardness is attributed to grain refinement within the fusion zone. The fusion zone exhibits the highest micro-hardness value of 420 $HV_{0.1}$, followed by the heat-affected zone at 346 $HV_{0.1}$, and the parent material at 310 $HV_{0.1}$.

7. Ultimate tensile strength of 169.1 MPa and yield strength of 106.9 MPa is achieved at optimal parameter settings.

8. Minimum fusion zone width of 926.32 μm and minimum heat affected zone width of 190.92 μm has been achieved at 330-watt laser power, 3.9 mm/s scanning speed, 5.67 mm defocussing distance and 2.56 bar gas pressure by Desirability function based optimization technique.

CHAPTER: 8

HIGH POWER LASER BEAM WELDING OF TITANIUM SUPERALLOYS

Titanium alloy, because of its exceptional fatigue behavior, enhanced corrosion resistance, and high strength to weight ratio, is being widely utilized in a variety of industries. The strong bio-compatibility of titanium alloys has expanded its use beyond the current scope of aerospace, nuclear, and automotive applications to include the manufacture of bio-medical devices. Since, titanium exhibits very low corrosion rates in human body fluids, therefore, it has numerous application in medical industry such as artificial heart pumps, heart valve parts, and hip bone replacement. Ti-6Al-4V, which is α-β allotropic phase alloy, are the mostly used among all titanium alloy. It has the ability to alter the mechanical and physical properties by changing the amount of alloying elements or by regulating the microstructural evolution during thermo-mechanical processing. The HCP structured α phase alloy remains stable up to 882°C before changing into BCC β structured material. Ti-6Al-4V is presently considered as the workhorse of titanium alloy because of its high strength and easy fabrication. It contains about 6% aluminium for α stabilization and 4% vanadium for β stabilization.

The welding of titanium is very much difficult because it is highly reactive toward atmospheric gases like oxygen, nitrogen, carbon, or hydrogen at temperatures exceeding 550°C, predominantly in the molten stage, which causes severe embrittlement and crack formation. Contamination in the weld region can be caused by inadequate cleaning of the joint, poor shielding environment in the vicinity of the weld zone, or impurities in the shielding gas, which results in a crack formation. Although there are variety of welding technique such as solid state welding and fusion welding are used to join titanium alloy, but advanced welding technique such as laser beam and electron beam welding, have clear cutting edge over the conventional welding processes. However, laser beam welding has certain advantages over electron beam welding, as it does not require vacuum. Laser beam welding produces fine seam width, high precision, and less thermal distortion for joining the intricate metal assemblies. In the current study, a high power Yb-fiber laser is used to examine the

effects of welding on the bead shape, microstructure, and micohardness variation during laser welding of 2-mm thick titanium sheet in butt joint arrangement.

8.1. Experimental Planning

Titanium super-alloy (Ti6Al4V) of size 50 mm x 25 mm with thickness of 2 mm are cut from the rectangular plates and selected as work material for laser beam welding. The work piece is cleaned with acetone before laser beam welding. A multi-diode pump CW fiber laser welding (SILFLDP004, Suresh Indu Lasers Pvt. Ltd.) is used to perform the butt welding of titanium alloy. The fiber laser beam welding used for the experimental work contains spot diameter of 500 µm, wavelength 1064 nm, and maximum power of 500 watt. A fiber laser source is used in continuous mode with active gain medium. Focusing lens with a focal length of 200 mm are used to deliver the laser beam to the work piece. The beam focus is positioned on the bottom surface. A focus spot with a near Gaussian distribution and a diameter of 500 µm is produced on the work piece. Mechanical clamping with four nut and bolts are used to fix the work piece for experimental work. Laser spot diameter of 500 µm at focused condition and single number of passes are used throughout the experimentation. Butt joint welding is performed along the width of 25 mm of selected work piece. Figure 8.1 represents the schematic view of experimental setup of laser welding system.

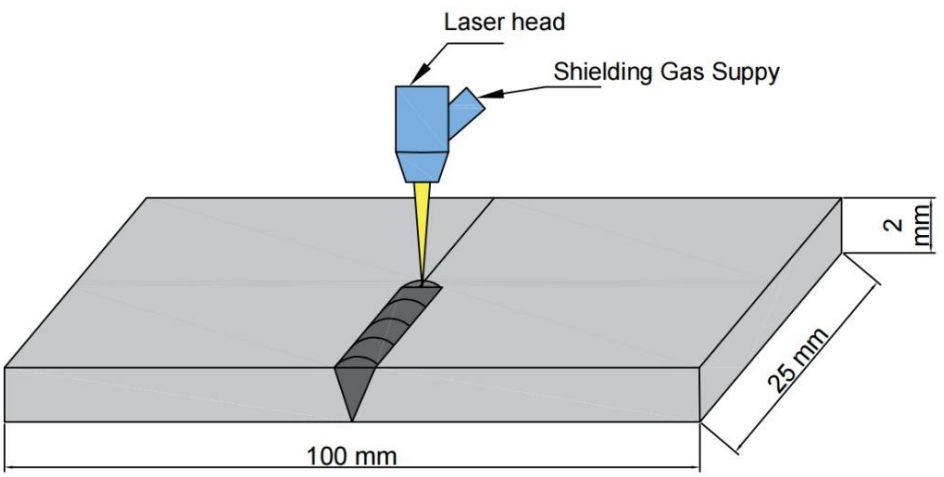

Figure 8.1. Schematic representation of experimental setup of laser welding system

Laser power (LP), scanning speed (SS), and defocusing distance (FD) are considered as process parameter while fusion zone width (FZ) and heat affected zone width (HAZ) are taken responses. Full factorial central composite design with three continuous factor and five level are used for the experimental design based on response surface method. Twenty number of

experiments with three time replications has to be conducted on the basis of this design which includes 8 factorial point, 6 axial point and 6 center point. Based on the literature survey and feasibility of the experimental setup, trial experiment are conducted to find out the possible ranges of process variables as given in Table 8.1. The width of fusion zone and heat affected zone is measured using a 3-dimensional optical measuring microscope (STM-6, OLYMPUS). Three measurements of each welded specimen are taken and average of them are considered for analysis. Morphological analysis and elemental composition of weld bead is analyzed using Scanning electron microscope with Energy Dispersive X-Ray Spectrometer (Model: JEOL JSM IT500).

Table 8.1. Process control parameters and their levels

Controllable Parameters	Units	Notations	Levels				
			-2	-1	0	+1	+2
Laser Power	W	LP (A)	400	410	425	440	450
Scanning Speed	mm/s	SS (B)	0.5	1	1.8	2.6	3.2
Defocusing Distance	mm	FD (C)	2.6	4	6	8	9.4

Using a Vickers micro hardness tester (model: S.Auto) from Omnitech, India, a microhardness test was performed on the etched cross section of the base material and bead. The diamond pyramid indenter is used to apply a normal load of 100 gf and a dwell period of 10 s in order to measure the variance in microhardness across different zones. The base material, HAZ, and fusion zone (FZ) are the three zones in which the hardness of the welded sample is evaluated.

Tensile test samples were cut utilizing the wire electrical discharge machining (wire-EDM) method in accordance with ASTM E8/E8M standards. Figure 8.2 shows a representation of a typical tensile sample with measurements. A standard gauge length of 32 mm was selected for mechanical tests, and a load cell-type universal testing equipment (Instron 8862) was used to execute the tensile test at a traverse head speed of 1 mm/min. The room temperature tensile tests were conducted using the 50 KN tensile testing device. Initially, a single loading cycle was used for the uniaxial tensile test until the rupture occurred.

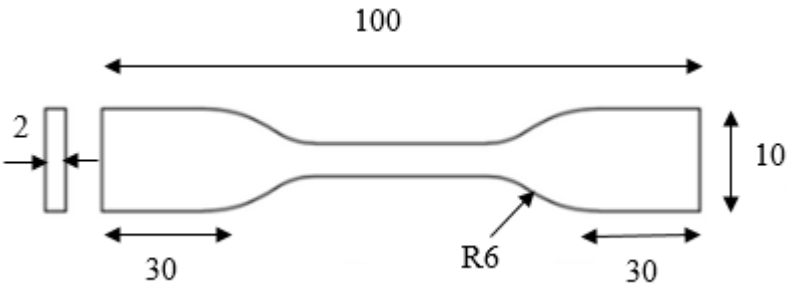

Figure 8.2. Tensile test sample with measurements

8.2 Parametric Analysis Based on RSM Modelling

Table 8.2 presents the experimental plan as well as the measured value of the responses. The Central Composite Design (CCD) of the RSM is employed to design the experiments, facilitating a systematic investigation of the variables influencing the welding process.

Table 8.2 Design matrix and measured experimental result

Experimental Information				Results	
Exp. No.	Welding Parameters			FZ width (µm)	HAZ width (µm)
	LP (Watt)	SS (mm/s)	FD(mm)		
1	410	1	4	1293.28	2184.56
2	440	1	4	1249.68	2286.52
3	410	2.6	4	1175.84	1988.36
4	440	2.6	4	1099.17	2165.54
5	410	1	8	1317.9	1960.32
6	440	1	8	1306.26	2439.85
7	410	2.6	8	1140.51	1922.07
8	440	2.6	8	1107	2421.76
9	400	1.8	6	1287.24	1433.49
10	450	1.8	6	1192.42	2029.32
11	425	0.5	6	1357	2498.88
12	425	3.2	6	1059	2337.67
13	425	1.8	2.6	1141.98	2266.91
14	425	1.8	9.4	1169.32	2389.41
15	425	1.8	6	1205.74	2007.04
16	425	1.8	6	1216.48	1928.78

17	425	1.8	6	1205.2	1997.32
18	425	1.8	6	1196.6	1987.2
19	425	1.8	6	1198.96	1974.32
20	425	1.8	6	1202.9	2029.44

8.3 Second Order Regression Equation of Responses

The model with the best fits has been estimated and the measured output has been analyzed using Design Expert® software. To determine the best fit model, the v17 program has employed the lack-of-fit test, sequential f-test, and ANOVA (analysis of variance) techniques to assess the model's adequacy. Mathematical models are developed to establish a correlation between input and output parameters to understand the behaviour of process parameters on responses. The final regression equation generated for fusion zone (Y_{FZ}) shows the quadratic relation between process variables and responses, which are given as follows:

(a) In terms of coded factors

$$Y_{FZ} = 1206.82 - 23.79\,A - 83.79\,B + 7.3\,C - 6.87\,AB + 9.39\,AC - 13.59\,BC + 14.37\,A^2 - 15.39\,C^2 \quad \text{..... (8.1)}$$

(b) In terms of actual factors

$$Y_{FZ} = 13716.36231 - 56.73270\ A + 189.30536\ B - 67.92292\ C - 0.57229\,AB + 0.31300\,AC - 8.49219\ BC + 0.063881\ A^2 - 3.84722\ C^2 \quad \text{..... (8.2)}$$

The final regression equation generated for heat affected zone (Y_{HAZ}) shows the quadratic relation between process variables and responses, which are given as follows:

(a) In terms of coded factors

$$Y_{HAZ} = 1987.30 + 165.52\ A - 47.20\ B + 23.80\,C + 87.51\,AC + 32.61\,BC - 90.19\,A^2 + 152.65\ B^2 + 120.79\,C^2 \quad \text{..... (8.3)}$$

(b) In terms of actual factors

$$Y_{FZ} = -65553.26102 + 334.25772\ A - 1039.94658\ B - 1626.88364\,C + 2.91700\,AC + 20.37813\,BC - 0.40085\,A^2 + 238.52065\,B^2 + 30.19819\ C^2 \quad \text{(8.4)}$$

8.4. Effect of Heat Input on Weld Surface Appearance

Firstly, trial and error experiments are performed to find the most suitable process variables and shielding gas pressure, so that crack can be avoided. Because of the ductile to brittle transition temperature above 550º C and presence of oxidation, most of the time longitudinal crack happens as shown in Figure 8.3.

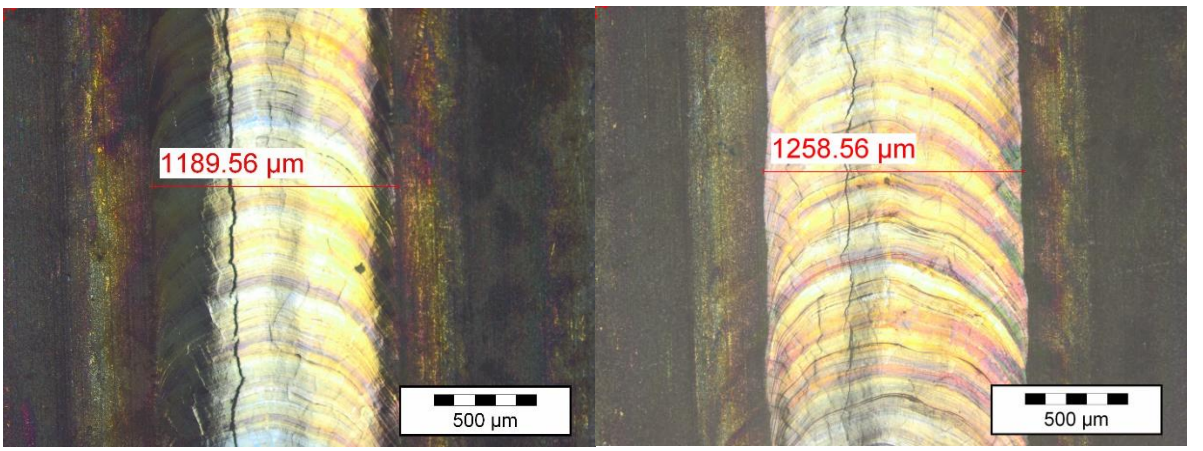

Figure 8.3. Longitudinal crack observed at unfavorable welding parameters

Suitable range of process parameter, defocusing distance and shielding gas pressure are required to be selected to find the range, and experiments are designed. The appearance of the top surface of the welded samples at different welding parameters is shown in Figure 8.4. It has been noted that the weld zone width rises with increasing heat input. Heat input is defined as laser power to scanning speed. Maximum heat input (850 J/mm) increases the fusion zone width as shown in Figure 8.4 (c) and minimum heat input (132.81 J/mm) decreases the fusion zone width as shown in Fig. 8.4 (d). The appearance of burn through weld defect can be clearly seen at high heat input (Exp. No. 11) Medium heat input of 410 J/mm produces uniform weld pool as shown in Fig. 8.4 (a).

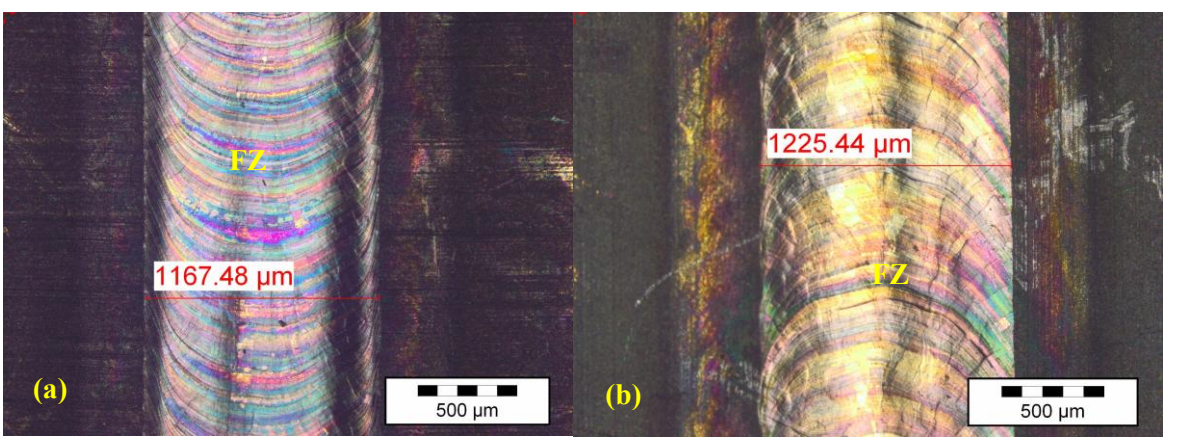

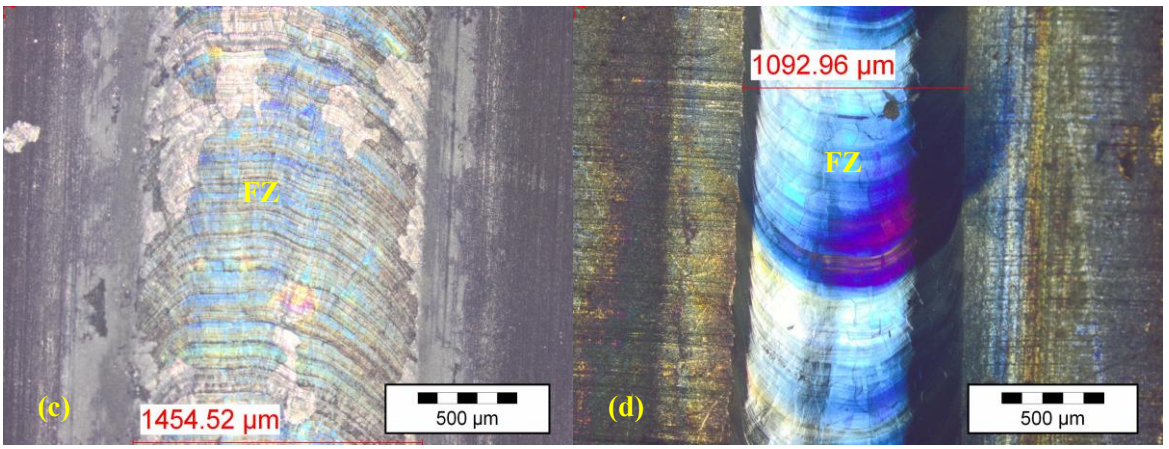

Figure 8.4. Weld bead appearance of the top surface of weld joint by varying heat inputs: (a) 410 J/mm, (b) 236.11 J/mm, (c) 850 J/mm, and (d) 132.81 J/mm

8.5. ANOVA Analysis for Responses

ANOVA technique is used to identify the significant variables and other model adequacy metrics such as R^2, R^2-adjusted and R^2-predicted of developed model. Critical F-ratio is lower than calculated F ratio at 95 % confidence level. P Values should be less than 0.05 for all considered responses. Model terms that have a value of "Prob > F" (less than 0.05) are significant. The remaining terms are non-significant terms which are excluded using a backward elimination approach in order to enhance the model's adequacy. Table 8.3 presents the ANOVA results for response surface model of fusion zone after backward elimination. F ratio and P value satisfies the model. The model F value of 134.13 indicates that the model is significant. The lack of fit has F value of 3.22, which specifies that lack of fit is not significant as comparison to pure error. The "Pred. R-Squared" of 0.9455 is in reasonable agreement with the "Adj. R-Squared" of 0.9825. Adequate Precision measures the signal to noise ratio. A ratio greater than 4 is desirable. Adequate precision ratio of 40.771 indicates an adequate signal of the model which can be used to navigate the design space.

Table 8.3 ANOVA results for fusion zone width (after backward elimination).

Source	FD	Adj. SS	Adj. MS	F-value	P-value
Model	8	114236.67	14279.58	134.131	0.000
LP	1	7728.86	7728.86	72.599	0.000
SS	1	96127.46	96127.46	902.945	0.000
FD	1	727.56	727.56	6.834	0.0241
LP × SS	1	377.3	377.3	3.544	0.0865

Source	FD	Adj. SS	Adj. MS	F-value	P-value
LP × FD	1	705.38	705.38	6.626	0.0259
SS × FD	1	1476.96	1476.96	13.873	0.0034
LP × LP	1	3006.87	3006.87	28.244	0.0002
FD × FD	1	3446.84	3446.84	32.377	0.0001
Residual	11	1171.06	106.46	-	-
Lack-of-fit	6	930.06	155.01	3.216	0.182
Pure error	5	241	48.20	-	-
R-sq. = 99 %, R-sq. (adjusted) = 98 %, R-sq. (predicted) = 94.55 %					

ANOVA technique is used to identify the significant variables and other model adequacy metrics such as R^2, R^2-adjusted and R^2-predicted of developed model. Critical F-ratio is lower than calculated F ratio at 95 % confidence level. P Values should be less than 0.05 for all considered responses. Significant model terms are those with a value of "Prob > F" (less than 0.05). The remaining terms are non-significant terms which are excluded using a backward elimination approach in order to enhance the model's adequacy. Table 8.4 presents the ANOVA results for response surface model of heat affected zone after backward elimination. F ratio and P value satisfies the model. The model F value of 157.81 indicates that the model is significant. The lack of fit has F value of 0.62, which specifies that lack of fit is not significant as comparison to pure error. The "Pred. R-Squared" of 0.9727 is in reasonable agreement with the "Adj. R-Squared" of 0.9851. An appropriate signal from the model that can be utilized to navigate the design space is indicated by an adequate precision ratio of 51.065.

Table 8.4 ANOVA results for heat affected zone width (after backward elimination).

Source	FD	Adj. SS	Adj. MS	F-value	P-value
Model	8	1174012.36	146751.54	157.81	0.000
LP	1	374135.24	374135.24	402.32	0.000
SS	1	30428.9	30428.90	32.72	0.000
FD	1	7736.10	7736.10	8.32	0.0149
LP × FD	1	61264.00	61264.00	65.88	0.000
SS × FD	1	8504.69	8504.69	9.15	0.0116
LP × LP	1	117230.05	117230.05	126.06	0.000

Source	FD	Adj. SS	Adj. MS	F-value	P-value
SS × SS	1	335826.36	335826.36	361.12	0.000
FD × FD	1	210273.53	210273.53	226.11	0.000
Residual	11	10229.43	929.95	-	-
Lack-of-fit	6	4370.51	728.42	0.62	0.712
Pure error	5	5858.91	1171.78	-	-
R-sq. = 99 %, R-sq. (adjusted) = 99 %, R-sq. (predicted) = 97.27 %					

8.6. Validation of the Developed Model

Fig. 8.5 and 8.6 represent the correlation between the measured and predicted values of the width of fusion zone and heat affected zone, respectively. These figure demonstrate that the models developed are satisfactory, as the predicted results closely align with the measured data. The generated models can produce extremely accurate results, as demonstrated by the validation trials, which show a small percentage difference between the estimated and experimental values.

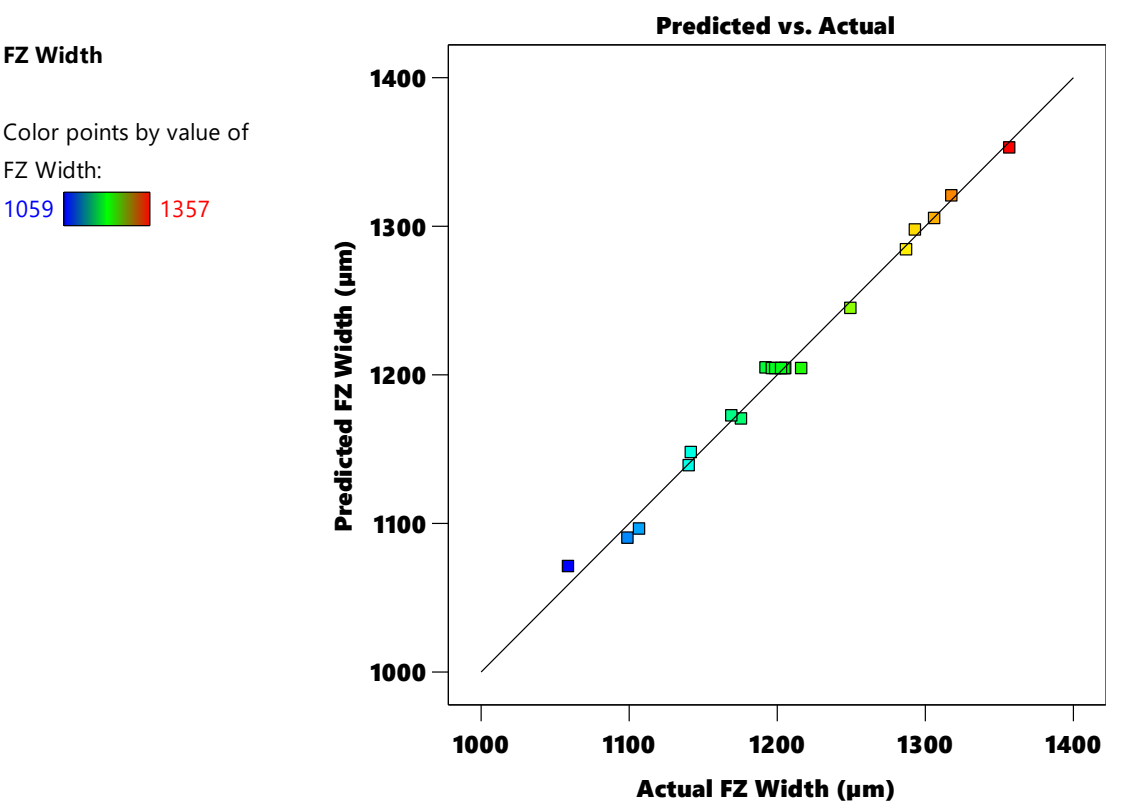

Figure 8.5. Plot of actual vs. predicted Fusion Zone Width

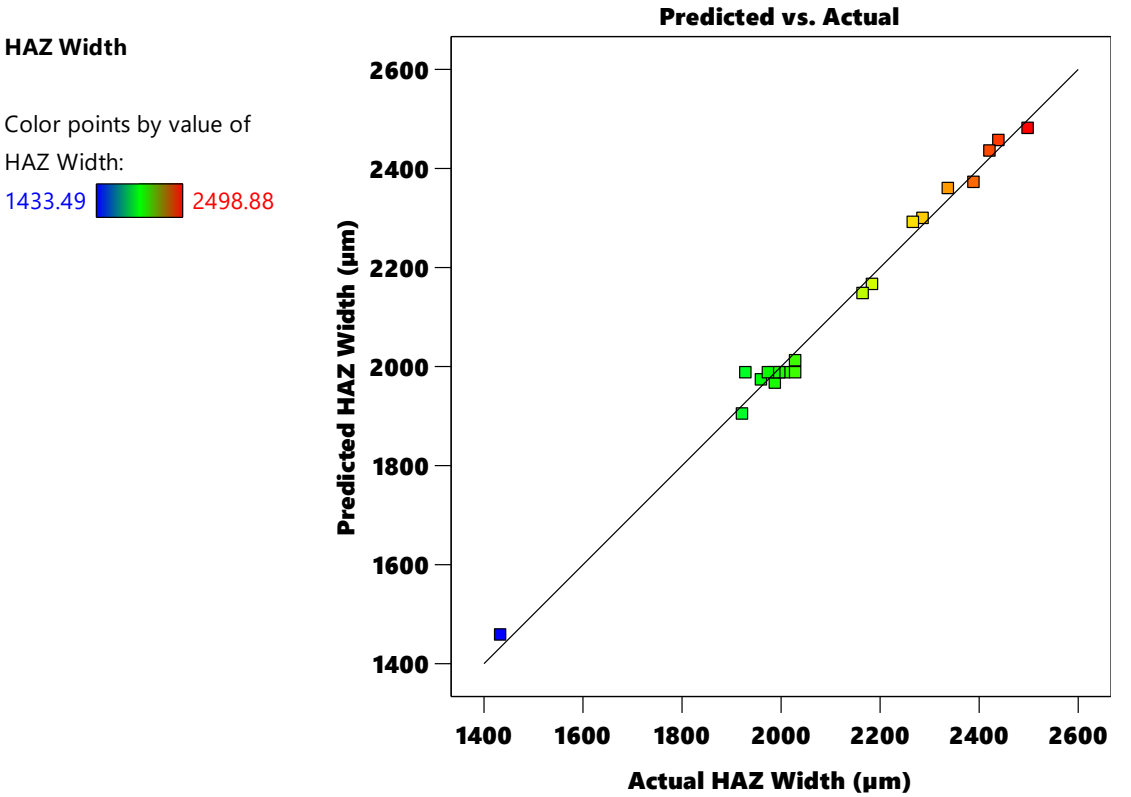

Figure 8.6. Plot of actual vs. predicted HAZ width

8.7. Parametric Analysis

The effects of process variables on weld quality characteristics such as weld shear strength and weld seam width, within the specified range, are thoroughly investigated. The surface interaction plot depicts the behaviour of responses as the value of the process variable changes; the rationale for this is discussed in detail.

8.7.1. Fusion zone width

The perturbation plot, which illustrates the impact of every process variable at the center point in a design space, is displayed in Fig. 8.7. The graph makes it evident that scanning speed reduces the width of the fusion zone. This is because a higher welding speed shortens the irradiation time, which lowers the amount of heat input into the weld zone and the amount of melted base material. The laser power has a direct impact on the heat input given to the base material, while the welding speed has an inverse effect. It is also found out that laser power has little negative effect on fusion zone. This happen because laser power increases the heat input and certain amount of heat input increases the penetration, and minimizes the fusion zone. Results indicate that focal distance or defocusing distance has little effect on fusion

zone width. Fusion zone width increases with an increase of defocusing distance up to center point, and after that it decreases.

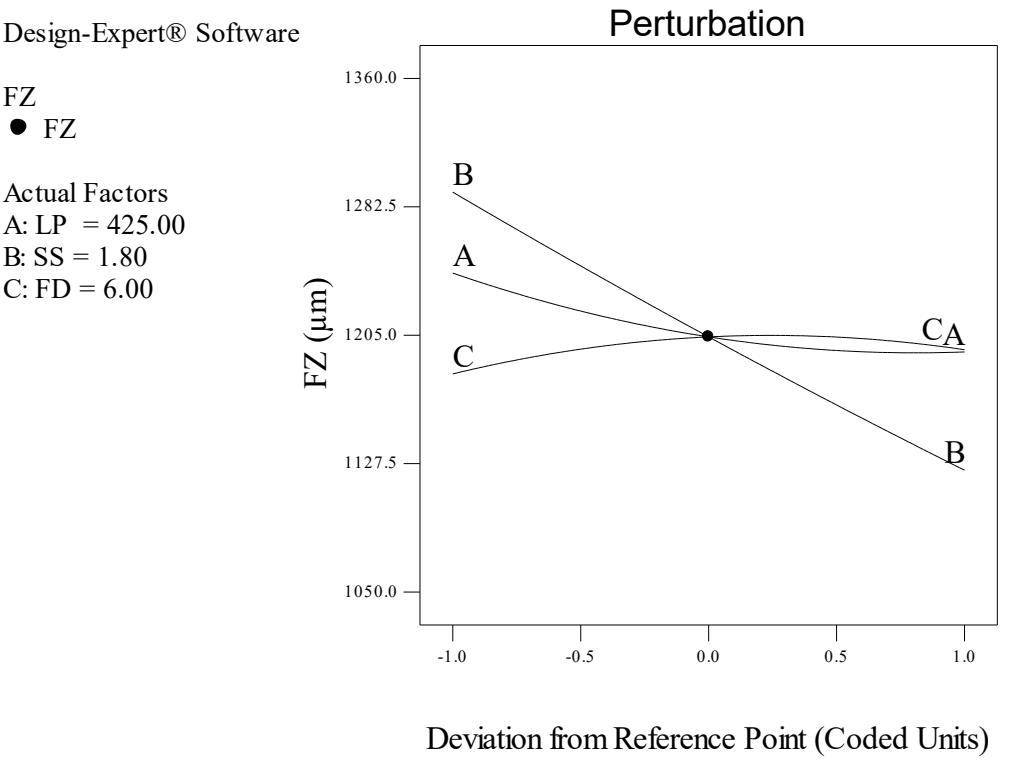

Figure 8.7. Perturbation plot for FZ width

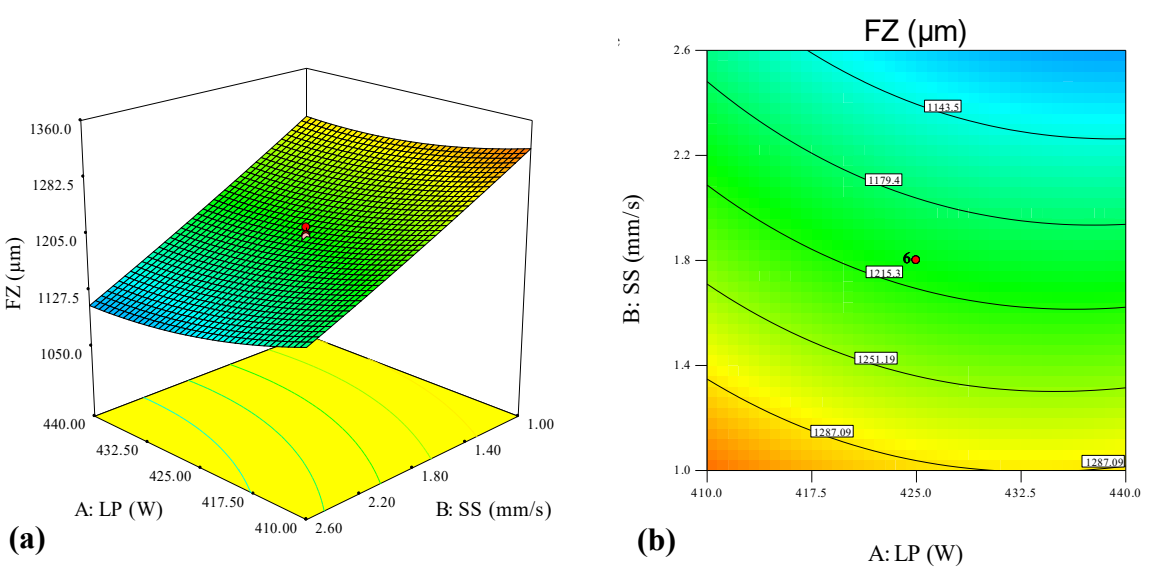

Figure 8.8. Interaction effects of laser power and scanning speed on FZ width (a) surface plot and (b) contour plot, when all other parameters are at their central values

As the defocusing distance increases, the beam spot diameter at the weld interface also increases. This, in turn, leads to a decrease in laser power density since it is inversely proportional to the spot diameter. Increasing the defocusing distance from the centre point generates higher line energy, which leads to overheating and partial decomposition of the material, which reduces the fusion zone width. Fig. 8.8 (a) & (b) shows the surface and contour plot of fusion zone width with respect to laser power and welding speed. The interaction plot represent that fusion zone decreases with an increase of laser power as well as welding speed. Increment of laser power as well as welding speed at the same time, reduces the line energy (laser power to the welding speed) to the material to be welded. Optimum amount of fusion zone width is required to obtain uniform weld strength as more fusion zone width deteriorates the material and less fusion zone width decreases the proper penetration. Insufficient line energy leads to inadequate penetration, inefficient heat transfer, and inadequate mixing of materials, resulting in an unsatisfactory weld. Conversely, excessive line energy can lead to degradation of the base material.

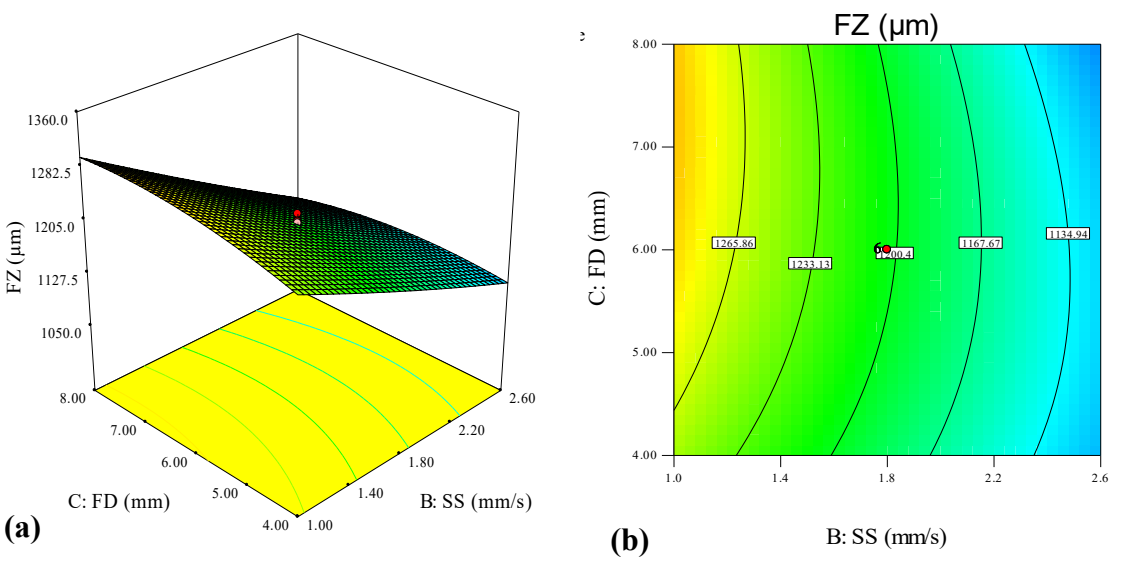

Figure 8.9. Interaction effects of scanning speed and defocussing distance on FZ width (a) surface plot and (b) contour plot, when all other parameters are at their central values

Fig. 8.9 (a) & (b) shows the surface and contour plot of fusion zone width with respect to welding speed and focal distance or defocussing distance. The interaction plot represent that fusion zone width decreases with an increase of welding speed and defocussing distance up to center point. The contour map makes it clear that a larger fusion zone results from both increasing the welding speed and the defocussing distance toward the central limit.

Nevertheless, the fusion zone's width shrinks when the defocussing distance rises over this threshold. At very high power density, the fusion zone becomes restricted due to material decomposition, while insufficient fusion occurs at very low power density.

8.7.2 Heat affected zone width

Fig. 8.10 depicts a perturbation plot that demonstrates the impact of all factors at the center point within the design space. It is evident from the figure that laser power has positive effect on heat affected zone. This is because laser power increases the power density, and high power density generates more heat affected zone. It is also observed from the figure that welding speed and defocussing distance shows similar pattern, i.e. heat affected zone decreases with an increase of welding speed and defocussing distance up to center point, and after that it increases. This could be attributed due to the following reasons. Laser material interaction time or irradiation time reduces with an increase of welding speed, and thus less heat is delivered to the workpiece, which reduces the heat affected zone. At high welding speed, irradiation time reduces, but heat input to the material dissipates rather than penetrate and melt the workpiece. Although, increment of defocussing distance increases the beam spot diameter, at the same time focussing is shifted towards the inside of the workpiece. At high defocussing distance, large spot beam size spreads the heat input into a wider area, which increases the heat affected zone.

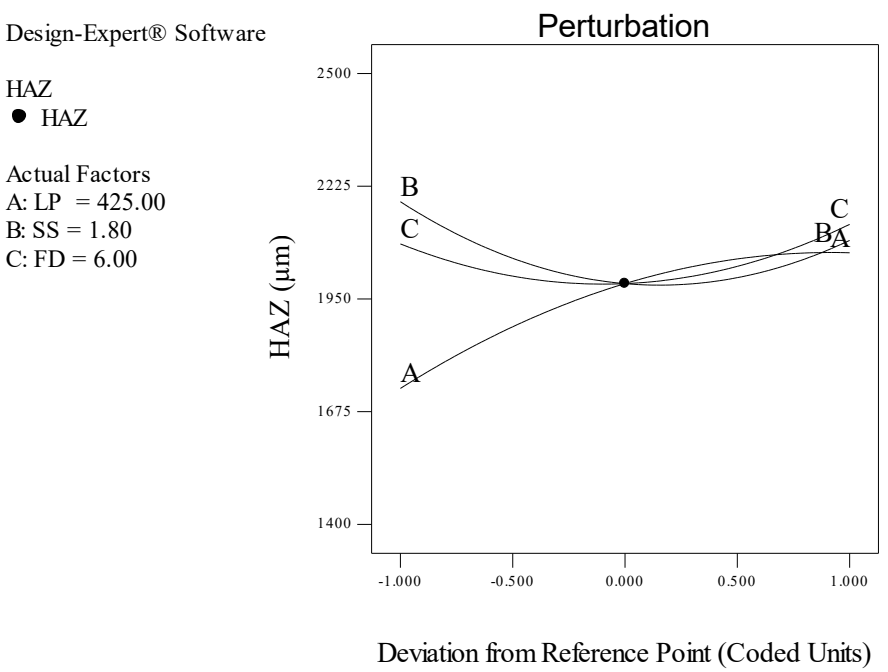

Figure 8.10. Perturbation plot for HAZ width

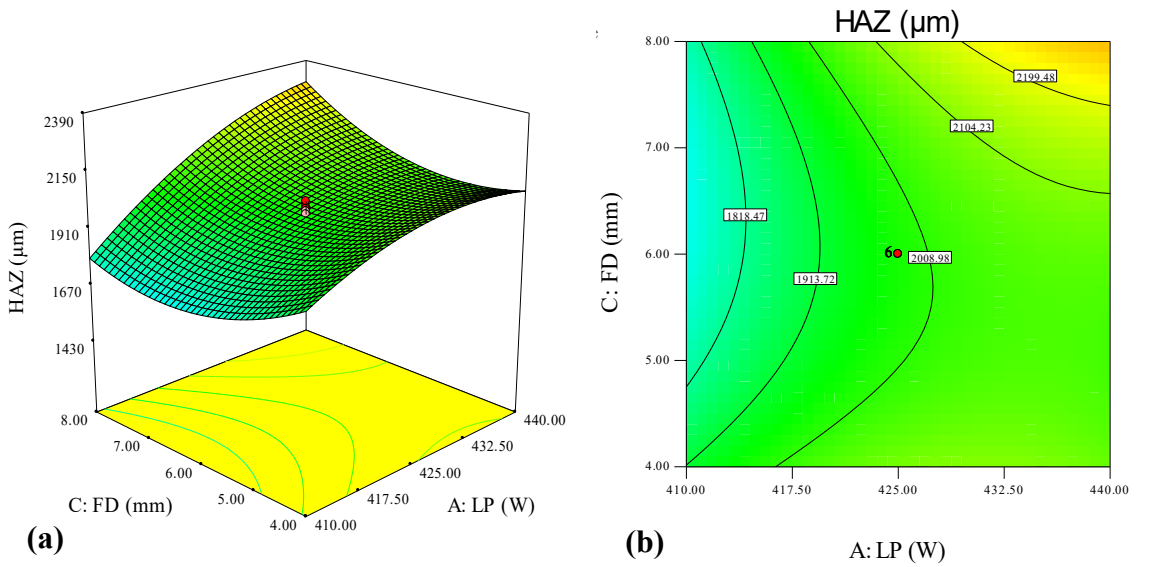

Figure 8.11. Interaction effects of laser power and defocussing distance on HAZ width (a) surface plot and (b) contour plot, when all other parameters are at their central values

Fig. 8.11 (a) & (b) shows the interaction effect of laser power and focal distance on heat affected zone. It is evident from the figure that laser power has positive effect on heat affected zone, because laser power increases the power density or overall heat input, and thus heat conduction takes place from fusion to the adjacent material. This leads to expansion of the HAZ. Based on contour plot, heat affected zone is minimum at Centre point of defocusing distance. As defocusing distance directly relates to the spot beam size, which spreads the heat to the material.

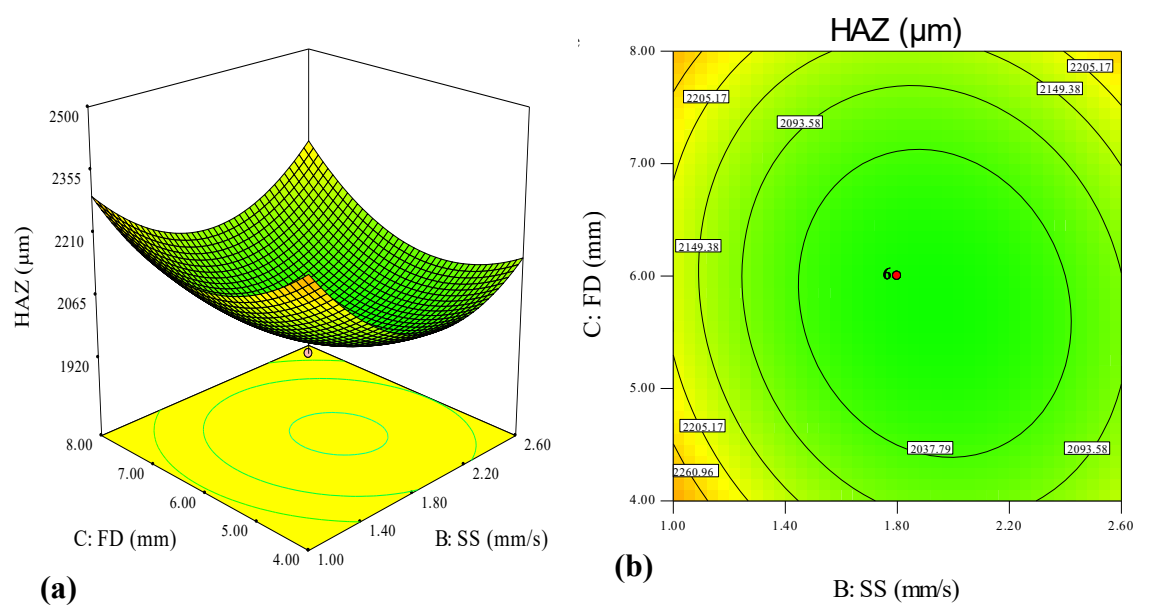

Figure 8.12. Interaction effects of scanning speed and defocussing distance on HAZ width (a) surface plot and (b) contour plot, when all other parameters are at their central values

Fig. 8.12 (a) & (b) illustrate the interaction plot of scanning speed and focal distance on heat affected zone. Both welding speed and defocusing distance exhibit a similar impact on the heat affected zone. Specifically, the minimum heat affected zone is observed at the mid values of welding speed and defocusing distance. This phenomenon occurs because as welding speed increases, the power density decreases, leading to a narrower heat affected zone. Conversely, increasing the defocusing distance at a constant laser power reduces the power density, resulting in a narrower heat affected zone. However, at high defocusing distances, the wider area of interaction caused by the defocused beam leads to a broader heat affected zone.

8.8. SEM Microstructure and EDX Analysis

The SEM (Scanning Electron Microscopy) and EDX (Energy Dispersive X-ray) analysis of the welded specimens, depicted in figure 8.13 and 8.14, reveal significant insights into the microstructural characteristics influenced by heat input during the of laser welding of titanium alloy. The microstructure of the weld zone at 170 N/mm of heat input is depicted in Figure 8.13 (a), and formation of acicular martensite α′ in the FZ is observed. Fig. 8.14 (a) shows the microstructure when heat input is 240 N/mm. Additionally, the acicular α′ and preceding β grains in the fusion zone get coarser as the heat input increases. Based on EDX analysis, it is observed that as heat input increases, i.e. higher laser power and lower scanning speed, oxidation can be reduced.

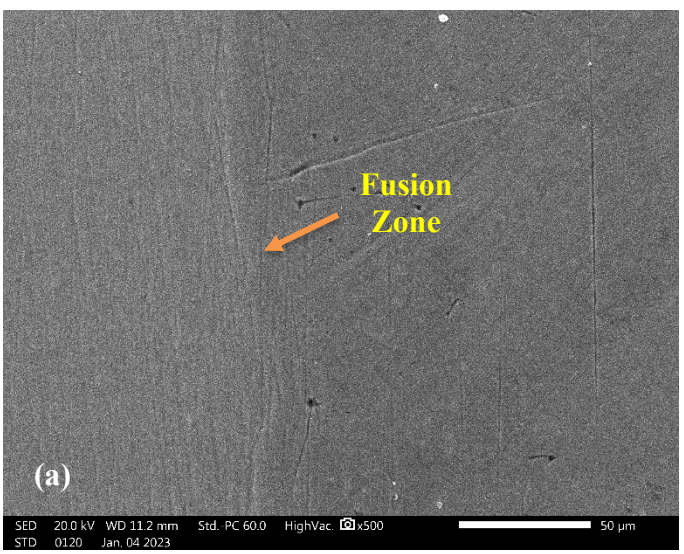

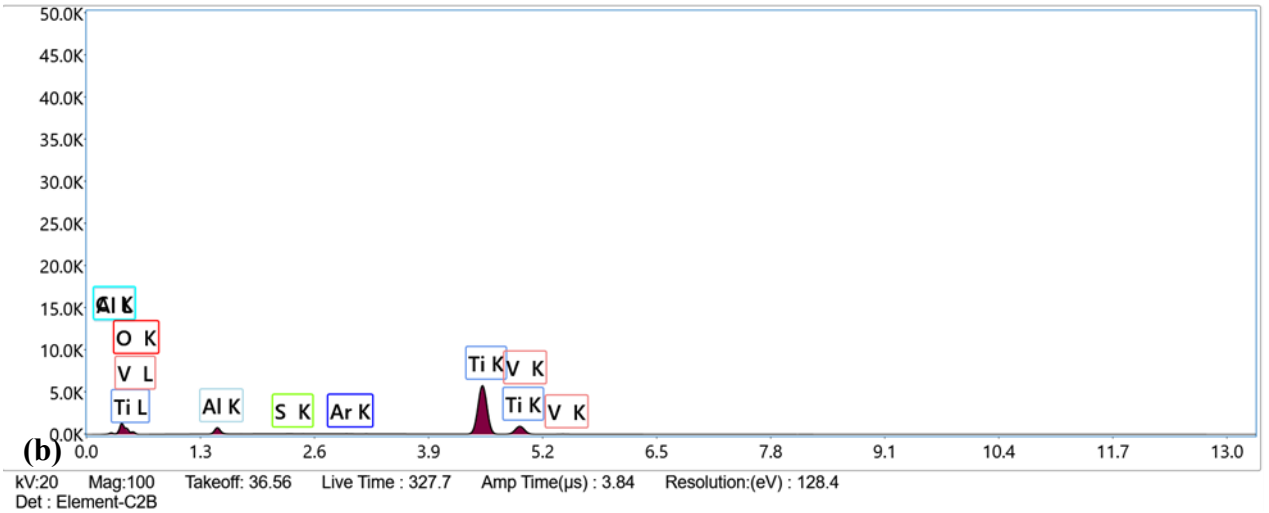

Figure 8.13. (a) SEM micrograph of weld zone and (b) EDX analysis of weld zone for Exp. No. 4

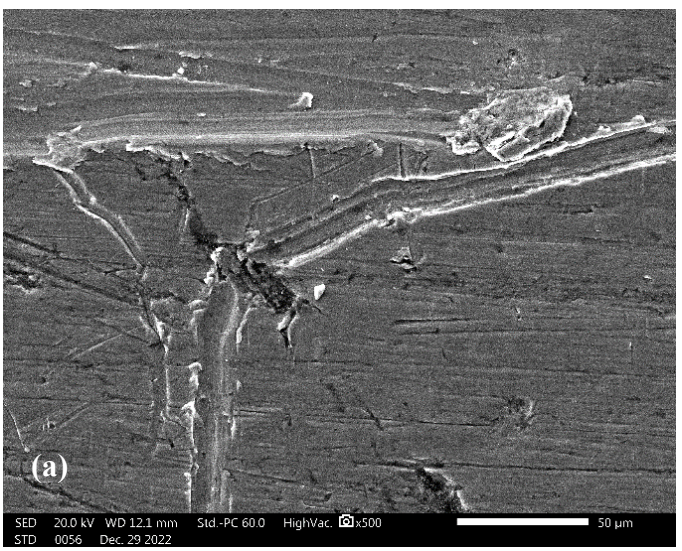

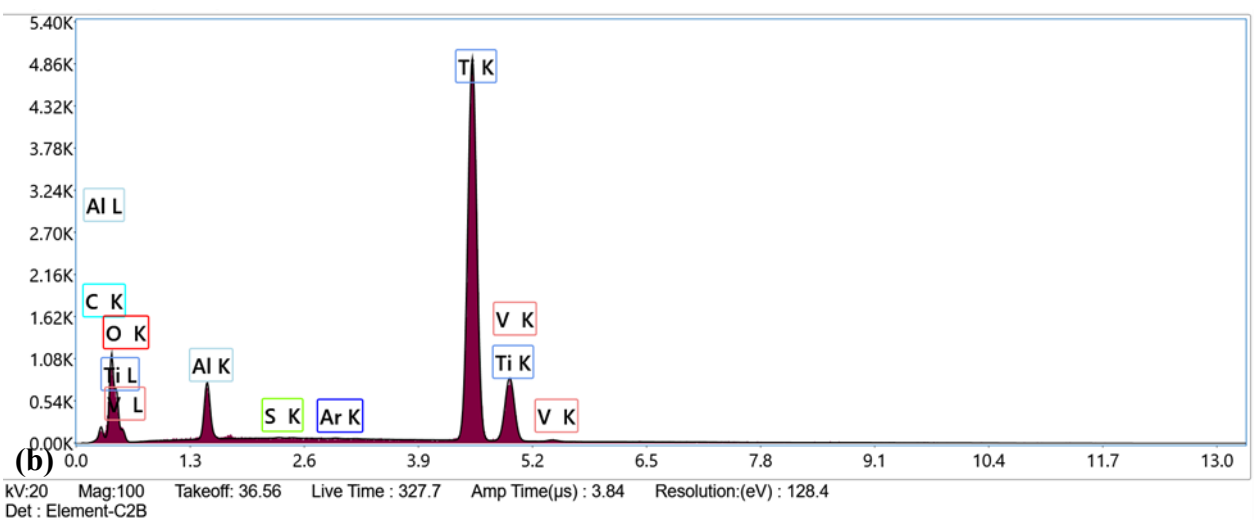

Figure 8.14. (a) SEM micrograph of weld zone at 1000x magnification, and (b) EDX analysis of weld zone for Exp. No. 10

8.9. Micro-Hardness Variation

The variations in microhardness across the weld bead, illustrated in Figure 8.15, reveal critical insights into the mechanical properties of the laser-welded titanium alloy. The plot distinctly outlines three hardness zones: the base material, FZ and HAZ. The results show that the micro-hardness of the fusion zone (FZ) is higher compared to the heat-affected zone (HAZ) and the base metal. This is attributed to the formation of acicular martensite α′ in the FZ. The parent metal has a micro-hardness value of approximately 357 HV, while the FZ exhibits a range of 475-498 HV. As the heat input increases, the average micro-hardness of the fusion zone decreases. This is because the acicular α′ and prior β grains in the fusion zone become coarser with higher heat input. At low heat input, the micro-hardness distribution across the HAZ decreases sharply from the fusion zone and HAZ interface to the base metal zone and HAZ interface. In contrast, at high heat input, the micro-hardness does not decrease sharply. This is because the original α- and β-phases of the base metal transform into the acicular α′ phase, which increases the micro-hardness of the HAZ to a level equivalent to the fusion zone.

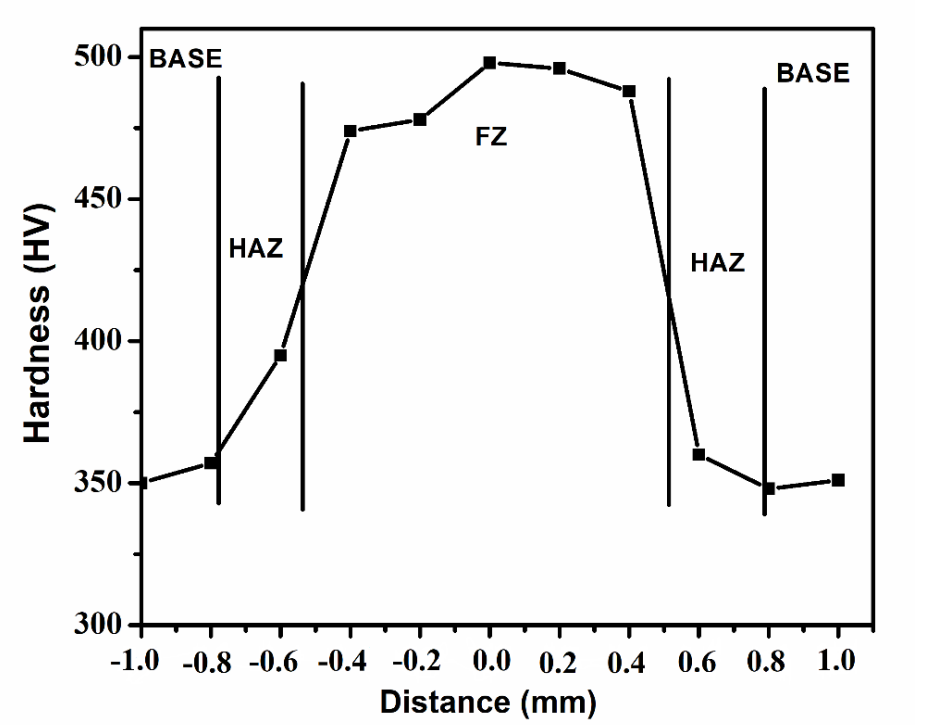

Figure 8.15. Variation of micro-hardness across the weld bead

8.10. Multi-Objective Optimization using Desirability Function Based Technique

The desirability function-based optimization method is employed to find the optimal process parameters that minimize both the fusion zone width and the heat-affected zone width simultaneously. It works by translating the responses in to corresponding value of desirability. Desirability value depends upon range and target response. When response reach its goal, then desired unity value is assigned. Desirability value is considered zero outside certain limit. Minimum fusion zone width of 1143.05 µm and minimum heat affected zone width of 1689.13 µm has been achieved at 400 watt laser power, 2.7 mm/s scanning speed and 8.85 mm defocussing distance as shown in Fig. 8.16. Fig. 8.17 shows the overlaid contour plot fusion zone width and heat affected zone width. Minimum seam width or fusion zone is achieved at higher scanning speed and minimum HAZ is achieved at lower laser power.

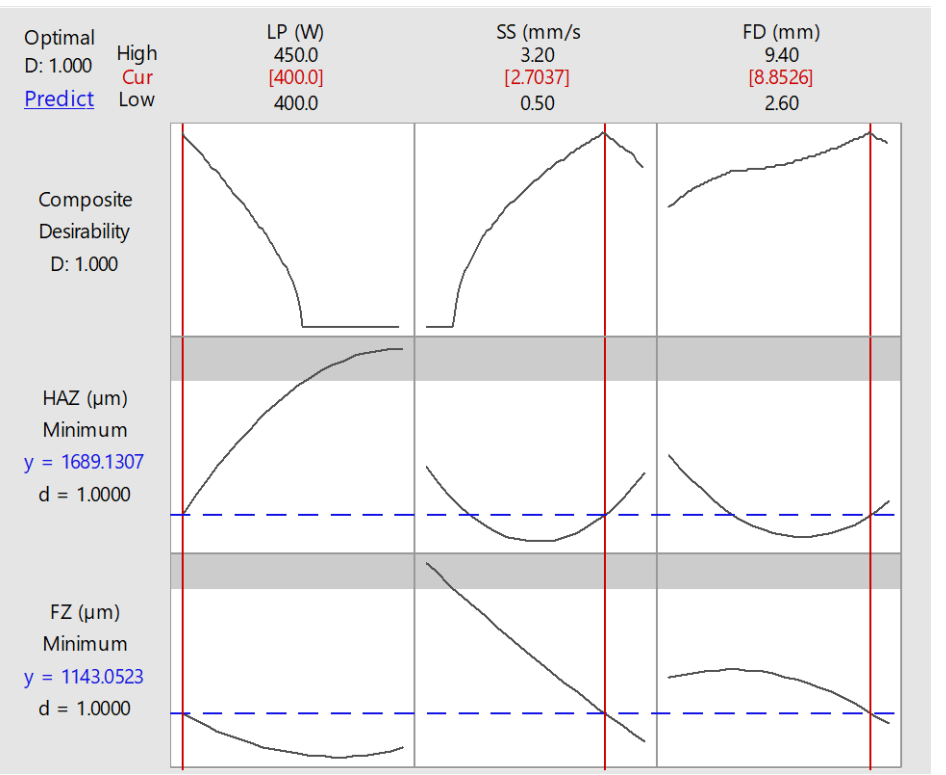

Figure 8.16. Optimization results for minimum FZ and minimum HAZ

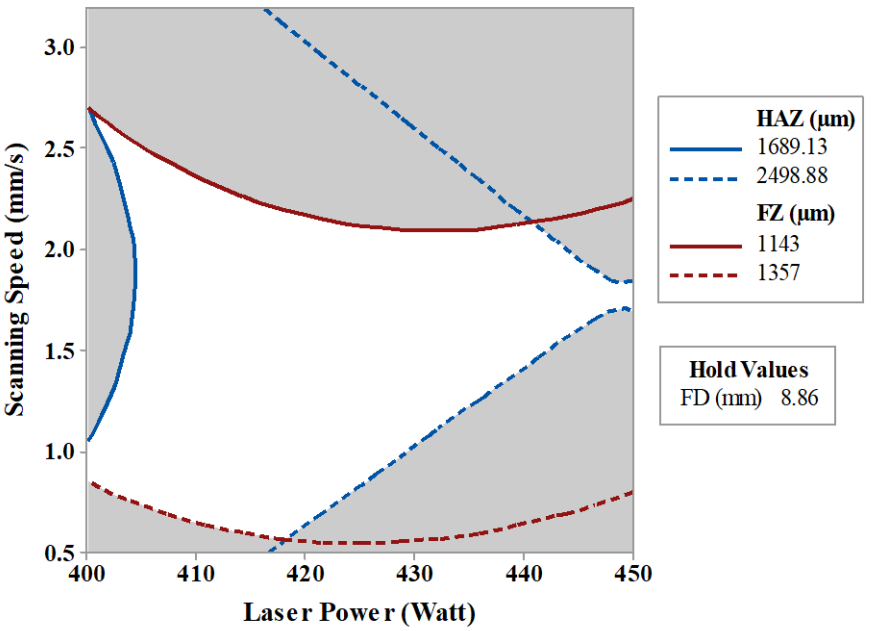

Figure 8.17. Overlaid contour plot of FZ and HAZ

8.11. Tensile Test

Tensile test is performed at optimal process parameter settings obtained by RSM based DFA technique to assess the weld strength. The welded samples undergo tensile testing to examine the relation between applied stress and strain, as seen in Fig. 8.18.

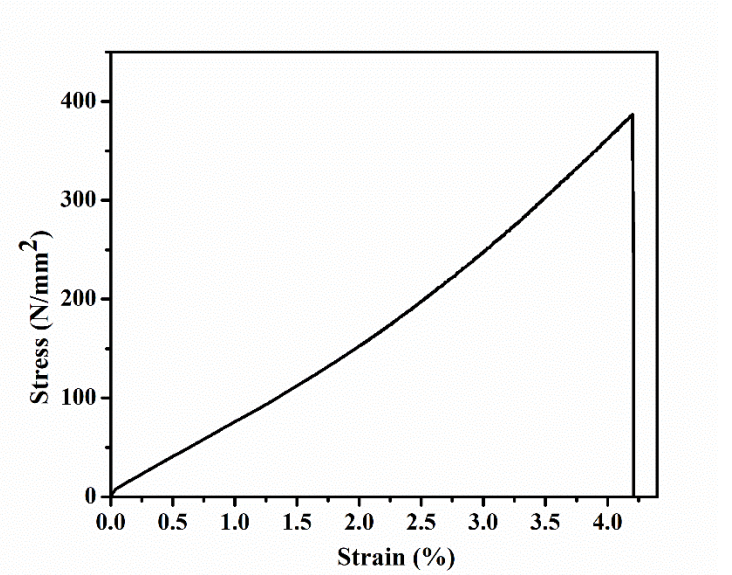

Figure 8.18. Graphs showing the tensile test results of welded samples

The welded specimens had an elongation to fracture of roughly 4.27% and ultimate tensile values of 386 MPa. Additionally, the welded sample exhibits a yield stress of 386 MPa. It is

observed that for the welded samples, the fracture occurred in the welding zone. It can be said that the welded sample's tensile strength is significantly lower than that of the base material. The decrease in tensile strength suggested that welding causes the material to become more brittle. The ductility of the welded samples began to decline because of the growth of fine dendritic structures in the weld pool.

8.12. Validation Experiment

A confirmation experiment has been performed at the optimal welding process parameter setting to find the error, and it is estimated that fusion zone width has an error of 4.51 % and heat affected zone width has an error of 3.17 % (Table 8.5), which is very minimum and less than 5%; thus it is acceptable.

Table 8.5 Confirmation test at optimal process parameter

Optimum value from Desirability function technique			Confirmation test	% Error
Process Parameters	LP (Watt)	400	400	
	SS (mm/s)	2.7	2.7	
	DF (mm)	8.85	8.85	
Response Parameters	FZ (µm)	1143	1197	4.51
	HAZ (µm)	1689	1637	3.17

8.13 Outcomes of the Present Research Work

The following conclusions can be drawn from the present research:

1. Laser butt welding of 2 mm thick titanium superalloy using a 500-watt continuous-wave fiber laser successfully produced smooth, uniform weld beads with shiny surfaces and no defects.

2. The weld defect has been reduced extensively under appropriate shielding gas environment with optimum selection of process parameters.

3. ANOVA results shows that welding speed has highest impact on fusion zone width, followed by laser power and defocusing distance of the laser beam, as welding speed directly governs the heat input to the weld region.

4. Laser power and welding speed both have negative impact on fusion zone width, while laser power shows the positive impact on HAZ width. The HAZ becomes minimum

at mid value of welding speed because it influences the thermal cycle and provides sufficient melting without excessive heat accumulation.

5. The fusion zone exhibits the highest micro-hardness value of 498 $HV_{0.1}$, followed by the heat-affected zone at 400 $HV_{0.1}$, and the parent material at 357 $HV_{0.1}$. This increase in micro-hardness is attributed to formation of acicular martensite α′ in the fusion zone.

6. Ultimate tensile strength of 386 MPa and yield stress of 386 MPa is achieved at optimal parameter settings.

7. Minimum fusion zone width of 1143 μm and minimum heat affected zone of 1689 μm has been achieved at optimal process parameter setting of laser power 400 watt, welding speed of 2.68 mm/sec. and defocusing distance of 8.92 mm using multi objective DFA based optimization method.

CHAPTER: 9

CONCLUSIONS

9.1. Conclusions

Within the limitation of the available resources, various experimental planning, mathematical modelling and extensive experimental observation based parametric analysis on laser beam welding system has been carried out. Based on the present set of research investigations, the following general conclusions have been drawn:

1. The laser weldability of acrylic and polypropylene copolymer is successfully assessed using a low power laser. Despite their inherent incompatibility and differing optical and thermal properties, the application of white ink as compatibilizer at the weld interface enabled acceptable joint formation. Additionally, the laser welding of clear transparent polymers is demonstrated to be feasible by employing black ink line as laser absorber at the weld interface. Morphological analysis confirmed consistent weld seam formation, and optimized process settings significantly improved joint strength, validating the approach for additive free laser welding of transparent polymers.
2. Laser transmission welding of acrylic and polypropylene copolymer has been performed using a low power diode laser. Based on ANOVA results, scanning speed is found to most dominant parameter, followed by pulse frequency and laser power on both weld strength and weld seam width. For a lap-shear joint, the maximum welding strength of 15.949 N/mm and minimum weld seam width of 222.225 μm have been achieved at optimal parameter setting by using multi-objective optimization technique. Morphological analysis shows that white ink absorbent seems to be effective for inducing fibrillation in to amorphous and thereby mechanical interlocking. It is observed that intermixing of these two polymer happens through white ink and molecular chain interfuse in molten state.

3. Laser transmission welding of polycarbonate and carbon black filled acrylic has been performed using a low power diode laser. It is observed that increasing the laser power increases the weld strength and weld seam width, however, welding speed has a negative impact on both responses. It is revealed that weld strength is limited by very high laser heat input, which causes material to overheat and degrade, while low laser heat input results in a lack of fusion or penetration. The maximum welding strength of 34.28 N/mm and minimum weld seam width of 2.6 mm have been achieved at optimal parameter setting by using multi-objective optimization technique.
4. Laser transmission welding of polycarbonate and carbon black filled acrylic has been performed with beam wobbling technique using a low power diode laser. Wobble width is found to be most dominant parameter affecting the weld seam width and an increase in wobble width leads to increase in weld seam width. It is observed that laser power, welding frequency, scanning speed, wobble width and wobble frequency have a strong interaction effect on both weld strength and weld seam width. These parameters control the laser heat input to the weld area. The maximum welding strength of 27.73 N/mm and minimum weld seam width of 1.37 mm have been achieved at optimal parameter setting by using multi-objective optimization technique.
5. Laser transmission welding of similar clear transparent acrylic materials has been performed with a black ink line serving as a laser absorber applied at the weld interface, using a low power laser. The maximum welding strength of 37 N/mm and minimum weld seam width of 180 µm have been achieved at optimal parameter setting by using multi-objective optimization technique. Morphological analysis indicates a number of small bubbles and some larger bubbles at weld zone, which can activate the micro-anchor mechanism and enhance the joining strength.
6. Laser transmission welding of clear transparent dissimilar thermoplastic polymers such as acrylic and polycarbonate can be conveniently and efficiently welded together utilizing beam wobbling technique with a black ink line serving as a laser absorber applied at the interface. According to the ANOVA, the wobble width has the greatest influence on weld shear strength, followed by scanning speed, wobble frequency, laser power, and pulse frequency. Beam wobbling is found to have a substantial effect on weld shear strength when beam wobbling parameters such as wobble width and wobble frequency are used. A circular beam oscillation with a wobble diameter of 0.6 mm and a frequency of 3 kHz is shown to have a substantial beneficial influence on

weld strength. Graphical representation of actual vs. predicted weld shear strength and weld-seam width results shows good agreement between actual and predicted weld quality. Morphological analysis indicates formation of bubbles near the fusion zone as well as small bits of polymer debris on the bubble's edges. The small bubble creates crack and pit on the contracting surfaces, pushing the molten polymer into cavity and activating the micro-anchoring process.

7. During the tensile tests, two types of breaking failure are observed: (a) shear failure from weld interface, and (b) fracture of base material starting from fusion zone.
8. The developed response surface models estimate the responses effectively within the ranges of welding process parameters. It is found that laser power, pulse frequency, scanning speed, defocussing distance, wobble width and wobble frequency have better interaction effect on weld strength and weld seam width, the parameters mentioned control the heat input of the laser to the weld area.
9. It is observed that beam wobbling has strong influence on seam width and provide high speed laser welding. Based on microstructure, a number of voids, spherulites and bubbles can be seen at the weld or fusion zone in conventional LTW. In the case of wobble LTW, beam wobbling can minimize the voids and porosity at weld zone by controlling the fusion and solidification process. The beneficial effect of beam wobbling on weld shear strength are attributed to homogenized heat input, melt pool turbulence and improved polymer intermixing in the weld pool.
10. Laser beam welding of NiTinol alloy has been performed using a high power fiber laser. Based on ANOVA results, scanning speed is found to be the most dominant parameter on fusion zone width and heat affected zone width. Weld-bead consisted of the columnar dendritic structure. Columnar dendritic grains are observed to orient almost perpendicular to the weld centerline, indicating uniform heat flow and solidification throughout the weld thickness. Micro-hardness value was gradually increased from the base material to weld center. This increase in micro-hardness is attributed to grain refinement within the fusion zone. The fusion zone exhibits the highest micro-hardness value of 420 $HV_{0.1}$, followed by the heat-affected zone at 346 $HV_{0.1}$, and the parent material at 310 $HV_{0.1}$. Minimum fusion zone width of 926.32 µm and minimum heat affected zone width of 190.92 µm has been achieved at optimal parameter settings by multi-objective optimization technique. Ultimate tensile strength of 169.1 MPa is achieved at optimal parameter settings.

11. Laser beam welding of Titanium super-alloy has been performed using a high power fiber laser. The weld defect have been reduced extensively under appropriate shielding gas environment with optimum selection of process parameters. It has been observed that as the heat input increases, the weld zone width increases. Laser power and welding speed both have negative impact on fusion zone width, while laser power shows the positive impact on HAZ width whereas HAZ is minimum at mid value of welding speed. The fusion zone exhibits the highest micro-hardness value of 498 $HV_{0.1}$, followed by the heat-affected zone at 400 $HV_{0.1}$, and the parent material at 357 $HV_{0.1}$. This increase in micro-hardness is attributed to formation of acicular martensite α' in the fusion zone. Minimum fusion zone width of 1143 μm and minimum heat affected zone width of 1689 μm has been achieved at optimal parameter settings by multi-objective optimization technique. Ultimate tensile strength of 386 MPa is achieved at optimal parameter settings.

9.2. Scope of Future Work

The present set of research findings will not only be opening up new insights to the fundamental and applied researchers in the area for better understanding of the laser beam welding of polymers and titanium alloys but also be quite useful to the manufacturing industries for taking a quantum jump to the arena of present day needs of utilization of varieties of newly developed biocompatible polymers, shape memory alloy, HSTR alloy irrespective of their solubility, melting point, optical properties, thermal and electrical properties. However, a number of recommendations for further research have arisen from the work in this thesis, these are:

1. To carry out further study of the laser beam welding of broader range of material combinations including dissimilar polymers, metals, ceramics, and composites – for better understanding of the physics of the welding with high speed video camera.
2. To develop the sensor based monitoring using predictive modelling and artificial intelligence, which can help in early detection and correction of defects, leading to improved weld reliability and automation.
3. The current study has focused primarily on tensile strength and weld morphology. Future work could include the assessment of impact strength, fatigue behaviour, and fracture mechanics of laser-welded joints under cyclic and high-stress loading conditions, particularly for critical applications.

4. To apply the two step model such as ANN-NSGA-II and ANN-NSTLBO for fine tuning the outcomes
5. To investigate laser beam welding of dissimilar material systems, especially polymer-to-metal or metal-to-ceramic interfaces, which can unlock potential for hybrid structures in lightweight and functional devices.
6. To utilize ultrafast lasers, hybrid welding processes (laser-MIG, laser-TIG), and spatial beam modulation techniques, which may enhance the weldability and quality of difficult-to-join materials.

BIBLIOGRAPHY

1. Pervaiz, M., Panthapulakkal, S., Sain, M., & Tjong, J. (2016). Emerging trends in automotive lightweighting through novel composite materials. *Materials sciences and Applications*, *7*(01), 26.
2. Cole, G. S., & Sherman, A. M. (1995). Light weight materials for automotive applications. *Materials characterization*, *35*(1), 3-9.
3. Acherjee, B. (2020). Laser transmission welding of polymers–A review on process fundamentals, material attributes, weldability, and welding techniques. *Journal of Manufacturing Processes*, *60*, 227-246.
4. Mistry, K. (1997). Tutorial plastics welding technology for industry. *Assembly Automation*, *17*(3), 196-200.
5. Jones, I. (2002). Laser welding for plastic components. *Assembly automation*, *22*(2), 129-135.
6. Hopmann, C., & Weber, M. (2012). New concepts for laser transmission welding of dissimilar thermoplastics. *Progress in Rubber Plastics and Recycling Technology*, *28*(4), 157-172.
7. Yang, Y. S., & Lee, S. H. (1999). A study on the joining strength of laser spot welding for automotive applications. *Journal of Materials Processing Technology*, *94*(2-3), 151-156.
8. Quintino, L., Costa, A., Miranda, R., Yapp, D., Kumar, V., & Kong, C. J. (2007). Welding with high power fiber lasers–A preliminary study. *Materials & Design*, *28*(4), 1231-1237.
9. Einstein, A. (1917). On the quantum theory of radiation. *Physikalische Zeitschrift*, *18*(121), 167-83.
10. Kopfermamm H, Ladenburg R 1928 Phys. Chem. Abt. A139: 375
11. Maiman, T. H. (1960). Stimulated optical radiation in ruby. *nature*, *187*(4736), 493-494.

12. Bachmann, F. G., & Russek, U. A. (2002, June). Laser welding of polymers using high-power diode lasers. In *Photon processing in Microelectronics and Photonics* (Vol. 4637, pp. 505-518). SPIE.
13. Van de Ven, J. D., & Erdman, A. G. (2006). Simultaneous measurement of laser reflection and transmission of poly (vinyl chloride). *Optical Engineering*, *45*(9), 094301-094301.
14. Bonten, C., & Tüchert, C. (2002). Welding of Plastics—Introduction into Heating by Radiation. *Journal of reinforced plastics and composites*, *21*(8), 699-709.
15. Katayama, S. (2020). *Fundamentals and details of laser welding*. Singapore: Springer Singapore.
16. Dutta Majumdar, J., & Manna, I. (2003). Laser processing of materials. *Sadhana*, *28*, 495-562.
17. Laser Welding Modes: Conduction, Transition, & Keyhole Welding https://amadaweldtech.com/blog/laser-welding-modes-conduction-transition-keyhole-welding/ (accessed on 15-01-2025)
18. In, J. B., Kwon, H. J., Yoo, J. H., Allen, F. I., Minor, A. M., & Grigoropoulos, C. P. (2017). Laser welding of vertically aligned carbon nanotube arrays on polymer workpieces. *Carbon*, *115*, 688-693.
19. Silvus Jr, H. J., & Wachtell, S. (1970). Perforating, welding, and cutting plastic films with a continuous CO_2 laser. *PA State University, Engineering Proceedings*, 88-97.
20. Duley, W. W., & Mueller, R. E. (1992). CO_2 laser welding of polymers. *Polymer Engineering & Science*, *32*(9), 582-585.
21. Grimm, R. A. (1995). Welding processes for plastics. *Advanced materials & processes*, *147*(3), 27-31.
22. Mingareev, I., Weirauch, F., Olowinsky, A., Shah, L., Kadwani, P., & Richardson, M. (2012). Welding of polymers using a 2 μm thulium fiber laser. *Optics & Laser Technology*, *44*(7), 2095-2099.
23. Genna, S., Leone, C., & Tagliaferri, V. (2017). Characterization of laser beam transmission through a High Density Polyethylene (HDPE) plate. *Optics & Laser Technology*, *88*, 61-67.
24. Borge, M. (2016). Transmission laser welding of large plastic components: lightweight automotive constructions require quantum jumps in technology. *Laser Tech J*, *13*(5), 34-37.

25. Laser transmission welding becomes the technology of choice. Medical Plastics News Magazine,https://www.medicalplasticsnews.com/news/technology/lasertransmission-welding-becomes-the-technology-of-choice/ (accessed on: 10 January 2025).
26. R. Ramachandramoorthy, Laser transmission welding of thermoplastic tubes and plates using laser refraction, Thesis (Masters in Engineering, Mechanical Engineering), McGill University, Canada, 2011
27. Kagan, V. A. (2002). Innovations in laser welding of thermoplastics: This advanced technology is ready to be commercialized. *SAE Transactions*, 845-864.
28. Kagan, V. A., & Woosman, N. M. (2004). Efficiency of clearwelding technology for polyamides. *Journal of reinforced plastics and composites*, *23*(4), 351-359.
29. Michaeli, W., Hoffmann, W. M., & Haberstroh, E. (2008). Laser welding of transparent plastics by means of the intermediate film method. In *66th Annual Technical Conference of the Society of Plastics Engineers (ANTEC 2008), Society of Plastics Engineers* (Vol. 14, pp. 06804-0403).
30. Acherjee, B., Misra, D., Bose, D., & Acharyya, S. (2011). Optimal process design for laser transmission welding of acrylics using desirability function analysis and overlay contour plots. *International Journal of Manufacturing Research*, *6*(1), 49-61.
31. Olowinsky, A., & Rösner, A. (2012). Laser welding of polymers: established process but still not at its best. *Laser Technik Journal*, *9*(2), 52-56.
32. Laserweldable materials. Leister Technologies AG; https://www.leister.com/en/laser-plastic-welding/know-how/principle/ materials. (Accessed on 15th January 2025)
33. Kagan, V. A., Bray, R. G., & Kuhn, W. P. (2002). Laser transmission welding of semi-crystalline thermoplastics—Part I: Optical characterization of nylon based plastics. *Journal of reinforced plastics and composites*, *21*(12), 1101-1122.
34. Kagan, V., Bray, R., & Chambers, A. (2003). Forward to better understanding of optical characterization and development of colored polyamides for the infra-red/laser welding: part I-efficiency of polyamides for infra-red welding. *Journal of reinforced plastics and composites*, *22*(6), 533-547.
35. Chen, Z., Huang, Y., Han, F., & Tang, D. (2018). Numerical and experimental investigation on laser transmission welding of fiberglass-doped PP and ABS. *Journal of Manufacturing Processes*, *31*, 1-8.

36. KIRKLAND, T. R. (2004). Practical joint designs for laser welding of thermoplastics. In *ANTEC... conference proceedings* (Vol. 1, pp. 1236-1240). Society of Plastics Engineers.
37. Ghasemi, H., Zhang, Y., Bates, P. J., Zak, G., & DuQuesnay, D. L. (2018). Effect of processing parameters on meltdown in quasi-simultaneous laser transmission welding. *Optics & Laser Technology*, *107*, 244-252.
38. Jansson, A., Kouvo, S., Salminen, A., & Kujanpää, V. (2003, October). The effect of parameters on laser transmission welding of polymers. In *ICALEO 2003: 22nd International Congress on Laser Materials Processing and Laser Microfabrication*. AIP Publishing.
39. Rodríguez-Vidal, E., Quintana, I., & Gadea, C. (2014). Laser transmission welding of ABS: Effect of CNTs concentration and process parameters on material integrity and weld formation. *Optics & Laser Technology*, *57*, 194-201.
40. Juhl, T. B., Bach, D., Larson, R. G., Christiansen, J. D., & Jensen, E. A. (2013). Predicting the laser weldability of dissimilar polymers. *Polymer*, *54*(15), 3891-3897.
41. Baylis, B. K., Prabhakaran, R., Bates, P. J., Huang, Y. P., Xu, X., & Watt, D. (2003). Pyrometer measurements during laser welding of thermoplastic elastomers to polypropylene and of nylon to itself. In *ANTEC-CONFERENCE PROCEEDINGS*- (Vol. 1, pp. 1111-1115).
42. Askadskii, A. A., Matseevich, T. A., Popova, M. N., & Kondrashchenko, V. I. (2015). Prediction of the compatibility of polymers and analysis of the microphase compositions and some properties of blends. *Polymer Science Series A*, *57*, 186-199.
43. Liu, H., Jiang, Y., Tan, W., & Wang, X. (2017). Enhancement of the laser transmission weldability between polyethylene and polyoxymethylene by plasma surface treatment. *Materials*, *11*(1), 29.
44. Liu, H., Jiang, Y., Tan, W., Chen, G., Liu, W., & Wang, X. (2017). The study of laser transmission joining PA66 and PVC with large compatibility difference. *Journal of Manufacturing Processes*, *26*, 252-261.
45. Wang, X., Liu, B., Liu, W., Zhong, X., Jiang, Y., & Liu, H. (2017). Investigation on the mechanism and failure mode of laser transmission spot welding using PMMA material for the automotive industry. *Materials*, *10*(1), 22.
46. Acherjee, B. (2021). Laser transmission welding of polymers–a review on welding parameters, quality attributes, process monitoring, and applications. *Journal of Manufacturing Processes*, *64*, 421-443.

47. Laser welding processes. Leister Technologies AG, https://www.leister.com/en/laser-plastic-welding/know-how/welding-concepts (accessed on 10th April 2025).
48. Smarra, M., Strube, A., & Dickmann, K. (2016, March). Micro drilling using deformable mirror for beam shaping of ultra-short laser pulses. In *Laser-based Micro- and Nanoprocessing X* (Vol. 9736, pp. 139-152). SPIE.
49. Kou, S. (2003). Welding metallurgy. *New Jersey, USA*, *431*(446), 223-225.
50. Davis, J. R. (1993). Hardfacing, weld cladding, and dissimilar metal joining.
51. JC, L. K. D., & Kotecki, D. J. (2005). Welding metallurgy and weldability of stainless steel. *New York: Willer Inder Science Publication*.
52. Katayama, S. (Ed.). (2013). *Handbook of laser welding technologies*. Elsevier.
53. Lippold, J. C. (2014). *Welding metallurgy and weldability*. John Wiley & Sons.
54. Tomashchuk, I., Sallamand, P., Belyavina, N., & Pilloz, M. (2013). Evolution of microstructures and mechanical properties during dissimilar electron beam welding of titanium alloy to stainless steel via copper interlayer. *Materials Science and Engineering: A*, *585*, 114-122.
55. Samson, B. R. Y. C. E., Hoult, T. O. N. Y., & Coskun, M. U. S. T. A. F. A. (2017). Fiber laser welding technique joins challenging metals. *Industrial Laser Solutions for Manufacturing*, *32*(2).
56. Mann, V., Hofmann, K., Schaumberger, K., Weigert, T., Schuster, S., Hafenecker, J., ... & Schmidt, M. (2018). Influence of oscillation frequency and focal diameter on weld pool geometry and temperature field in laser beam welding of high strength steels. *Procedia CIRP*, *74*, 470-474.
57. Acherjee, B. (2021). State-of-art review of laser irradiation strategies applied to laser transmission welding of polymers. *Optics & Laser Technology*, *137*, 106737.
58. Puetz, H., Haensch, D., Treusch, H.G., Pflueger, S., 1997. Laser welding offers array of assembly advantages. *Modern Plastics International 27 (9)*, 127–130.
59. Baylis, B., Huang, Y. P., & Watt, D. (2002, October). Welding thermoplastic elastomers to polypropylene with a diode laser. In *ICALEO 2002: 21st International Congress on Laser Materials Processing and Laser Microfabrication*. AIP Publishing.
60. Amanat, N., Chaminade, C., Grace, J., McKenzie, D. R., & James, N. L. (2010). Transmission laser welding of amorphous and semi-crystalline poly-ether–ether–ketone for applications in the medical device industry. *Materials & design*, *31*(10), 4823-4830.

61. Amanat, N., James, N. L., & McKenzie, D. R. (2010). Welding methods for joining thermoplastic polymers for the hermetic enclosure of medical devices. *Medical engineering & physics*, *32*(7), 690-699.
62. Newaz, G., Sultana, T., Nusier, S., & Herfurth, H. J. (2008). Miniaturized samples for bond strength and hermetic sealing evaluation for transmission laser joints. *Laser*, *30*(10).
63. Klein, J. & Kraus, A.. (2004). Is laser welding economical?. *Kunststoffe Plast Europe*. 94. 49-52.
64. https://www.imeche.org/news/news-article/light-strong-and-defect-free-laser welding-perfecting-the-process-for-the-automotive-industry (accessed on: 10 January 2025).
65. Potente, H., Fiegler, G., Haferkamp, H., Fargas, M., Von Busse, A., & Bunte, J. (2006). An approach to model the melt displacement and temperature profiles during the laser through-transmission welding of thermoplastics. *Polymer Engineering & Science*, *46*(11), 1565-1575.
66. Ghorbel, E., Casalino, G., & Abed, S. (2009). Laser diode transmission welding of polypropylene: Geometrical and microstructure characterisation of weld. *Materials & Design*, *30*(7), 2745-2751.
67. Sa, Y., Guo, Y., Feng, X., Wang, M., Li, P., Gao, Y., ... & Jiang, T. (2017). Are different crystallinity-index-calculating methods of hydroxyapatite efficient and consistent?. New journal of chemistry, 41(13), 5723-5731.
68. Mayboudi, L. S., Birk, A. M., Zak, G., & Bates, P. J. (2009). A three-dimensional thermal finite element model of laser transmission welding for lap-joint. *International Journal of Modelling and Simulation*, *29*(2), 149-155.
69. Acherjee, B., Kuar, A. S., Mitra, S., & Misra, D. (2010). Selection of process parameters for optimizing the weld strength in laser transmission welding of acrylics. *Proceedings of the Institution of Mechanical Engineers, Part B: Journal of Engineering Manufacture*, *224*(10), 1529-1536.
70. Acherjee, B., Kuar, A. S., Mitra, S., Misra, D., & Acharyya, S. (2012). Experimental investigation on laser transmission welding of PMMA to ABS via response surface modeling. *Optics & Laser Technology*, *44*(5), 1372-1383.
71. Acherjee, B., Kuar, A. S., Mitra, S., & Misra, D. (2012). Effect of carbon black on temperature field and weld profile during laser transmission welding of polymers: A FEM study. *Optics & Laser Technology*, *44*(3), 514-521.

72. Acherjee, B., Kuar, A. S., Mitra, S., & Misra, D. (2012). Modeling and analysis of simultaneous laser transmission welding of polycarbonates using an FEM and RSM combined approach. *Optics & Laser Technology*, *44*(4), 995-1006.
73. Acherjee, B., Kuar, A. S., Mitra, S., & Misra, D. (2013). Finite element simulation of laser transmission thermoplastic welding of circular contour using a moving heat source. *International Journal of Mechatronics and Manufacturing Systems*, *6*(5-6), 437-454.
74. Singare, S. K., Chen, S. G., Zou, J. J., & Lin, Y. Z. (2014). Laser transmission welding of thermoplastic: effect of process parameters on weld strength. *Advanced Materials Research*, *852*, 463-466.
75. Aden, M., Mamuschkin, V., & Olowinsky, A. (2015). Influence of carbon black and indium tin oxide absorber particles on laser transmission welding. *Optics & Laser Technology*, *69*, 87-91.
76. Berger, S., Oefele, F., & Schmidt, M. (2015). Laser transmission welding of carbon fiber reinforced thermoplastic using filler material—A fundamental study. *Journal of laser Applications*, *27*(S2).
77. Xu, X. F., Bates, P. J., & Zak, G. (2015). Effect of glass fiber and crystallinity on light transmission during laser transmission welding of thermoplastics. *Optics & Laser Technology*, *69*, 133-139.
78. Wang, X., Zhong, X., Liu, W., Liu, B., & Liu, H. (2016). Investigation on enhancement of weld strength between PMMA and PBT in laser transmission welding—Using intermediate material. *Journal of Applied Polymer Science*, *133*(44).
79. Gisario, A., Veniali, F., Barletta, M., Tagliaferri, V., & Vesco, S. (2017). Laser transmission welding of poly (ethylene terephthalate) and biodegradable poly (ethylene terephthalate)–based blends. *Optics and Lasers in Engineering*, *90*, 110-118.
80. Herthoge, M., De Pelsmaeker, J., Boone, M., De Baere, I., Van Paepegem, W., & Van Vlierberghe, S. (2020). Laser welding of carbon fibre filled polytetrafluoroethylene. *Journal of Materials Processing Technology*, *282*, 116681.
81. El-Batahgy, A. M. (1997). Effect of laser welding parameters on fusion zone shape and solidification structure of austenitic stainless steels. *Materials letters*, *32*(2-3), 155-163.

82. Reed, C. B., Natesan, K., Xu, Z., & Smith, D. L. (2000). The effect of laser welding process parameters on the mechanical and microstructural properties of V–4Cr–4Ti structural materials. *Journal of nuclear materials*, *283*, 1206-1209.
83. Caiazzo, F., Curcio, F., Daurelio, G., & Minutolo, F. M. C. (2004). Ti6Al4V sheets lap and butt joints carried out by CO2 laser: mechanical and morphological characterization. *Journal of Materials Processing Technology*, *149*(1-3), 546-552.
84. MI, K. (2008). Effects of welding parameters on the mechanical performance of laser welded nitinol. *Materials transactions*, *49*(11), 2702-2708.
85. Schneider, A., Gumenyuk, A., Lammers, M., Malletschek, A., & Rethmeier, M. (2014). Laser beam welding of thick titanium sheets in the field of marine technology. *Physics Procedia*, *56*, 582-590.
86. Fang, X., Liu, H., & Zhang, J. (2015). Reducing the underfill rate of pulsed laser welding of titanium alloy through the application of a transversal pre-extrusion load. *Journal of Materials Processing Technology*, *220*, 124-134.
87. Deepan Bharathi Kannan, T., Ramesh, T., & Sathiya, P. (2016). A review of similar and dissimilar micro-joining of nitinol. *Jom*, *68*, 1227-1245.
88. Kumar, C., Das, M., Paul, C. P., & Singh, B. (2017). Experimental investigation and metallographic characterization of fiber laser beam welding of Ti-6Al-4V alloy using response surface method. *Optics and Lasers in Engineering*, *95*, 52-68.
89. Datta, S., Raza, M. S., Saha, P., & Pratihar, D. K. (2019). Effects of process parameters on the quality aspects of weld-bead in laser welding of NiTinol sheets. *Materials and Manufacturing Processes*, *34*(6), 648-659.
90. Kramár, T., Tauer, J., & Vondrouš, P. (2019). Welding of nitinol by selected technologies. *Acta Polytechnica*, *59*(1), 42-50.
91. Boglea, A., Olowinsky, A., & Gillner, A. (2007, October). TWIST–a new method for the micro-welding of polymers with fibre lasers. In *ICALEO 2007: 26th International Congress on Laser Materials Processing, Laser Microprocessing and Nanomanufacturing*. AIP Publishing.
92. Kuryntsev, S. V., & Gilmutdinov, A. K. (2015). The effect of laser beam wobbling mode in welding process for structural steels. *The international journal of advanced manufacturing technology*, *81*, 1683-1691.
93. Barbieri, G., Cognini, F., Moncada, M., Rinaldi, A., & Lapi, G. (2017, February). Welding of automotive aluminum alloys by laser wobbling processing. In *Materials Science Forum* (Vol. 879, pp. 1057-1062). Trans Tech Publications Ltd.

94. Khodabakhshi, F., Shah, L. H., & Gerlich, A. P. (2019). Dissimilar laser welding of an AA6022-AZ31 lap-joint by using Ni-interlayer: Novel beam-wobbling technique, processing parameters, and metallurgical characterization. *Optics & Laser Technology*, *112*, 349-362.
95. Shah, L. H., Khodabakhshi, F., & Gerlich, A. (2019). Effect of beam wobbling on laser welding of aluminum and magnesium alloy with nickel interlayer. *Journal of Manufacturing Processes*, *37*, 212-219.
96. Jeng, J. Y., Mau, T. F., & Leu, S. M. (2000). Prediction of laser butt joint welding parameters using back propagation and learning vector quantization networks. *Journal of Materials Processing Technology*, *99*(1-3), 207-218.
97. Nagesh, D. S., & Datta, G. L. (2002). Prediction of weld bead geometry and penetration in shielded metal-arc welding using artificial neural networks. *Journal of materials processing technology*, *123*(2), 303-312.
98. Okuyucu, H., Kurt, A., & Arcaklioglu, E. (2007). Artificial neural network application to the friction stir welding of aluminum plates. *Materials & design*, *28*(1), 78-84.
99. Rao, R. V., Pawar, P. J., & Shankar, R. (2008). Multi-objective optimization of electrochemical machining process parameters using a particle swarm optimization algorithm. *Proceedings of the Institution of Mechanical Engineers, Part B: Journal of Engineering Manufacture*, *222*(8), 949-958.
100. Chandrasekaran, M., Muralidhar, M., Krishna, C. M., & Dixit, U. S. (2010). Application of soft computing techniques in machining performance prediction and optimization: a literature review. *The International Journal of Advanced Manufacturing Technology*, *46*, 445-464.
101. Rao, R. V., Savsani, V. J., & Vakharia, D. P. (2012). Teaching–learning-based optimization: an optimization method for continuous non-linear large scale problems. *Information sciences*, *183*(1), 1-15.
102. Rao, R. V., & Kalyankar, V. D. (2013). Parameter optimization of modern machining processes using teaching–learning-based optimization algorithm. *Engineering Applications of Artificial Intelligence*, *26*(1), 524-531.
103. Rao, R. V., & Patel, V. (2013). Multi-objective optimization of heat exchangers using a modified teaching-learning-based optimization algorithm. *Applied Mathematical Modelling*, *37*(3), 1147-1162.

104. Satapathy, S. C., Naik, A., & Parvathi, K. (2013). A teaching learning based optimization based on orthogonal design for solving global optimization problems. *SpringerPlus*, *2*(1), 130.
105. Yildiz, A. R. (2013). Cuckoo search algorithm for the selection of optimal machining parameters in milling operations. *The International Journal of Advanced Manufacturing Technology*, *64*, 55-61.
106. Mohamad, A. B., Zain, A. M., & Nazira Bazin, N. E. (2014). Cuckoo search algorithm for optimization problems—a literature review and its applications. *Applied Artificial Intelligence*, *28*(5), 419-448.
107. Rao, R. V., Kalyankar, V. D., & Waghmare, G. (2014). Parameters optimization of selected casting processes using teaching–learning-based optimization algorithm. *Applied Mathematical Modelling*, *38*(23), 5592-5608.
108. Huang, L., Ding, S., Yu, S., Wang, J., & Lu, K. (2016). Chaos-enhanced Cuckoo search optimization algorithms for global optimization. *Applied Mathematical Modelling*, *40*(5-6), 3860-3875.
109. Gupta, M. K., Sood, P. K., & Sharma, V. S. (2016). Machining parameters optimization of titanium alloy using response surface methodology and particle swarm optimization under minimum-quantity lubrication environment. *Materials and Manufacturing Processes*, *31*(13), 1671-1682.
110. Rakhshani, H., & Rahati, A. (2017). Snap-drift cuckoo search: A novel cuckoo search optimization algorithm. *Applied Soft Computing*, *52*, 771-794.
111. Joshi, A. S., Kulkarni, O., Kakandikar, G. M., & Nandedkar, V. M. (2017). Cuckoo search optimization-a review. *Materials Today: Proceedings*, *4*(8), 7262-7269.
112. Elsheikh, A. H., & Abd Elaziz, M. (2019). Review on applications of particle swarm optimization in solar energy systems. *International Journal of Environmental Science and Technology*, *16*, 1159-1170.
113. Abdel-Basset, M., Mohamed, R., Chakrabortty, R. K., Sallam, K., & Ryan, M. J. (2021). An efficient teaching-learning-based optimization algorithm for parameters identification of photovoltaic models: Analysis and validations. *Energy Conversion and Management*, *227*, 113614.
114. Diyaley, S., & Chakraborty, S. (2021). Teaching-learning-based optimization of ring and rotor spinning processes. *Soft Computing*, *25*(15), 10287-10307.

115. Gómez Díaz, K. Y., De León Aldaco, S. E., Aguayo Alquicira, J., Ponce-Silva, M., & Olivares Peregrino, V. H. (2022). Teaching–learning-based optimization algorithm applied in electronic engineering: A survey. *Electronics*, *11*(21), 3451.
116. Hassan, A. M., Ayoub, M. A., Mohyadinn, M. E., Al-Shalabi, E. W., & Alakbari, F. S. (2022, March). A new insight into smart water assisted foam SWAF technology in carbonate rocks using artificial neural networks ANNs. In *Offshore Technology Conference Asia* (p. D041S040R002). OTC.
117. Ali, U., Karim, K. J. B. A., & Buang, N. A. (2015). A review of the properties and applications of poly (methyl methacrylate)(PMMA). *Polymer Reviews*, *55*(4), 678-705.
118. Polycarbonate. https://en.wikipedia.org/wiki/Polycarbonate (accessed on: 15 January 2025).
119. Polypropylene copolymer. https://www.azom.com/article.aspx?ArticleID=832 (accessed on: 15 January 2025).
120. Buehler WJ and Wiley RC. *Nickel-base alloys*. Patent 3174851, USA, 1965.
121. Morgan, N. B. (2004). Medical shape memory alloy applications—the market and its products. *Materials Science and Engineering: A*, *378*(1-2), 16-23.
122. Li, Z. C., Zhao, X. K., Zhang, H., Liu, L., & Xu, Y. B. (2003). Microstructure and superelasticity of severely deformed TiNi alloy. *Materials Letters*, *57*(5-6), 1086-1090.
123. Derringer, G., & Suich, R. (1980). Simultaneous optimization of several response variables. *Journal of quality technology*, *12*(4), 214-219.
124. KHEZRI, V., Panahi, M., & Yasari, E. (2020, October). Comparing performance of evolutionary algorithms for optimizing synthetic and real-world case studies. In *The 11th International Chemical Engineering Congress and Exhibition (IChEC 2020)*.
125. Karaboga, D. (2010). Artificial bee colony algorithm. *scholarpedia*, *5*(3), 6915.
126. Ranjan, A. (2020). An investigation on surfactant added PMWEDM of Inconel 718. *International journal of automotive and mechanical engineering*.
127. Gandomi, A. H., Yang, X. S., & Alavi, A. H. (2013). Cuckoo search algorithm: a metaheuristic approach to solve structural optimization problems. *Engineering with computers*, *29*, 17-35.
128. Al-Salami, N. M. (2009). System evolving using ant colony optimization algorithm. *Journal of Computer Science*, *5*(5), 380.

129. Acherjee, B., Maity, D., Prakash, S., Kuar, A. S., & Mitra, S. (2018). Optimal Process Parameter Selection of Underwater Nd: YAG Laser Micro-channeling on PMMA by Firefly Algorithm and Flower Pollination Algorithm. *Chinese Soc. Mech. Eng*, *39*(5), 515-533.

130. Acherjee, B., Maity, D., Karia, D., & Kuar, A. S. (2019). Selection of laser micro-drilling process parameters using novel bat algorithm and bird swarm algorithm. In *Optimization Using Evolutionary Algorithms and Metaheuristics* (pp. 83-100). CRC Press.

131. Yang, X. S., & Deb, S. (2009, December). Cuckoo search via Lévy flights. In *2009 World congress on nature & biologically inspired computing (NaBIC)* (pp. 210-214). Ieee.

132. Holland, J. H. (1992). *Adaptation in natural and artificial systems: an introductory analysis with applications to biology, control, and artificial intelligence*. MIT press.

133. Lambora, A., Gupta, K., & Chopra, K. (2019, February). Genetic algorithm-A literature review. In *2019 international conference on machine learning, big data, cloud and parallel computing (COMITCon)* (pp. 380-384). IEEE.

134. Pal, K., Panwar, V., Friedrich, S., & Gehde, M. (2016). An investigation on vibration welding of amorphous and semicrystalline polymers. *Materials and Manufacturing Processes*, *31*(3), 372-378.

Abhiraj Kumar 26/11/25

Arunanshu Shekhar Kuar 26/11/25

Dr. Arunanshu Shekhar Kuar
PROFESSOR
Production Engineering Department
Jadavpur University
Kolkata - 700 032, India

Arabian Journal for Science and Engineering (2024) 49:2411–2441
https://doi.org/10.1007/s13369-023-08238-1

RESEARCH ARTICLE-MECHANICAL ENGINEERING

Performance Evaluation of TWIST Welding Using Machine Learning Assisted Evolutionary Algorithms

Dhiraj Kumar[1] · Samriddhi Ganguly[1] · Bappa Acherjee[2] · Arunanshu Shekhar Kuar[1]

Received: 2 April 2023 / Accepted: 17 August 2023 / Published online: 12 September 2023

Abstract
The Transmission welding using incremental scanning technique (TWIST) combines linear feed with an oscillating laser beam to enhance weld quality and expand the process window. However, TWIST welding is influenced by nonlinear process variables, and achieving multiple objectives concurrently is challenging due to conflicting performance attributes. In industrial practice, time constraints and project specifications limit the effectiveness of methodologies tailored to specific workpiece materials or single performance optimization. The present study employs an artificial neural network (ANN) to establish a correlation between TWIST welding parameters and desired performance attributes. Various ANN model architectures are evaluated, with the 5-11-6-2 architecture achieving the highest accuracy (correlation coefficient of 0.998). For multi-objective optimization, the non-dominated sorted genetic algorithm (NSGA-II) and non-dominated sorted teaching learning-based optimization (NSTLBO) algorithm are employed, utilizing the ANN model's fitness function as the objective. The newly developed two-step model provides operators with the flexibility to prioritize factors based on project requirements, resulting in improved outcomes. Comparative analysis of the algorithms using seven metrics demonstrates that NSGA-II outperforms NSTLBO in solution prediction, albeit with slightly increased computing time. NSGA-II offers a broader range of Pareto optimum solutions compared to NSTLBO, which converges narrowly and restricts non-dominated sets. Validation experiments confirm the adequacy of both algorithms, supporting the effectiveness of the two-step model. The proposed methodology enables practitioners to achieve better weld quality, accommodate conflicting performance attributes, and effectively optimize multiple objectives in industrial applications.

Keywords Laser transmission welding · TWIST · Artificial neural network · Evolutionary algorithm · Machine learning · Multi-objective optimization

1 Introduction

Polymers have a significant role in our daily life, which is difficult to comprehend. Nowadays, polymers are employed everywhere, from essential everyday items to very complicated industrial goods. The fabrication of well-designed electronic products and microfluidic devices is made possible by the wide variety of polymeric materials that are now readily available [1–3]. Polymers are widely used due to their low weight, durability, and ease of manufacturing and recycling. Increasing the use of polymer composites in the automotive and aviation sectors helps to improve fuel economy and thereby reduce greenhouse gas emissions, making it more fuel efficient and environmentally friendly [4]. For polymers and polymer composites to have a broader range of applications in many sectors, high-quality joining is necessary. Although there have been decades of traditional polymer welding options available, laser transmission welding (LTW) is gradually taking the place of friction, electromagnetic, and thermal traditional polymer welding processes in industrial applications

✉ Dhiraj Kumar
dhirajk.production.rs@jadavpuruniversity.in

Samriddhi Ganguly
samriddhiganguly2000@gmail.com

Bappa Acherjee
bappa.rana@gmail.com

Arunanshu Shekhar Kuar
askuar@rediffmail.com

[1] Department of Production Engineering, Jadavpur University, Kolkata 700032, India

[2] Department of Production and Industrial Engineering, Birla Institute of Technology: Mesra, Ranchi 835215, India

Optics & Laser Technology 146 (2022) 107603

Contents lists available at ScienceDirect

Optics and Laser Technology

journal homepage: www.elsevier.com/locate/optlastec

Beam wobbling effects on laser transmission welding of dissimilar polymers: Experiments, modeling, and process optimization

Dhiraj Kumar [a,*], Niladri Shekhar Sarkar [b], Bappa Acherjee [c], Arunanshu Shekhar Kuar [a]

[a] Department of Production Engineering, Jadavpur University, Kolkata 700032, India
[b] School of Laser Science and Engineering, Jadavpur University, Kolkata 700032, India
[c] Department of Production and Industrial Engineering, Birla Institute of Technology, Mesra, Ranchi 835215, India

ARTICLE INFO

Keywords:
Laser transmission welding
Wobble welding
Welding parameters
Transparent polymer welding
Dissimilar polymer welding
Process optimization

ABSTRACT

Because of numerous advantageous characteristics of polymers and their expanding usage in microfluidic devices, automotive, household, packaging, and biomedical sectors, laser transmission welding (LTW) has emerged to meet the need for a potent polymer welding technology for industrial use. This paper presents an experimental investigation, mathematical modeling, and parameters optimization of wobble LTW of dissimilar transparent polymers. A low-power Nd:YVO_4 laser is used to fuse transparent acrylic and polycarbonate plaques using a black marker ink line applied at the weld interface. Planned experiments and corresponding analyses are performed to develop the mathematical models and investigate the effect of beam wobbling on the process responses. The wobbling of the beam creates homogenized heat distribution and turbulence inside the weld pool, which improves material intermixing and joint strength. Morphological analysis reveals the presence of a number of tiny bubbles on the top surface of the weld bead, which strengthens the micromechanical joining at the weld interface. Artificial intelligence-based teaching learning-based optimization (TLBO) algorithm and desirability function analysis (DFA)-based optimization method are employed to improve the weld quality and to obtain the desired response. TLBO produces more accurate results than DFA because of its strong convergence towards global optima.

1. Introduction

Polymeric materials are increasingly being used in a variety of applications, including aerospace, automotive, electronics, medical, microfluidics and packaging [1-5]. With the ever-increasing need for polymer components, joining methods are becoming increasingly important in their production. Laser transmission welding (LTW) emerged at the end of the twentieth century as a viable and competitive technique for meeting the polymer joining criteria [6,7]. The optical characteristics of the polymer components to be welded using LTW should differ. The top polymer part of the assembly must be laser-transparent, while the bottom must be laser-absorbent (Fig. 1). An intermediate layer is added at the weld interface to ensure absorption of laser radiation while welding both transparent polymers [8-10]. The laser radiation passes through the top transparent part and is absorbed by the absorbent part, causing optical radiation to be converted into heat energy via thermo-optic interaction. The heat produced in the absorbent part is transferred to the upper transparent polymer part via heat conduction. The clamping pressure is required to create the weld because it provides adequate pressure to keep the molten metal at the weld interface while improving heat conduction. As a result, both parts melt at interface and a strong bond between the polymer parts is produced. LTW has the advantage of being simple to automate and control. With the increased usage of polymers and the capacity of LTW to weld thin as well as thick components, LTW is now extensively recognized in industries. LTW is a non-contact, high energy density joining method that results in a small heat-affected zone [11,12]. The laser polymer interaction, optical properties of polymers, additives or carbon content of polymers, and laser radiation wavelength all influence the effectiveness of the LTW process [13,14]. Controllable welding parameters such as laser power, pulse frequency, scanning speed, clamping pressure, and laser beam size affect heat input to the weld fusion zone, which is utilized to adjust temperature during welding [15-17]. Weld quality is also affected by the polymer properties and the extent of the air gap at the interface [16,18]. For LTW of polymers, diode, Nd:YAG, and fiber lasers operating in the wavelength range 0.8–1.1 μm are employed, since

* Corresponding author.
E-mail address: dhirajk.production.rs@jadavpuruniversity.in (D. Kumar).

https://doi.org/10.1016/j.optlastec.2021.107603
Received 11 July 2021; Received in revised form 23 September 2021; Accepted 11 October 2021
Available online 21 October 2021

Lasers in Eng., Vol. 49, pp. 205–225
Reprints available directly from the publisher
Photocopying permitted by license only

Enhancement of Laser Transmission Welds in Acrylic and Polypropylene Copolymer (PPCP) Using Snap Drift Cuckoo Search (SDCS) Optimization

D. KUMAR[1,*], S. GHOSH[1], A.S. KUAR[1] AND N. MAITY[2]

[1]*Department of Production Engineering, Jadavpur University, Kolkata-700032, West Bengal, India*
[2]*School of Laser Science and Engineering, Jadavpur University, Kolkata-700032, West Bengal, India*

Laser transmission welding (LTW) is widely recognized as an effective joining method for thermoplastic polymers. Excellent mechanical, physical and thermal properties of polypropylene makes it suitable for many application in aerospace, automotive manufacturing and laboratory accessories; however, joining of semi-crystalline and amorphous polymers is very difficult due to their poor compatibility or different crystal structure. To overcome this problem, white ink is applied at the interface of weld to increase the solubility and retain the laser heat input. As white ink is an opaque, containing copolymer resins which helps to enhance the bonding strength. Here, acrylic (amorphous) and polypropylene copolymer (PPCP) (semi-crystalline) each of 4 mm thickness have been joined by low power diode laser. Experimental analysis of the effect of process parameters such as laser power, scanning speed and pulse frequency on the weld zone has been studied. Greater weld strength is achieved at low scan speed. A novel multi objective snap drift cuckoo search (SDCS) optimization technique has been implemented for betterment of weld strength and weld width. A scanning electron microscope (SEM) has been used to observe the welded zone morphology. It is observed that weld strength is primarily dependent on mechanical interlocking between the two layers of polymers.

Keywords: Nd:YVO4, acrylic, polypropylene copolymer (PPCP), amorphous, semi-crystalline, laser transmission welding (LTW), low power, morphology, snap drift cuckoo search (SDCS) technique

*Corresponding authors: E-mail: erdhirajkumar3@gmail.com

Lasers in Eng., Vol. 50, pp. 311–330
Reprints available directly from the publisher
Photocopying permitted by license only

Low Power Laser Transmission Welding (LTW) of Clear to Clear Acrylic Transparent Polymers

D. KUMAR[1,*], A.S. KUAR[1] AND N. MAITY[2]

[1]*Department of Production Engineering, Jadavpur University, 188, Raja Subodh Chandra Mallick Rd, Kolkata-700032, West Bengal, India*
[2]*School of Laser Science and Engineering, Jadavpur University, 188, Raja Subodh Chandra Mallick Rd, Kolkata-700032, West Bengal, India*

Owing to the growing applications in medical equipment, the marine sector and automotive industries, laser transmission welding (LTW) is gaining increasing importance. LTW of two transparent acrylic thermoplastic materials, each of 4 mm thickness, was demonstrated using a diode laser-pumped solid-state Nd:YVO_4 pulsed laser. The effect of process parameters such as laser power, pulse frequency and scanning speed have been investigated and a multi-objective optimization based on desirability function technique was used for the betterment of the results. A validation test has been performed which shows that the predicted results are compatible with actual value. Scanning speed was found to be the process parameter that mostly affects the weld strength. A scanning electron microscope (SEM) was used to study the morphology of the weld zone. It was observed from SEM micrographs that the heating zone in the weld area often generates bubbles and ablation which enhance the joining strength.

Keywords: Nd: YVO_4 laser, acrylic, transparent polymer, laser transmission welding (LTW), low power, morphology, multi-objective optimization, response surface methodology (RSM)

1 INTRODUCTION

Laser transmission welding (LTW) over the years has developed to become an indispensable technology that offers reliable solutions for joining of polymers. It is a well known fact that LTW is widely being accepted as an impor-

*Corresponding author: E-mail: erdhirajkumar3@gmail.com

Materials Today: Proceedings 56 (2022) 2063–2069

Contents lists available at ScienceDirect

Materials Today: Proceedings

journal homepage: www.elsevier.com/locate/matpr

Sensitivity analysis for process parameters in laser transmission welding of transparent polymers

D. Kumar [a,*], U. Pratap [a], N. Roy [b], A.S. Kuar [a]

[a] Jadavpur University, Kolkata 700032, India
[b] Swami Vivekananda Institute of Science & Technology, Kolkata 700145, India

ARTICLE INFO

Article history:
Available online 6 December 2021

Keywords:
Laser transmission welding
Sensitivity analysis
Transparent polymer welding
Optimization

ABSTRACT

Owing to the increasing use of polymers in microfluidic devices, lightweight automotive and modern industries, laser transmission welding has evolved as a reliable method over the years. In this paper, sensitivity analysis has been performed to find out the critical parameters and to compare the relative impact of process variables on weld quality. Two transparent PMMA materials have been joined using low power laser with 1064 nm wavelength. The results are analyzed for laser transmission welding processes by considering corresponding parameters such as laser power, pulse frequency and scanning speed. Scanning speed is found to be dominant parameter based on statistical method while sensitiveness of weld strength and weld width are maximum for laser power. Optimization of process variable helps to obtain desired responses. A novel metaheuristic Teaching Learning Based Algorithm has been used to maximize the weld strength and minimize the weld width.

Selection and peer-review under responsibility of the scientific committee of the International Conference on Applied Research and Engineering 2021

1. Introduction

Polymers have been popular material choice for microfluidic devices because of the ease of surface modification and shape, low cost and optical characteristics. With increasing application of microfluidic devices in recent years, there is a need to explore the possible advancement in the field of polymer joining, which helps to obtain leak proof joint in sealing of microfluidic devices. The use of polymeric materials is growing now a days in many applications such as aerospace, automotive, electronics, medical, packaging etc. PMMA (poly-methyl methacrylate) is widely used in microfluidic chips, aircraft windshields and automotive panels etc. due to its robust, longevity and lightweight [1]. Excellent thermal, electrical, mechanical and chemical properties of PMMA makes suitable for biological and micro electro mechanical applications.

Laser technology plays a vital role in fulfilling the necessary plastic processing requirements. Joining of polymers is a challenging process and various joining techniques have been developed over the past few years. The plastic joining can be broadly divided into three types: chemical or adhesive, mechanical and welding. Initially, traditional welding solved the challenges of welding of polymers in the early days. Now a days, many industries are looking for several demands that cannot be met by conventional laser welding and thus, laser transmission welding is introduced to fulfil the demands. Laser transmission welding (LTW) is recognized as most promising technology for welding of polymers. LTW is generally applied to join laser transparent polymers and opaque or laser absorbent thermoplastic polymers. It works on the transmission of laser through upper part, absorption of laser at bottom part, heat conduction to the top layer, melting and interfusion of polymers at weld interface [2]. The working principle of LTW is shown in Fig. 1.

Several researchers focused on examining various facets of LTW technique in order to improve the weld quality. Ilie et al., [3] explored the laser weldability of dissimilar polymers considering ABS and PA11 as work material using design of experiment. Optical properties of the polymer plays vital role while welding of polymers. Xu et al., [4] studied the behavior of laser when it passes through the transparent part and also reported the effect of glass fiber and crystallinity on welding of various polymers. Carbon black (CB) is frequently used in welding of polymers and its influence on light transmission has been discussed by Chen et al., [5].

* Corresponding author.
E-mail address: erdhirajkumar3@gmail.com (D. Kumar).

https://doi.org/10.1016/j.matpr.2021.11.404
2214-7853/
Selection and peer-review under responsibility of the scientific committee of the International Conference on Applied Research and Engineering 2021

Materials Today: Proceedings 103 (2024) 481–492

Contents lists available at ScienceDirect

Materials Today: Proceedings

journal homepage: www.elsevier.com/locate/matpr

Modeling and optimization of conflicting responses in the laser transmission welding process using RSM, PSO, and TLBO algorithm

Dhiraj Kumar [a,*], Utkarsh Pratap [a], Bappa Acherjee [b], Arunanshu Shekhar Kuar [a]

[a] Department of Production Engineering, Jadavpur University, Kolkata 700032, India
[b] Department of Production and Industrial Engineering, Birla Institute of Technology: Mesra, Ranchi, Jharkhand 835215, India

ARTICLE INFO

Keywords:
Laser transmission welding
Transparent polymer welding
RSM-based desirability function approach
Meta-heuristic algorithm
Nature-inspired methods

ABSTRACT

Laser transmission welding (LTW) is a widely used polymer welding technology in industries today. The performance of LTW is governed by a number of process parameters, and fine-tuning those parameters is critical for the process to achieve the intended results. Optimization of process parameters for enhancing LTW performance, like weld strength and weld width, is always tricky since they are inherently contradictory. Therefore, in this research, an effort is made to optimize the LTW parameters utilizing the three best-known optimization approaches, and the performance of those optimization approaches in LTW process optimization is compared. First, the response surface method (RSM) is employed to build empirical equations that establish an empirical correlation between process variables and desired performance features. These empirical equations are then employed as objective functions for process optimization utilizing the RSM-based desirability function approach (DFA), particle swarm optimization (PSO), and teaching learning-based optimization (TLBO) algorithms. The performance of the chosen optimization approaches is compared with reference to optimum results, accuracy, convergence rate, and computing time. PSO and TLBO algorithms outperform the DFA approach for single and multi-objective optimizations. TLBO is found to have faster convergence, whereas PSO takes less time for computation.

1. Introduction

Polymers are indispensable in various industries, from electronics to food packaging. They find applications in construction, appliances, transportation, and more. Their advantages, like durability and lightness, have led to their use in aerospace, automotive, and consumer goods. Polymer composites, like fiber-reinforced variants, have gained use in sectors such as boat manufacturing [1–3]. As polymers expand into biomedical and food packaging sectors, a need arises for eco-friendly polymer welding methods [4]. Over fifteen polymer welding processes exist, including established ones like hot gas welding, vibration welding, ultrasonic welding, dielectric welding, and resistive implant welding [5]. Laser welding of polymers emerged in the 1970s, employing CO_2 lasers for processing and CO_2 lasers for cutting and welding [6]. By the late 1980s, Nd:YAG and diode lasers (0.8–1.1 μm wavelengths) advanced the laser welding of polymers beyond thin films. Laser transmission welding (LTW), illustrated in Fig. 1, emerged as a prominent polymer welding method and fills the gap where conventional polymer welding methods fall short. In LTW, the optical properties of polymer parts are crucial. One part needs to be laser-transparent, while the other must be laser-absorbing. Transparent polymer-to-polymer welding requires an absorbing interlayer for energy transfer. The laser penetrates the upper transparent polymer, absorbed by the lower absorbing polymer, transmitting the heat to the top polymer, softening or melting them at the interface [7,8]. This creates a solidified joint through molecular diffusion. Polymers' inherent transparency can be turned laser-absorbing with colorant additives.

The effectiveness of the LTW process relies on intricate factors like laser-polymer interactions, polymer compositions, optical characteristics, laser wavelength, and processing parameters. Acherjee et al. [9] conducted research on optimizing welding parameters for acrylic and also investigated the LTW of dissimilar polymers, specifically acrylic and ABS (acrylonitrile butadiene styrene), utilizing response surface methodology (RSM) to establish connections between variables and responses [10]. Kumar et al. [11] explored LTW between acrylic and polycarbonate, identifying pivotal process parameters. Liu et al. [12] delved into transparent polymer LTW using metal absorbers, observing that metal absorbers outperformed dye absorbers, yielding stronger,

* Corresponding author.
E-mail address: erdhirajkumar3@gmail.com (D. Kumar).

https://doi.org/10.1016/j.matpr.2023.09.189
Received 13 June 2023; Received in revised form 2 September 2023; Accepted 23 September 2023
Available online 27 September 2023

Materials Today: Proceedings 26 (2020) 808–813

Contents lists available at ScienceDirect

Materials Today: Proceedings

journal homepage: www.elsevier.com/locate/matpr

Laser transmission welding of thermoplastic with beam wobbling technique using particle swarm optimization

D. Kumar *, S. Ghosh, A.S. Kuar, S. Paitandi

Jadavpur University, Kolkata 700032, India

ARTICLE INFO

Article history:
Received 6 December 2019
Accepted 31 December 2019
Available online 28 January 2020

Keywords:
Low power laser
Polycarbonate
Acrylic
Beam wobbling
Weld strength
Particle swarm optimization

ABSTRACT

Laser transmission welding is growing day by day with an increase of the uses of thermoplastic materials. This article presents the effect of various process parameters on weld strength and weld seam width obtained. The transparent polycarbonate and black carbon filled PMMA, each of 2.8 mm thickness have been joined by using low power laser. Here, effect of wobble frequency and wobble width are studied along with other process parameters. It is observed that weld seam width much depends upon the wobble width and the effect of wobble frequency is minimum. It has been observed that laser beam wobbling provides the greater weld strength by enlargement of joint area. Moreover, Beam wobbling plays a significant role to achieve better weld strength and weld width. Response surface methodology has been used to model the laser welding process parameters and responses of welding through regression analysis. The results of ANOVA reveal that the models formed appropriately predict the responses within the range of process parameters. A confirmation experiment has also been conducted to validate the results. A multi objective optimization has been used to find the optimum solution by Particle swarm optimization technique.

Selection and peer-review under responsibility of the scientific committee of the 10th International Conference of Materials Processing and Characterization.

1. Introduction

Plastics have been the fastest growing basic material. The applications of plastics are essentially limitless. Plastics are lightweight, robust, flexible, complex shape fabrication and relatively cheap. Plastics do not deteriorate, but can be reused quickly. Now a days, plastic are replacing metals and non-metals in certain applications due to its light weight, flexibility, weather resistant, strong and relatively inexpensive. Major applications have been found for plastics in the aerospace, adhesives, coating, construction, electrical, electronic, medical, packaging, textile, household products and automotive industries [1]. The ever-increasing demand for plastic products and the widespread use both in technologically advanced fields and in everyday life require new methods that are more versatile, quicker and environmentally friendly. As a new alternative to meeting these criteria, laser processing of plastic materials arises. Laser transmission welding offers an attractive alternative option to weld plastics where traditional plastic joining technique fails. The flexibility of Laser eliminates the plastic welding based on friction, ultrasonic energy, vibration and hot tool. The gradual replacement of traditional tools by Laser in welding in plastics industries can be justified by process reproducibility, process efficiency, and increased productivity.

1.1. Laser transmission welding

Laser transmission welding technologies for thermoplastics have already been incorporated into industrial manufacturing. The fundamental principle of the transmission laser welding is to pass or transmit laser radiation to form a weld through one piece of plastic. Unlike standard welding, where the energy is applied to the material surface, transmission laser welding aims to apply the energy to the interface between two plastic parts. There is criteria to perform laser transmission welding like first part has to be transparent and second part need to absorbent to the laser radiation. Laser radiation transmittance should not be same as plastic optical transparency. Upon passing through the upper layer, the laser beam still needs to be transformed into thermal energy. The lower one needs the ability to consume the laser energy to produce heat. Once it converts the laser energy into heat, the thermal

* Corresponding author.
E-mail address: dhirajk.production.rs@jadavpuruniversity.in (D. Kumar).

https://doi.org/10.1016/j.matpr.2019.12.422

Selection and peer-review under responsibility of the scientific committee of the 10th International Conference of Materials Processing and Characterization.